Technical University of Munich
TUM School of Engineering and Design

Biotechnological Production of Microbial Oils from Carbon Dioxide Using Microalgae and Oleaginous Yeasts in an Integrated Process

Ayşe Özlem Koruyucu

Complete reprint of the dissertation approved by the TUM School of Engineering and Design of the Technical University of Munich for the award of the

Doktorin der Ingenieurwissenschaften (Dr.-Ing.)

Chair: Prof. Dr. Thomas Hamacher

Examiners:

1. Prof. Dr.-Ing. Dirk Weuster-Botz
2. Prof. Dr. Thomas Brück

The dissertation was submitted to the Technical University of Munich on 21.03.2024 and accepted by the TUM School of Engineering and Design on 11.06.2024.

The explorer who will not come back or send back his ships to tell his tale is not an explorer, only an adventurer; and his sons are born in exile.

— Ursula K. Le Guin, The Dispossessed: An Ambiguous Utopia —

Acknowledgements

This dissertation came into existence during my work as a research assistant at the Chair of Biochemical Engineering, Technical University of Munich, under the lead of Prof. Dr.-Ing. Dirk Weuster-Botz. I would like to express my heartfelt gratitude to all those who contributed to the development of this work in various ways.

First of all, I want to thank Prof. Dr.-Ing. Dirk Weuster-Botz for his excellent supervision, which made this dissertation possible. I am very grateful to him for his guidance, for always providing helpful insights when needed, and for the critical evaluation of my scientific work. His support and encouraging attitude helped me stay determined and enthusiastic about my work.

I would like to thank Prof. Dr. Thomas Brück for examining my dissertation and Prof. Dr. Thomas Hamacher for taking the chair for my thesis defence.

Furthermore, I am thankful to Daniel Garbe for the great management of the GreenCarbon project. I extend my thanks to all of my project colleagues, particularly Sophia Prem and Felix Melcher, for their enthusiastic engagement and excellent collaboration.

Special thanks go to Torben Schädler for the great assistance at the TUM-AlgaeTec Center in my first year, as well as to Jeremy von Poschinger and Emil Korzin for the immense support at the TUM Pilot Plant for Industrial Biotechnology. Moreover, I really appreciate the support of Patrick Meins, Nelson Vogel, and Markus Amann with administrative tasks, paperwork, technical issues, and organizational needs, which make up a significant portion of the work as a research assistant.

Additionally, I am very grateful to all of my colleagues at the Chair of Biochemical Engineering and the Professorship of Systems Biotechnology for their excellent cooperation, many exciting academic discussions and the wonderful working environment. Working with them has been a pleasure for me.

I would also like to acknowledge the contributions of my many former students Karlis Blums, Tillmann Peest, Amelie Gniffke, Laura Schmack-Rauscher, Konrad Mundt, Susann Krippendorf, Peter Urban, İpek Dere, Patricia, Billy Halim, Lukas Gröninger, Annika Pfeffer and Yisha Liu. Working with so many brilliant students has been my luck over these years.

I thank my dear friend Daniel Caballero, who has accompanied and supported me through a big part of my academic journey, first as a college mate and then as a colleague during my dissertation.

A big thanks go to my beloved family, particularly my mom Şerife and my dad Mustafa for their unconditional support. It is a bliss to have you always by my side.

Finally, I must express my greatest gratitude to my dear partner, Fabian, for actively supporting me through the periods of intense work, always being there as my safe haven and giving me the home that enables me to be who I am and do what I do.

Contents

1. Introduction

The current climate crisis and the limited supply of fossil oils demand a rapid energy transition and a switch to renewable, sustainable resources as raw materials in the industry. Due to the urgency of the crises and the need for international cooperation for solutions, policy makers have already taken steps towards regulating the future course of the industry (UNFCCC, 2016; European Comission, 2022). As a result, research focusing on alternative green production ways and low carbon energy supplies has intensified substantially.

Microbial oils present a great potential for a sustainable change in the industry contributing to a circular economy. Industrial waste streams and biogenic resources, such as biomass residues from the forestry and agriculture sectors, are low-cost carbon sources that could be used for microbial oil production. Moreover, industrial exhaust gases with high CO_2 content or CO_2 captured from the atmosphere using efficient novel technologies could be utilized as feedstocks for the production of these oils. The main candidates producing microbial or single-cell oils (SCOs) are oleaginous microalgae and yeasts, both being intensively researched in recent years. Oleaginous microorganisms can accumulate lipids of at least 20% of their dry weight (Thorpe & Ratledge, 1972), and some oleaginous yeast strains are known to achieve a cellular lipid content of up to almost 90% (Abeln & Chuck, 2021).

Microalgae are interesting SCO producers, in particular due to their ability to fixate CO_2 into their biomass with fixation efficiency reaching up to 90% (Schädler et al., 2019). However, due to their relatively low lipid productivity, current application areas of microalgae remain limited to mainly wastewater treatment (Brenner & Abeliovich, 2013; Kaplan, 2013), aquaculture supplying foodstuffs (Becker, 2013; Muller-Feuga, 2013), and production of specific polyunsaturated fatty acids (PUFAs) for use as nutraceuticals (Ratledge & Wynn, 2020). Oil production by oleaginous yeast, on the other hand, can achieve very high productivities with high efficiency of carbon conversion into oils (Abeln & Chuck, 2021). Nevertheless, yeast are heterotrophic microorganisms producing CO_2 in the process, so the advantages of yeast oil production depend on the carbon source used and the end use of the oils.

Microbial oils can be an alternative to petroleum and vegetable oils, some of which are linked to global deforestation, such as palm oil and cacao oil. Moreover, first-generation feedstocks used for biodiesel production, such as rapeseed or soy bean competing with land and fresh water supplies for food production, can be substituted by microbial oils (Abeln & Chuck, 2021). Techno-economic analysis of the process shows the potential of microbial oils especially for production of oleochemicals and other high-added-value products, but possibly also for biodiesel production in the future as fossil oils become scarcer and prices rise (Koutinas et al., 2014; Ratledge & Wynn, 2020).

2. Objectives

Microbial oil production from CO_2 using microalgae has been researched intensively in recent decades, receiving particular attention due to its potential for the carbon-neutral sustainable production of fuels and other valuable biochemicals based on algal lipids. Still, microalgae processes remain uncompetitive for the production of low-value-added products due to high production costs entailed by low lipid productivity. This study suggests an alternative pathway to improve the productivity of microbial oil production from CO_2, utilizing microalgae and oleaginous yeasts in a single integrated process.

Marine microalgae can fixate CO_2 into their biomass with an efficiency of up to 90% using sunlight as the energy source (Schädler et al., 2019). Lipid production in oleaginous microorganisms, such as microalgae, is induced by the limitation of an essential nutrient such as nitrogen, phosphorus or sulphur in the presence of a carbon source in excess. It has been previously shown that microalgae growing fast without any nutrient limitation achieve a much higher areal productivity than lipid production under growth-limiting conditions (Schädler et al., 2019). Therefore, it would be a reasonable approach to utilize microalgae not for lipid production, but only for the fast and efficient CO_2 fixation. Microalgae biomass generated in this way can then be hydrolysed and used as a cultivation medium for an oleaginous yeast to produce microbial oils with high productivity. Thus, utilizing microalgae biomass as a carbon source, rather than a single-cell oil (SCO) producer, could be a better option for a microbial oil factory, considering the advantages regarding process productivity. Previous studies have already demonstrated it to be possible to utilize lipid-extracted and enzymatically hydrolysed microalgae biomass with an oleaginous yeast on a laboratory scale (Younes et al., 2020; Meo et al., 2017). Figure 2.1 illustrates the flowchart of the integrated oil production process studied in this work, in which CO_2 is fixated into microalgae biomass, which is then processed into a phosphorus-depleted biomass hydrolysate and finally converted into microbial oils by oleaginous yeasts.

Cultivation systems for microalgal biomass production are divided into open and closed photobioreactors (PBRs). While the microalgae suspension in open PBRs is in direct contact with the atmosphere, the culture in closed reactors is wholly separated from its surroundings. Closed cultivation systems offer better control of the growth conditions, protection from external contamination to some extent, and reduced evaporation. Still, the installation and operation of closed PBRs are considered too expensive for the industrial production of low-value-added products due to their high complexity and poor scalability (Zittelli et al., 2013). Therefore, the general assumption is that only simple open cultivation systems can economically produce microalgae biomass as a raw material for the industry. Accordingly, an open PBR is preferred for microalgal biomass production in this work.

Microalgal biomass production requires large areas due to the dependence of biomass growth on energy influx per culture volume through sunlight. Hence, high areal productivity is crucial for the profitability of any open microalgae cultivation system. Apel et al. (2017) applied a new type of scalable open thin-layer cascade (TLC) PBR to investigate microalgal growth under physical simulation of suitable climate zones. The first objective of this study is to determine the necessary conditions to achieve high biomass productivities and >90% CO_2 fixation efficiency of microalgal biomass pro-

duction in a TLC reactor on a pilot scale (50 m^2) under realistic climate conditions. Additionally, a suitable mode of operation with high efficiency is to be determined for continuous biomass production.

One of the main challenges of microalgae cultivation in open PBRs is, alongside productivity issues, the risk of contamination (Ratledge & Wynn, 2020). Thus, it is crucial to reduce this risk by growing microalgae that require extreme conditions unfavourable for potential contaminants. The marine microalgae *Microchloropsis salina* is known to achieve relatively high growth rates of 0.03 h^{-1} with a salinity optimum at 35 ppt and a pH optimum of 7.5–8.0 (Boussiba et al., 1987), which significantly reduces the amount of contaminants in an open culture. High salinity of the algae culture also makes it possible to use seawater as the cultivation medium, reducing freshwater consumption and, thus, the cost and environmental footprint of microalgae production. Moreover, multiple studies have shown that *M. salina* is well suited for biomass production in open TLC PBRs (Apel et al., 2017; Pfaffinger et al., 2019; Schädler et al., 2019, 2021). Hence, *M. salina* is chosen for microalgal biomass production in this work.

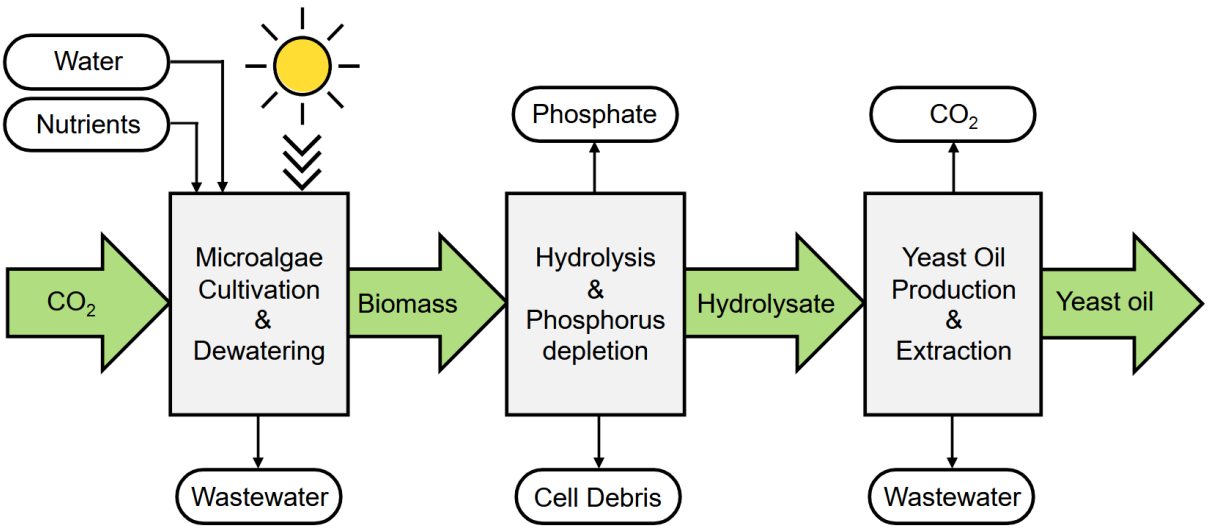

Figure 2.1: Flowchart of the integrated process for microbial oil production from CO_2 using microalgae and oleaginous yeasts. CO_2 is fixated into microalgae biomass using sunlight, water and nutrients. After biomass separation, hydrolysis and phosphorus depletion, microalgal biomass hydrolysate is used as the carbon source for yeast oil production. Central substrate, intermediate and product streams of interest are highlighted in green, while the remaining inflow and side-product streams are marked in white.

Microalgae cultivation is followed by hydrolysis of the biomass, to be used as cultivation medium for the oleaginous yeast. Generally, microalgae biomass grown under nutrient-replete conditions has around 25% *(w/w)* carbohydrates and 50% *(w/w)* proteins (Schädler et al., 2019), both of which could be converted into valuable carbon sources that can be utilized by oleaginous yeasts. This would, for instance, correspond to around 50 g L^{-1} sugar concentration in a microalgal biomass hydrolysate produced using a concentrated biomass with 250 g dry cell weight per litre (Meo et al., 2017). Although considered typical for the waste streams or biomass hydrolysates generally used as substrate for yeast cultivation (Moon et al., 1978; Masri et al., 2017; Yousuf et al., 2010; Yu et al., 2011), such a low concentration of the carbon source is still very diluted in comparison to synthetic media used in industrial processes. Therefore, it is important to employ an efficient biomass harvest

and dewatering method to obtain a high-density whole-cell microalgae paste to keep the sugar concentration in the resulting biomass hydrolysate as high as possible.

Marine microalgae have rather complex and structurally stable cell walls, which are hard to disrupt both mechanically and chemically (Spiden et al., 2013; Scholz et al., 2014; Hernández et al., 2015). Besides, microalgae grown in nutrient-replete medium have a potential to build even stronger cell walls than the cells grown in nutrient-limited medium (Jeong et al., 2017). Therefore, a combination of different cell disruption and hydrolysis methods will be examined in this study for the efficient hydrolysis of the whole-cell microalgae paste. Mechanical cell disruption methods studied are selected to be scalable and suited for continuous production, targeting high cell disintegration degree with minimum energy input, whereas enzymatic hydrolysis of the disrupted microalgae cells aims for maximum saccharification efficiency of the carbohydrates present in the microalgal biomass. For process scalability, combinations of various commercially available enzyme mixtures will be tested for biomass hydrolysis.

Lipid accumulation by oleaginous yeast cells is induced by deficiency of a nutrient required for growth, accompanied by an excess of carbon sources in the medium. Phosphate elimination using precipitating agents is an uncomplicated and cheap option to create nutrient-depleted conditions applicable on an industrially relevant scale (Sabelfeld & Geißen, 2011). Accordingly, in this study, the preferred method for induction of lipid production by oleaginous yeast is limiting the phosphor source. Inducing the oleaginous metabolism in yeasts by phosphor-limitation require a very high ratio of carbon to phosphorus in the cultivation medium, and thus very low phosphorus concentrations below 100 mg per litre (G. Zhang et al., 2011; Meo et al., 2017). Consequently, a very efficient phosphor elimination method providing over 99% depletion is essential for the effectiveness of the biomass hydrolysate as substrate for the yeast oil production.

Use of a diluted substrate as a cultivation medium means low product concentration in the end, which results in higher costs in downstream processing. Utilization of a membrane bioreactor (MBR) is very appropriate to be able to carry out high-cell-density yeast cultivation with a diluted medium at low sugar concentrations. In this way, the residence time of the yeast cells in the bioreactor is decoupled from that of the medium, enabling feeding of large amounts of substrate solution without diluting the yeast suspension inside the bioreactor. In this study, an MBR (stirred-tank bioreactor with cross-flow microfiltration in a bypass) will be employed with total cell retention to prevent any loss of valuable lipid-producing and lipid-accumulating yeast cells.

The objective of the MBR operation is to achieve high volumetric lipid productivity with the yeast while keeping the carbon conversion yield into microbial oils as high as possible. A very high cellular lipid content at the end of the process is crucial to the latter. Also, while using an MBR, an accumulation of sugars in the reaction medium would mean the loss of valuable carbon sources in the permeate stream. In order to prevent that by keeping the sugar concentration as low as possible, the dilution rate has to be kept relatively low. Hence, a favourable compensation state has to be found in determining a low enough dilution rate while still supplying adequate substrate to achieve high lipid productivity.

Cutaneotrichosporon oleaginosus has been noted to be capable of utilizing a vast spectrum of substrates as carbon source and accumulating over 70% of its dry weight as lipids (Moon et al., 1978; Yaguchi, Rives, & Blenner, 2017). Furthermore, this yeast strain displays high tolerance against growth inhibitors (Bracharz, Beukhout, et al., 2017; Yu et al., 2011, 2014; Yaguchi, Robinson, et al., 2017), an ability to co-utilize various substrates and to grow in variable and harsh conditions found in wastewater streams. All of these speak for the great potential of *C. oleaginosus* in the valorization of wastes and residues. Therefore, *C. oleaginosus* is selected as the biocatalyst for oil production in this study, considering the variety of carbon sources present in microalgal biomass hydrolysate, which is to be used as the cultivation medium for microbial oil production.

Some conventional downstream processing possibilities are also explored in order to present a concept covering a complete microbial oil production process. For the separation of microbial oils from fermentation broth, solvent extraction is the method preferred. Hence, various solvents and pretreatment methods will be tested and compared based on the separation efficiency and the fatty acid composition of the resulting extract.

Finally, a very detailed overall carbon balance of the integrated lipid production process will be worked out making use of an elemental analysis of all the intermediate products, as well as the final products. The aim of this study is to demonstrate the feasibility of the combined use of microalgae and oleaginous yeasts to produce microbial oils from CO_2 in an integrated process. A final comparison regarding productivity, conversion efficiency and costs of the two processes show potential improvements to the microalgal lipid production and points out the most important aspects to be considered for future process optimization.

3. Theoretical Background

This chapter outlines the theoretical foundations used in this work. First of all, properties of oleaginous microorganisms, in particular of microalgae and yeast, and their metabolic peculiarities regarding carbon dioxide fixation and lipid production are described. Then, fundamental models used in bioprocess engineering to characterize microbial cultivation processes in bioreactors are elucidated in consideration of various modes of operation and special types of bioreactors of relevance to this study. Finally, conventional cell disruption and hydrolysis methods are illustrated.

3.1. Oleaginous microorganisms

Microorganisms that can accumulate more than 20% of their biomass as storage lipids are called oleaginous. Most microorganisms accumulate only a few percent of their biomass as lipids and store energy in form of starch or glycogen or produce secondary metabolites instead. Oleaginous species, on the other hand, convert excess carbon and energy into intracellular oil as storage, up to 90% of the cell weight being extractable oil (Ratledge & Wynn, 2020; Abeln & Chuck, 2021).

Microbial storage oils are referred to as single-cell oils (SCOs) and are typically composed of triacylglycerols (TAG) (Ratledge & Wynn, 2020). Although there are also mould and bacterial species known to be oleaginous, the main candidates for production of SCOs on industrially relevant scales are oleaginous microalgae and yeast, both being intensively researched in recent years (Abeln & Chuck, 2021). The following subsections give an overview of the lipid metabolism in oleaginous species, as well as a summary of important features of microalgae and oleaginous yeast.

3.1.1. Lipid metabolism

Lipid production in oleaginous microorganisms is induced by limitation of an essential nutrient such as nitrogen, phosphorus or sulphur in the presence of a carbon source in excess. The underlying mechanism of lipid accumulation in oleaginous species under nitrogen limitation has been extensively studied (Ratledge & Wynn, 2002; Ratledge, 2014; Abeln & Chuck, 2021). A schematic outline of involved metabolites and enzymes is given in Figure 3.1. Shortly as described by Ratledge and Wynn (2020):

- Adenosine monophosphate (AMP) is degraded to inosine monophosphate (IMP) by the enzyme adenosine deaminase (AD), which is activated under nitrogen starvation. Subsequently, the activity of isocitrate dehydrogenase (ICDH) is reduced due to the lowered concentration of AMP, which is a crucial cofactor of ICDH. This results in the accumulation of isocitrate in the mitochondrion.
- Simultaneously, excess isocitrate is converted to citrate in a recation catalyzed by aconitase.
- Transport of citrate from the mitochondrion into the cytosol occurs, where it is cleaved under adenosine triphosphate (ATP) consumption, yielding acetyl coenzyme A (acetyl-CoA) and oxaloacetate. This reaction is catalyzed by ATP:citrate lyase (ACL).
- Acetyl-CoA is used for fatty acid biosynthesis through the action of fatty acid synthase (FAS).

- Oxaloacetate is converted to malate by malate dehydrogenase (MDH) and malate is subsequently oxidized to pyruvate by malic enzyme (ME) generating NADPH (nicotinamide adenine dinucleotide phosphate).

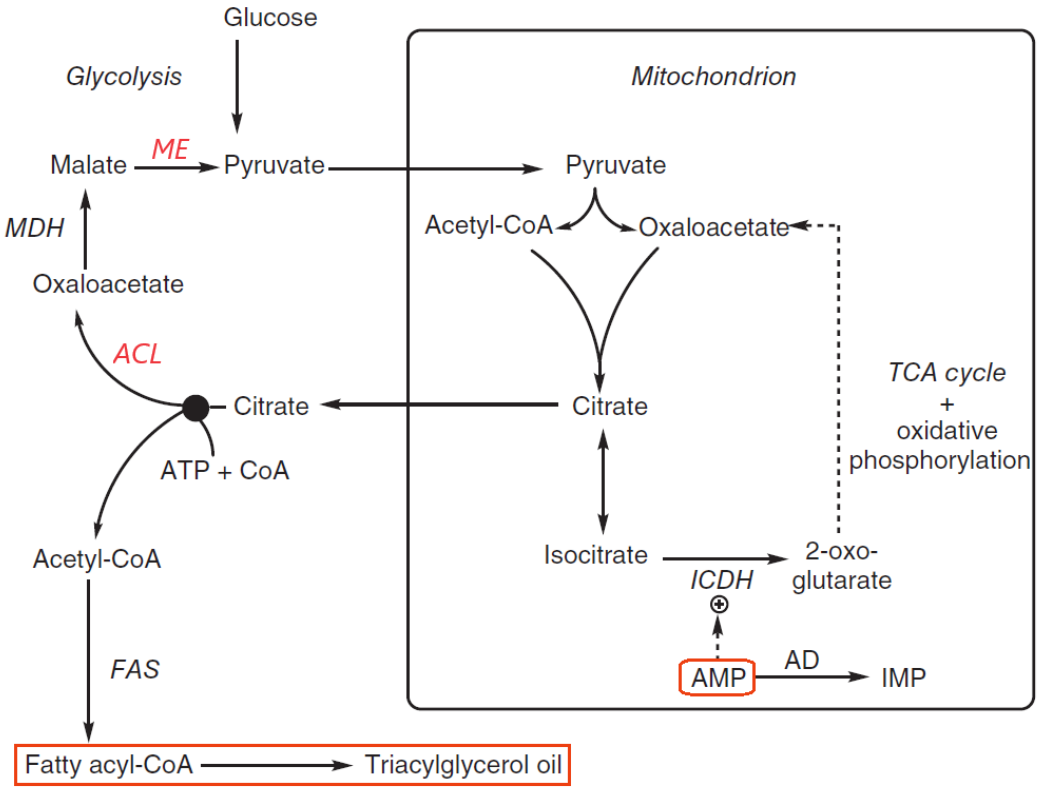

Figure 3.1: Outline of the main biochemical events leading to lipid accumulation in oleaginous microorganisms. The key enzymes involved are adenosine deaminase (AD), isocitrate dehydrogenase (ICDH), TCA cycle tricarboxylic acid cycle, ATP:citrate lyase (ACL), fatty acid synthase (FAS), malate dehydrogenase (MDH), and malic enzyme (ME). Figure modified from Ratledge and Wynn (2020).

ACL and ME are crucial components in lipid metabolism of oleaginous species. These enzymes contribute to elevated acetyl-CoA and NADPH levels, which are required to promote fatty acid (FA) biosynthesis (Ratledge & Wynn, 2002). ACL is present only in oleaginous cells and thus is a key enzyme to attribute oleaginicity to a microorganism (Ratledge & Wynn, 2020), whereas the function of ME could be fulfilled also by other enzymes (Kourist et al., 2015). Variation in the amount of storage lipids accumulated by different oleaginous microorganisms is mainly a result of their differences regarding NADPH production. Cells, in which ME synthesis stays switched on during nitrogen starvation, also achieve the highest amounts of lipid content, compared to those, in which ME synthesis is down-regulated after nitrogen exhaustion (Ratledge & Wynn, 2020).

3.1.2. Microalgae

The term algae covers a wide spectrum of eukaryotic, photosynthetic organisms that differ from higher plants in their structure by having no specialized tissues like roots, stems, or leaves (Andersen, 2013). It includes both unicellular (microalgae) and multicellular organisms, such as seaweed. Although most of them are aquatic organisms, some algae occupy terrestrial areas growing loosely on soil, plants, and animals (Andersen, 2013).

Microalgal cells vary in size in a range from a few micrometers typically to a few hundred micrometers in rare cases and can build aggregates. They are conventionally grouped according to their light-harvesting photosynthetic pigments: Rhodophyta (red algae), Chrysophyceae (golden algae), Phaeophyceae (brown algae), and Chlorophyta (green algae) (Masojídek et al., 2013). Due to their similarities to microalgae, cyanobacteria, also called blue-green algae, are usually considered as microalgae despite being prokaryotic (Andersen, 2013).

Even though microalgae can accumulate SCOs, they have rather low lipid productivities not allowing a cost competitive commercial application to replace petrochemical oils for now (Ratledge & Wynn, 2020). At present, microalgae are used mainly for wastewater treatment (Brenner & Abeliovich, 2013; Kaplan, 2013), aquaculture supplying foodstuffs (Becker, 2013; Muller-Feuga, 2013), and production of specific polyunsaturated fatty acids (PUFAs), such as docosahexaenoic acid, eicosapentaenoic acid, or arachidonic acid, for use as nutraceuticals (Ratledge, 2005). The FA composition of microalgal oils can vary a lot depending on the strain and can consist of FAs with a chain length of 14 to 22 carbons (Ratledge & Wynn, 2020).

Phototrophic metabolism

Photosynthesis is a redox reaction driven by light energy captured by chlorophyll molecules, in which carbon dioxide and water are converted into carbohydrates as follows:

$$\mathrm{H_2O} + \mathrm{CO_2} \rightarrow (\mathrm{CH_2O}) + \mathrm{O_2}$$

This net balance can be split into two steps as light reactions and dark reactions as shown in Figure 3.2 (Masojídek et al., 2013). In the light reactions light energy is converted to chemical energy in form of NADPH and ATP as follows:

$$2\mathrm{H_2O} \rightarrow 4\mathrm{H^+} + \mathrm{O_2} + 4\mathrm{e^-}$$

In the dark reactions, these reducing agents, NADPH and ATP, are utilised to convert carbon dioxide to carbohydrates as follows:

$$\mathrm{CO_2} + 4\mathrm{H^+} + 4\mathrm{e^-} \rightarrow (\mathrm{CH_2O}) + \mathrm{H_2O}$$

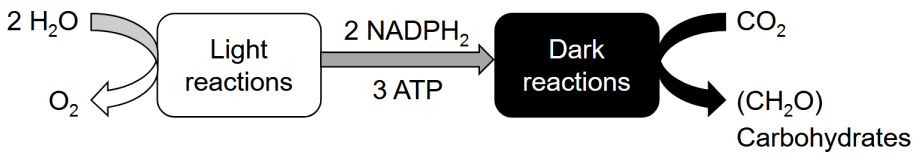

Figure 3.2: Net balance of light and dark reactions of photosynthesis. Figure modified from Masojídek et al. (2013).

The dark reactions are commonly refferred to as Calvin Benson Bassham cycle (CBB cycle) and govern carbon fixation into biomass (Masojídek et al., 2013; Barsanti & Gualtieri, 2022). The key enzyme in the CBB cycle is ribulose-1,5-bisphosphat-carboxylase (RuBisCO) using ribulose-1,5-

bisphosphate (RuBP) and carbon dioxide as substrate to produce two molecules of 3-phosphoglycerate (G3P), which then undergo several reactions before being integrated into biomass. However, RuBisCO also has oxygenase function and can use RuBP and oxygen as substrate generating one G3P and one 2-Phosphoglycolate (2-PG) molecule. While one of the two carbons in G3P can be recovered in the process of photorespiration, one carbon is lost as CO_2. In most cases 2-PG is excreted adding to the carbon loss, which represents a significant inefficiency in the carbon assimilation process also wasting photosynthetic energy (Beardall & Raven, 2016).

Factors affecting microalgae growth

For choosing the optimal growth conditions for biomass production it is important to know the parameters that affect the growth and the lipid productivity of microalgae. The most important of these are light and nutrient availability. Light as energy source is one of the two main substrates of photosynthesis. Since light is attenuated exponentially in microalgae suspensions, the influx and the distribution of light in a culture is very important in a reactor system. In dense cultures with above 1 g L^{-1} dry biomass around 90% of the photons would be absorbed in the first centimetre causing severe light inhibition for algae in this section, while the algae below this layer are severely light limited (Beardall & Raven, 2013). Reducing the optical pathway and ensuring sufficient mixing of the microalgae suspension is therefore very crucial to achieving high biomass productivity in algal cultures by allowing the cells to switch adequately between light and dark reactions and thus CO_2 fixation to catch up with photon capture.

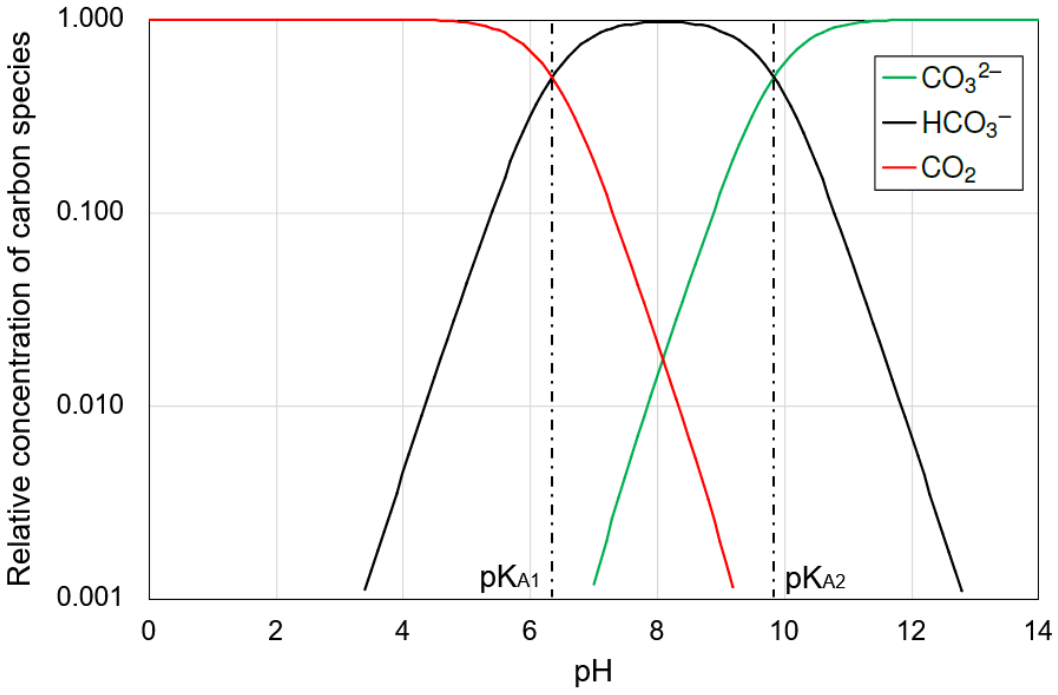

Figure 3.3: Influence of pH on the relative concentration of different carbon species for water under standard conditions (25 °C, 1 atm) plotted using pK_{A1} = 6.35 and pK_{A2} = 9.84 at zero ionic strength (Pines et al., 2016).

The second main substrate of photosynthesis is CO_2 as the carbon source. Atmospheric CO_2 only is not enough to achieve high productivities in dense microalgae suspensions, which requires additional CO_2 supply. In open reactor systems CO_2 dissolved in water is in equilibrium with atmospheric CO_2 at the gas-liquid phase boundary and in the liquid phase present in equilibrium with other forms

of dissolved inorganic carbon (DIC) being carbonic acid, bicarbonate, and carbonate as follows:

$$\mathrm{CO_2 + H_2O \rightleftharpoons H_2CO_3 \rightleftharpoons HCO_3^- + H^+ \rightleftharpoons CO_3^{2-} + 2H^+}$$

Increasing acidity of the aqueous phase shifts the equilibrium towards CO_2, while in basic solutions bicarbonate and carbonate dominate as shown in Figure 3.3 (Acién et al., 2016).

CO_2 can enter the cells by diffusion across the plasmalemma, whereas cell membranes are essentially impermeable to bicarbonate. However, many algae possess an active transport system for both CO_2 and bicarbonate, which gets activated depending on the dissolved CO_2 level (Beardall & Raven, 2013). As microalgae in a suspension take up dissolved CO_2, more CO_2 is produced from bicarbonate and carbonate under consumption of H^+, which causes an increase in the pH. On the other hand, when CO_2 supplied into a microalgae suspension in gaseous form dissolves, it generates more bicarbonate and carbonate as well as H^+, causing a drop in the pH. Hence, it is possible to keep the pH of a microalgae suspension constant at a set-point by controlling the CO_2 supply only.

While pH determines the distribution of individual DIC species, the absolute concentrations depend on total alkalinity (TA), which is the acid neutralization capacity of water based on its negatively charged ion content consisting mostly of carbonates and can be approximated as follows:

$$\mathrm{TA = [HCO_3^-] + 2[CO_3^{2-}] + [OH^-] - [H^+]}$$

By definition, TA has an influence on both the pH control of the microalgae suspension due to buffering capacity and the CO_2 uptake efficiency by determining the concentrations of DIC species. At lower TA of the suspension, the concentration of dissolved CO_2 in the liquid phase is lower reducing the loss of CO_2 into the atmosphere due to being in equilibrium with the atmospheric CO_2. This in return increases the CO_2 uptake efficiency in the microalgae suspension.

Oxygen being one of the main products of photosynthesis accumulates in microalgae suspensions over time. As mentioned before, the key enzyme of carbon fixation (RuBisCO) in microalgae has both carboxylase and oxygenase activity. This means, at high oxygen to CO_2 ratios the rate of photorespiration increases compared to photosynthesis reducing the overall carbon fixation and energy utilization efficiencies (Jacobi & Posten, 2013). This problem can be circumvented in closed reactor systems via stripping the oxygen out of the liquid phase by active supply of an oxygen-deplete gas stream, whereas open reactor systems require a surface to volume ratio high enough to allow adequate material exchange surface with the atmosphere to keep the dissolved oxygen concentration low. In both systems keeping the partial pressure of CO_2 high in the inlet gas stream is very important to minimize photorespiration (Jacobi & Posten, 2013).

Temperature affects all metabolic processes in a cell through various mechanisms and optimal temperature range of a particular algae strain has a significant effect on productivity. In general, reaction and material transport rates are higher at higher temperatures. When at their optimum temperature, algae are better able to utilise the available light and are less likely to be significantly photoinhibited. Higher temperatures are coupled with increased photorespiration, whereas lower temperatures

favour increased photoinhibition (Borowitzka, 2016). Furthermore, lower temperatures also reduce the biomass loss at night caused by respiration (Borowitzka, 2016).

Salinity is an important factor at reducing the susceptibility of a culture to contaminations as mentioned before. In most industrial applications saline or brackish water is used for algae cultivation to diminish the fresh water consumption. This, however, creates a challenge in open reactor systems due to water evaporation causing an increase of salinity over time. Thus, using a microalgae species with a broad range of tolerated salinity is an advantage. Microalgae in nature grow in waters of varying salinity, ranging from freshwater to hypersaline lakes. The salinity range tolerated by each species depends on its osmoregulatory system, by which an adaptation to higher salinity occurs via accumulation of osmoregulatory solutes inside the cell (Borowitzka, 2016).

There are many more complex interactions between the factors mentioned, the metabolism of the specific microalgae strain, and the composition of the reaction medium, as well as the environmental conditions for the open pond systems, which affect the microalgal biomass and lipid production. For instance, the availability of other nutrients such as nitrogen, phosphorous, and iron has a significant influence on cellular growth. Also temperature, pH, alkalinity and salinity all affect CO_2 solubility and thus microalgal growth and other process metrics such as CO_2 fixation efficiency. The effects explained here are limited to the ones having the greatest influence on microalgae cultivation.

3.1.3. Oleaginous Yeasts

Yeasts are eukaryotic microorganisms classified as fungi. They are predominantly unicellular, although some can become multicellular via formation of strands of elongated buds or formation of true hyphae like typical filamentous fungi (Kurtzman & Piskur, 2006). Yeast cell size varies greatly. Some may be only 2–3 µm in length, whereas others may reach 20–50 µm, while having a width of 1–10 µm (Feldmann, 2012). Yeasts are chemoorganotrophs, using organic compounds as carbon and energy source. They use mainly sugars as carbon source, although some are known to be able to utilize nonconvential carbon sources. Yeasts can grow in both aerobic and anaerobic conditions and produce energy by oxidative respiration or fermentation (Feldmann, 2012). In a review on the taxonomic diversity of oleaginous yeasts Sitepu et al. (2014) report over 70 oleaginous species. Considering there are more than 2000 yeast species (Radecka et al., 2015) oleaginicity is a rare property among yeasts.

Oleaginous yeasts are reported to be superior for possible commercial lipid production over other microorganisms such as microalgae, due to their fast growth, high lipid content and productivity (Sawangkeaw & Ngamprasertsith, 2013). Some oleaginous yeast strains are known to achieve a cellular lipid content of up to almost 90% (Abeln & Chuck, 2021). The FA composition of yeast oils can vary a bit depending on the strain, but is limited to FAs with a chain length of 16 and 18 carbons consisting of palmitic acid, palmitoleic acid, stearic acid, oleic acid, and linoleic acid similar to vegetable oils (Ratledge & Wynn, 2020). In recent years, more research has been focused on advancing yeast lipid technology as a sustainable oil source of oil replace palm, cacao and soybean oil, mostly as a novel route to advanced biofuels, but not excluding the potential use in other industries (Abeln & Chuck, 2021).

Growth and lipid production of oleaginous yeasts are affected mainly by the availability of nutrients and oxygen, type of carbon source utilized, as well as pH and temperature of the cultivation medium. To achieve a high cellular lipid content a pH range of 5.0–6.0 and a temperature range of 25–35 ℃ were reported as optimal in literature (Moon et al., 1978). The type of nutrient being limited and the degree of nutrient limitation, commonly specified as a C-to-nutrient ratio, also have a substantial influence on lipid productivity.

Lipid metabolism

General lipid metabolism of oleaginous microbes under nitrogen limitation was described in Subsection 3.1.1. However, the exact metabolic pathway activated for lipid production depends on the specific strain, the type of nutrient limitation, and the carbon source used. Even though lipid metabolism in oleaginous yeasts under nitrogen limitation is well studied, there is still little information on lipid metabolism under limitation of other nutrients, such as phosphorus or sulphur.

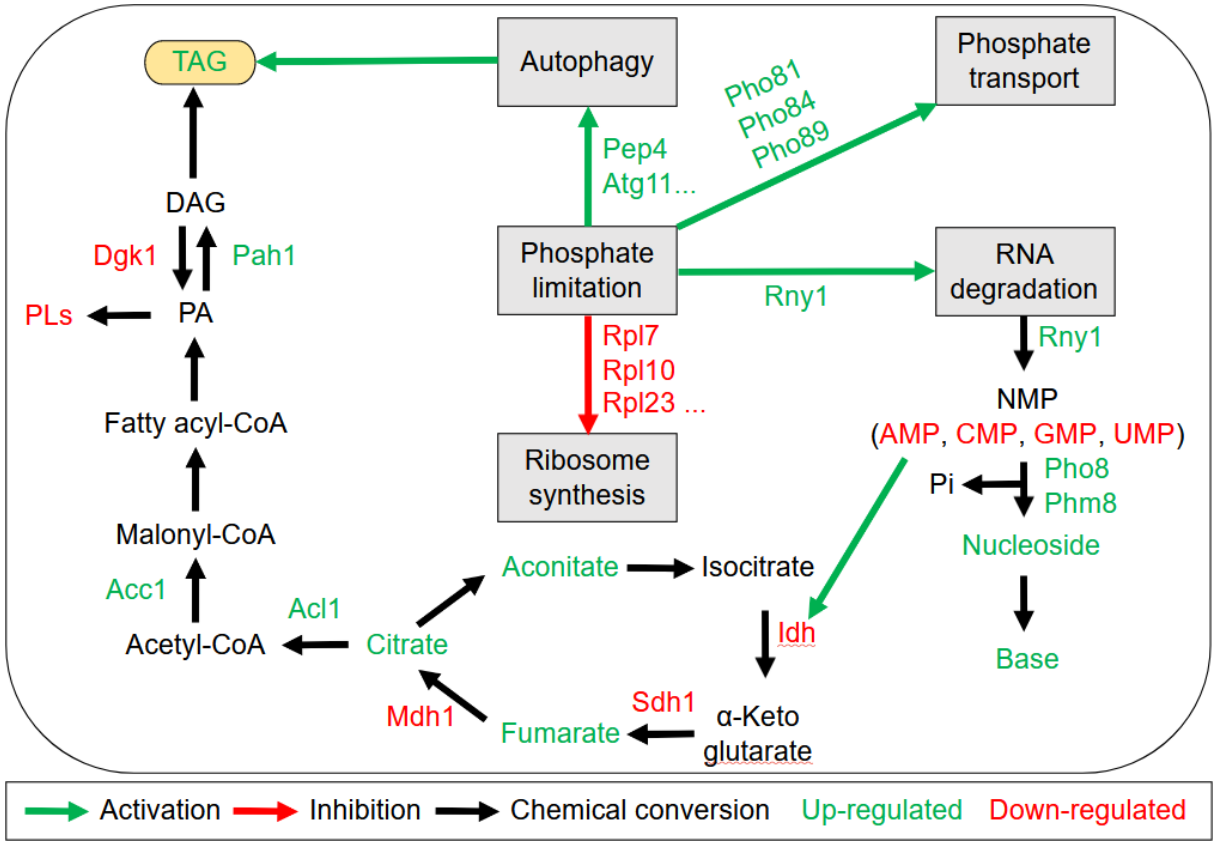

Figure 3.4: Multi-omic responses to phosphorus limitation and lipid accumulation by *R. toruloides*. Green indicates up-regulated gene, protein, or enriched metabolite, while red indicates down-regulated gene, protein, or lowered metabolite. TAG: triacylglyceride; DAG: diacylglyceride; PA: phosphatidate; PL: phospholipid; CoA: coenzyme A; RNA: ribonucleic acid; NMP: nucleoside monophosphate; AMP: adenosine monophosphate; CMP: cytidine monophosphate; GMP: guanosine monophosphate; UMP: uridine monophosphate; Pi: inorganic phosphate. Figure modified from Y. Wang et al. (2018).

Y. Wang et al. (2018) investigated the lipid accumulation in *Rhodosporidium toruloides* under phosphorus limitation and revealed potential mechanisms taking place as shown in Figure 3.4. First, mechanisms involving inorganic phosphate (Pi) scavenging are activated leading to degradation of polyphosphate, nucleic acids, and phospholipids (PLs). Secondly, Pi depletion results in ribonucleic

acid (RNA) degradation and represses ribosome biosynthesis, which in return reduces cell reproduction. Thirdly, genes contributing to protection of lipids from degradation are up-regulated. In addition, levels of enzymes producing acetyl-CoA from citrate, pyruvate, and acetate increase notably. Moreover, consumption of acetyl-CoA for production of other metabolites is reduced. Finally, citrate and isocitrate accumulate due to reduced AMP levels leading to increased flow of carbon into lipid biosynthesis, similarly to nitrogen-limited conditions.

Inducing lipid production without any nutrient limitation using acetate as the sole carbon source or as a co-substrate is also reported to be possible and suggested as a higher lipid productivity alternative to nutrient limitation, since the latter also affects cell growth negatively (Masri et al., 2019; Gong et al., 2015). The reason for a shift of metabolism towards lipid production in the presence of acetate is likely due to the activity of the enzyme acetyl-CoA synthetase (ACS) using ATP to convert acetate directly to acetyl-CoA, which is the main precursor of the FA biosynthesis pathway, although the effects on the whole transcriptome and lipid metabolism are still to be investigated.

3.2. Growth kinetics and process models

3.2.1. Growth kinetics

Nowadays it's not uncommon to build metabolic network models of a microorganism based on genomic data available to estimate key process figures such as growth rate, product formation rate or substrate uptake rate. However, it remains a challenge to identify thousands of parameters of a kinetic model for a single cell, let alone for more complex heterogeneous cell populations. Therefore, the most conventional method for describing cellular growth is still the use of a black-box model, where biomass is assumed to be not segregated, not structured and completely homogeneous (Weuster-Botz & Takors, 2018). In this case, the determination of cell dry weight (CDW) only is sufficient to characterize the biocatalyst.

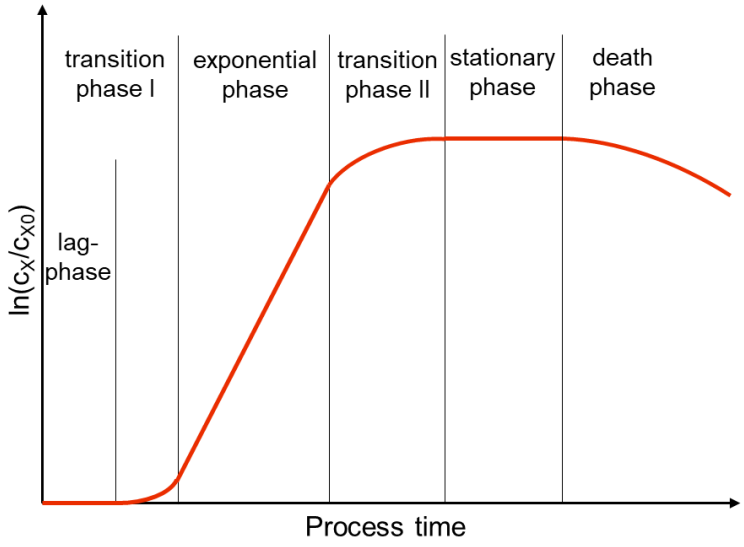

Figure 3.5: Growth curve with an initial cell dry weight concentration of $c_{X,0}$.

In a batch cultivation with nutrient-replete medium under ideal reaction conditions, the increase in cell mass can be described as a function of time, which comprises of different growth phases as shown in Figure 3.5. In the beginning a lag-phase is observed, in which cells adapt to the new reaction conditions. Once they start to take up and utilize substrate from the medium, they grow with an ever increasing rate (transition phase I) until their growth becomes exponential and the maximum growth rate possible is reached (exponential phase). After a while, growth rate starts to decrease again (transition phase II), which may be due to a variety of reasons such as substrate depletion, accumulation of toxic metabolites or a growth inhibiting product. At some point, growth rate decreases so much to equal the cell death rate resulting in constant cell mass (stationary phase). Finally, cells start dying out and to lyse, which leads to a decrease in cell mass (death phase).

The cell-specific growth rate (μ) is defined as follows:

$$\mu = \frac{1}{c_X} \cdot \frac{dc_X}{dt} \tag{3.1}$$

where c_X is the CDW concentration and t is the process time. In exponential phase cells grow without limitation and the maximum growth rate is achieved and maintained. Thus, when μ is constant and equal to μ_{max}, Equation (3.1) can be integrated to yield:

$$\int_{c_{X,0}}^{c_X} \frac{1}{c_X} \cdot dc_X = \mu_{max} \cdot \int_0^t dt \tag{3.2a}$$

$$ln\left(\frac{c_X}{c_{X,0}}\right) = \mu_{max} \cdot t \tag{3.2b}$$

$$c_X = c_{X,0} \cdot e^{\mu_{max} \cdot t} \tag{3.2c}$$

Growth rate can also be described as a function of a limiting substrate concentration, which is often the case during transition phase II (see Fig. 3.5). For this, the saturation kinetics introduced by Monod (1949) is most commonly used:

$$\mu = \mu_{max} \cdot \frac{c_S}{K_S + c_S} \tag{3.3}$$

where c_S is the substrate concentration and K_S is the saturation constant, which is equal to the substrate concentration, at which growth rate is equal to half of μ_{max}.

There are many substrates, that can inhibit cellular growth, when present in excess such as alcohols and sugars. In this case, as suggested by Andrews (1968), growth rate can be expressed as:

$$\mu = \mu_{max} \cdot \frac{c_S}{K_S + c_S + \frac{c_S^2}{K_I}} \tag{3.4}$$

where K_I is the inhibition constant, which is equal to the substrate concentration, at which growth rate is approximately equal to half of μ_{max} if $K_I \gg K_S$.

In order to grow, cells first need to take up substrate from their environment. Analogous to the specific growth rate, a specific rate for substrate uptake (q_S) and a specific rate of product formation

(q_P) can be defined:

$$-q_S = \frac{1}{c_X} \cdot \frac{dc_S}{dt} = \frac{r_S}{c_X} \tag{3.5}$$

$$q_P = \frac{1}{c_X} \cdot \frac{dc_P}{dt} = \frac{r_P}{c_X} \tag{3.6}$$

where c_P is the product concentration, r_S is the volumetric substrate uptake rate, and r_P is the volumetric product formation rate. Growth rate and substrate uptake rate can be related to define a biomass yield coefficient ($Y_{XS,\mu}$):

$$Y_{XS,\mu} = \frac{\mu}{q_S} = \frac{dc_X}{dc_S} = \frac{r_X}{r_S} \tag{3.7}$$

where r_X is the rate of biomass production. If the limiting substrate is used also for product formation, then product yield coefficients related to substrate uptake rate (Y_{PS}) and to biomass formation rate (Y_{PX}) can be defined as follows:

$$Y_{PS} = \frac{q_P}{q_S} = \frac{dc_P}{dc_S} = \frac{r_P}{r_S} \tag{3.8}$$

$$Y_{PX} = \frac{q_P}{\mu} = \frac{dc_P}{dc_X} = \frac{r_P}{r_X} \tag{3.9}$$

Y_{PS} is commonly referred to as product selectivity, whereas Y_{PX} as specific productivity.

Substrate taken up by cells can be used for growth ($q_{S,\mu}$), cell maintenance ($q_{S,m}$), and product formation ($q_{S,P}$). This can be expressed as:

$$q_S = q_{S,\mu} + q_{S,m} + q_{S,P} \tag{3.10}$$

If there is no product formation and the cell specific uptake rate of a limiting substrate for maintenance of the cellular metabolism is assumed to be constant, following can be applied to Equation (3.10):

$$\begin{aligned} q_{S,P} &\stackrel{!}{=} 0 \\ q_{S,m} &= m_S \\ q_{S,\mu} &= \frac{\mu}{Y_{XS,\mu}} \end{aligned}$$

The consideration of substrate consumption for cell maintenance requires, however, a slight modification to the model used for describing growth rate, which finally provides a more explicitly defined version of Equation (3.10) as follows:

$$\mu = \mu_{max} \cdot \frac{c_S}{K_S + c_S} - m_S \cdot Y_{XS,\mu} \tag{3.11a}$$

$$q_S = \frac{1}{Y_{XS,\mu}} \cdot \mu + m_S \tag{3.11b}$$

$$= \frac{1}{Y_{XS,\mu}} \cdot \left(\mu_{max} \cdot \frac{c_S}{K_S + c_S} - m_S \cdot Y_{XS,\mu} \right) + m_S \tag{3.11c}$$

3.2.2. General material balance of ideal stirred-tank bioreactors

A bioreactor is any device or system, in which a chemical conversion of materials is carried out in the presence of and assisted by a biocatalyst. Growing or inactive whole cells as well as isolated enzymes can be a biocatalyst. Each process model and equation presented here is based on the assumption of a single-phase, ideally mixed, homogeneous reaction medium. In other words, all component concentrations, for example of a substrate, and physical properties, such as temperature, are the same at every point of the reaction volume. Thus, all reaction rates are independent of location inside the reactor. This assumption is sufficiently justified for laboratory-scale bioreactors with adequate energy input (Takors & Weuster-Botz, 2018). In a bioreactor, as well as in any system with defined boundaries, the change of mass of a species i is equal to the mass of i entering the system minus the mass of i exiting the system plus the mass of i generated inside the system, which can be formulated as:

$$\frac{dm_i}{dt} = \dot{m}_{i,in} - \dot{m}_{i,out} + r_i \cdot V_R \tag{3.12a}$$

$$= \dot{V}_{in} \cdot c_{i,in} - \dot{V}_{out} \cdot c_{i,out} + r_i \cdot V_R \tag{3.12b}$$

m_i	Mass of species i, g
t	Time, h
$\dot{m}_{i,in}$	Mass flow of species i entering the system, g h^{-1}
$\dot{m}_{i,out}$	Mass flow of species i exiting the system, g h^{-1}
r_i	Volumetric rate of generation reaction of species i, g L^{-1} h^{-1}
V_R	Reaction volume, L
$\dot{V}_{in}$	Volumetric flow of species i entering the system, L h^{-1}
$c_{i,in}$	Concentration of species i in the inlet stream, g L^{-1}
$\dot{V}_{out}$	Volumetric flow of species i exiting the system, L h^{-1}
$c_{i,out}$	Concentration of species i in the outlet stream, g L^{-1}

Notice that r_i can be positive or negative depending on if i is generated or consumed. Using the product rule used to find the derivative of the product of multiple functions, following applies for the change of mass of species i:

$$\frac{dm_i}{dt} = \frac{d(c_i \cdot V_R)}{dt} = V_R \cdot \frac{dc_i}{dt} + c_i \cdot \frac{dV_R}{dt} \tag{3.13}$$

where c_i is the concentration of species i in the reaction volume. Combining equations (3.12b) and (3.13), the general mass balance equation for i is derived:

$$V_R \cdot \frac{dc_i}{dt} + c_i \cdot \frac{dV_R}{dt} = \dot{V}_{in} \cdot c_{i,in} - \dot{V}_{out} \cdot c_{i,out} + r_i \cdot V_R \tag{3.14}$$

Mass balance equations used for different process types elaborated in following subsections are all modified versions of this general mass balance equation. Further specification of the generation term (r_i) depends on the growth and reaction kinetics of species i as described in Subsection 3.2.1.

3.2.3. Batch and fed-batch processes

Batch process

Batch processes are characterized by the initial availability of all ingredients required for a bioconversion process. In case of microbial cultivation, this means that all desired nutrients required for cellular growth are provided at the beginning of the process. Minimal amounts of agents for pH and foam control can be added, but these are presumed to be negligible changes to the reaction volume. Additionally, in some cases such as in aerobic cultivations, where active aeration takes place, or in photosynthetic cultivations, where active CO_2 supply is required, the exchange of gaseous phases are ignored and the process is still considered to be a batch process, unless there is an exchange of liquid medium.

Since there are no inlet and outlet streams in batch processes, $(dV_R/dt) = 0$, $\dot{V}_{in} = 0$, and $\dot{V}_{out} = 0$ hold true. Thus, for batch processes Equation (3.14) is simplified to:

$$\frac{dc_i}{dt} = r_i \tag{3.15}$$

By combining the mass balance described in Equation (3.15) and the kinetics described in equations (3.5) and (3.6), the change in the concentrations of substrate (c_S), CDW (c_X), and product (c_P) can be expressed as:

$$\frac{dc_S}{dt} = r_S = -q_S \cdot c_X = -\frac{\mu}{Y_{XS,\mu}} \cdot c_X \tag{3.16}$$

$$\frac{dc_X}{dt} = r_X = \mu \cdot c_X \tag{3.17}$$

$$\frac{dc_P}{dt} = r_P = q_P \cdot c_X = \left(Y_{PS} \cdot \frac{\mu}{Y_{XS,\mu}} \right) \cdot c_X \tag{3.18}$$

In aerobic processes oxygen acts as a further substrate, so that equations (3.5) and (3.7) pertaining to the cell specific substrate uptake rate (q_S) and the yield coefficient ($Y_{XS,\mu}$), respectively, are valid for oxygen as well. In such processes ensuring sufficient oxygen supply is very critical and dissolved oxygen levels are usually monitored and controlled. The mass balance for dissolved oxygen concentration in reaction medium of a batch cultivation can be formulated as follows:

$$\frac{dc_{O_2}}{dt} = OTR - OUR = k_L a \cdot (c^*_{O_2} - c_{O_2}) - \frac{\mu}{Y_{XO_2}} \cdot c_X \tag{3.19}$$

OTR	Oxygen transfer rate, g L^{-1} h^{-1}
OUR	Oxygen uptake rate, g L^{-1} h^{-1}
$k_L a$	Volumetric gas transfer coefficient of oxygen, h^{-1}
$c^*_{O_2}$	Saturation concentration of oxygen in reaction medium, g L^{-1}
c_{O_2}	Concentration of oxygen dissolved in reaction medium, g L^{-1}
Y_{XO_2}	Biomass yield coefficient of oxygen, g g^{-1}

Another way for calculating the change of a gaseous component in a reactor system over time is to make up a molar balance of inlet and outlet gas streams. This method has a broader applicability,

since it can be used for any gaseous component as long as the composition of inlet and outlet gas streams are known. Under the assumption of an ideal gas as well as constant temperature and pressure, the molar balance of O_2 is given as (Takors & Weuster-Botz, 2018):

$$\frac{dn_{O_2}}{dt} = \dot{n}_{O_2,in} - \dot{n}_{O_2,out} = \frac{P}{R \cdot T} \cdot (\dot{V}_{g,in} \cdot Y_{O_2,in} - \dot{V}_{g,out} \cdot Y_{O_2,out}) \tag{3.20}$$

n_{O_2}	Molar amount of O_2, mol
$\dot{n}_{O_2,in}$	Molar flow rate of O_2 at the inlet stream, mol h^{-1}
$\dot{n}_{O_2,out}$	Molar flow rate of O_2 at the outlet stream, mol h^{-1}
P	Absolute pressure, atm
R	Ideal gas constant ($R = 0.0821$ L atm mol^{-1} K^{-1})
T	Temperature, K
$\dot{V}_{g,in}$	Volumetric flow rate of gas inlet stream, L h^{-1}
$Y_{O_2,in}$	Molar fraction of O_2 in the inlet gas stream, -
$\dot{V}_{g,out}$	Volumetric flow rate of gas outlet stream, L h^{-1}
$Y_{O_2,out}$	Molar fraction of O_2 in the outlet gas stream, -

However, the volumetric flow rate of the outlet gas stream is not equal to that of the inlet stream, since O_2 is consumed, CO_2 is generated, and the exhaust gas stream can have humidity up to the saturation point after being in contact with the liquid phase. Therefore, the total moles of gas going in and out of the reactor system are not the same. However, air supplied to the reactor has an inert component, namely N_2, around which a molar balance can be made as (Takors & Weuster-Botz, 2018):

$$\dot{n}_{N_2,in} = \dot{n}_{N_2,out} \Rightarrow \frac{\dot{V}_{g,in}}{\dot{V}_{g,out}} = \frac{Y_{N_2,out}}{Y_{N_2,in}} \tag{3.21}$$

where $\dot{n}_{N_2,in}$ and $\dot{n}_{N_2,out}$ are the molar flow rate of N_2 at the inlet and the outlet stream, and $Y_{N_2,in}$ and $Y_{N_2,out}$ are the molar fractions of N_2 in inlet and outlet gas streams, respectively. This equation enables the expression of $\dot{V}_{g,out}$ in terms of known parameters. Assuming that air consists of only 3 components being N_2, O_2, and CO_2, molar balance of O_2 can be rewritten as:

$$\frac{dn_{O_2}}{dt} = \frac{P \cdot \dot{V}_{g,in}}{R \cdot T} \cdot \left(Y_{O_2,in} - \frac{1 - Y_{O_2,in} - Y_{CO_2,in}}{1 - Y_{O_2,out} - Y_{CO_2,out}} \cdot Y_{O_2,out} \right) \tag{3.22}$$

where $Y_{CO_2,in}$ and $Y_{CO_2,out}$ are the molar fractions of CO_2 in inlet and outlet gas streams, respectively. Following the definition, oxygen uptake rate (OUR) can be expressed in molar units as:

$$OUR = -\frac{dn_{O_2}}{dt} \cdot \frac{1}{V_R} \tag{3.23}$$

Similarly to Equation (3.20), molar balance on CO_2 can be expressed as:

$$\frac{dn_{CO_2}}{dt} = \frac{P \cdot \dot{V}_{g,in}}{R \cdot T} \cdot \left(Y_{CO_2,in} - \frac{1 - Y_{O_2,in} - Y_{CO_2,in}}{1 - Y_{O_2,out} - Y_{CO_2,out}} \cdot Y_{CO_2,out} \right) \tag{3.24}$$

where n_{CO_2} is the molar amount of CO_2. Thus, a molar carbon emission rate (CER) can be defined as:

$$CER = -\frac{dn_{CO_2}}{dt} \cdot \frac{1}{V_R} \tag{3.25}$$

The ratio of CER to OUR is called respiratory quotient (RQ):

$$RQ = \frac{CER}{OUR} \tag{3.26}$$

which is dependent on the metabolism of a specific strain as well as the substrate used and can be used as a signal for on-line process quality assessment (Takors & Weuster-Botz, 2018).

Fed-batch process

In a fed-batch process there is an inlet stream of components into the bioreactor, but no outlet stream exiting the reactor, so that the reaction volume increases over time. This implies $\dot{V}_{out} = 0$ and $(dV_R/dt) = \dot{V}_{in}$ for fed-batch processes. Applying these to Equation (3.14) and rearranging the equation gives:

$$\frac{dc_i}{dt} = \frac{\dot{V}_{in}}{V_R} \cdot (c_{i,in} - c_i) + r_i \tag{3.27}$$

So the change in substrate concentration (c_S) can be expressed as:

$$\frac{dc_S}{dt} = \frac{\dot{V}_{in}}{V_R} \cdot (c_{S,in} - c_S) - q_S \cdot c_X \tag{3.28}$$

which shows, that the substrate concentration increases by addition of feed medium and decreases due to dilution of the reaction medium as well as consumption by cells, simultaneously. In a fed-batch process it is possible to adjust the medium feed rate so that a low substrate concentration is maintained, which can be desirable in cases of excess substrate inhibition or toxic by-product formation. Moreover, by adjusting the medium feed rate accordingly, the growth rate can be kept constant over a certain period of time using an exponential feeding method. Assuming a constant substrate concentration ($dc_S/dt = 0$), a highly concentrated feeding solution ($c_{S,in} \gg c_S$), as well as exponential growth (see Eq. 3.2c), volumetric flow rate for a constant growth rate (μ_{set}) can be calculated from Equation (3.28) as follows:

$$\dot{V}_{in} = \frac{V_R \cdot \mu_{set} \cdot c_{X,0}}{Y_{XS,\mu} \cdot c_{S,in}} \cdot e^{\mu_{set} \cdot t} \tag{3.29}$$

Since $c_{X,in} = 0$ and $c_{P,in} = 0$ in the feed stream, Equation (3.27) yields following expressions for CDW (c_X) and product (c_P) concentrations:

$$\frac{dc_X}{dt} = \frac{\dot{V}_{in}}{V_R} \cdot (-c_X) + \mu \cdot c_X \tag{3.30}$$

$$\frac{dc_P}{dt} = \frac{\dot{V}_{in}}{V_R} \cdot (-c_P) + q_P \cdot c_X = c_X \cdot \left(q_P - \frac{\dot{V}_{in}}{V_R} \right) \tag{3.31}$$

3.2.4. Continuous and semi-continuous processes

Continuous process

Continuous processes are characterized by simultaneous addition of feed medium and removal of reaction medium with the same volumetric flow rate to maintain a constant reaction volume. In this way, after a certain process time a steady state is achieved, in which all component concentrations (CDW, substrate, and product) are constant over time. Since $\dot{V}_{in} = \dot{V}_{out} = \dot{V}$, and thus $(dV_R/dt) = 0$ in continuous processes, applying these to Equation (3.14) and rearranging the equation gives:

$$\frac{dc_i}{dt} = \frac{\dot{V}}{V_R} \cdot (c_{i,in} - c_{i,out}) + r_i \tag{3.32}$$

The dilution rate (D) for a continuous process is defined as the ratio of volumetric flow rate to reaction volume as follows:

$$D = \frac{1}{\tau} = \frac{\dot{V}}{V_R} \tag{3.33}$$

whereas the inverse of the dilution rate is known as the mean hydraulic residence time (τ). Under the assumption of an ideally mixed homogeneous reaction volume, all component concentrations in the outlet stream are equal to their concentrations in the reaction medium ($c_{i,out} = c_i$). Using Equation (3.33) with $c_{S,out} = c_S$ the substrate concentration in a continuous process is expressed as follows:

$$\frac{dc_S}{dt} = D \cdot (c_{S,in} - c_S) - q_S \cdot c_X \tag{3.34}$$

Similarly, applying $c_{X,in} = 0$ and $c_{X,out} = c_X$ to Equation (3.33) the CDW concentration can be described as:

$$\frac{dc_X}{dt} = D \cdot (-c_X) + \mu \cdot c_X = c_X \cdot (\mu - D) \tag{3.35}$$

In the same manner, applying $c_{P,in} = 0$ and $c_{P,out} = c_P$ gives the following for the change of product concentration over time:

$$\frac{dc_P}{dt} = D \cdot (-c_P) + q_P \cdot c_X = q_P \cdot c_X - D \cdot c_P \tag{3.36}$$

After a sufficiently long process time a steady-state is achieved, where component concentrations are constant over time ($(d/dt) = 0$). In this case, the above equations can be modified as follows:

$$\mu = D \tag{3.37}$$

$$q_S = \frac{D}{c_X} \cdot (c_{S,in} - c_S) \tag{3.38}$$

$$q_P = \frac{D}{c_X} \cdot c_P \tag{3.39}$$

Equation (3.37) directly implies that a stable operation of a continuous process with dilution rates higher than the maximum growth rate ($D > \mu_{max}$) is not possible. In this case, since the dilution rate exceeds the generation rate of new cells, a wash-out of the cells from the reactor occurs, as shown in Figure 3.6 for $D \geq D_{max}$.

For a continuous production process, space-time-yield (STY) is defined as:

$$STY_i = D \cdot c_i \tag{3.40}$$

The ideal operation point is thus achieved using the dilution rate, at which the STY of the desired product is at maximum.

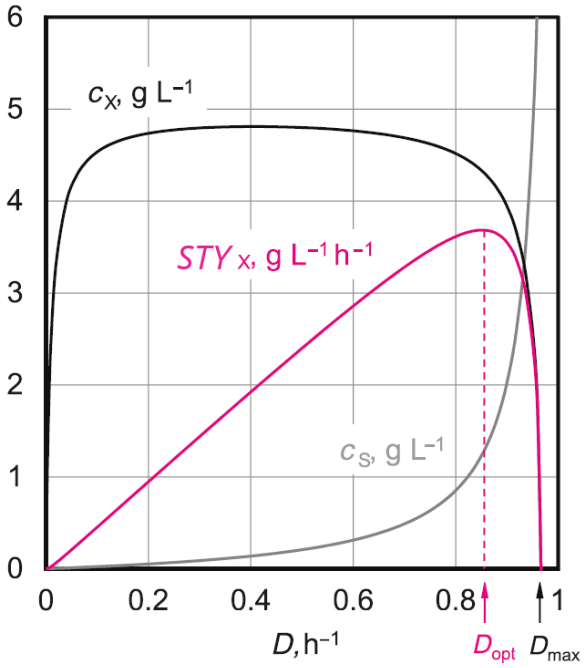

Figure 3.6: Plot of STY_X, CDW concentration (c_X), and substrate concentration (c_S) as a function of dilution rate in steady state of a continuously operated stirred-tank reactor (STR) modified from Takors and Weuster-Botz (2018).

Semi-continuous process

In semi-continuous processes, also called a repetitive batch process, process operation is very similar to a batch process. However, in this case, a partial harvest of the reaction medium takes place in predetermined time intervals. The culture remaining inside the reactor acts as inoculum for the following batch cycle. The reaction volume removed from the reactor is immediately replaced with fresh medium to avoid nutrient depletion for the next batch cycle. This mode of operation might also be called repetitive fed-batch, if there is a continuous medium feed into the reactor. In principle, a semi-continuous process can be treated analogously to a batch or fed-batch process regarding process modelling.

3.2.5. Photobioreactors

A photobioreactor (PBR) is a reactor system used for photosynthetic cultivation of microalgae, which transforms the environmental conditions to be suited for optimal growth in microalgal suspensions. These can be open or closed, while the open PBR are also described as ponds. Examples to the closed systems are flat plate and tube bioreactors, whereas open systems can be, for instance, designed as raceway ponds or thin-layer cascade (TLC) bioreactors (Apel et al., 2017).

PBRs differ from other bioreactors by having a light supply to sustain photosynthetic cells. Here light can be regarded like a fourth phase in the reactor overlapping with the other three being cells, liquid medium, and gas phase (Chmiel & Weuster-Botz, 2018). The gas phase supplied contains CO_2, either pure or enriched, unlike in aerobic processes, since it acts as the carbon source for autotrophic growth. However, light is the most important substrate for phototrophic cells. Around 43% of sunlight is in the photosynthetically usable wavelength range (400–700 nm), which is called photosynthetically active radiation (PAR) (Chmiel & Weuster-Botz, 2018). Radiation intensity, also called photon flux density (PFD), is described as amount of photons flowing onto a unit area per unit time and considered as the limiting substrate in microalgae cultivation processes. Pfaffinger et al. (2016) demonstrated that the Beer-Lambert law, formulated as follows, is valid for microalgae processes:

$$I = I_0 \cdot e^{l \cdot c_X \cdot \varepsilon} \tag{3.41}$$

I	Light transmitted over the layer thickness, µmol m^{-2} s^{-1}
I_0	Incident photon flux density, µmol m^{-2} s^{-1}
l	Thickness of the optical path, cm
ε	Specific extinction coefficient, L g^{-1} cm^{-1}

In their model Pfaffinger et al. (2016) used the concept of mean integral PFD (I^*) defined by Molina Grima et al. (1997) as follows:

$$I^* = \frac{1}{L} \cdot \int_0^L I(c_X, l) \cdot dl = \frac{I_0 \cdot (1 - e^{L \cdot c_X \cdot \varepsilon})}{L \cdot c_X \cdot \varepsilon} \tag{3.42}$$

where L is the layer thickness of the PBR. Considering light as a limiting substrate combining equations (3.4) and (3.42) yields:

$$\mu = \mu_{max} \cdot \frac{I^*}{K_{SP} + I^* + I^* \cdot \left(\frac{I^*}{K_{IP}}\right)^{\varphi}} \tag{3.43}$$

K_{SP}	Saturation constant for photon flux density, µmol m^{-2} s^{-1}
K_{IP}	Photoinhibition constant, µmol m^{-2} s^{-1}
φ	Sensitivity factor, -

which is a model describing a mean specific growth rate validated by Pfaffinger et al. (2019) for processes with the microalgae strain *Microchloropsis salina* in flat plate and TLC PBRs used in this work.

3.2.6. Membrane bioreactors

A membrane bioreactor (MBR) is a device with an integrated membrane-based separation module and a bioreactor to enable retention of a biocatalyst inside the reactor, either partially or completely. This might be desirable in cases, where excess amounts of a substrate or a product inhibit product formation. Additionally, for continuous processes, in which the concentration of a biocatalyst in reaction medium is directly proportional to STY, it might be advantageous to retain the biocatalyst in the

reactor to allow much higher productivities than possible in a standard continuous process. Hence, the use of an MBR enables decoupling of the residence time of the cells in a reactor from that of the medium, reducing technical limitations to the productivity of a continuous process.

Table 3.1: Filtration types used for MBR processes distinguished by the size of retained solids as specified by Koros et al. (1996).

Process	**Size range**	**Retained substance**
Microfiltration	$>$ 0.1 µm	Particles (yeast, bacteria, pollen, cells)
Ultrafiltration	2.0 nm – 0.1 µm	Macromolecules (virus, proteins)
Nanofiltration	$<$ 2.0 nm	Molecules

An MBR system can be set up both by placing a filter module inside the reactor or by connecting an external filtration unit to the reactor as a bypass. In principle, filtration processes used in MBR systems differ by the size of particles to be retained as stated in Table 3.1 and by the technical design of the filter unit as shown in Figure 3.7.

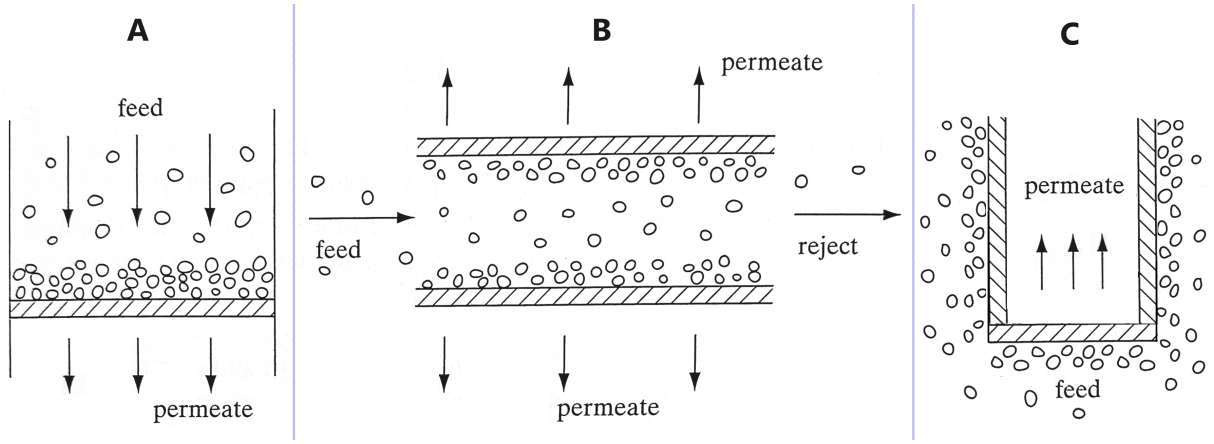

Figure 3.7: Process flow for microfiltration. **A**: dead-end flow; **B**: cross-flow; **C**: dead-end flow with a filter module suspended inside an STR to reduce cake formation on filter surface utilizing agitation of reaction medium. Figure was modified from Geankoplis (2003).

If a cross-flow filter is used as an external bypass, cell suspension is pumped externally through the filter module. Permeate flow through the membrane is driven by pressure drop through the membrane, known as the trans membrane pressure (TMP):

$$TMP = \frac{P_{in} + P_{out}}{2} - P_{perm} \tag{3.44}$$

where P_{in} and P_{out} are the pressure values at the inlet and outlet streams across the filter module, whereas P_{perm} is the pressure on the permeate outlet stream. A portion of the retentate can be directed to the outlet stream, whereas the remaining retentate flows back into the reactor, which is also called the reflux stream. Thus, volumetric flow rates of all inlet and outlet streams for a continuous process in an MBR can be described as:

$$\dot{V} = \dot{V}_{in} = \dot{V}_{out} = \dot{V}_{out,perm} + \dot{V}_{out,ret} = \dot{V}_{in,filter} - \dot{V}_{reflux} \tag{3.45}$$

$\dot{V}_{out,perm}$	Volumetric flow rate of permeate outlet stream, L h^{-1}
$\dot{V}_{out,ret}$	Volumetric flow rate of retentate outlet stream, L h^{-1}
$\dot{V}_{in,filter}$	Volumetric flow rate of feed into the filter module, L h^{-1}
$\dot{V}_{reflux}$	Volumetric flow rate of retentate fed back to the reactor , L h^{-1}

In an MBR process the degree of cell retention can be adjusted by changing $\dot{V}_{reflux}$ from partial to total retention, which is characterized by a parameter called reflux ratio (α) as follows:

$$\alpha = \frac{\dot{V}_{reflux}}{\dot{V}_{out}} \tag{3.46}$$

where $\alpha = 1$ corresponds to a standard continuous process without cell retention, while $\alpha = 0$ indicates a continuous process with total cell retention. For $0 < \alpha < 1$ Equation (3.35) becomes:

$$\frac{dc_X}{dt} = \frac{\dot{V}_{out,ret}}{V_R} \cdot (-c_X) + \mu \cdot c_X = c_X \cdot (\mu - \frac{\dot{V}_{out,ret}}{V_R}) \tag{3.47}$$

In case of total cell retention, where $\alpha = 0$ since $\dot{V}_{out,ret} = 0$, the change of CDW concentration in reaction medium is described analogously to a batch process by Equation (3.17). For substrate and product concentrations equations (3.34) and (3.36) hold, similarly to a continuous process. However, Equation (3.37) equating growth rate to dilution rate in steady state does not apply here, which allows setting a dilution rate higher than the maximum growth rate ($D > \mu_{max}$) for stable steady state operation of a continuous production process.

To prevent fouling and consequent blocking of a membrane in a cross-flow filtration module, some critical parameters should be adjusted carefully. Among these are the shear rate across the fibres or capillaries of a filter unit and the Reynolds number. Shear rate ($\dot{\gamma}$) is the rate of change in velocity, at which a fluid layer passes over an adjacent one, and is determined for Newtonian fluids in stationary tube flow as follows (Chmiel & Walitza, 2018):

$$\dot{\gamma} = \frac{4}{\pi} \cdot \frac{\dot{V}}{r^3} \tag{3.48}$$

where $\dot{V}$ is the volumetric flow rate through a single tube and r is the tube radius. In a cross-flow filtration process, the shear rate of a suspension flowing through individual tubes of the filtration module should be kept high enough to reduce fouling layer formation on the membrane by washing off the membrane surface. As Equation (3.48) suggests, this can be achieved by ensuring an adequately high volumetric flow rate through the filter unit depending on the inner diameter of a single tube inside the filter and the total number of tubes.

Reynolds number (Re) characterizes the type of flow inside the capillaries and is defined as follows for flow through a tubular structure:

$$Re = \frac{\rho \cdot \dot{V} \cdot (2 \cdot r)}{\mu \cdot A} \tag{3.49}$$

where ρ is the fluid density, $\dot{V}$ is the volumetric flow rate through a single capillary, r is the capillary radius, μ is the dynamic viscosity of the fluid, and A is the cross-sectional area of the capillary (Chmiel & Walitza, 2018). For $Re < 2100$ the flow is always laminar and for $Re > 4000$ turbulant in most cases (Geankoplis, 2003). Between these values the flow is in transition state with $Re = 2300$ generally accepted as the critical point, at which the transition to turbulent flow occurs (White, 2011). Sustaining turbulent flow in cross-flow filtration is important in an MBR process to ensure sufficient mixing of the suspension flowing through individual tubes and prevent clogging due to fouling layer formation on the membrane.

3.3. Cell disruption and biomass hydrolysis

Disruption of cell wall and membrane is an important step in bioprocesses to recover intracellular products or to make intracellular contents available for further processing. There is a variety of disruption methods applicable for cell disruption, which are divided into two main groups according to their working mechanism. Figure 3.8 summarizes the classification of cell disruption methods examined in this work along with their working principles and important parameters influencing their effectiveness (Günerken et al., 2015). These methods were selected specifically for their applicability in continuous processes on an industrial scale.

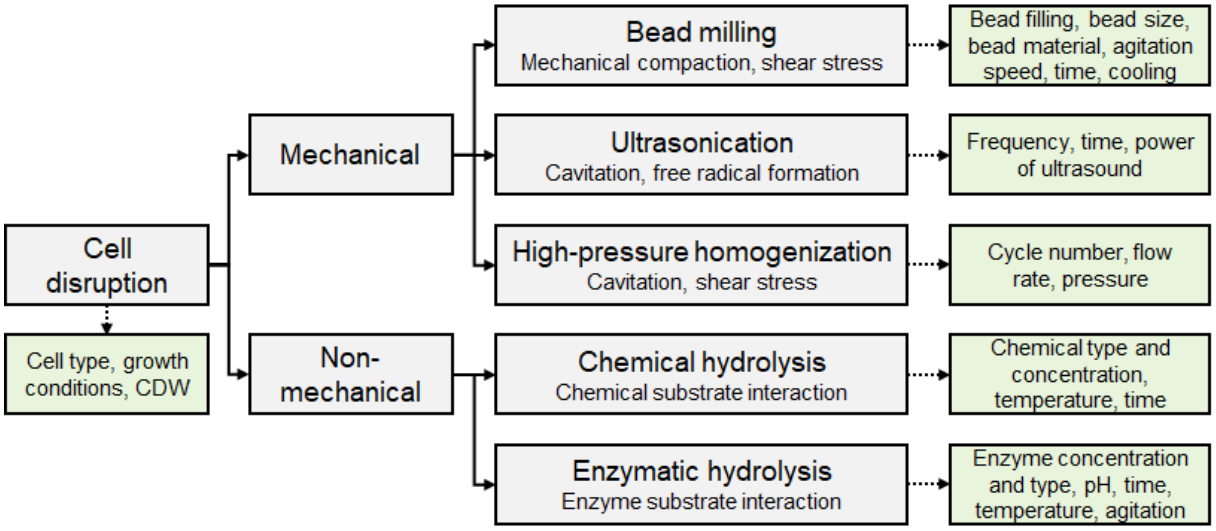

Figure 3.8: Classification of cell disruption methods examined divided into mechanical and non-mechanical methods, presented together with the specific working mechanism of each. Green highlighted boxes indicate important process parameters specifically for each method. Information illustrated here originates from a review article by Günerken et al. (2015).

Bead milling

Bead mills are used for grinding both wet and dry materials mainly for particle size reduction, but also for cell disruption in bioprocessing. Beads and cell material are filled into a horizontally positioned cylindrical container, which either rotates on a horizontal axis or swings vertically. In this way, cells are disrupted both by getting mechanically smashed between beads and container wall and by frictional forces applying solid shear stress. For industrial-scale continuous bead milling processes

commonly an agitator bead mill is used. Laboratory-scale devices such as a table-top mixer mill can be used in preliminary experiments to determine the bead properties and expected milling duration suitable for a certain cell type and density. The most important aspect is the determination of suitable bead size and material for the disruption of a certain cell type with a certain cell density (dry material or wet mass with a certain CDW content). As a general rule for wet grinding applications, it is important to use bead materials with a higher density than that of the cell mass to be ground. The density of beads is positively proportional to the energy they can transfer into mechanical compaction upon collision. Examples to different bead materials commonly used are low density materials such as glass and high density materials like steal or zirconium oxide. Bead sizes usually vary between 0.1–5 mm depending on application. Growth phase and conditions also affect cell composition and durability of cell wall, and are thus to be taken into account in bead selection. Bead filling of the grinding container, agitation speed, milling duration, and cooling of cell material are further parameters to be determined with the actual milling equipment used. Despite its many advantages for industrial processes, such as high disruption efficiency and throughput, good temperature control, commercial availability, easy scale-up, and low labour requirement, bead milling is still considered less favourable for low-cost production processes because of its high energy demand due to inefficient energy transfer (Günerken et al., 2015).

Ultrasonication

Ultrasonication is a liquid-shear method for cell disruption, which is used primarily in laboratory-scale applications. Ultrasound, sound of frequency higher than 15 kHz, is known to disrupt cells in suspension at high acoustic power inputs (Chmiel, 2018). High frequency acoustic waves initiate a cavitation process and a propagating shock wave forms jet streams in the surrounding liquid medium causing cell disruption by high shear forces (Günerken et al., 2015). Cavitation is the formation and sudden implosion of gas bubbles in liquids as a result of quick changes in pressure. Basically, micro-bubbles in a liquid form spontaneously if the pressure drops below the evaporation pressure of the liquid, while they collapse if the pressure suddenly rises again, which releases immense amounts of energy locally in form of pressure and temperature (Chmiel, 2018). In these micro-regions of extreme conditions temperatures as high as 5000 °C and pressures up to 100 MPa are estimated to prevail (Günerken et al., 2015). Thus, average temperature of the treated material rises very quickly during ultrasonication, which requires cooling, especially for high cell density suspensions. There are two main types of ultrasound devices on a bench-top scale: ultrasonic baths and ultrasonic horn homogenizers, the second being the suitable option for continuous applications. For scale-up it is important to keep ultrasonic amplitude, frequency and time spent in the active cavitation zone unchanged. However, in industrial-scale implementations ultrasonication loses its effectiveness drastically (Chmiel, 2018) and is generally not preferred due to high energy consumption concerns.

High-pressure homogenization

In a high-pressure homogenizer (HPH) cell suspension flowing against a valve functioning as a piston pump enters the valve chamber in a pulsating flow at very high pressures up to 2000 bar, which

causes a sudden pressure drop upon opening of the valve for a very short duration, accelerating the suspension across the valve opening with a 90° angle against an impact ring before exiting the valve chamber. In this way, cell disruption is achieved through high-pressure impact of the accelerated fluid as well as hydrodynamic cavitation caused by rapid pressure drop (Chmiel, 2018), as described above for ultrasonication. Even small changes to the design and construction of the valve of a HPH affect the disruption efficiency significantly. Effectiveness of cell disruption is mostly influenced by working pressure as well as number of passes and flow rate through the HPH. Since the rheology and flow characteristics of a cell suspension depend largely on cell density, HPH applications for highly viscous cell suspensions with high CDW concentrations are reported to be less efficient and entail technical limitations. The main drawback of using HPH is thus the use of low CDW concentrations under 100 g L^{-1} increasing the energy demand of downstream processing, although it is among the most preferred methods for industrial-scale cell disruption (Günerken et al., 2015).

Chemical hydrolysis

Chemical hydrolysis is commonly used for digestion of lignocellulosic biomass. It covers acid and alkali treatments of cell masses both requiring high temperatures around 120 °C to be efficient, although acid treatments at high temperatures (around 160 °C) generally lead to a higher degree of cell disruption (Günerken et al., 2015). Acid hydrolysis is catalysed by strong Brønsted acids such as H_2SO_4, which are applied at 3-5% *(v/v)* of the cell suspension. Higher concentrations cause side reactions leading to degradation of sugars to other molecules, therefore reducing sugar yield (Talukder et al., 2012). Besides, high temperature and alkali induced protein denaturation make these techniques less favourable in many cases (Molina Grima et al., 2003). Additionally, chemical alterations of desired products, low effectiveness in cases of strong recalcitrant cell walls, and large amounts of acid or base required are further downsides of chemical cell disruption and hydrolysis for industrial applications.

Enzymatic hydrolysis

Enzymatic cell disruption is an excessively studied method due to its biological specificity, mild operating conditions, low energy requirements, and low capital investment with many applications in medicine, food industry, agriculture, and for recovery of intracellular products (Günerken et al., 2015). Enzymes bind to and act on specific molecules in cell membrane and cell wall structures causing their degradation. Since the discovery of lysozyme, which is an antimicrobial enzyme hydrolysing bacterial cell walls, many studies have contributed to the understanding of working mechanisms of lytic enzymes (Salazar & Asenjo, 2007). Recombinant production and protein engineering also contribute to the potential for new applications. Depending on the structure and composition of the cells to be hydrolysed different enzymes acting on polysaccharides, peptides or lipids are utilized. Choosing the right combination of hydrolytic enzymes requires caution and should take into account the desired product or end-use of the resulting hydrolysate. If the desired product is a protein, for example, proteases should be avoided. Major applications of lysozymes are related to the extraction of nucleic acids and release of recombinant proteins from susceptible cells (Salazar & Asenjo, 2007).

On the other hand, for a biorefinery process, in which biomass hydrolysate, rich in monosaccharides and proteins, itself is the desired product, a combination of various hydrolytic enzyme activities would be required (Masri et al., 2017; Younes et al., 2020). Apart from cell type, growth phase and conditions also significantly affect cell composition, and thus enzyme activities required for hydrolysis.

Major parameters influencing the efficiency of enzymatic hydrolysis are enzyme type and dosing with respect to CDW concentration, treatment duration, and adequate agitation of the reaction medium, which provides for sufficient enzyme-substrate contact. Additionally, optimal pH and temperature specific to the selected enzymes should prevail to achieve maximum enzymatic activity. Generally, an enzymatic treatment is gentle, has a high selectivity and scale-up is relatively easy. Nevertheless, long process times, low production capacity compared to mechanical or chemical methods, and product inhibition are disadvantages of enzymatic cell disruption (Harun & Danquah, 2011; Günerken et al., 2015). However, enzymatic biomass hydrolysis can be combined with mechanical cell disruption techniques to improve hydrolysis efficiency.

4. Materials and Methods

4.1. Strain information

The microalgae strain *Microchloropsis salina* (SAG 40.85), formerly known as *Nannochloropsis salina*, was obtained from the Culture Collection of Algae at the University of Göttingen (Göttingen, Germany). Figure 4.1 shows a light microscope image of *M. salina* cells, which are typically spherical with a diameter of 2–4 µm. They are single cells without motility accessories such as flagella or haptonema and aren't prone to form colonies, aggregates or biofilm (Andersen, 2013).

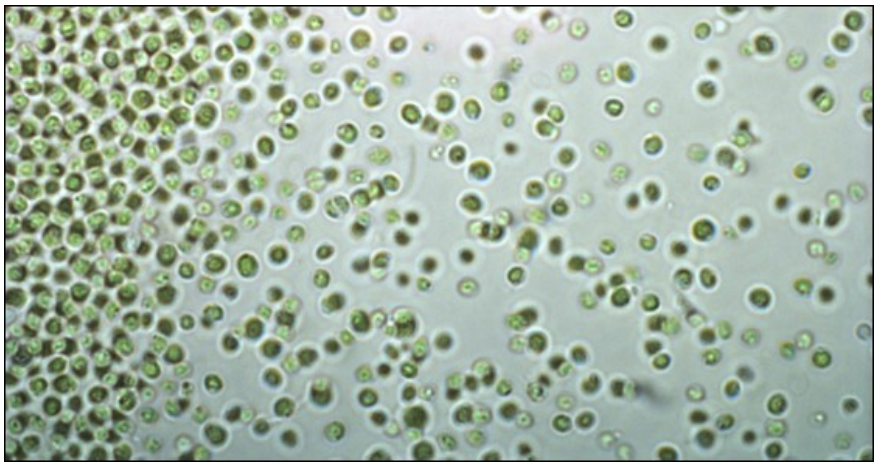

Figure 4.1: Light microscope image of *Microchloropsis salina* with 50x magnification in bright field.

The oleaginous yeast strain, *Cutaneotrichosporon oleaginosus* (ATCC 20509), was purchased from the German Collection of Microorganisms and Cell Cultures (DSMZ) (Braunschweig, Germany) as a dried culture, where it is registered under DSM number 11815. This strain was formerly known as *Candida curvata D*, *Apiotrichum curvatum*, *Cryptococcus curvatus*, *Trichosporon cutaneum*, and *Trichosporon oleaginosus*, respectively (Yaguchi, Rives, & Blenner, 2017).

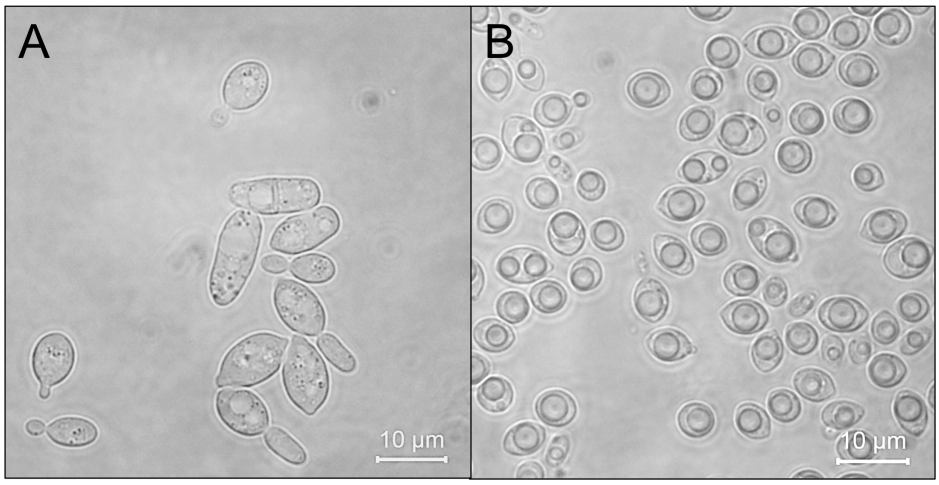

Figure 4.2: Light microscope image of *Cutaneotrichosporon oleaginosus* with 50x magnification in bright field **A**: grown in nutrient-replete medium **B**: grown in phosphorus-depleted medium.

Figure 4.2 shows light microscope images of *C. oleaginosus* cells (A) grown in nutrient-replete conditions and (B) grown in phosphorus-depleted medium with single-cell oils (SCOs) clearly visible as intracellular droplets. The morphology yeast cells vary a lot depending on culture conditions and growth stage. Cells growing in nutrient-replete complex medium are typically elliptic with a width of 2–8 µm and a length from 5 up to 20 µm varying greatly in size and shape. Lipid accumulating *C. oleaginosus* cells are on the other hand morphologically more homogeneous being rather spherical with a diameter of 3–10 µm.

4.2. Cultivation media and solutions

The microalga strain *M. salina* was cultivated with a modified version of the artificial seawater (ASW) medium (see Table 4.1 and 4.2) described by Boussiba et al. (1987). The modification is the usage of urea as nitrogen source instead of KNO_3. The concentrations of the salts NaCl, $MgSO_4$ and $CaCl_2$ were kept constant in the reaction medium, whereas the remaining medium components were supplied as a concentrated solution additionally throughout the cultivation to keep the urea concentration at 0.5–1.5 g L^{-1}.

Table 4.1: Composition of the artificial seawater (ASW) medium modified from Boussiba et al. (1987).

Salts	**Concentration, g L^{-1}**
NaCl	27.0
$MgSO_4 \cdot 7\ H_2O$	6.6
$CaCl_2 \cdot 2\ H_2O$	1.5
Nutrients	**Concentration, g L^{-1}**
Urea	0.297
KH_2PO_4	0.070
$FeCl_3 \cdot 6\ H_2O$	0.014
$Na_2EDTA \cdot 2\ H_2O$	0.021
	Concentration, mL L^{-1}
Trace element solution (20,000×)	0.05

Table 4.2: Composition of the 20,000× concentrated trace element solution for ASW medium.

Component	**Concentration, g L^{-1}**
$ZnCl_2$	0.80
H_3BO_3	12.00
$CuCl_2 \cdot 2\ H_2O$	0.80
$MnCl_2 \cdot 4\ H_2O$	12.58
$(NH_4)_6Mo_7O_{24} \cdot 4\ H_2O$	7.40

Long-term maintenance of the yeast *C. oleaginosus* was realized using cryo-stocks of the cells in 25% (*v/v*) glycerine containing medium stored at –80 °C. The preculture medium used to suspend the cryo-stocks and for the fed-batch cultivations on a 3 L scale was yeast-peptone-dextrose (YPD) medium (see Table 4.3). The culture was incubated in 4 x 0.5 L shaking flasks with 100 mL filling volume each at 30 °C and 150 rpm for 1 d.The preculture used for other experiments on a litre scale and in the membrane bioreactor on a 50 L scale was incubated in concentrated YPD medium (see Table 4.4) in 8 x 2 L shaking flasks with 400 mL filling volume each at 30 °C and 150 rpm for 3 d.

Table 4.3: Composition of the yeast-peptone-dextrose (YPD) medium for preculture.

Component	**Concentration, g L^{-1}**
Yeast extract	20
Peptone from casein	10
Glucose	20

Table 4.4: Composition of the concentrated YPD medium for preculture.

Component	**Concentration, g L^{-1}**
Yeast extract	60
Peptone from casein	20
Glucose	60

Table 4.5: Composition of the defined medium modified from Hassan et al. (1996) for the cultivation of *C. oleaginosus*.

Component	**Concentration, g L^{-1}**
Glucose	40.0
Mannose	10.0
$(NH_4)_2SO_4$	12.0
KH_2PO_4	0.025
$MgSO_4 \cdot 7\ H_2O$	1.0
	Concentration, mL L^{-1}
Antifoam 204	1.0
Trace element solution (100×)	10.0
Vitamin solution (100×)	10.0
Kanamycin sulphate (1,000×)	1.0
Tetracycline hydrochloride (1,000×)	1.0

The medium used for fed-batch and semi-continuous cultivations in the membrane bioreactor was a modified version of the defined medium published by Hassan et al. (1996) as given in Table 4.5. The changes to the medium aimed to imitate the sugar content and the composition of a microalgae hydrolysate based on literature data (Meo et al., 2017) and to achieve the desired degree of phosphorus-depletion in the medium by adjusting a certain C/P mass ratio. This was done by changing the concentration of KH_2PO_4 in the medium in dependence of the sugar concentration and the desired C/P ratio. The concentrations given in Table 4.5 correspond to a C/P ratio of 3515 g g^{-1}. This is the standard medium composition used in this work unless stated otherwise specifically. The compositions of the trace element and vitamin solutions used for this medium are given in Table 4.6 and 4.7.

Kanamycin and tetracycline solutions contained 100 g L^{-1} kanamycin sulphate in deionized water and 100 g L^{-1} tetracycline hydrochloride in 50% (*v/v*) ethanol in water mixture. The vitamin and antibiotic solutions were filter-sterilized (0.22 µm filter) and added into the medium prior to inoculation. All other medium components were sterilized at 121 °C for 20 min.

Table 4.6: Composition of the trace element solution (100×) for the yeast cultivation medium.

Component	**Concentration, g L^{-1}**
$CaCl_2$	2.72
$ZnSO_4 \cdot 7\ H_2O$	0.75
$CuSO_4 \cdot 5\ H_2O$	0.13
$CoCl_2 \cdot 6\ H_2O$	0.13
$MnSO_4 \cdot H_2O$	0.50
$(NH_4)_6Mo_7O_{24} \cdot 4\ H_2O$	0.61

Table 4.7: Composition of the vitamin solution (100×) for the yeast cultivation medium.

Component	**Concentration, g L^{-1}**
Myo-inositol	12.5
Nicotinic acid	0.5
Calcium D(+)-pantothenate	0.678
Thiamine hydrochloride	0.560
Pyridoxine hydrochloride	0.753
D(+)-Biotin	0.0125

Phosphate buffered saline (PBS) and washing saline (see Table 4.8 and 4.9) were used to wash the preculture cells if needed. In cases where a complete phosphorus-depletion of the inoculum was required, washing saline was used instead of PBS.

Table 4.8: Composition of phosphate buffered saline (PBS).

Component	Concentration, g L^{-1}
NaCl	8.00
KCl	0.20
Na_2HPO_4	1.44
KH_2PO_4	0.24

Table 4.9: Composition of the saline used for washing the preculture cells.

Component	Concentration, g L^{-1}
NaCl	8.00
KCl	0.20

4.3. TUM-AlgaeTec Center and climate simulation

In this study all experiments regarding the production of microalgal biomass were conducted at the TUM-AlgaeTec Center, a facility for pilot-scale microalgae research at realistically simulated climate conditions located in Taufkirchen, Germany. The TUM-AlgaeTec Center and the specifications of the climate simulation were described previously in detail by Apel et al. (2017). Figure 4.3 shows the external view of the TUM-AlgaeTec Center with green light-emitting diode (LED) lighting in the glass halls, where the thin-layer cascade (TLC) photobioreactors were located. The first hall containing two TLC reactors with 4 m^2 surface area was used for preculture generation. The second hall with six TLC reactors, each with 8 m^2 surface area, was used for preliminary examination of the cultivation conditions. The third hall containing the pilot-scale TLC reactor with 50 m^2 surface area was used for scale-up and for biomass production at large.

Figure 4.3: Exterior view of the TUM-AlgaeTec Center with green LED-lighting in the reactor halls with climate simulation.

The glass facade of the halls allowed natural sunlight to reach the reactors, the amplitude and the wavelength of which were measured by a spectroradiometer (Flame, Ocean Optics, Dunedin, USA) located directly under the glass roof. The solar radiation measured was complemented by local radiation with LED-based artificial sunlight (FutureLED, Berlin, Germany) in the 400–750 nm range to achieve the target photosynthetically active radiation (PAR) according to the simulated climate data. Air temperature and humidity were automatically controlled by air conditioning and natural ventilation depending on the local outdoor conditions. For the physical climate simulation, the data chosen was from 15 June 2012 in Almería, Spain, as depicted in Figure 4.4.

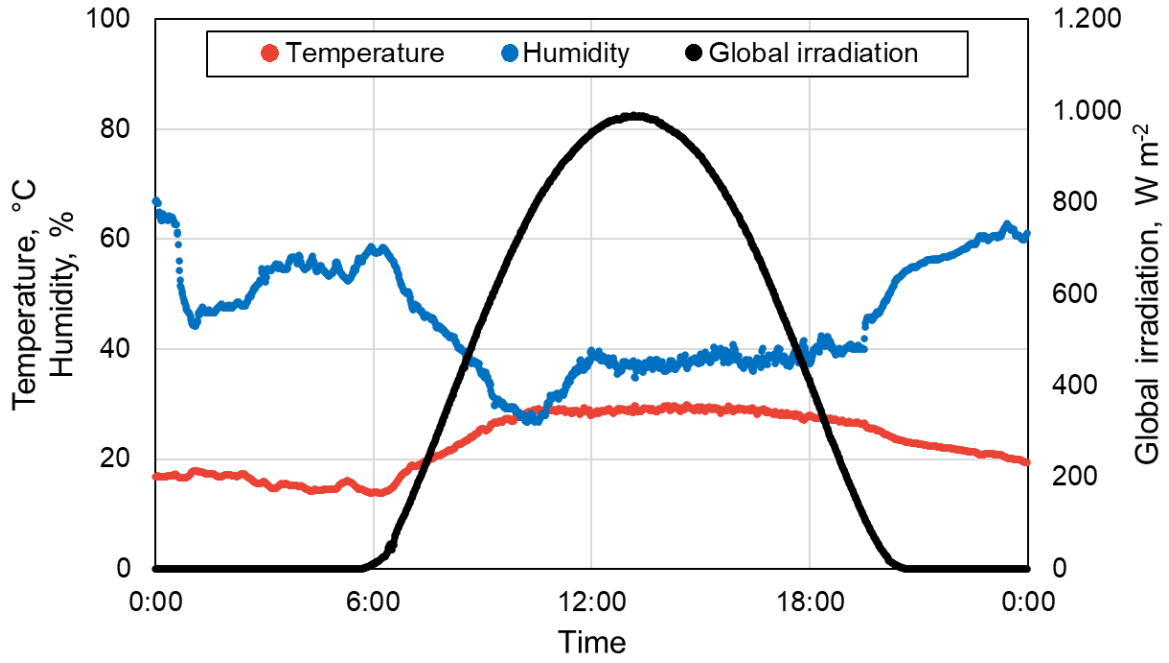

Figure 4.4: Daily time courses of air temperature (red), air humidity (blue) and global irradiation (black) of June 15, 2012 in Almería, Spain as the target climate for physical climate simulation.

4.4. Design and operation of thin-layer cascade photobioreactors

Design and construction of the thin-layer cascade (TLC) photobioreactors in the TUM-AlgaeTec Center were described previously in detail by Apel et al. (2017). As shown in Figure 4.5, these consisted of two polyethylene channels with an inclination of 1° in opposite directions placed next to each other and connected with a flow reversal module, so that the microalgae suspension fed from the highest point of the upper channel can flow through both channels freely reaching the retention tank at the lowest point of the lower channel. The microalgae suspension is then circulated back into the inlet module using a centrifugal pump (MKPG, Ventaix, Monschau, Germany). This was different only for the pilot-scale TLC photobioreactor, which has a retention tank and a circulation pump at the end of each channel, making it possible to connect any amount of channels in sequence. pH of the microalgae suspension was controlled at pH 8.5 during the day by addition of pure CO_2 through a gassing unit with perforated hoses (Solvocarb® and Solvox® B, Linde, Pullach, Germany) installed in the retention tanks. pH and temperature of the microalgae suspension were measured using a combination electrode (tecLine 201020/51-18-04-18-120, Jumo, Fulda, Germany) located in the

retention tank and connected to a transmitter (ecoTrans pH 03, Jumo, Fulda, Germany). The temperature of the suspension was only measured, not controlled. Volumetric flow rate of the microalgae suspension was measured using a magnetic-inductive sensor (MIK, Kobold, Hofheim, Germany) placed after the circulation pump. Additionally, a level sensor (LFFS, Baumer, Friedberg, Germany) was placed in the retention tank to check the liquid level inside the tank. When this fell below the pre-adjusted level due to evaporation, tap water was automatically added through a solenoid valve (Type 52, Gemü, Ingelfingen, Germany) to keep the suspension volume in the reactor constant. Design and operational specifications of the TLC photobioreactors on different scales are presented in Table 4.10. Salinity and total alkalinity (TA) of the microalgae suspension were measured at-line and the TA was controlled by manual addition of sulphuric acid into the suspension.

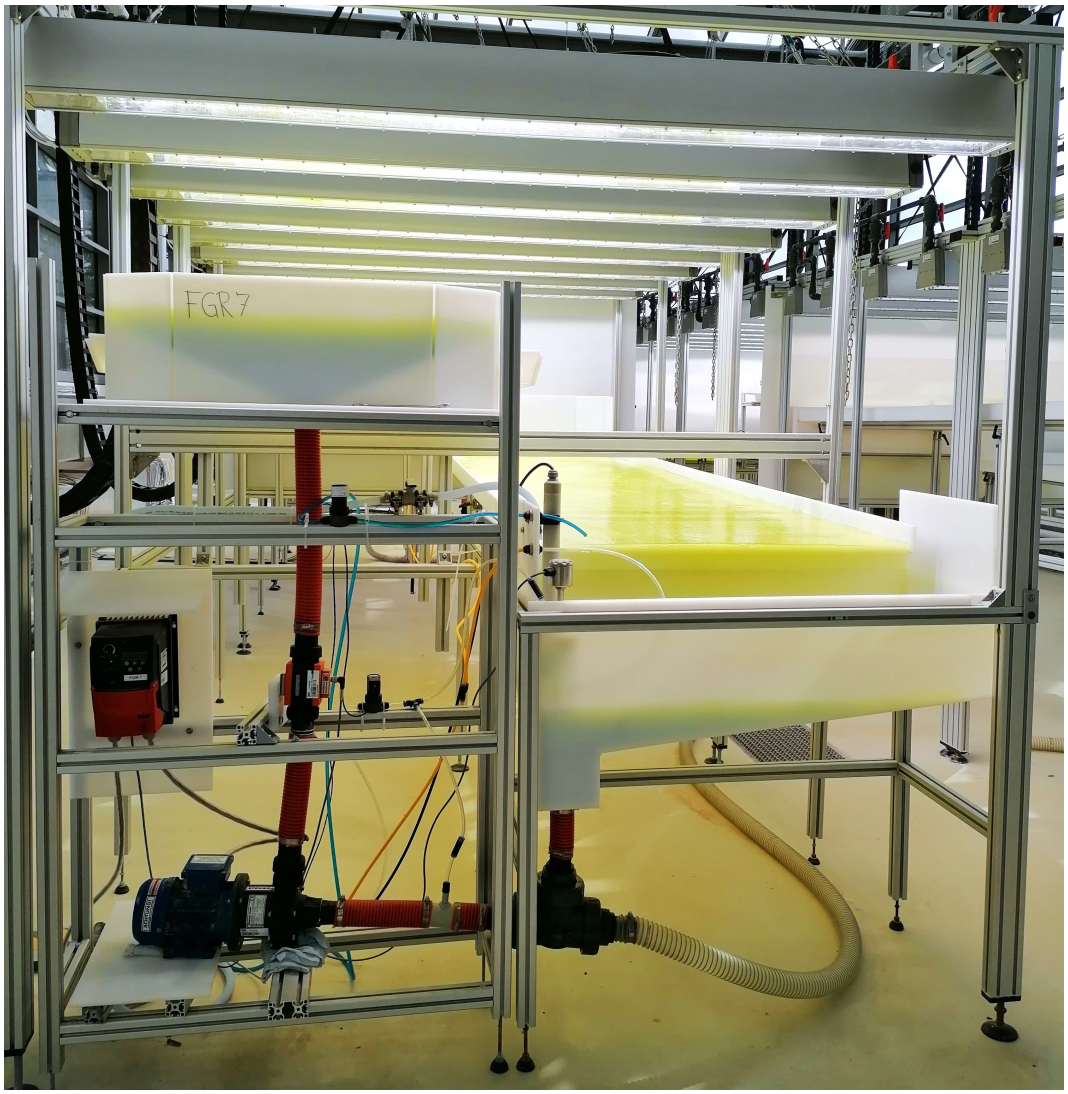

Figure 4.5: Image of a TLC photobioreactor in operation for microalgae cultivation.

In each experiment the reactors were inoculated with enough microalgae suspension from the preculture reactor to achieve a starting CDW concentration of 0.3-0.5 g L^{-1} in order to prevent a previously observed photoinhibition at the beginning of the cultivation. The minimum initial CDW concentration required for the pilot-scale reactor was determined to be 0.7 g L^{-1} empirically. After inoculation all reactors were run under a physical climate simulation as described in Section

4.3. Feed medium was supplied into the reactor always in concentrated form to avoid a significant change of the reaction volume. Three different modes of operation were examined in this study to determine, which one of them allows maximum biomass productivity: batch mode, semi-continuous mode, and continuous mode.

Table 4.10: Specifications of the TLC photobioreactors on different scales.

Specification	**Preculture scale**	**Experimental scale**	**Pilot scale**
Surface area	4 m^2	8 m^2	50 m^2
Working volume	40 L	55 L	330 L
A/V ratio	100 m^{-1}	145 m^{-1}	152 m^{-1}
Flow rate	2.0 L s^{-1}	2.4 L s^{-1}	4.8 L s^{-1}
Channel length	1.7 m	3.7 m	12 m
Channel width	1 m	1 m	2 m
Channel slope	1 °	1 °	1 °
Layer thickness	0.6 cm	0.6 cm	0.6 cm

In all processes, concentrations of the medium salts (NaCl, $MgSO_4$ and $CaCl_2$) were kept constant in the reaction medium, whereas the remaining medium components were supplied as a concentrated solution additionally over the whole process to avoid nutrient depletion in the medium and to keep the urea concentration at 0.5–1.5 g L^{-1}. For easier description, the average nutrient feed rate ($r_{feed,ave}$) in batch and semi-continuous experiments is expressed in terms of a factor (F) of the nutrient concentration in the ASW medium as follows:

$$r_{feed,ave} = \frac{m_{nutrient,in}}{V_R \cdot t} = \frac{F \cdot c_{nutrient,ASW}}{t} = F \times \text{ASW per day} \tag{4.1}$$

where $m_{nutrient,in}$ is the mass of nutrients fed, V_R is the reaction volume (i.e. volume of algae suspension inside the reactor), t is the process time in days, and $c_{nutrient,ASW}$ is the nutrient concentration in the ASW medium as given in Table 4.1.

All batch processes were started with a nutrient concentration of 2× that of ASW medium. Batch processes were ended after reaching the maximum integral productivity. Semi-continuous processes were started the same way as batch processes. Semi-continuous operation began after the microalgae suspension had reached the desired CDW concentration, which corresponds to the preselected biomass density value at the start of each day. Thereafter, everyday at 10 a.m. except on weekends, a portion of the suspension was harvested from the reactor and was replaced with fresh ASW medium in order to bring the CDW concentration to the desired value. Additional concentrated feed medium was added manually whenever needed to keep the urea concentration in the desired range throughout the process.

Figure 4.6 depicts the process flow for continuous operation of TLC photobioreactors. Continuous processes also began the same way as batch processes. The switch to continuous operation was started after the microalgae suspension had reached the desired CDW concentration. This CDW concentration was estimated based on the corresponding expected growth rate, which is equal to the dilution rate in a continuous process (see Subsection 3.2.4). Thereafter, concentrated feed medium in an external feed tank (Type TR 5/L made of black polyethylene, Aricon Kunststoffwerk GmbH, Solingen, Germany) was supplied into the reactor continuously by a peristaltic pump. Microalgae suspension was pumped into an external collection tank (Type TR 5/L made of standard polyethylene, Aricon Kunststoffwerk GmbH, Solingen, Germany) for 12 hours everyday from 7 a.m. to 7 p.m. to avoid washing out of the cells in the night time when the cell growth is minimal due to the lack of light supply. Volumetric flow rate of the outlet stream in these 12 hours is set to twice that of the inlet stream, so that the daily harvested suspension volume equals the daily feed medium volume supplied into the reactor. Hence, the dilution rate specified for each experiment is a daily average. Figure 4.7 shows the actual set-up of the pilot-scale TLC photobioreactor in continuous operation.

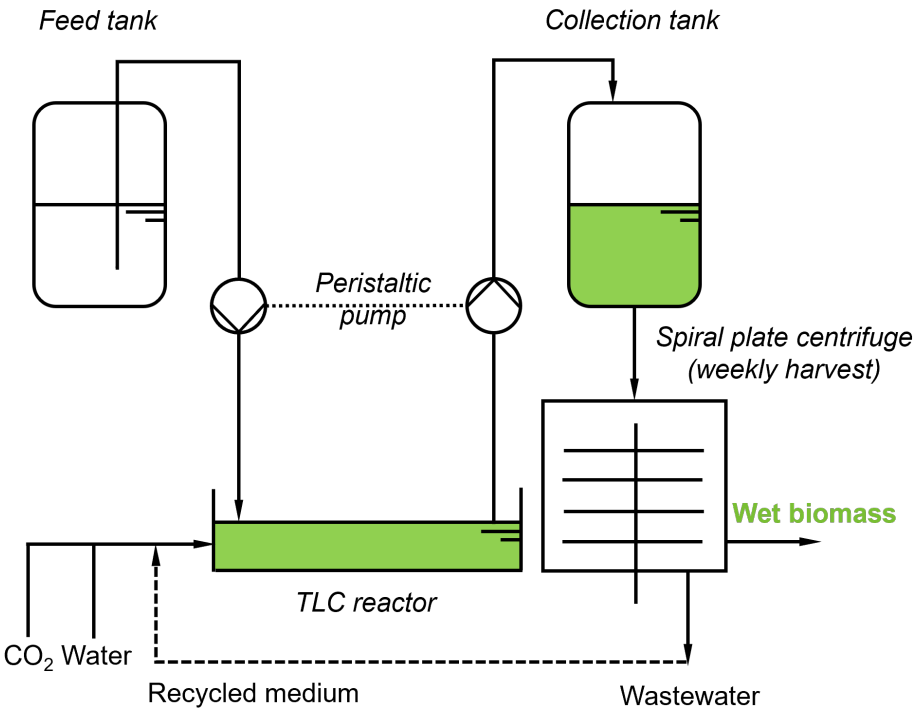

Figure 4.6: Process flow for continuous microalgal biomass production in TLC photobioreactors. Concentrated feed medium in an external feed tank is supplied into the reactor continuously by a peristaltic pump and microalgae suspension is pumped into an external collection tank with the same volumetric flow rate as the feed stream. Once enough suspension has been accumulated in the collection tank, the microalgal biomass is harvested by centrifugation. The dashed line refers to a possible recycling of the waste medium (clear phase) exiting the centrifuge as feed.

In continuous processes, the concentration of the feed medium was adjusted to a factor (CF) of the nutrient concentration in the ASW medium without changing the concentration of medium salts (i.e. NaCl, $MgSO_4$ and $CaCl_2$), depending on the dilution rate (D) and the desired feed rate. Similarly to batch and semi-continuous processes, the nutrient feed rate (r_{feed}) in each continuous experiment

is expressed in terms of a factor (F) of the nutrient concentration in the ASW medium as follows:

$$r_{feed} = \frac{m_{nutrient,in}}{V_R \cdot t} \tag{4.2a}$$

$$= \frac{c_{nutrient,feed} \cdot V_{feed}}{V_R \cdot t} \tag{4.2b}$$

$$= \frac{CF \cdot c_{nutrient,ASW} \cdot (V_R \cdot D \cdot t)}{V_R \cdot t} \tag{4.2c}$$

$$= CF \cdot D \cdot c_{nutrient,ASW} \tag{4.2d}$$

$$= F \times \text{ASW per day} \tag{4.2e}$$

where $m_{nutrient,in}$ is the mass of nutrients fed, V_R is the reaction volume (i.e. volume of algae suspension inside the reactor), t is the process time in days, V_{feed} is the volume of the feed medium supplied, D is the dilution rate, and $c_{nutrient,ASW}$ is the nutrient concentration in the ASW medium as given in Table 4.1. For instance, with a 20× concentrated feed medium ($CF = 20$) and a dilution rate of 0.175 d^{-1}, the feed rate (r_{feed}) is expressed as 3.5× ASW per day, meaning $F = 3.5$.

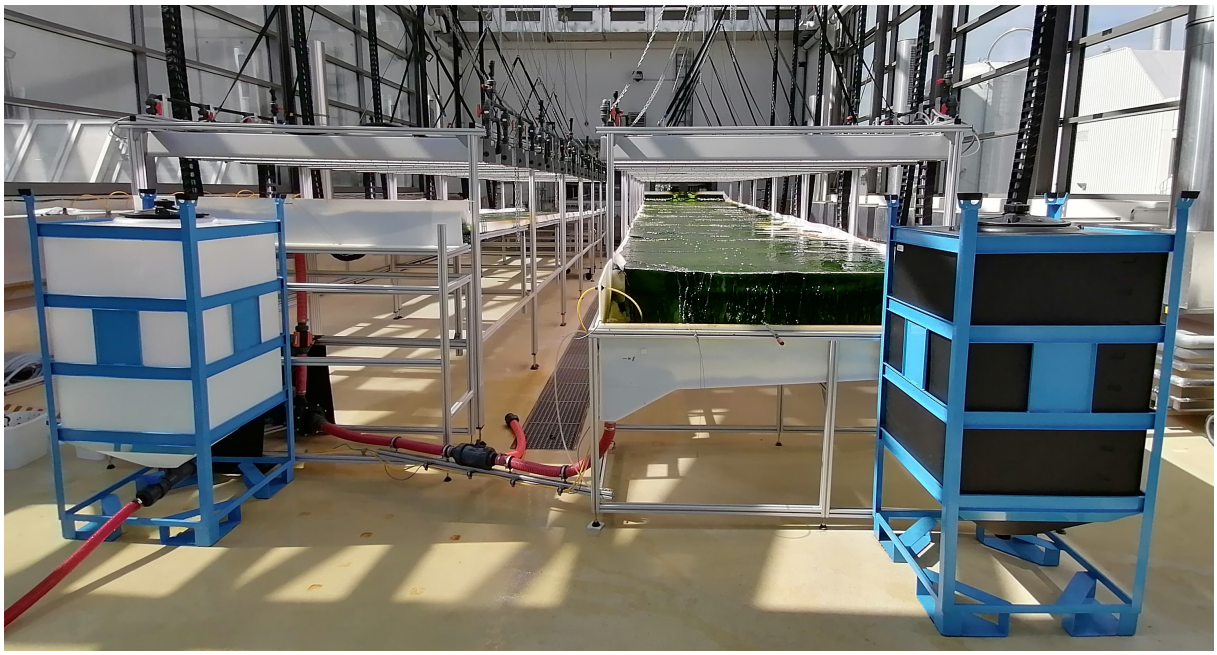

Figure 4.7: Pilot-scale TLC photobioreactor in continuous operation.

After enough microalgae suspension had been accumulated in the collection tank, the microalgal biomass was harvested by centrifugation. In Figure 4.6 a dashed line was used to emphasize a possible recycling of the waste medium (clear phase) exiting the centrifuge as feed to facilitate an efficient use of resources.

4.5. Microalgal biomass harvest

In this work, microalgal biomass generated is further processed into a hydrolysate in a process requiring high CDW concentrations up to 250 g L^{-1}. Therefore, the collected microalgae suspension had to be dewatered and concentrated significantly into a wet paste. To this end, microalgal biomass

was harvested using a continuous centrifuge with spiral plate technology (Evodos 50A, Evodos B.V., Raamsdonksveer, Netherlands).

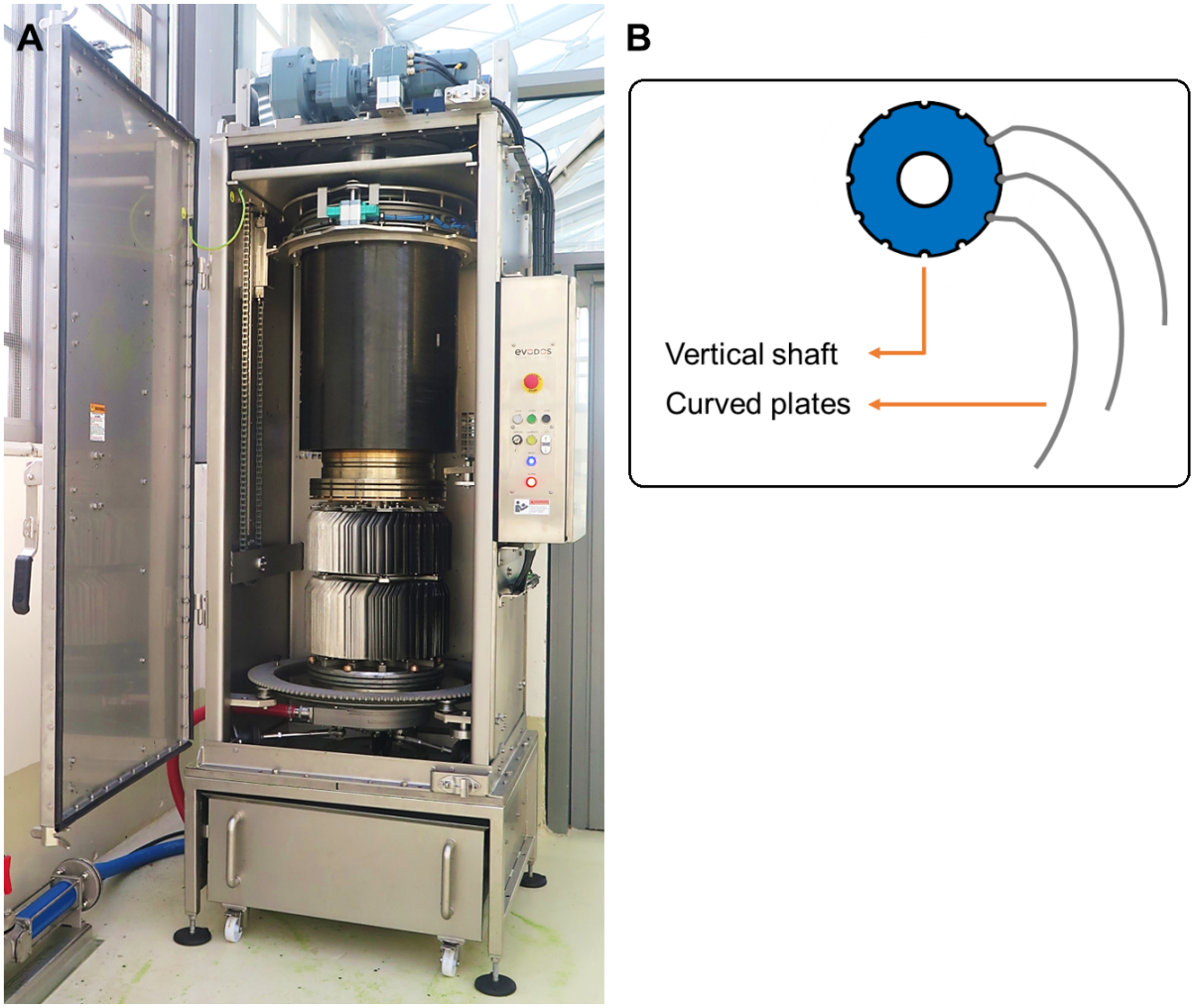

Figure 4.8: Evodos™ centrifuge with spiral-plate technology. **A**: Interior view of the centrifuge; **B**: depiction of the spiral plate technology showing curved plates hinged onto a vertical shaft viewed from the top.

Spiral plate technology encompasses rotating curved plates hinged onto a vertical shaft inside a sliding cylindrical drum to reduce particle settling distances as shown in Figure 4.8. This technology combined with the continuous and fully automated design of the centrifuge provides a major improvement in the dewatering efficiency of microalgae biomass and a reduction in the overall operational costs (Pahl et al., 2012).

Dewatering of microalgal biomass was conducted with Evodos™ 50A centrifuge using the settings given in Table 4.11 and the equipment set-up shown in Figure 4.9. Biomass in form of microalgae paste was discharged with 30 minutes intervals and was gathered from the collecting tray below the centrifuge drum at the end of centrifugation. Water content of the harvested biomass was determined by gravimetric measurement to be around 70% *(w/w)* for all batches. The microalgal biomass was frozen and stored at –20 °C until further processing.

Figure 4.9: Exterior view of Evodos™ centrifuge connected to the pilot-scale TLC photobioreactor. Microalgae suspension pumped into the collection tank continuously is fed to the centrifuge using the associated progressing cavity pump located on the floor to the left of the centrifuge compartment. The control cabinet with a touch screen display panel is located on the right side of the hall door.

Table 4.11: Operational settings of Evodos™ 50A centrifuge with spiral plate technology.

Separation	**Parameter**	**Value**
Step 1	Rotor speed	4.000 min^{-1}
	Feed rate	500 L h^{-1}
	Duration	1 min
Step 2	Rotor speed	4.200 min^{-1}
	Feed rate	500 L h^{-1}
	Duration	2 h
General	Start of centrifuge by rotor speed	4.000 min^{-1}
	Drum prefill settling time	240 s
	Solids compressing time	120 s
	Pump Pulsing time	0 s (Pulsing off)
	Pump Pulsing off time	10 s

4.6. Design and operation of the stirred-tank bioreactor

Batch and fed-batch processes on a litre scale were carried out in a baffled glass stirred-tank bioreactor (Labfors 3, Infors HT, Bottmingen, Switzerland) with a working volume of 1–6 L. The reactor had an agitator with three 6-bladed Rushton turbines, a curved drilled hole sparger for gassing, a tempering jacket, a pH and a dissolved oxygen sensor, a thermometer, addition ports on the reactor cover for inoculum, feed and titration solutions, and an exhaust gas port with a condenser and a foam trapping unit. In fed-batch processes feed medium was added via a peristaltic pump (BVP Easy-Load II, Ismatec, Wertheim, Germany). The stirred-tank bioreactor used in this work is depicted in Figure 4.10 together with the flow diagram of a fed-batch process.

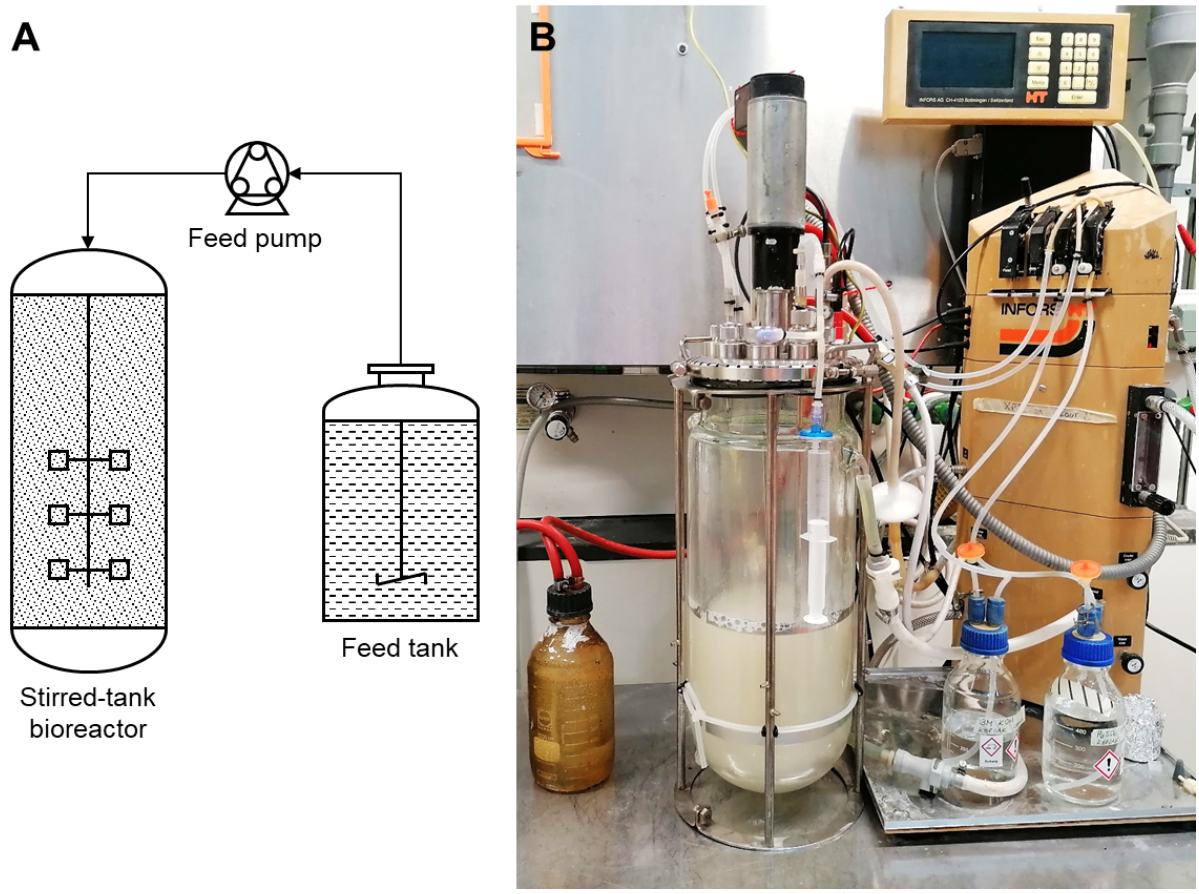

Figure 4.10: Stirred-tank bioreactor used for batch and fed-batch processes on a litre scale. **A**: Flow diagram of a fed-batch process; **B**: stirred-tank bioreactor with an STR, control station, pH control solutions, and foam trapping unit (coated glass bottle) on exhaust gas line.

Process parameters such as temperature, agitation rate, aeration rate, pH and dissolved oxygen level (pO_2) were controlled via a control station connected to a PC using the software Iris v5. For controlling pO_2 a control sequence adjusting agitation and aeration rates was run using the software. For automated pH control 1 M H_2SO_4 and 1 M KOH solutions were used. In cases where nitrogen depletion was to be omitted ammonia solution (25% (*w/w*)) was used as base for pH regulation. pH and pO2 sensors were calibrated using two-point calibration method before each cultivation. pH sensor calibration was carried out using standard calibration solutions with pH 4 and pH 10. For the pO_2 sensor 0% and 100% values were adjusted after gassing with N_2 and pressurized air, re-

spectively, and achieving a constant measured value. Process parameter settings applied for all experiments carried out in this stirred-tank reactor (STR) are given in Table 4.12.

Table 4.12: State variables for operation of the stirred-tank bioreactor.

Process parameter	**Value**
Working volume	3 L
Temperature	30 °C
pH	6.5
pO_2	>20%
Aeration rate	2–6 NL min^{-1}
Agitation	400–1200 rpm

4.7. Design and operation of the membrane bioreactors

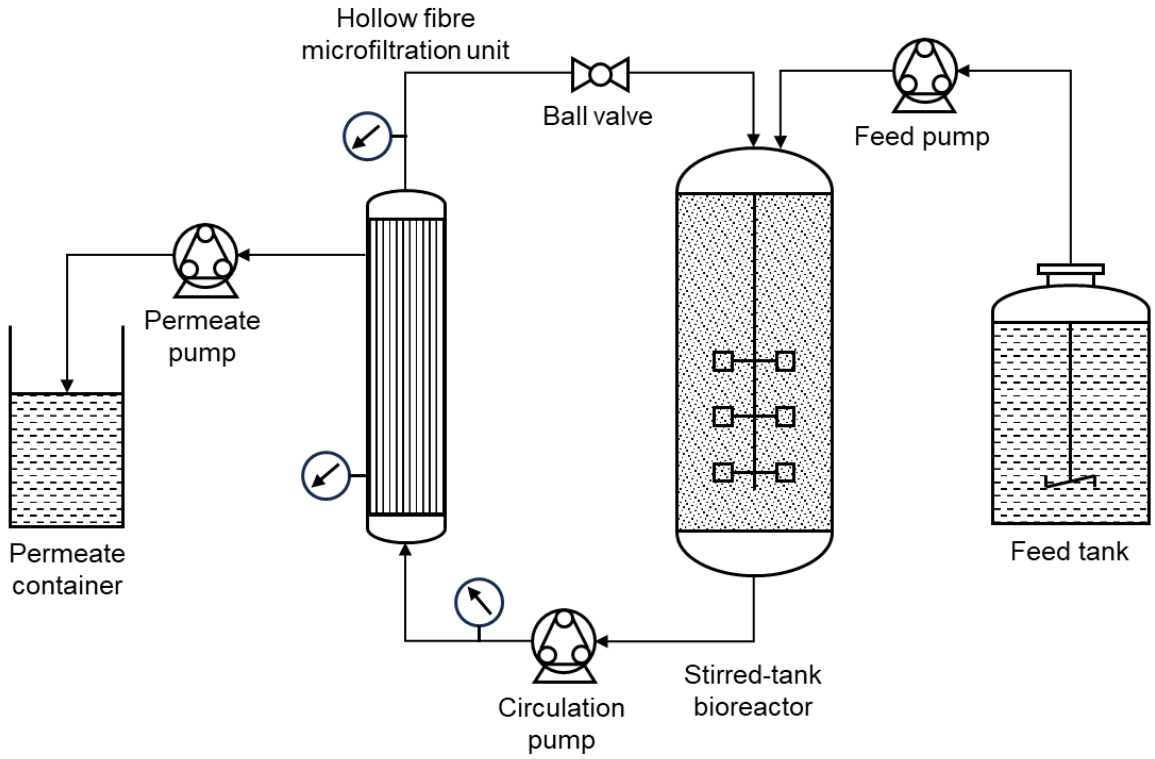

Figure 4.11: Flow diagram of the MBR with total cell retention on a 1.5 L scale.

For high-cell-density yeast cultivation two membrane bioreactors (MBRs) with total cell retention were used. The MBR used for experiments on a 1.5 L scale consisted of the stirred-tank bioreactor (Labfors 2, Infors HT,Bottmingen, Switzerland) described in Section 4.6 and a hollow fibre microfiltration module (CFP-2-E-4A, Cytiva Europe GmbH, Freiburg, Germany) connected to it as an external bypass as shown in Figure 4.11. The microfilration unit had a membrane area of 0.042 m^2. Feed medium was added via a peristaltic pump. Fermentation broth was circulated through the bypass

across the hollow fibre module by a peristaltic pump, whereas permeate was drawn via another. TMP was kept in the range of 0.5–1.0 bar by manually regulating the volumetric flow rate of the reflux stream via a ball valve.

Figure 4.12 shows the actual setup used for the MBR system on a 1.5 L scale during a running experiment. Each cultivation was started in batch mode. After complete consumption of sugars in the fermentation medium marked by a sudden increase in pO_2, the MBR operation was switched to semi-continuous mode. In the semi-continuous mode of operation, the feed is supplied into the MBR continuously with a constant rate, whereas filtering out of the used up medium from the reactor is done only for 8 hours during the day. This method entails a constant change in liquid volume inside the reactor in a preset range; however, it also reduces the time of microfiltration per process time so that energy consumption associated with medium filtration is reduced by two thirds compared to a fully continuous operation.

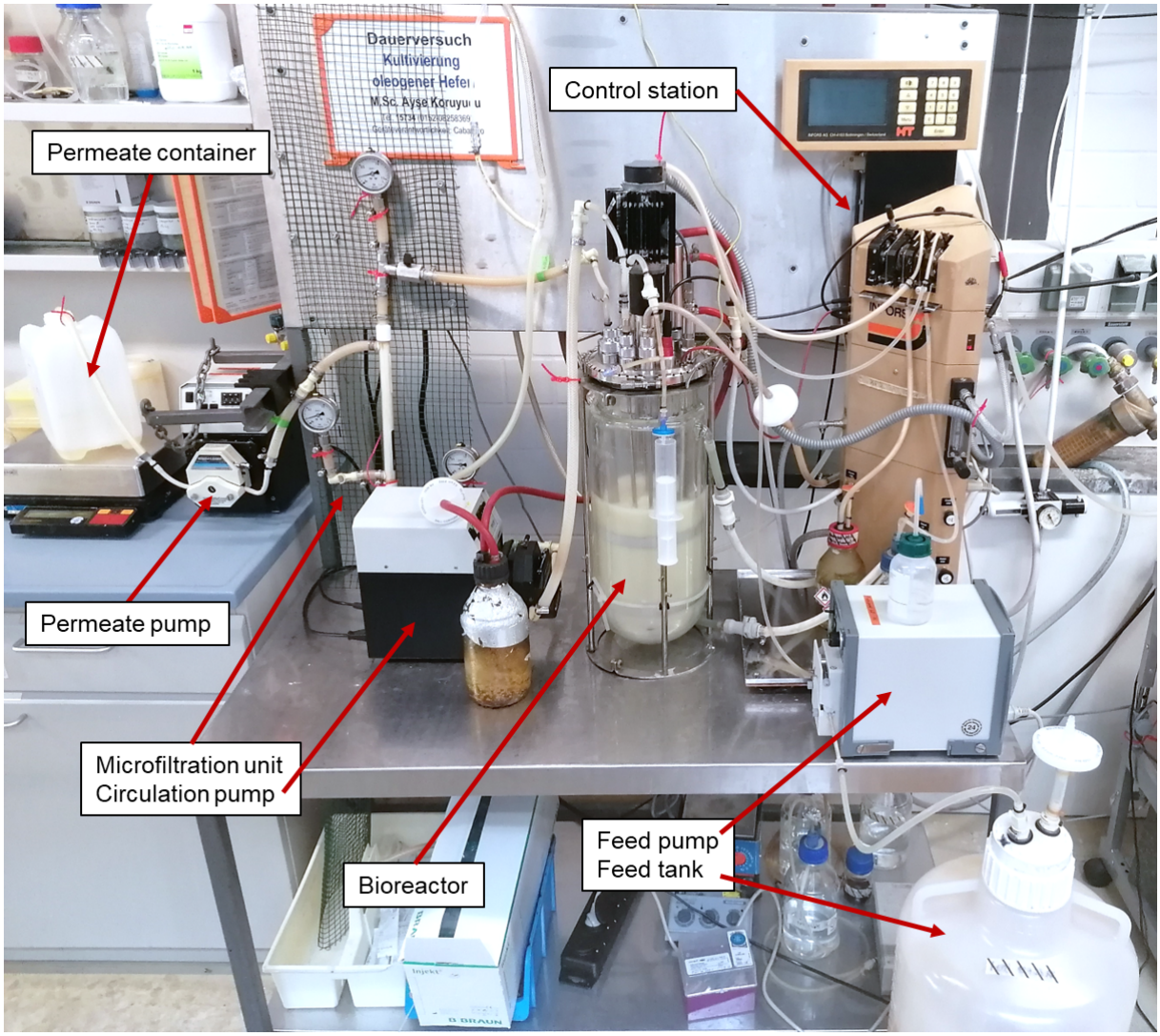

Figure 4.12: MBR with total cell retention on a 1.5 L scale.

The feed was started with and kept constant at a rate of 1.1 g sugars L^{-1} h^{-1} based on initial liquid volume in the MBR. From this value, volumetric flow rate of the feed stream ($\dot{V}_{in}$) was calculated

based on initial fermentation volume and sugar concentration of feed medium as follows:

$$\dot{V}_{in} = \frac{Q_S \cdot V_{R,0}}{c_{S,feed}} \tag{4.3}$$

where Q_S is the sugar feed rate based on initial fermentation volume, $V_{R,0}$ is the initial liquid volume in the reactor, and $c_{S,feed}$ is the substrate concentration in feed medium. In addition, permeate flow rate was adjusted depending on the feed flow rate so that the liquid volume inside the MBR was reduced from 5.26 L at the beginning of each day to 1.20 L at the end of the day within 8 h. Since there was no filtration but only the feed flow into the reactor at night, the liquid volume inside the MBR increased from 1.20 L to 5.26 L overnight within 16 h. In this manner, the liquid volume inside the MBR was kept in the desired range and the initial volume of 1.5 L was achieved in the MBR once a day midway into the filtration phase.

Before each experiment, the 1.5 L MBR was sterilized. The STR with all of its components was heat-sterilized (at 121 °C for 20 min), whereas the hallow fibre cartridge was sterilized using 80% ethanol in water mixture. For this, first 1 L of 80% ethanol solution was pumped through the whole bypass unit for 10 min, followed by rinsing with 2 L of heat-sterilized (at 121 °C for 20 min) distilled water. Finally, remaining liquid inside the bypass module was drained into a sterile bottle via filter-sterilized pressurized air. For cleaning the unit after a cultivation, same procedure as described above was applied under non-sterile conditions and the hallow fibre cartridge was allowed to dry at room temperature with pressurized airflow.

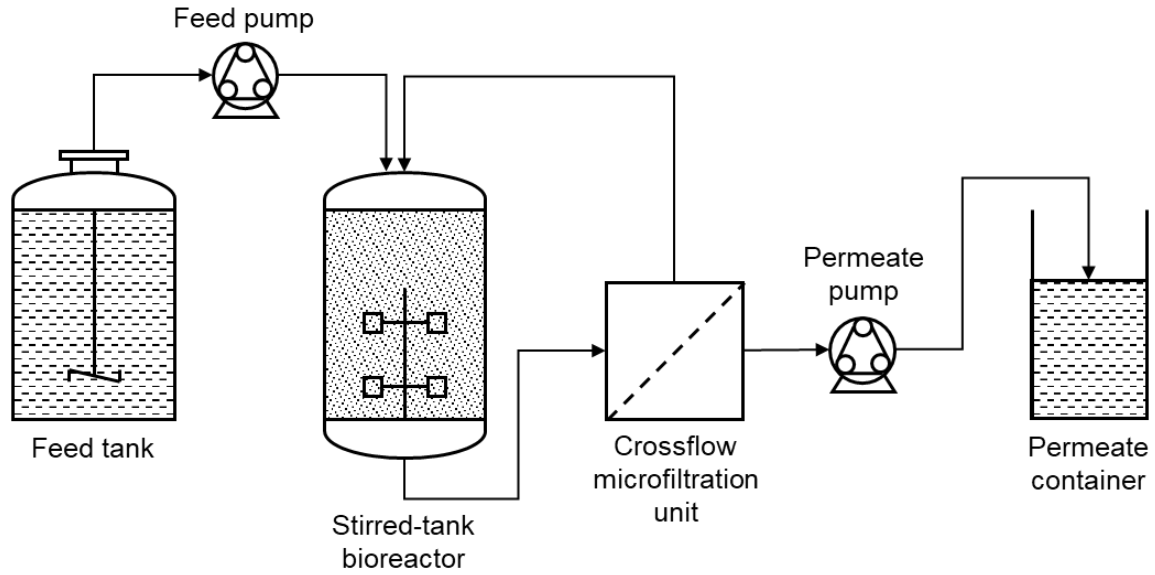

Figure 4.13: Flow diagram of the MBR with total cell retention on a 50 L scale.

The MBR used for experiments on a 50 L scale was composed of two main units: a stirred-tank bioreactor with a 50 L working volume (LP75L, Bioengineering, Wald, Switzerland) and a cross-flow microfiltration unit (Clearflow MF X 01, Heinrich Frings, Rheinbach, Germany) connected to it as an external bypass as shown in Figure 4.13. The state variables were controlled via BioSCADALab (Bioengineering, Wald, Switzerland) software using local IFM controllers and a peristaltic pump station provided by the manufacturer (Bioengineering, Wald, Switzerland). Additionally, a control cascade was used to keep the dissolved oxygen level over 40% air saturation at all times by regulat-

ing the agitation and aeration rate. 1 M sulfuric acid, 25% *(w/w)* ammonia, and 10% *(v/v)* antifoam (Antifoam 204, Sigma-Aldrich, Taufkirchen, Germany) solutions were connected to the pump station for automated software control of the pH and foam. The cross-flow microfiltration unit had a central control cabinet with a programmable logic controller (PLC, Siemens, Munich, Germany) and a touch panel. The microfilter used was a 1.2 m long ceramic module (Crystar 41-61-3.0 FT250, Compagnie de Saint-Gobain, Courbevoie, France) with capillaries (61 $\times$ 3.2 mm inside diameter), and a filtration area of 0.8 m^2. A sterile vessel with 200 L capacity (Rütten Engineering Ltd., Tagelswangen, Switzerland) equipped with a magnetic stirrer, a sterile filter, a manometer, a thermometer, and a cooling jacket was used as the feed tank. The feed medium was supplied to the bioreactor by a peristaltic pump with manually adjustable pump speed at the pump station.

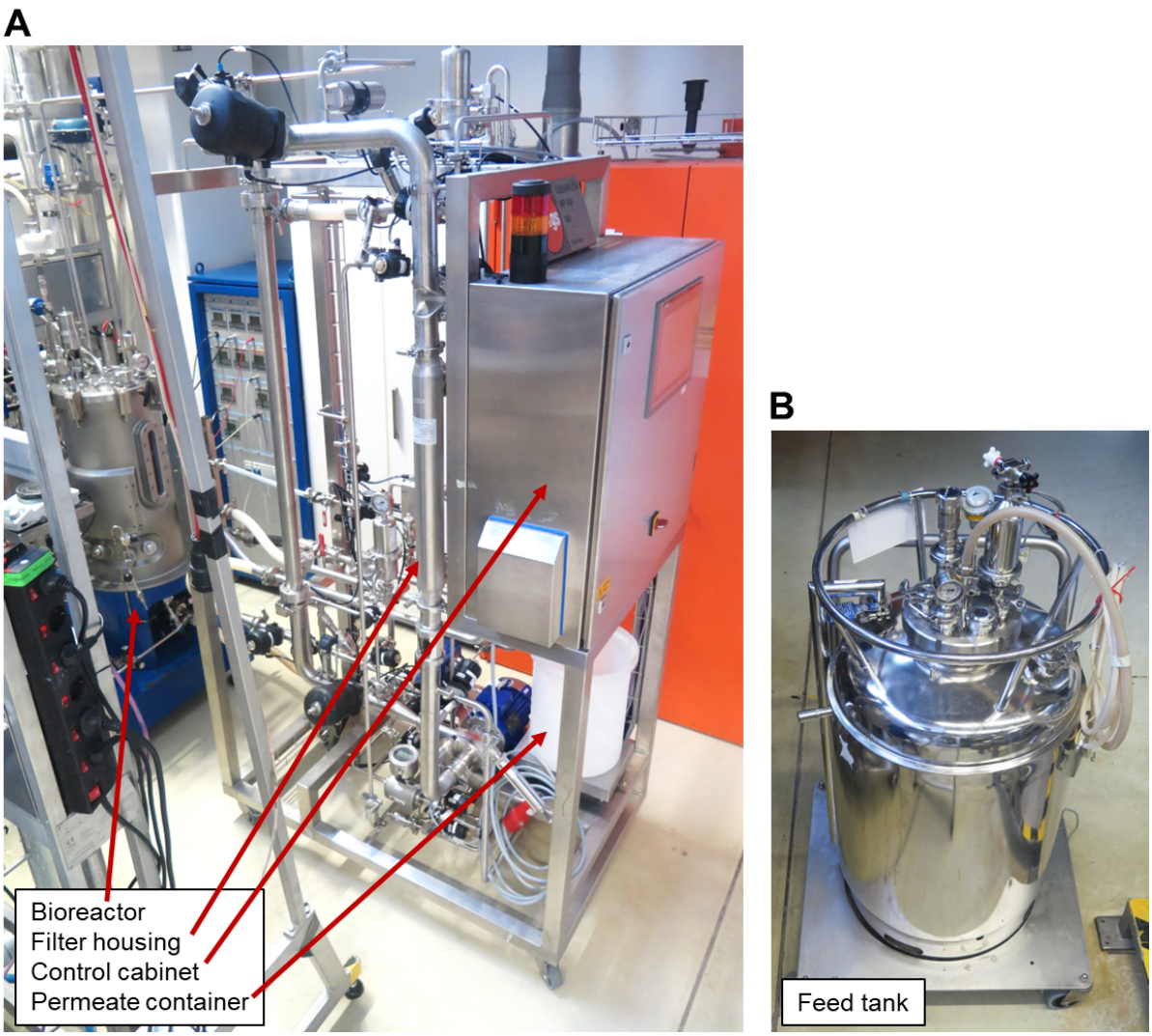

Figure 4.14: MBR with total cell retention on a 50 L scale. **A**: Photograph of the steam-sterilizable 50 L MBR; **B**: photograph of the steam-sterilizable feed tank.

Figure 4.12 shows the actual setup used for the MBR system on a 50 L scale. Each cultivation was started in batch mode. After complete consumption of sugars in the medium, the mode of operation was switched to semi-continuous as described above for the 1.5 L scale. Similarly, the feed was started with and kept constant at 1.1 g sugars L^{-1} h^{-1} based on initial liquid volume in the MBR. Required volumetric flow rate of the feed stream was calculated to be 1.1 L h^{-1} using Equation 4.3 considering a sugar concentration of 50 g L^{-1} and an initial cultivation volume of 50 L. Likewise, the

microfiltration unit was operated only for 8 h during the day. Accordingly, the permeate flow through the filter was adjusted to 3.3 L h^{-1} so that the liquid volume inside the MBR was reduced from 61.6 L at the beginning of each day to 44 L at the end of the day. The dilution rate resulting from these settings was D = 0.528 d^{-1}, which corresponds to 0.022 h^{-1} on a daily average.

Before and after each experiment, the 50 L MBR was heat-sterilized (at 121 °C for 20 min). After sterilization, at the end of an experiment, the MBR was cleaned using a standard machine cleaner dissolved in water, stirring at 70 °C for 40 min and then rinsed with tap water. No formation of persistent biofilm was observed on the filter material and no further cleaning of the MBR was required. The data and state variables applied for operation of both MBRs, as well as some key values important for proper scale-up of the MBR, are summarized in 4.13.

Table 4.13: Specifications, process data and state variables applied for the operation of the MBRs.

Process parameter	**1.5 L scale**	**50 L scale**
Working volume including bypass	1–6 L	40–67 L
Bypass volume	0.11 L	7.25 L
Temperature	30 °C	30 °C
pH	6.5	6.5
pO_2	>20%	>20%
Aeration rate	2–6 NL min^{-1}	50–100 NL min^{-1}
Agitation	400–1200 rpm	350–800 rpm
Cross-flow filter type	Hollow fibre microfilter	Microfilter with capillaries
Cross-flow filter material	Polysulfone (PS)	Ceramic (>99% SIC)
Cross-flow filter pore size	0.20 µm	0.25 µm
Inner diameter of fibres/capillaries	1.0 mm	3.2 mm
Volumetric flow rate in bypass	47.8 L h^{-1}	150 L h^{-1}
Mean residence time in bypass	0.13 min	2.9 min
Relative membrane area	0.028 m^2 L^{-1}	0.016 m^2 L^{-1}
Bypass-to-working volume ratio	7.0%	14.5%
Shear rate across filter module	2705 sec^{-1}	212 sec^{-1}

4.8. Separation of microbial oils

The main focus of this work is the process integration for yeast oil production. Nonetheless, some conventional downstream processing possibilities were also explored in order to present a concept covering a complete production process. The preferred method for the separation of microbial oils from fermentation broth was solvent extraction. For this, various solvents and pre-treatment methods were tested and compared based on the separation efficiency and the purity of the resulting product.

Solvents selected for examination were ethyl acetate, n-hexane, and ethanol in combination with potassium carbonate (K_2CO_3) to induce or enhance phase separation in water-solvent mixtures. Additionally, effects of the following pre-treatment methods on solvent extraction of yeast oil from actual fermentation broth were investigated in different combinations with each other:

- Enzymatic hydrolysis of yeast cells
- Mechanical disruption of yeast cells by high-pressure homogenization
- Treatment with a demulsifier

For enzymatic disruption of *C. oleaginosus* cells commercial enzyme mixtures listed in Table 4.14 were used. These were selected based on previous work by Masri et al. (2019) stating the enzyme activities required for enzymatic cell disruption of this yeast strain. It was also considered that the enzymes should be commercially available in large amounts and cost efficient enough to be used on an industrial scale. Using these enzymes the procedure stated in Table 4.15 was applied on lipid containing yeast cells. For pH adjustment and control acetic acid (98% (*w/w*) and ammonia (25% (*w/w*) solutions were used.

Table 4.14: Commercial enzymes used for yeast cell hydrolysis.

Enzyme	**Activity**	**Manufacturer**
Cellic® CTec3 HS	Cellulase, ß-glucosidase, hemicellulase	Novozymes (Denmark)
Rohalase® GMP	Endo-mannanase	AB Enzymes (Germany)
Protamex®	Endo-protease	Novozymes (Denmark)

Table 4.15: Procedure applied for enzymatic treatment of yeasts for cell wall hydrolysis.

Step	**Enzyme**	**Dosage**	**Temperature**	**pH**	**Duration**
1	Cellic® CTec3 HS	23.8% (*w/w*) g g^{-1} CDW	50 °C	5.0	24 h
	Rohalase® GMP	2.38% (*w/w*) g g^{-1} CDW			
2	Protamex®	11.9% (*w/w*) g g^{-1} CDW	37 °C	7.0	8 h

Mechanical disruption of yeast cells was carried out using an industrial high-pressure homogenizer (HPH) (Ariete NS3015H, GEA Group AG, Düsseldorf, Germany) with an external manually operated diaphragm pump (SartoJet, Sartorius AG, Göttingen, Germany) as the inlet pump. During operation of the HPH inlet pressure was manually adjusted to 3.5 bar at all times. Homogenization took place at 900 bar outlet pressure and a volumetric flow rate of 200 L h^{-1} with three passes through the homogenizer.

Since formation of an emulsion consisting of solvent, aqueous phase and cell debris was observed in all cases of solvent extraction, a pre-treatment with various emulsion breaking agents, also called demulsifiers, was performed. This the included addition of H_2SO_4 with 1% *(v/v)* of the yeast broth to be extracted and incubation at room temperature for 2 h unless stated otherwise.

For solvent extraction of yeast oil after pre-treatment with one or more of the methods mentioned above, solvent was added to broth to be extracted with 2:1 volumetric ratio of solvent to yeast suspension unless specified otherwise. After incubation for at least 2 h at room temperature under mixing, the mixture was allowed to settle to facilitate phase separation. In case of ethanol as extraction solvent, phase separation was facilitated by addition of 82% *(w/w)* K_2CO_3 with regard to the initial mass of yeast suspension. Since no spontaneous phase separation only by settling was observed in case of ethyl acetate, either addition of K_2CO_3 or centrifugation at 3260 rcf was necessary to promote it. After phase separation the upper phase containing solvent and lipids was transferred into another vessel. Solvent evaporation and recovery was performed using a rotary evaporator at 50 °C and pressures listed in Table 4.16. Extracted oil was further purified of solvents in an explosion-proof vacuum drying chamber at 50 °C and 4 mbar for 2 h.

Table 4.16: Evaporation pressure of different solvents in rotary evaporator used for lipid extraction.

Solvent	**Pressure**
Ethyl acetate	450 mbar
n-Hexane	200 mbar
Ethanol	75 mbar

Extraction efficiency (η_{ext}) was determined based on gravimetric analysis by weighing the extracted oil at the end in pre-dried and pre-weighed vessels as follows:

$$\eta_{ext} = \frac{m_{L,ext}}{V_{ext} \cdot c_{L,ext}} \tag{4.4}$$

where $m_{L,ext}$ is the mass of oil extracted, V_{ext} is the volume and $c_{L,ext}$ is the total lipid concentration of the yeast suspension prior to extraction. Determination of total lipid concentration is thoroughly described in Subsection 4.10.5.

4.9. Cell disruption and hydrolysis of microalgae

4.9.1. Rheology of microalgal biomass

Flow characteristics of a cell suspension have a big influence on the applicability and the efficiency of the method applied for cell disruption. Rotational viscometer are especially suited for examining the flow properties of non-Newtonian fluids such as concentrated cell suspensions (Schramm, 2004). Therefore, a rotational rheometer (RheolabQC, Anton-Paar, Graz, Austria) equipped with a tempered measuring cup (standard measuring system DG42/SS/QC-LTD) and a measuring cylinder (B-DG42 RFID) was used, which functions according to the Searle principle, where the cup is stationary and the cylinder rotates.

To measure the shear stress in dependence of the varying shear rate 12 mL of each sample was transferred into the measuring cup, tempered at 25 °C unless stated otherwise, and a predefined protocol was started using a PC connection with the software Rheoplus. In this way the shear stress (τ) and thus the dynamic viscosity (μ) were measured over 8 sec at constant shear rate ($\dot{\gamma}$) in a

range of 500–5000 s^{-1} with an upper limit of 170 Pa for the shear stress measurement. The acquired data sets were used to plot the flow and viscosity curves of the corresponding biomass.

4.9.2. Ultrasonication

A sonotrode (Sonopuls, Bandelin electronic GmbH, Berlin, Germany) consisting of a high-frequency generator (Sonopuls GM-2070) and an ultrasonic transducer (Sonopuls UW-2070) equipped with a titanium micro tip (Sonopuls MS 73) was used for the ultrasonic disruption of microalgal cells. The parameter settings given in Table 4.17 were adjusted on the homogenizer device. 25 mL of each sample was transferred into a 50 mL centrifuge tube, which was placed into an ice bath for cooling during the treatment, was homogenized for a specified duration of time.

Table 4.17: Parameter settings for disruption of *M. salina* cells with an ultrasonic homogenizer.

Sonotrode	Power	Frequency	Amplitude	Pulsation
MS73	70 W	20 kHz	97%	100%

4.9.3. Bead milling

For the disruption of microalgal cells through bead milling a mixer mill (MM 400, Retsch GmbH, Haan, Germany) equipped with stainless steel grinding jars with a nominal volume of 25 mL was used. Both the sample and the bead filling were at 40%, so that the total filling volume of the jars was at 80% corresponding to 20 mL. The jars were placed into an ice bath for cooling during sampling. Each sample was homogenized for a specified duration of time at a mixing frequency of 30 s^{-1}. The specifications of the various beads (Retsch GmbH, Haan, Germany) used for cell disruption are given in Table 4.18.

Table 4.18: Specifications of the various beads used for cell disruption of *M. salina* by bead milling.

#	**Material**	**Diameter, mm**	**Density, g mL^{-1}**
1	Zirconium oxide	1	6.13
2	Zirconium oxide	0.5	6.91
3	Agate	1	6.02
4	Glass	3	2.88
5	Stainless steel	5	7.72
6	Stainless steel	2	7.72
7	Tungsten carbide	3	14.94

4.9.4. High-pressure homogenization

For microalgal cell disruption by high-pressure homogenization on a 200 mL scale a tabletop high-pressure homogenizer (HPH) (HPL6, Maximator GmbH, Nordhausen, Germany) was used. In this case, 200 mL of each sample was processed at a flow rate of 4 L h^{-1} for up to 10 passes at a specified outlet pressure. For homogenization at scales larger than 30 L an industrial HPH (Ariete NS3015H, GEA Group AG, Düsseldorf, Germany) with an external manually operated diaphragm pump (SartoJet, Sartorius AG, Göttingen, Germany) as the inlet pump was used. In this case, for practical reasons the biomass was circulated in a tank with a cooling jacket and an external stirrer unit during homogenization. Thus, instead of counting the actual number of passes, the time equivalent of passes was calculated, which is defined as the homogenization time divided by the total volume and multiplied by the volumetric flow rate. The biomass was processed at a flow rate of 150–200 L h^{-1} for up to 5 passes at an outlet pressure of 1000 bar. During the homogenization process the inlet pressure was manually adjusted to 3.5 bar at all times using a diaphragm pump.

4.9.5. Enzymatic hydrolysis

Hydrolysis of the microalgal biomass was carried out on different scales. The preliminary experimentation with various enzyme doses on a mL scale was performed in 5 mL screw-cap glass vials in triplicate using a thermal shaker (Thermomixer Basic, CellMedia GmbH & Co. KG, Zeitz, Germany) incubating the reaction mixture for 72 hours with an agitation rate of 550 rpm. Scale-up experiments on a 60 L scale were performed in an STR (LP 75L, Bioengineering AG, Wald, Switzerland) with an agitation rate of 550 rpm. Scale-up to 200 L was done in a tempered stirred-tank (M500L, Bioengineering AG, Wald, Switzerland). CDW concentration of the microalgal biomass to be hydrolysed was adjusted to 150 g L^{-1} unless stated otherwise. Experiments were carried out both with and without mechanical cell disruption prior to enzymatic hydrolysis, which is indicated for each experiment individually. The commercial enzymes used for biomass hydrolysis are listed in Table 4.19.

Table 4.19: Commercial enzymes used for microalgal biomass hydrolysis.

Enzyme	Activity	Manufacturer
Cellic® CTec3 HS	Cellulase, ß-glucosidase, hemicellulase	Novozymes (Denmark)
Hemicellulase from *A. niger*	Hemicellulase	Sigma-Aldrich (Germany)
Protamex®	Endo-protease	Novozymes (Denmark)
Protease from *A. saitoi*	Protease, ß-glucosidase	Sigma-Aldrich (Germany)
Rohalase® GMP	Endo-mannanase	AB Enzymes (Germany)
Rohament® CEP	Cellulase, ß-glucosidase, hemicellulase	AB Enzymes (Germany)

In some cases, a pretreatment with proteases was performed prior to the addition of polysaccharide-degrading enzymes to determine, if this would increase the accessibility of carbohydrates for the latter enzymes. Since the optimal pH and temperature conditions to achieve maximum activity is

different for each enzyme, these parameters were adjusted differently for the proteolysis and the following polysaccharide hydrolysis, which are listed in Table 4.20.

Table 4.20: Hydrolysis conditions set for different enzymes for optimal enzyme activity according to manufacturer specifications.

Enzyme	pH	Temperature
Protamex®	7.0	37 °C
Protease from *A. saitoi*	3.5	37 °C
Other enzymes	5.0	50 °C

4.9.6. Phosphorus elimination

For phosphorus elimination a phosphate precipitation method including the addition of a precipitating agent, namely $FeCl_3$, was adopted. Initial experiments were carried out using a phosphate buffer containing 0.209 g L^{-1} Na_2HPO_4 and 0.035 g L^{-1} KH_2PO_4 corresponding to a Na_2HPO_4:KH_2PO_4 stoichiometric ratio of 5.75 and a phosphate concentration of 164.3 mg L^{-1}. 50 mL of phosphate buffer was transferred into a 50 mL centrifugation tube and the amount of 0.24 M $FeCl_3 \cdot 6\ H_2O$ solution required to achieve the desired Fe:P stoichiometric ratio was added. The pH of the reaction mixture was adjusted to pH 4.5–5.5 by addition of 3 M KOH solution. Then, the reaction mixture was thoroughly mixed using a vortex mixer and incubated for 20 minutes. Finally, the reaction tubes were centrifuged at 3260 rcf and phosphate concentration of the supernatant was determined using a colorimetric test kit (Phosphate colorimetric kit, Sigma-Aldrich, Munich, Germany).

Preliminary experimentation for phosphorus elimination of microalgae hydrolysate was carried out in 50 mL centrifugation tubes as described above. Deviations from the standard procedure are given for each experiment specifically in Section 7.4. Scale-up of phosphate precipitation of microalgae hydrolysate to 200 L was performed in a tempered stirred-tank (M500L, Bioengineering AG, Wald, Switzerland) with pH monitoring. For phosphate precipitation on a 200 L scale, required amounts of $FeCl_3 \cdot 6\ H_2O$ and KOH were added to microalgae hydrolysate in solid form to prevent a significant dilution of the resulting hydrolysate and multiple successive precipitation step were required to achieve sufficiently low phosphate depletion. Detail procedure of the phosphorus elimination of microalgae hydrolysate is given in Section 7.4. Separation of the precipitated iron(III) phosphate on a 200 L scale was done by centrifugation using a disk separator (CSA 08-06-476, GEA Westfalia Separator Group, Oelde, Germany).

4.9.7. Final processing and sterilization

After phosphorus elimination and centrifugation with a disk separator, microalgae hydrolysate was centrifuged again at 14,000 rcf for 15 minutes to separate the remaining fine cell debris, which could not be eliminated using the disk separator with lower centrifugal force. Subsequently, the hydrolysate sterilized by filtration (0.22 µm) and stored at –4 °C until further use.

4.10. Analytical methods

4.10.1. Optical density

Cell density of the yeast culture was determined by optical density measurement at 600 nm (OD_{600}) against culture medium in triplicate using a UV–vis spectrophotometer (Genesys 10S UV–VIS, Thermo Fisher Scientific Inc., Waltham, MA, USA). PBS (see Table 4.8) was used for dilution of the samples into the linear correlation range of the photometer. Whenever dilution of a sample was necessary, the blank was also diluted with the same dilution factor using PBS.

Cell density of the microalgae culture was measured by determining the optical density at 750 nm (OD_{750}) against a salt solution (2.7% *(w/w)* NaCl) in triplicate, using a UV–Vis spectrophotometer (Genesys 10S UV–VIS, Thermo Fisher Scientific Inc., Waltham, MA, USA). The same salt solution, matching the salinity of the ASW medium, was also utilized to dilute the samples into the linear correlation range of the photometer.

4.10.2. Cell dry weight concentration

Cell dry weight (CDW) concentration was determined using different methods in experiments with different microorganisms. For yeast processes CDW of each sample was measured in triplicate gravimetrically by centrifugation (at 20,817 rcf for 5 min) of the samples in pre-dried and pre-weighed tubes and drying the pellet for at least 48 h at 70 °C before weighing a second time. The CDW concentration was then calculated by dividing the difference in dry weight by the volume of the sample initially centrifuged.

CDW of each microalgae sample was measured in triplicate gravimetrically by pipetting at least 2 mg of the samples onto pre-dried and pre-weighed glass microfibre filters (Whatman® glass microfibre filters Grade GF/C, Cytiva Europe GmbH, Munich, Germany) using a Büchner funnel, washing with 1 mL of distilled water and drying the filters for at least 48 h at 70 °C before weighing a second time. The CDW concentration was then calculated by dividing the difference in dry weight by the volume of the sample pipetted onto the filter. A linear correlation was observed between CDW and OD_{750}, allowing for the estimation of a correlation factor for processes on different scales. These factors were used to derive CDW from OD_{750} measurements.

CDW of high cell density microalgae biomass (100–250 g L^{-1} CDW) with high viscosity was determined in triplicate gravimetrically by spreading a certain amount of sample onto pre-dried and pre-weighed aluminum dishes and drying for at least 72 h at 70 °C before weighing again. The CDW content was then calculated by dividing the difference in dry weight by the mass of the sample spread onto the dish initially.

4.10.3. Salinity and alkalinity

For the determination of salinity and total alkalinity (TA) of the culture medium, each sample was first centrifuged at 14,600 rcf for 4 min. The salinity of the supernatant was measured at least once daily

with a refractometer (Hanna Instruments, Voehringen, Germany), whereas the TA was determined with a colorimetric test according to the manufacturer's instructions (HI755 Checker HC, Hanna Instruments, Woonsocket, RI, USA).

4.10.4. Substrate concentrations

Each sample was centrifuged at 20,817 rcf for 5 min and the supernatant was filtered (0.2 µm) before substrate measurement. Concentrations of glucose, galactose, acetate, urea and ammonia were determined photometrically using enzymatic assays (D-Glucose, Lactose/D-Galactose, Acetate, Urea/Ammonia and Ammonia assay kits, R-Biopharm AG, Darmstadt, Germany). Similarly, concentrations of mannose, rhamnose and xylose were also determined photometrically using enzymatic assays (D-Mannose/D-Fructose/D-Glucose, L-Rhamnose and D-Xylose assay kits, Megazyme, Wicklow, Ireland). Phosphate concentration was measured using a colorimetric test kit (Phosphate colorimetric kit, Sigma-Aldrich, Munich, Germany). Protein content was determined in duplicate using the Pierce™BCA Protein Assay Kit (Thermo Fisher Scientific, Schwerte, Germany).

4.10.5. Lipid concentration and cellular lipid content

The total lipid concentration of a sample was determined using the sulfo-phospho-vanillin (SPV) assay described by Mishra et al. (2014). For preparation of the phospho-vanillin reagent, 0.3 g of vanillin was dissolved in 50 mL of 10% (*v/v*) ethanol in water mixture and mixed with 200 mL of phosphoric acid. 50 µL of each sample was incubated in 1 mL sulfuric acid (98% (*v/v*)) for 10 min at 90 °C in glass vials and cooled at –4 °C for 5 min. Then, 2.5 mL phospho-vanillin reagent was added into each vial and the mixture was incubated in a thermomixer at 37 °C and 900 rpm for 15 min (Thermomixer basic, CellMedia, Elsteraue, Germany). After incubation, the absorption at 530 nm wavelength against air was measured with a UV–vis spectrophotometer (Genesys 10S UV–VIS, Thermo Fisher Scientific Inc., Waltham, MA, USA). Blank values were measured separately and subtracted from the measured absorption values manually. Each sample was measured in triplicate and the sugar-containing samples were washed with demineralized water or PBS (see Table 4.8) to avoid additional color formation, which would interfere with absorption at 530 nm. An external standard of rapeseed oil was used to create a correlation line between absorption and total lipid concentration. For this, different amounts of an oil in hexane solution with known concentration (1 g L^{-1}) was transferred into glass vials. After the hexane was evaporated, 50 µL of demineralized water (same as the sample volume) was added and the standard assay procedure described above was applied. The resulting correlation line had a range of 0.0–2.0 g L^{-1} lipids. Cellular lipid content was calculated from total lipid concentration by dividing it by CDW concentration measured as described in Subsection 4.10.2.

4.10.6. Fatty acid composition

A gas chromatograph with a flame ionization detector (GC–FID) was used to determine the fatty acid (FA) composition of the yeast oil, but also to verify the results of the total lipid concentrations measured using the SPV assay. The samples were prepared by freezing at –80 °C and subsequent lyophilization at –50 °C and 0.12 mbar for at least 48 h (Lyophilizer ALPHA 1–2 LDplus, Martin Christ Gefriertrocknungsanlagen GmbH, Osterode am Harz, Germany). For preparation of the fatty acid

methyl esters (FAME), a direct transesterification procedure by Griffiths et al. (2010) was applied with slight modifications as described previously (Meo et al., 2017): 9–12 mg of lyophilized biomass per sample was used; a 2 mg mL^{-1} solution of C12-TAG (Glyceryl tridodecanoate, Sigma-Aldrich, Taufkirchen, Germany) in toluene was used as internal standard instead of C17-TAG in toluene; as acid catalyst, HCl in methanol solution (5% (*v/v*) concentrated HCl in methanol) was used; use of methyl nonadecanoate (C19-ME) as a secondary internal standard was omitted. After phase separation, the upper layer with the FAME containing hexane–toluene mixture was analyzed via GC–FID (GC-2010 Plus, Shimadzu Deutschland GmbH, Duisburg, Germany) with a fused silica separation column (FAMEWAX, Restek GmbH, Bad Homburg, Germany) using helium as carrier gas (as described previously by Thurn et al. (2022)). The column temperature was started at 120 °C, increased to 220 °C with 7 °C min^{-1}, and finally held at 220 °C for 20 min. The injector and FID temperatures were 220 °C and 250 °C, respectively. Peaks were identified by retention time based on an external standard (Marine Oil Test Mix, Restek GmbH, Bad Homburg, Germany). FA composition was determined by division of the corresponding FAME peak area by the sum of all peaks excluding the internal standard. The individual FA contents of the biomass were calculated by correlating the peak area of the FA to that of the standard with known concentration and normalizing the value to the dry sample weighed initially.

4.10.7. Elemental and macromolecular composition

Carbon, hydrogen, nitrogen, and sulfur (CHNS) contents were analysed using a CHNS elemental analyser (Euro EA CHNS Elemental Analyzer, HEKAtech GmbH, Wegberg, Germany). In the analyser, each sample is combusted using pure oxygen at 1800 °C, and the resulting gas mixture containing CO_2, H_2O, N_2, and SO_2 is fed into a gas chromatography column for separation using helium as carrier gas. Subsequently, the separated gases are measured by a thermal conductivity detector. The C, H, N, and S contents are then calculated as the mass of the element measured per mass of the initially weighed sample. Cell samples were freeze-dried for the analysis, and the oil sample was handled in liquid form. Each sample was measured in triplicate.

Phosphorus content was determined using a colorimetric method. Samples were mineralized in round bottom flasks at 400 °C using concentrated sulphuric acid and fuming nitric acid. Then, the nitrous gases were boiled away. An aliquot part of ammonium vanadate and ammonium molybdate was added to the mixture, and the resulting phosphomolybdic acid was measured against standards photometrically at 650 nm (Cary 100 UV–Vis Spectrophotometer, Agilent, Waldbronn, Germany). Each sample was measured in duplicate.

Macromolecular composition was determined using a combination of measurements from analysis of the samples in this work and literature values. Lipid content was calculated based on measurements of CDW and lipid concentrations as described in subsections 4.10.2 and 4.10.5. Total protein content was calculated from nitrogen content using a correlation factor of 4.4 for microalgal biomass (López et al., 2010) and 5.8 for yeast biomass (Bertolo et al., 2019). Ash content of *M. salina* biomass cultivated in a nutrient-replete medium under the same conditions as in this work was measured to be 10.0% by Schädler et al. (2019). Ash content of *C. oleaginosus* was assumed to be 7.0% based on the average of the ash content data reported by Agboola et al. (2021) for various

yeast species. The remaining portion of the biomass is assumed to be carbohydrates.

4.10.8. Degree of cell disruption

For quantitative evaluation of the mechanical disruption of *M. salina* cells each sample was measured using a flow cytometer (CytoFLEX V0-B4-R2, Beckman Coulter GmbH, Krefeld, Germany). The proportion of intact cells and cell debris as a frequency in total incidence count was based on shifts in the measured forward-scattered light (FSC) and the fluorescence in the wavelength range of 640–780 nm ($F_{640–780}$). The use of $F_{640–780}$ for the analysis is based on an empirical approach making use of the fluorophore content of microalgae, such as allophycocyanin with an emission peak at 660 nm, which would presumably be released upon cell disruption (Yeh et al., 1987). In order to ensure an accurate measurement each sample was diluted to an OD_{600} of around 0.150 using distilled water and the flow rate was adjusted to a value corresponding to less than 3,000 incidences per second. Per sample 100,000 incidences were recorded and used to plot a log–log graph of $F_{640–780}$ values with respect to FSC. The areas occupied by distilled water, intact *M. salina* cells, and cell debris as well as an unknown fraction were marked on this dot-plot to sort the incidences accordingly. The degree of cell disruption (DCD) was then calculated as:

$$DCD = \frac{i_{cells}}{(i_{cells} + i_{debris})} \tag{4.5}$$

where i_{cells} and i_{debris} are the incidence counts of intact cells and cell debris, respectively.

4.11. Process metrics

4.11.1. Specific rates and yields

Cell specific substrate uptake rate (q_S) is used to evaluate the utilization of different substrates by the yeast and is calculated using a differential method as follows:

$$q_S = \frac{(m_{S,up,2} - m_{S,up,1})}{(t_2 - t_1) \cdot \left(\frac{m_{X,1} + m_{X,2}}{2}\right)} \tag{4.6}$$

where m_X is the mass of lipid-free biomass produced, $m_{S,up}$ is the mass of substrate taken up, and t is process time.

Biomass yield (Y_{XS}) was calculated cumulatively over the process time using the following equation:

$$Y_{XS} = \frac{(m_{X,t} - m_{X,0})}{m_{S,up,t}} \tag{4.7}$$

Lipid yield (Y_{LS}) was also determined cumulatively over the process time as:

$$Y_{LS} = \frac{(m_{L,t} - m_{L,0})}{m_{S,up,t}} \tag{4.8}$$

where m_L is the mass of lipids produced. In all equations $m_{S,up}$ was calculated by subtracting the remaining substrate mass from the sum of substrate mass added into the system with the batch and

feed media until the indicated process time as follows:

$$m_{S,up} = m_{S,in} - m_{S,R} = (c_{S,0} \cdot V_{R,0} + c_{S,feed} \cdot \dot{V}_{in} \cdot t) - (c_{S,t} \cdot V_{R,t} + c_{S,out} \cdot \dot{V}_{out} \cdot t) \quad (4.9)$$

where $m_{S,in}$ is the mass of substrate supplied into the reactor, $m_{S,R}$ is the total mass of remaining unused substrate, $c_{S,0}$ is the initial substrate concentration, $V_{R,0}$ is the initial reaction volume, $c_{S,feed}$ is the substrate concentration of the feed medium, $\dot{V}_{in}$ is the volumetric flow rate of the feed stream, c_S is the substrate concentration, V_R is the liquid volume in the reactor, $c_{S,out}$ is the substrate concentration in the outlet stream, and $\dot{V}_{out}$ is the volumetric flow rate of the outlet stream (permeate).

4.11.2. Areal and volumetric productivities

Volumetric productivity (P_V) is calculated from the produced amount of product mass between process time t and the starting time of the process t_0 per initial reaction volume:

$$P_V = \frac{(m_{P,t} - m_{P,0})}{V_{R,0} \cdot (t - t_0)} \quad (4.10)$$

In microalgae processes the areal and volumetric productivities pertain to biomass productivity, whereas in yeast processes they refer to total lipid productivity, since these are the desired products of each process in this work.

Although volumetric productivity is usually referred to as the main performance indicator of an industrial process, areal productivity is a better suited indicator for microalgae cultivation in TLC photobioreactors. The reason for this is the solar energy input, or in other words the photosynthetic photon flux density (PPFD), being dependent on the unit surface area of the reactor and not the reaction volume. Hence, areal productivity is used to evaluate the performance of microalgae processes carried out in this work. Areal productivity (P_A) is calculated from the volumetric productivity using the specific volume to area ratio of the TLC reactor used in the process:

$$P_A = P_V \cdot \frac{V_R}{A} \quad (4.11)$$

For microalgae processes in this work, integral areal productivity is calculated cumulatively over the process time, whereas daily areal productivity is determined for the last 24 h starting at 10 a.m..

4.11.3. Carbon dioxide fixation efficiency

In the production of microalgal biomass CO_2 and urea serve as the only carbon sources. CO_2 fixation efficiency (η_{CO_2}) was defined as the mass of carbon fixated in biomass divided by the total carbon mass supplied to the system. Using the carbon content of *M. salina* measured by elemental analysis ($x_{C,Ms} = 0.53$, see Subsection 4.10.7) the CO_2 fixation efficiency can be expressed as:

$$\eta_{CO_2} = \frac{0.53 \cdot (m_{CDW,t} - m_{CDW,0})}{x_{C,CO_2} \cdot \int_0^t \dot{m}_{CO_2} dt + x_{C,Urea} \cdot m_{Urea,t}} \quad (4.12)$$

where x_{C,CO_2} and $x_{C,Urea}$ are the mass fractions of carbon in CO_2 and urea, respectively, $\dot{m}_{CO_2}$ is the CO_2 mass flow rate and $m_{Urea,t}$ is the total supplied mass of urea at time t.

4.11.4. Carbon conversion efficiency

The carbon initially present in the medium in the form of sugars and vitamins is used by the yeast cells for cell growth, lipid production, and for energy gain by respiration generating CO_2. The overall carbon balance was calculated based on this premise using the measured elemental composition of the cells and the yeast oil. The carbon balance can be formulated as:

$$m_{C,in} - m_{C,out} = (m_{S,in} - m_{S,out}) \cdot x_{C,S} + m_{Vit,in} \cdot x_{C,Vit} = m_X \cdot x_{C,X} + m_L \cdot x_{C,Lipid} + R_{rest} \quad (4.13)$$

where $m_{C,in}$ is the total carbon mass fed into the system, $m_{C,out}$ is the carbon mass leaving the system through the permeate stream, $m_{S,in}$ is the total sugar mass fed, $m_{Vit,in}$ is the total vitamin mass fed, $m_{S,out}$ is the total sugar mass exiting the system, m_X is the lipid-free CDW produced, m_L is the lipid mass generated, $x_{C,S}$ is the overall carbon fraction of the sugars, $x_{C,Vit}$ is the carbon fraction of the vitamins, $x_{C,X}$ is the carbon fraction of the lipid-free CDW, $x_{C,Lipid}$ is the carbon fraction of the lipids, and R_{rest} is the remaining carbon mass, which is presumed to be oxidized by respiration and thus can be expressed as follows:

$$R_{rest} = m_{CO_2} \cdot x_{C,CO_2} \quad (4.14)$$

where m_{CO_2} is the mass of carbon dioxide generated and x_{C,CO_2} is the fraction of carbon in CO_2. An alternative way to calculate the amount of carbon mass exiting the system in form of CO_2 (m_{C,CO_2}) based on process data on gas inlet and outlet streams is integrating Eq. (3.24) over process time to get the total amount of CO_2 generated as follows:

$$m_{C,CO_2} = \frac{dn_{CO_2}}{dt} \int_0^t \cdot M_{CO_2} \cdot x_{C,CO_2} \quad (4.15)$$

where M_{CO_2} is the molar mass of CO_2. Such a calculation using gas analysis data can also be used to verify the validity of Equation (4.14).

Carbon conversion efficiency (η_C) is defined as the fraction of total carbon taken-up by the cells in form of sugars and vitamins, which is converted into lipids at the end of the process:

$$\eta_C = \frac{m_L \cdot x_{C,Lipid}}{m_{C,in} - m_{C,out}} \quad (4.16)$$

Carbon conversion efficiency was calculated differently, when microalgae biomass hydrolysate was used as feeding medium. Here, the fraction of total carbon taken-up by the cells ($m_{C,in} - m_{C,out}$) was the sum of carbon present in the batch medium in form of sugars and carbon supplied with hydrolysate feed minus carbon leaving the system through the permeate stream, based on the carbon content of hydrolysate and permeate determined by elemental analysis.

4.11.5. Saccharification efficiency

Saccharification efficiency (η_{sac}) is defined as the ratio of sugars released from the carbohydrates in a biomass to the theoretical maximum of releasable sugars and is calculated for microalgae biomass

hydrolysis as follows:

$$\eta_{sac} = \frac{(c_{glucose} + c_{mannose})}{c_X \cdot x_{X,carb} \cdot (x_{carb,glucose} + x_{carb,mannose})} \tag{4.17}$$

where $c_{glucose}$ and $c_{mannose}$ are the glucose and mannose concentrations in the hydrolysate, respectively, $x_{X,carb}$ is the carbohydrate fraction of the CDW of the microalgae, and $x_{carb,glucose}$ and $x_{carb,mannose}$ are the glucose and mannose mass fractions in the carbohydrates of the microalgae, respectively. Here, only glucose and mannose were taken into account, since these make up over 80% of the total sugar content of *M. salina* and were the target of enzymatic hydrolysis. Schädler et al. (2019) determined the carbohydrate fraction of *M. salina* grown in TLC PBR in nutrient-replete medium to be 26% of its CDW and its sugar composition as listed in Table 4.21. These literature values were used to calculate the saccharification efficiency in this study.

Table 4.21: Sugar composition of *M. salina* grown in TLC PBR in nutrient-replete medium as measured by Schädler et al. (2019).

Carbohydrate moiety	**Mass fraction in CDW, mg g^{-1}**	**Mass fraction in total sugars, %**
Glucose	161.5	62.7
Mannose	50.1	19.5
Galactose	17.2	6.8
Rhamnose	12.8	5.0
Other sugars	15.9	6.0

5. Production of *Microchloropsis salina* Biomass in Open Thin Layer Cascade Photobioreactors [1]

In this chapter, the production of microalgal biomass with *M. salina* in open thin-layer cascade (TLC) photobioreactors (PBRs) is examined by applying different modes of operation. Microalgae were cultivated in an artificial seawater (ASW) medium controlled at pH 8.5, unless stated otherwise, by the addition of CO_2 under physical simulation of the Mediterranean summer climate in Spain. Biomass productivity and CO_2 fixation efficiency were maximized by studying various operational parameters in reactors with an 8 m^2 surface area, followed by a scale-up of the processes with the highest areal productivity onto a pilot scale reactor with a 50 m^2 surface area. Additionally, the effect of pH on process performance and a switch-off of the circulation pumps overnight to reduce energy consumption were investigated. A productivity comparison with a summary of the determined conditions to achieve optimal biomass productivity and CO_2 fixation efficiency, as well as the harvest of the biomass produced, are presented at the end of this chapter.

5.1. Batch production

A series of experiments for biomass production on an 8 m^2 scale in batch mode were carried out to determine the maximum possible areal productivity, as well as when and at which cell dry weight (CDW) concentration it is reached. Thereupon, an experiment in batch mode on a 50 m^2 scale was performed to determine how the results compare to the scaled-up process metrics. In all processes, concentrations of the medium salts (NaCl, $MgSO_4$ and $CaCl_2$) were kept constant in the reaction medium, whereas the remaining medium components were supplied as a concentrated solution additionally over the whole process to avoid nutrient depletion in the medium and to keep the urea concentration at 0.5–1.5 g L^{-1}. For easier description, the average nutrient feed rate ($r_{feed,ave}$) in batch processes is expressed in terms of a factor (F) of the nutrient concentration in the ASW medium as follows using Equation (4.1):

$$r_{feed,ave} = \frac{m_{nutrient,in}}{V_R \cdot t} = \frac{F \cdot c_{nutrient,ASW}}{t} = F \times \text{ASW per day}$$

where $m_{nutrient,in}$ is the mass of nutrients fed, V_R is the reaction volume (i.e. volume of algae suspension inside the reactor), t is the process time in days, and $c_{nutrient,ASW}$ is the nutrient concentration in the ASW medium as given in Table 4.1. All batch processes were started with a nutrient concentration of 2× that of the ASW medium.

Figure 5.1 shows the results of all experiments performed in batch operational mode. Experiments in TLC PBRs with 8 m^2 surface area were carried out with similar nutrient supply rates. In experiments B1, B2, and B3, averaged over the whole process time, the resulting average feed rate ($r_{feed,ave}$) was 1.5×, 1.6×, and 1.4× ASW per day, respectively. As seen in Figure 5.1 A, a CDW concentration

[1] Part of the results presented here has already been published in: Koruyucu, A., Schädler, T., Gniffke, A., Mundt, K., Krippendorf, S., Urban, P., Blums, K., Halim, B., Brück, T., Weuster-Botz, D (2024). Energy-Efficient Production of *Microchloropsis salina* Biomass with High CO_2 Fixation Yield in Open Thin-Layer Cascade Photobioreactors. *Processes*, *12*, 1303. doi:10.3390/pr12071303

of 43–48 g L^{-1} was reached after 17 days in all experiments. In experiments B1 and B2 maximum integral areal productivities of 17.2 g m^{-2} d^{-1} and 19.1 g m^{-2} d^{-1} were recorded on day 17, respectively, while in experiment B3 the maximum of 19.4 g m^{-2} d^{-1} was achieved after 11 days and kept decreasing from there on until the end of the process as shown in Figure 5.1 B. In any case, no significant increase of the integral areal productivity was observed in any of the experiments after day 11. The CDW concentration achieved at the end of day 11 ranged between 25.2–31.9 g L^{-1}.

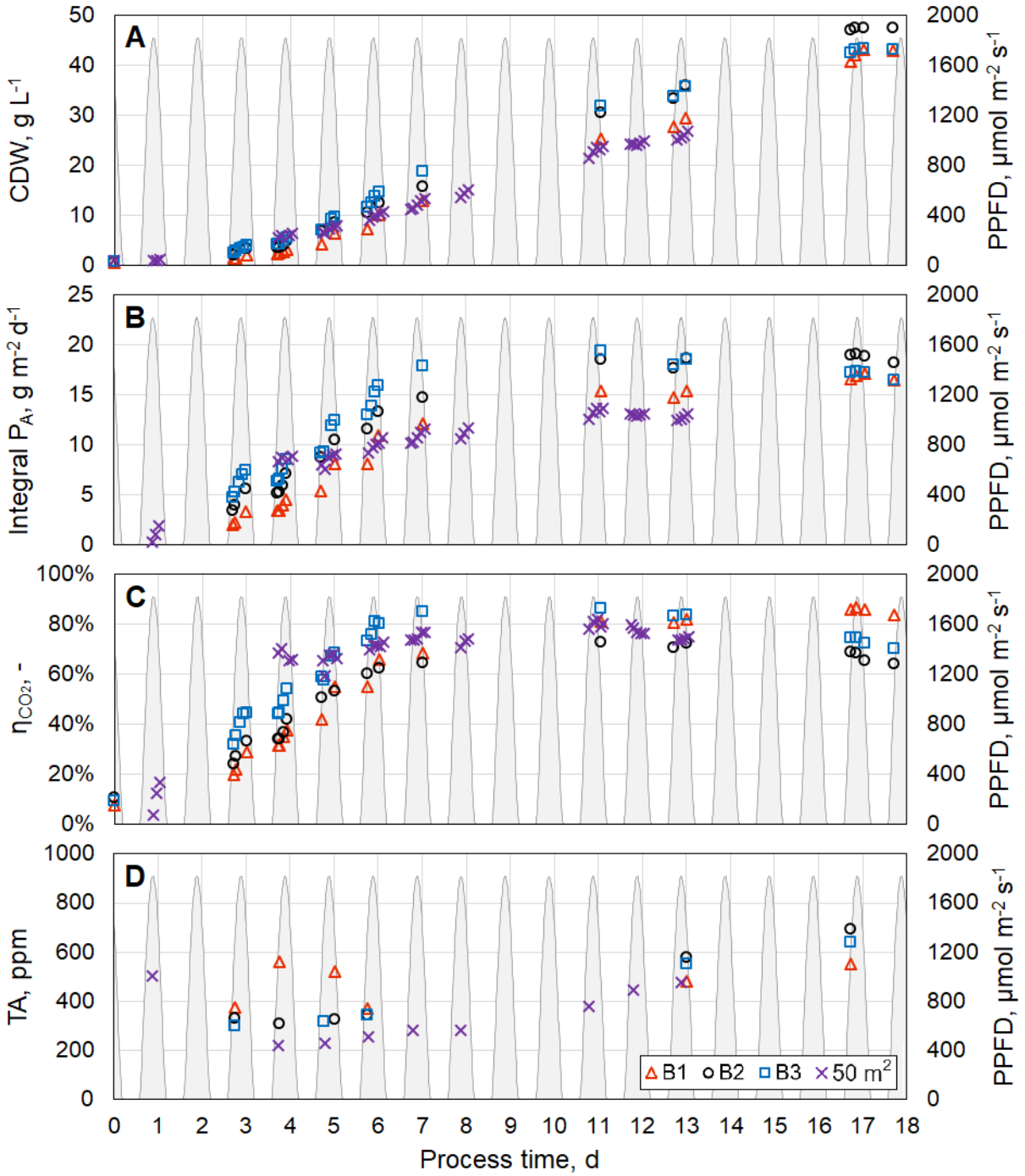

Figure 5.1: Biomass production with *M. salina* in open TLC photobioreactors in batch mode. Presented are three experiments B1 (△), B2 (○), and B3 (□) on an 8 m^2 scale and the scale-up experiment on a 50 m^2 scale (×). **A**: CDW concentration (c_X); **B**: integral areal productivity (P_A); **C**: CO_2 fixation efficiency (η_{CO_2}); **D**: total alkalinity (TA). Photosynthetic photon flux density (PPFD) is given on the secondary vertical axis and marked in grey to highlight the daytime.

The scale-up of the batch process to the TLC PBR with 50 m^2 surface area was carried out success-

fully. Manual supply of the concentrated nutrient solution to keep the urea concentration at 0.5–1.5 g L^{-1} resulted in an average nutrient feed rate of 1.62× ASW per day. Although the experiment was terminated after 13 days, which is a bit shorter than the preliminary experiments on the 8 m^2 scale, the maximum integral areal productivity of 13.6 g m^{-2} d^{-1} was observed similarly after 11 days and started to decrease after that. On the 50 m^2 scale, a CDW concentration of 23.7 g L^{-1} was documented on the day of maximum integral areal productivity, which is rather at the lower end of the range observed in processes on the 8 m^2 scale.

In Figures 5.1 C and D, CO_2 fixation efficiency and total alkalinity (TA) during all batch processes are plotted. In experiment B1, a maximum of 86.6% CO_2 fixation efficiency was achieved on day 17, whereas in experiments B2 and B3, the maximum values of 72.9% and 86.5%, respectively, were observed after 11 days simultaneously with the maximum productivity. In the scale-up experiment in the 50 m^2 TLC PBR, the maximum CO_2 fixation efficiency of 81.9% was reached after 11 days likewise. In all experiments, the TA was kept under 700 ppm by intermittent addition of sulphuric acid.

Discussion

In batch processes for microalgal biomass production with *M. salina* in TLC PBR, biomass concentrations of 43–48 g L^{-1} CDW were reached in 17 days. Using the same set-up under nutrient-replete conditions, Apel et al. (2017) reported achieving a CDW concentration of 38–42 g L^{-1} in the same time frame, after which the microalga growth stagnated, reaching a maximum of 50 g L^{-1} CDW concentration after 24 days. Similarly, under the same conditions, Schädler et al. (2019) stated to reach 30 g L^{-1} in 14 days. Thus, the results regarding CDW concentration are consistent with the literature data. Areal productivity achieved on an 8 m^2 scale ranged between 17–19 g m^{-2} d^{-1}, which is very similar to 15–18 g m^{-2} d^{-1} documented by Apel et al. (2017), although a lower areal productivity of 12–13 g m^{-2} d^{-1} was observed on a 50 m^2 scale in this study. Apel et al. (2017) also reported for a batch process that the maximum integral areal productivity was achieved after 9 days, remaining stable until day 16 and declining after that until the end of the process, which is very much in conformity with the course of areal productivity observed in this study.

Comparing the data on CO_2 fixation efficiency and TA on the last days of the experiments on the 8 m^2 scale, the inverse proportionality of these two becomes apparent. The timing of the decline in CO_2 fixation efficiency correlates with an increase in TA in all processes. Thus, it is suggested that a lower TA value directly correlates with a higher CO_2 fixation efficiency. Keeping the TA under 500 ppm would help prevent a decrease in CO_2 fixation efficiency. This was already suggested by Schädler et al. (2019) reporting a 20–30% increase in CO_2 fixation efficiency in a TLC PBR with 8 m^2 surface area, achieving a stable 84% for a one-week period, which was also verified in this study on an 8 m^2 scale as well as on the pilot scale.

5.2. Semi-continuous production

A series of experiments for biomass production with *M. salina* in semi-continuous mode was carried out in TLC reactors with 8 m^2 surface area to find out if a higher maximum of integral areal productivity can be achieved and sustained over a longer period of time in comparison to the batch operation.

Semi-continuous operation of TLC PBRs was performed as described in Section 4.4 with only the daily starting CDW concentration being varied between individual experiments.

In all processes, concentrations of the medium salts (NaCl, $MgSO_4$ and $CaCl_2$) were kept constant in the reaction medium, whereas the remaining medium components were supplied in the form of a concentrated solution over the whole process to avoid nutrient depletion in the algae suspension and to keep the urea concentration at 0.5–1.5 g L^{-1} at all times. Similarly to batch processes, the average nutrient feed rate ($r_{feed,ave}$) in semi-continuous processes is expressed in terms of a factor (F) of the nutrient concentration in the ASW medium as follows using Equation (4.1):

$$r_{feed,ave} = \frac{m_{nutrient,in}}{V_R \cdot t} = \frac{F \cdot c_{nutrient,ASW}}{t} = F \times \text{ASW per day}$$

All semi-continuous processes were started the same way as batch processes, with a nutrient concentration of 2× that of the ASW medium. The semi-continuous operation began after the microalgae suspension reached the desired CDW concentration, corresponding to the preselected biomass density at the start of each day. After that, every day at 10 a.m. except on weekends, a portion of the suspension was harvested from the reactor and replaced with fresh ASW medium in order to bring the CDW concentration to the desired value. Additional concentrated feed medium was manually added whenever needed to keep the urea concentration in the desired range throughout the process.

Figure 5.2 shows the results of this experimental series in the semi-continuous mode of operation. After an initial batch phase to achieve the desired biomass concentration, the daily starting CDW concentration during semi-continuous operation was kept at different set-points of 8 g L^{-1}, 11 g L^{-1}, 13 g L^{-1}, and 20 g L^{-1} in these experiments. The average nutrient feed rate ($r_{feed,ave}$) was 1.5–1.7× ASW per day in all four experiments. As seen in Figure 5.2 A, the length of the batch phase for initial biomass production was different between experiments, lasting 10 days for a daily starting CDW concentration of 8 g L^{-1} and 13–14 days in the remaining experiments. Throughout the semi-continuous operation, the integral areal productivity kept on increasing in all experiments, as apparent in Figure 5.2 B. For experiments with a similar daily starting biomass concentration of 8–13 g L^{-1} CDW, the areal productivity reached 11.3–12.4 g m^{-2} d^{-1}. The maximum areal productivity of 21.1 g m^{-2} d^{-1} was achieved with a CDW concentration of 20 g L^{-1}, which is the highest in this experiment series.

Figures 5.2 C and D show the change of CO_2 fixation efficiency and TA over the process time. The initial CO_2 fixation efficiency in experiments with a CDW concentration of 8 g L^{-1} and 13 g L^{-1} fall slightly higher than the rest due to a difference in inoculation conditions. In these experiments, the TA was at 555–557 ppm on average, and it stayed around 700 ppm for one week during the batch phase. Maximum CO_2 fixation efficiency reached with a CDW concentration of 8 g L^{-1} and 13 g L^{-1} was 62% and 71%, respectively. Although the fixation efficiency kept increasing throughout these two experiments and did not reach a final value, it should be noted that the TA has also declined over the process time, thus having a positive effect on the CO_2 fixation efficiency. On the other hand, in experiments with a CDW concentration of 11 g L^{-1} and 20 g L^{-1}, maximum CO_2 fixation efficiencies of 83% and 89% were recorded with an average TA of 403 ppm and 402 ppm, respectively.

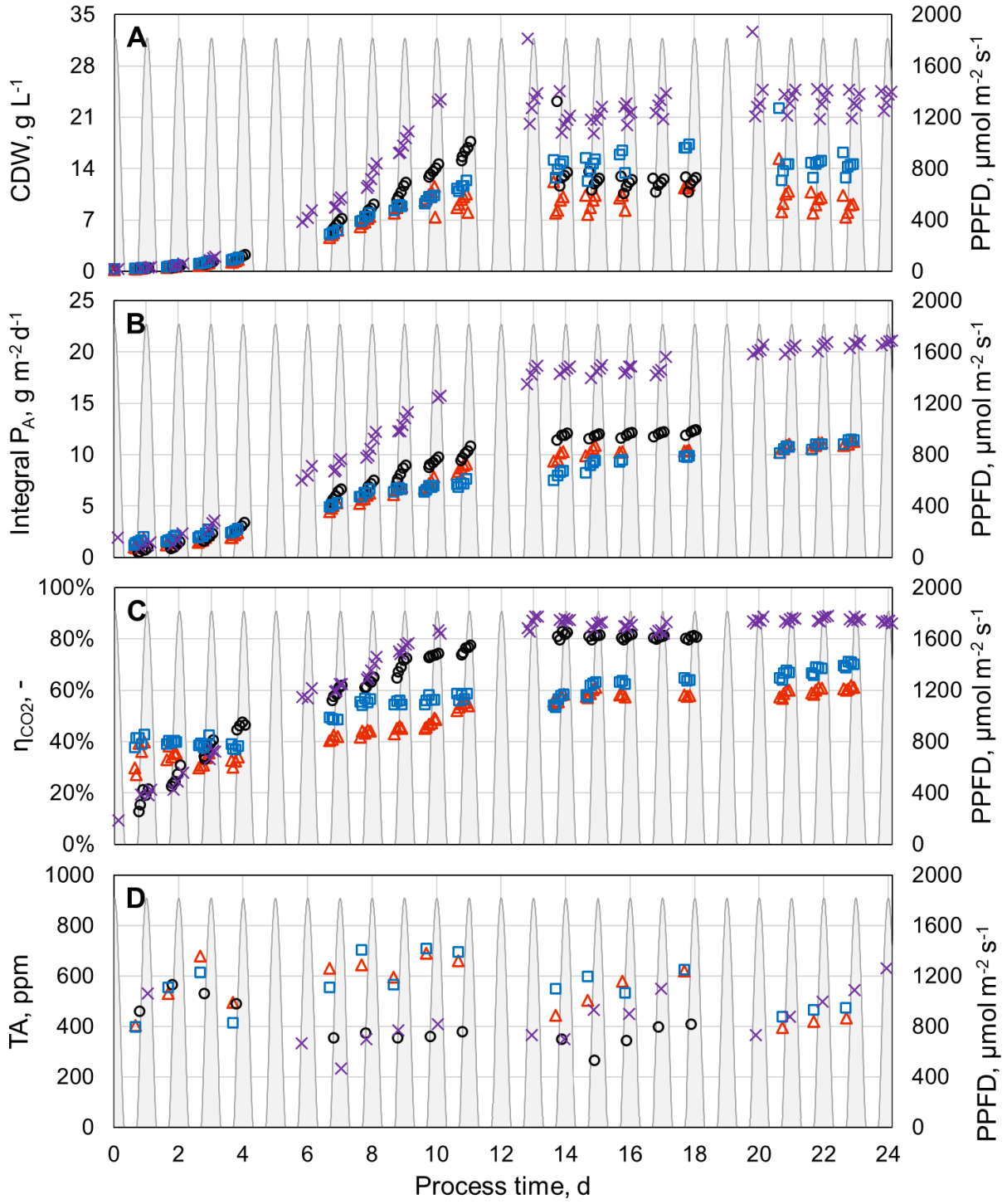

Figure 5.2: Variation of CDW concentration for biomass production with *M. salina* in open TLC photobioreactors in semi-continuous mode. Presented are experiments with a daily starting CDW concentration of 8 g L^{-1} (△), 11 g L^{-1} (○), 13 g L^{-1} (□), and 20 g L^{-1} (×) on an 8 m^2 scale. **A**: CDW concentration (c_X); **B**: integral areal productivity (P_A); **C**: CO_2 fixation efficiency (η_{CO_2}); **D**: total alkalinity (TA). Photosynthetic photon flux density (PPFD) is given on the secondary vertical axis and marked in grey to highlight the daytime.

Two experiments were carried out to scale up the semi-continuous biomass production with *M. salina* to the pilot scale in the TLC PBR with 50 m^2 surface area as illustrated in Figure 5.3. In both cases, the daily starting CDW concentration in the semi-continuous phase was kept at 18.5 g L^{-1}. However, the nutrient feed rates were adjusted differently, namely to 1.8× and 2.8× ASW per day on average. As can be seen in Figure 5.3 A, with a lower feeding rate, the batch phase took longer, namely 13

days, compared to the 7 days of batch phase with a higher feeding rate. However, this is also partly due to a technical issue with the light-emitting diode (LED) lights, which caused the light supply to be cut off completely for a whole day on day 5 of the experiment with a lower nutrient feeding rate.

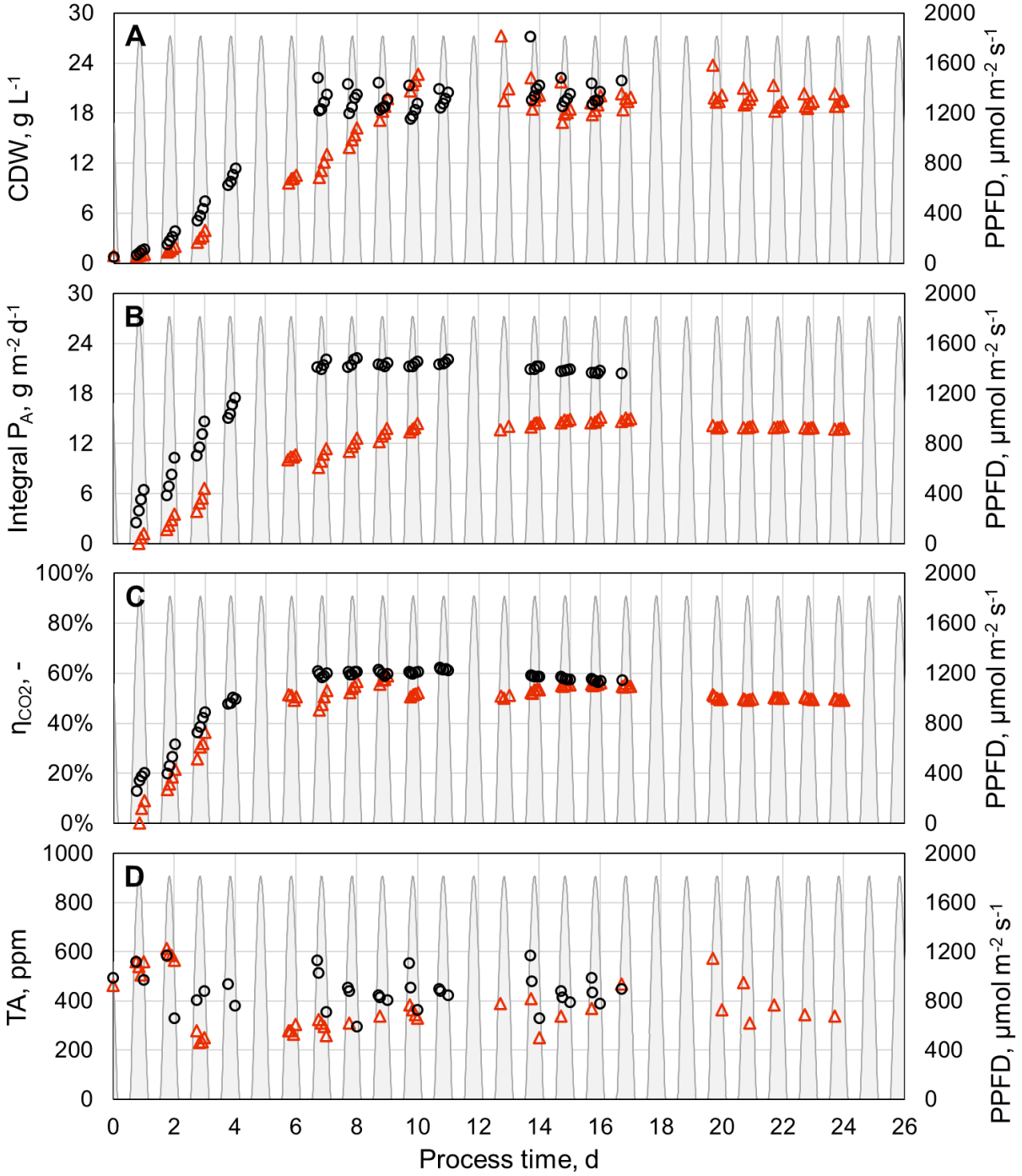

Figure 5.3: Scale-up of biomass production with *M. salina* in semi-continuous mode to 50 m^2 TLC photobioreactor. Presented are two experiments carried out with a daily starting CDW concentration of 18.5 g L^{-1} during semi-continuous operation with average nutrient feed rates of 1.8× ASW per day (△) and 2.8× ASW per day (○). **A**: CDW concentration (c_X); **B**: integral areal productivity (P_A); **C**: CO_2 fixation efficiency (η_{CO_2}); **D**: total alkalinity (TA). Photosynthetic photon flux density (PPFD) is given on the secondary vertical axis and marked in grey to highlight the daytime.

The influence of the feed rate on the integral areal productivity is apparent in Figure 5.3 B. With an average nutrient feed rate of 1.8× ASW per day, maximum integral areal productivity achieved during

semi-continuous operation was 15.2 g m^{-2} d^{-1} and the maximum daily areal productivity recorded on a single day was 22.4 g m^{-2} d^{-1}. With an average nutrient feed rate of 2.8× ASW per day, the maximum integral areal productivity achieved during semi-continuous operation was much higher, namely 21.3 g m^{-2} d^{-1}. Still, the maximum daily areal productivity reached on a single day was similar with 22.2 g m^{-2} d^{-1}. With an average nutrient feed rate of 2.8× ASW per day, the estimated urea concentration in the microalgae suspension was kept between 0.3–3.1 g L^{-1} at all times, with an average of 1.0 g L^{-1} over the whole process.

In Figures 5.3 C and D, CO_2 fixation efficiency and TA in these scale-up experiments with different nutrient feeding rates are shown. With an average nutrient feed rate of 1.8× ASW per day and an average TA of 385 ppm, an average CO_2 fixation efficiency of 52% was achieved during the semi-continuous operation, with a temporary maximum at 56%. With an average nutrient feed rate of 2.8× ASW per day, a slightly higher average CO_2 fixation efficiency of 59% was recorded, with a maximum at 62%, although the average TA of 445 ppm was higher than with a lower feed rate. However, it is visible that the CO_2 fixation efficiency kept declining until the end of the process in both experiments, holding the same value of 57% on day 17. Regarding the process scale-up to 50 m^2, it was noted that the areal productivities reached are very similar between the 8 m^2 and the 50 m^2 scales, when the same CDW concentration is adjusted at the beginning of each day and there is no nutrient limitation. Nonetheless, CO_2 fixation efficiency is much lower in processes on the 50 m^2 scale, namely around 25–30% less than on the 8 m^2 scale.

Discussion

As expected, the areal productivity of microalgal biomass production in TLC PBRs depends very much on the CDW concentration. In semi-continuous processes operated at a CDW concentration range of 8–25 g L^{-1}, areal productivity was higher for higher CDW concentrations in the investigated range. In comparison to batch mode, areal productivity was increased from 17–19 g m^{-2} d^{-1} to 20–21 g m^{-2} d^{-1} using semi-continuous operation without any sign of productivity decline until the end of the process after 24 days.

It has already been suggested in the literature that higher integral areal productivity can be achieved in a semi-continuous mode compared to batch production. He et al. (2016) reported that switching to semi-continuous operational mode increased areal productivity by 35–88% compared to batch mode. Similarly, Yadav et al. (2020) stated that switching from batch to semi-continuous operation increased areal productivity from 3.3 g m^{-2} d^{-1} to 11.5 g m^{-2} d^{-1} in outdoor raceway ponds. Thus, the results are in line with the literature.

In semi-continuous experiments on an 8 m^2 scale, CO_2 fixation efficiency ranged between 80–90% if the TA was kept below 500 ppm, which is consistent with the CO_2 fixation efficiencies observed in batch processes. In addition, Figure 5.2 implies that even though both TA and CDW concentration affect the CO_2 fixation efficiency, the influence of TA is much more significant than that of biomass concentration, since it was possible to achieve over 80% efficiency also at lower CDW concentrations of 10–14 g L^{-1} as long as the TA was kept below 500 ppm (10 mM) throughout the process.

On the pilot scale, maximum integral areal productivity achieved with an average nutrient feed rate of 1.8× ASW per day was 15.2 g m^{-2} d^{-1} during the semi-continuous operation, which is lower than 17–19 g m^{-2} d^{-1} achieved under very similar conditions on the 8 m^2 scale. With an average nutrient feeding rate of 2.8× ASW per day, on the other hand, the maximum integral areal productivity achieved on the pilot scale was much higher, namely 21.3 g m^{-2} d^{-1} during the semi-continuous operation. The only difference between the two experiments on the pilot scale was the average daily medium feeding rate. Hence, it can be concluded that higher productivity can be reached by increasing the nutrient feeding rate, most likely to a sufficient level to prevent nutrient limitation. It should, however, be considered that high ammonia concentrations in cultivation medium can be toxic for microalgae, meaning that the urea concentration should be kept in a certain range that allows the fast growth of microalgae without nutrient limitation and without causing ammonia intoxication.

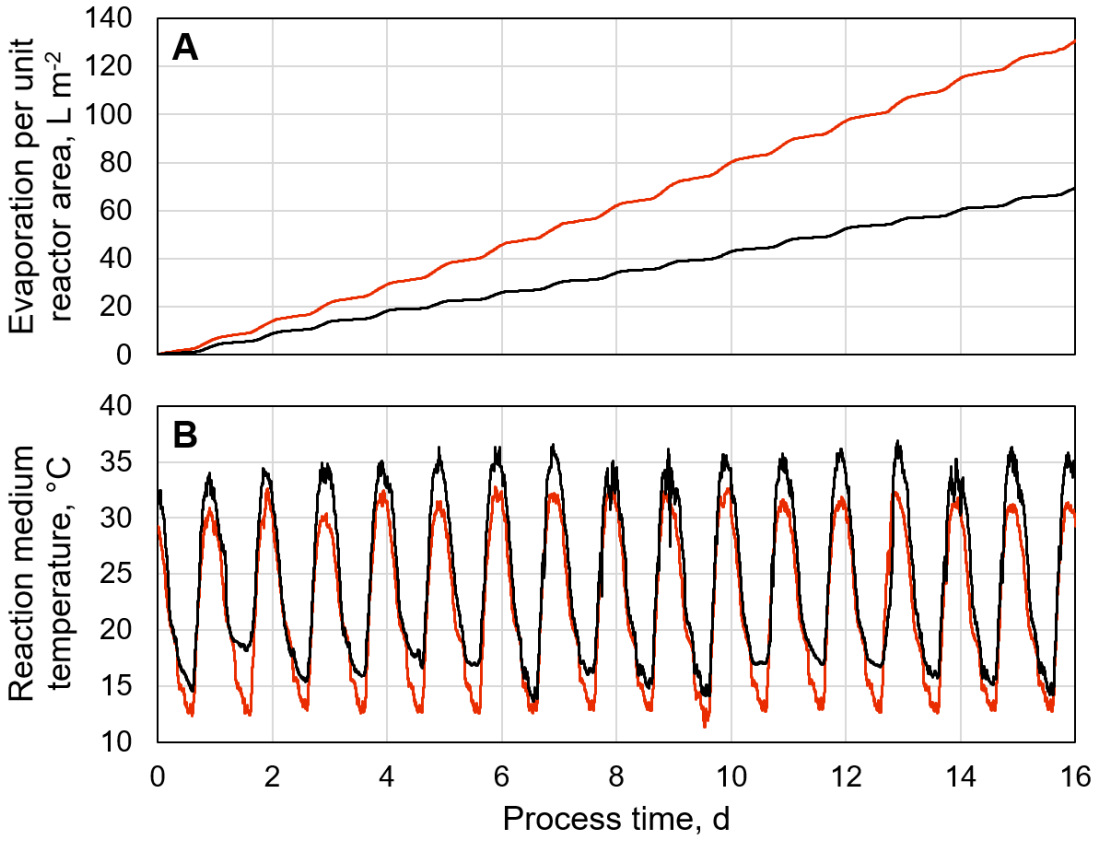

Figure 5.4: Comparison of the water evaporation rate and the reaction medium temperature in TLC PBRs in semi-continuous mode on different scales. Presented are two semi-continuous processes: one operated at a CDW concentration of 20 g L^{-1} on an 8 m^2 scale marked in red (–), and the other operated at a CDW concentration of 18.5 g L^{-1} on a 50 m^2 scale marked in black (–). **A**: Water evaporation rate per unit reactor area; **B**: temperature of the reaction medium (i.e. microalgae suspension).

In semi-continuous processes in the TLC PBR on a 50 m^2 scale, areal productivities similar to that on the 8 m^2 scale were achieved. However, CO_2 fixation efficiency was by 25–30% lower than on the 8 m^2 scale, although CDW concentration and TA values were the same. On the pilot scale TLC PBR with 50 m^2 surface area, the volumetric ratio of the microalgae suspension falling freely from the reactor channels into the retention tanks to the total reaction medium inside the reactor is smaller than on the 8 m^2 scale. This results in a lower evaporation rate in the pilot scale reactor, leading to partially higher temperatures of the microalgae suspension under the same climate conditions,

which is illustrated in Figure 5.4 comparing two semi-continuous processes in TLC PBRs on different scales. In this example, the process on the 8 m^2 scale had a mean water evaporation rate of 8.0 L m^{-2} d^{-1}, whereas it was 4.3 L m^{-2} d^{-1} on the 50 m^2 scale (Fig. 5.4 A). Consequently, the mean temperature of the microalgae suspension was higher on the 50 m^2 scale (24.4 °C) than on the 8 m^2 scale (22.3 °C), with the most significant temperature differences observed during the highest irradiation periods at midday and the cool-down periods overnight (Fig. 5.4 B). Higher temperatures of the microalgae suspension would also mean a lower gas solubility and a shift in the distribution of the dissolved organic carbon (DIC) species in water by affecting the carbonic acid dissociation constants (Woosley, 2021). Hence, higher temperatures of the reaction medium might be the reason for lower CO_2 fixation efficiency on the pilot scale. Another reason could be the smaller volume-specific gas transfer surface area of the pilot scale reactor compared to that on the 8 m^2 scale resulting from the CO_2 supply system being slightly different.

5.3. Continuous production

Series of experiments for biomass production with *M. salina* in continuous mode were carried out in TLC reactors with 8 m^2 surface area to find out if a higher maximum of integral areal productivity can be achieved and sustained over a longer time period in comparison to the batch operation. Another objective was to determine if higher CO_2 fixation efficiencies can be achieved in a continuous mode of operation compared to the batch and semi-continuous processes. In the following subsections, an experiment series investigating the variation of dilution rate, another experiment series examining the variation of feed rate, and the scale-up of the continuous biomass production to pilot scale in a TLC PBR with 50 m^2 surface area are presented. Additionally, a modification of the CO_2 supply system to increase CO_2 fixation efficiency in the pilot scale TLC reactor was examined.

Continuous processes began the same way as batch processes with a nutrient concentration of $2\times$ that in the ASW medium. The switch to continuous operation was started after the microalgae suspension had reached the desired biomass concentration, which was estimated based on the selected dilution rate, since the dilution rate is equal to the biomass growth rate in a continuous process (see Subsection 3.2.4). After that, a concentrated feed medium in an external feed tank was continuously supplied to the reactor. Microalgae suspension was pumped into an external collection tank only for 12 hours every day from 7 a.m. to 7 p.m. to avoid washing out of the cells at night when the cell growth was minimal due to the lack of light supply. The volumetric flow rate of the outlet stream in these 12 hours is set to twice that of the inlet stream so that the daily harvested suspension volume equals the daily feed medium volume supplied to the reactor. Hence, the dilution rate specified for each experiment is a daily average.

Nutrient concentration in the feed medium was adjusted to avoid nutrient depletion in the microalgae suspension, keeping the urea concentration at 0.5–1.5 g L^{-1} over the whole process. In continuous processes, the nutrient concentration in the feed medium was adjusted to a factor (CF) of the nutrient concentration in the ASW medium without changing the concentration of medium salts (i.e. NaCl, $MgSO_4$ and $CaCl_2$). The ratio of nutrient concentration in the feed medium to that in the ASW medium (CF) was selected depending on the dilution rate (D) and the desired nutrient feed rate. Similarly to batch and semi-continuous processes, the nutrient feed rate (r_{feed}) in each continuous

experiment is expressed in terms of a factor (F) of the nutrient concentration in the ASW medium as follows using Equation (4.2):

$$r_{feed} = \frac{m_{nutrient,in}}{V_R \cdot t} = CF \cdot D \cdot c_{nutrient,ASW} = F \times \text{ASW per day}$$

where $m_{nutrient,in}$ is the mass of nutrients fed, V_R is the reaction volume (i.e. volume of algae suspension inside the reactor), t is the process time in days, D is the dilution rate, and $c_{nutrient,ASW}$ is the nutrient concentration in the ASW medium as given in Table 4.1. For instance, with a 20× concentrated feed medium ($CF = 20$) and a dilution rate of 0.175 d^{-1}, the nutrient feed rate (r_{feed}) is expressed as 3.5× ASW per day, meaning $F = 3.5$.

5.3.1. Variation of the dilution rate

In this series of experiments for continuous biomass production with *M. salina* in TLC PBRs with 8 m^2 surface area, the dilution rate was varied between 0.075–0.200 d^{-1}, while the nutrient feed rate was set to 2.5× ASW per day for all experiments. For a continuous process to achieve an actual steady state, the operation must be kept running for at least three times the mean hydraulic residence time calculated from the dilution rate. In this experiment series, this was the case only with a dilution rate of 0.200 d^{-1} requiring 15 days of operation after the start of the continuous phase. For the remaining experiments with lower dilution rates, no significant change in the biomass concentration was observed after continuous operation for one mean hydraulic residence time, so a steady state was assumed after that.

Figure 5.5 A shows the CDW concentrations achieved with various dilution rates. In experiments with dilution rates of 0.075 d^{-1}, 0.100 d^{-1}, 0.150 d^{-1}, and 0.200 d^{-1}, average CDW concentrations of 35.9 g L^{-1}, 31.5 g L^{-1}, 24.4 g L^{-1}, and 14.9 g L^{-1} were recorded at steady state, respectively. Integral areal productivity was highest with 23 g m^{-2} d^{-1} at CDW concentrations between 24.4–31.5 g L^{-1}. At a CDW concentration of 35.9 g L^{-1}, which is above this specified biomass concentration range, the productivity dropped slightly to 21.3 g m^{-2} d^{-1}. Lowest integral areal productivity of 17.6 g m^{-2} d^{-1} was measured in experiment with 14.9 g L^{-1} CDW concentration.

Figures 5.5 C and D show CO_2 fixation efficiency and TA in these experiments. Interestingly, CO_2 fixation efficiencies over 100% were measured temporarily in some cases. However, the values stabilized towards the end of each process. In experiments with dilution rates of 0.075 d^{-1}, 0.100 d^{-1}, 0.150 d^{-1}, and 0.200 d^{-1}, CO_2 fixation efficiencies recorded on the last day were 91%, 96%, 73%, and 77%, respectively. The results suggest that the CO_2 fixation efficiency correlates with areal productivity except for the process with a dilution rate of 0.150 d^{-1}, in which TA was over 450 ppm for the last two weeks, resulting in the lowest CO_2 fixation efficiency measured in this series.

Discussion

In the continuous operation of TLC PBRs, higher dilution rates yielded lower CDW concentrations at a steady state, as expected. In general, it was concluded that with a continuous mode of operation, higher integral areal productivities can be achieved and sustained over longer periods of time in

comparison to batch operation. Additionally, slightly higher areal productivities and CO_2 fixation efficiencies were reached compared to semi-continuous processes at similar CDW concentrations and TA values. This is, however, most likely the result of a higher feed rate of 2.5 $\times$ ASW per day applied in continuous processes in this experiment series compared to the semi-continuous processes presented in Section 5.2 with an average nutrient feed rate of 1.5–1.7$\times$ ASW per day.

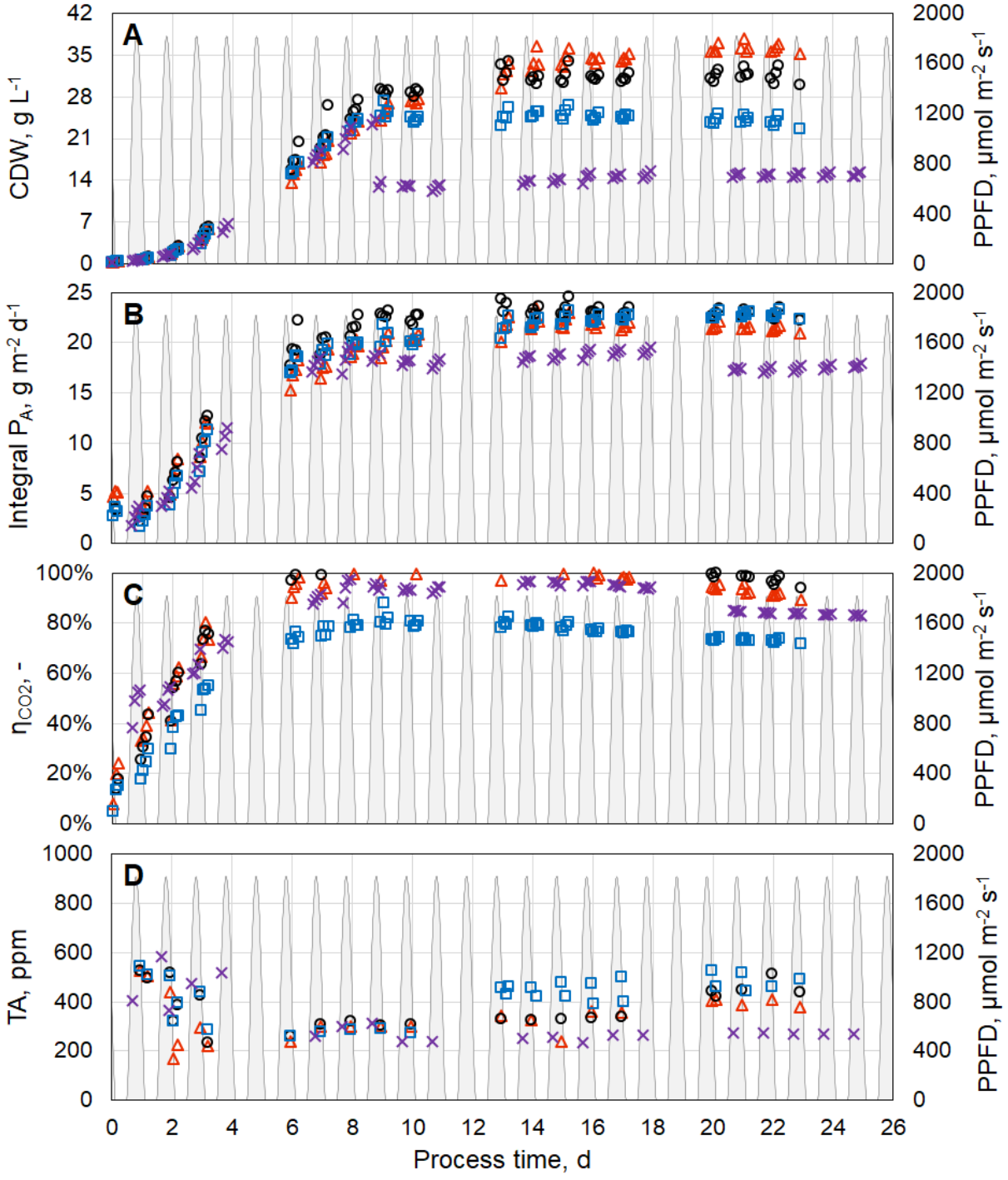

Figure 5.5: Variation of dilution rate for biomass production with *M. salina* in open TLC photobioreactors in continuous mode. Presented are experiments with a dilution rate of 0.075 d^{-1} (△), 0.100 d^{-1} (○), 0.150 d^{-1} (□), and 0.200 d^{-1} (×) on an 8 m^2 scale. Feed rate was adjusted to 2.5× ASW per day for all experiments. **A**: CDW concentration (c_X); **B**: integral areal productivity (P_A); **C**: CO_2 fixation efficiency (η_{CO_2}); **D**: total alkalinity (TA). Photosynthetic photon flux density (PPFD) is given on the secondary vertical axis and marked in grey to highlight the daytime.

5.3.2. Variation of the feed rate

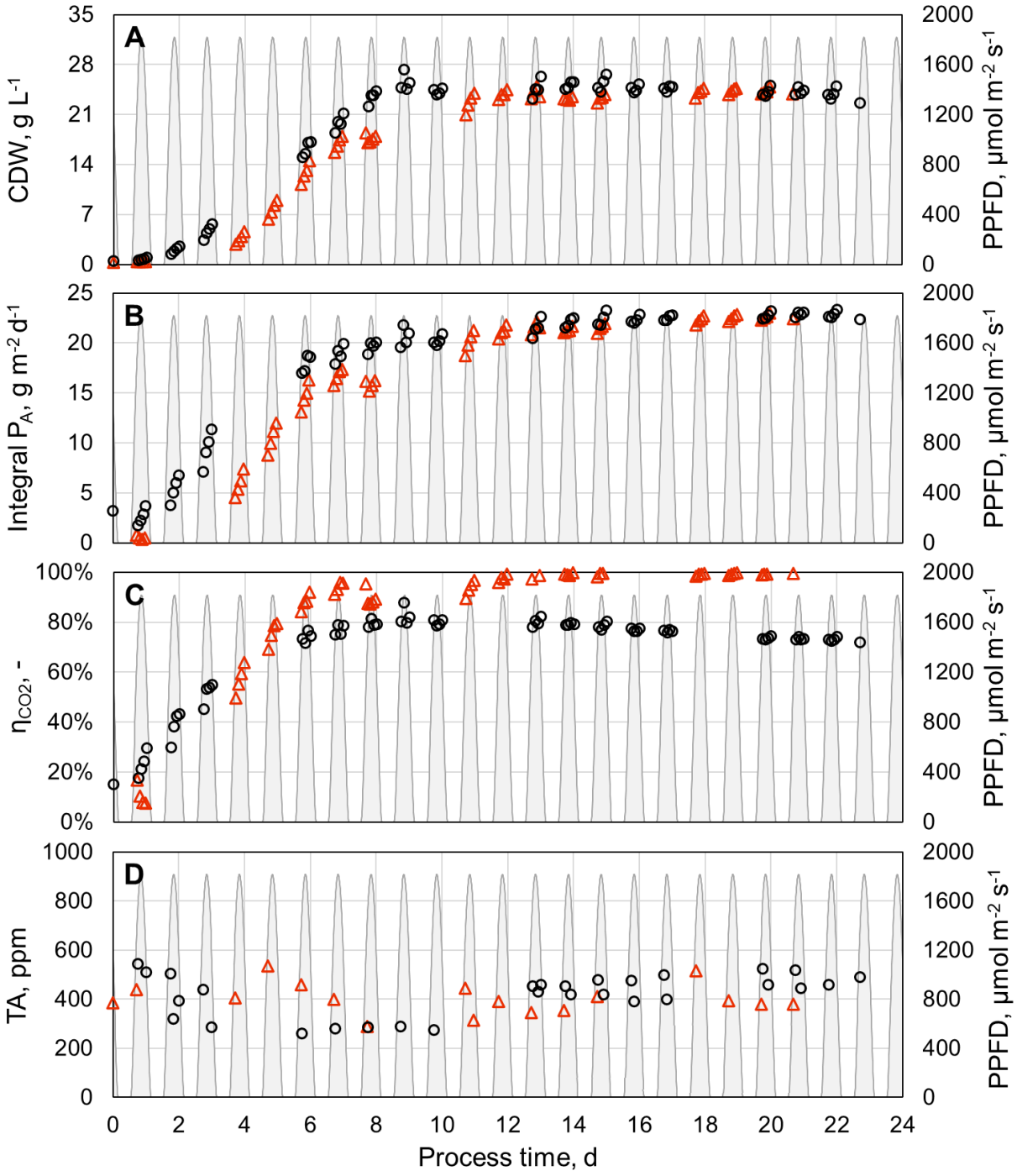

Figure 5.6: Variation of feed rate for biomass production with *M. salina* in open TLC photobioreactors on an 8 m^2 scale in continuous mode with a dilution rate of 0.150 d^{-1}. Presented are experiments with a nutrient feed rate of 2.5× ASW per day (△) and 3.0× ASW per day (○). **A**: CDW concentration (c_X); **B**: integral areal productivity (P_A); **C**: CO_2 fixation efficiency (η_{CO_2}); **D**: total alkalinity (TA). Photosynthetic photon flux density (PPFD) is given on the secondary vertical axis and marked in grey to highlight the daytime.

Two experiments were performed for continuous biomass production with *M. salina* in TLC reactors with 8 m^2 surface area, in which the dilution rate was kept constant at 0.150 d^{-1}, while the nutrient concentration in the feed medium was adjusted differently. Using a feed medium with a nutrient concentration factor (CF) of 16.7× and 20.0× that of the ASW medium, resulted in a nutrient feed

rate of 2.5× ASW per day and 3.0× ASW per day, respectively. The results of the experiment with the lower nutrient feeding rate were already presented in Subsection 5.3.1. In the experiment with a higher nutrient feeding rate, a CDW concentration of 24.0 g L^{-1} and an integral areal productivity of 22.2 g m^{-2} d^{-1} were recorded in the steady state of the continuous operation. As seen in Figure 5.6, increasing the nutrient feed from 2.5× to 3.0× ASW per day did not affect the biomass concentration and integral areal productivity. However, it resulted in an increase in the CO_2 fixation efficiency. Despite the TA being very similar to each other in these two processes, in the experiment with a higher nutrient feed rate, CO_2 fixation efficiency reached 99% on the last day of the experiment, showing an increase by 26% compared to the experiment with the lower nutrient feed rate.

Discussion

In a continuous process on an 8 m^2 scale with a dilution rate of 0.150 d^{-1}, increasing the nutrient feeding rate from 2.5× to 3.0× ASW per day did not affect areal productivity, but increased CO_2 fixation efficiency by 26%. In contrast, in Section 5.2, it was demonstrated in a semi-continuous process that increasing the average nutrient feed rate from 1.8× to 2.8× ASW per day results in a higher areal productivity, but makes almost no difference in the CO_2 fixation efficiency. This might suggest that an increase in the nutrient feeding rate positively affects biomass productivity at low nutrient concentrations, causing nutrient-limited growth of the microalgae. However, when the nutrient concentration is already so high that the microalgae can grow without nutrient limitation, a further increase of the nutrient feed rate might contribute to a higher CO_2 fixation efficiency. Since the urea-containing feed medium is acidic, higher feed supply to the microalgae suspension under nutrient-replete conditions might contribute to reduced TA of the reaction medium and thus have a positive effect on the CO_2 fixation efficiency.

5.3.3. Scale-up of continuous microalgal biomass production to 50 m^2

Two continuous processes with an integral areal productivity above 20 g m^{-2} d^{-1} were transferred from 8 m^2 to 50 m^2 scale. The first of these processes to be scaled-up was with a dilution rate of 0.150 d^{-1} and a nutrient feed rate of 2.5× ASW per day. Figure 5.7 shows the results of this scale-up experiment together with the reference process performed on the 8 m^2 scale for easy comparison. The time axis of the experiment on the 8 m^2 scale was shifted slightly to allow a comparison between the processes starting at a similar CDW concentration of around 0.8 g L^{-1}. In both cases a steady state was observed after one mean hydraulic residence time in continuous operation.

As can be seen in Figures 5.7 A and B, a CDW concentration of 22.5 g L^{-1} and an integral areal productivity of 21.5 g m^{-2} d^{-1} were achieved in continuous operation on a 50 m^2 scale, which are slightly lower but very similar to the values of 24.4 g L^{-1} CDW concentration and 22.6 g m^{-2} d^{-1} areal productivity on the 8 m^2 scale with the same dilution and feed rates. Figure 5.7 D shows that the TA was also very similar between the two experiments and successfully kept below 600 ppm at all times. However, the CO_2 fixation efficiency was much lower on the 50 m^2 scale compared to the 73% measured on the 8 m^2 scale. As seen in Figure 5.7 C, the CO_2 fixation efficiency recorded on the last day of continuous operation on the pilot scale was 48%, which is by 25% lower than on the 8 m^2 scale.

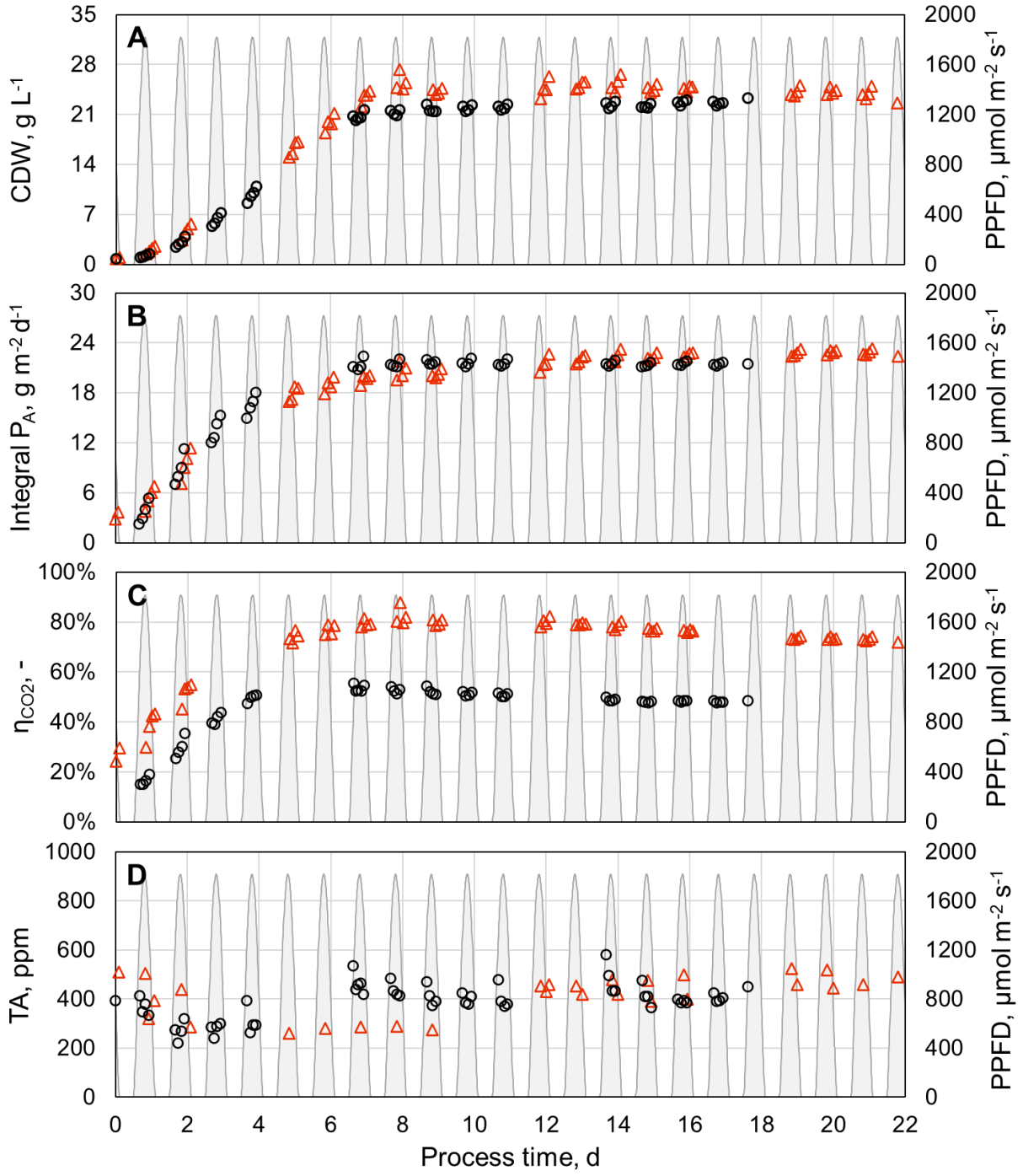

Figure 5.7: Scale-up of biomass production with *M. salina* in continuous mode to 50 m^2 TLC photobioreactor. Presented are continuous processes with a dilution rate of 0.150 d^{-1} on an 8 m^2 scale (△) and on a 50 m^2 scale (○). Nutrient feed rate was 2.5× ASW per day. **A**: CDW concentration (c_X); **B**: integral areal productivity (P_A); **C**: CO_2 fixation efficiency (η_{CO_2}); **D**: total alkalinity (TA). Photosynthetic photon flux density (PPFD) is given on the secondary vertical axis and marked in grey to highlight the daytime.

The second continuous process to be scaled-up was with a dilution rate of 0.175 d^{-1} and a feed rate of 3.5× ASW per day. Also here, the time axis of the experiment on the 8 m^2 scale was shifted slightly to have a similar initial CDW concentration of around 0.8 g L^{-1} in both processes. After a batch phase of 9-10 days, the microalgae suspension in the reactor was diluted to around 14 g L^{-1} CDW concentration and the continuous operation was started. In both experiments an actual steady

state after three times of the mean hydraulic residence time in continuous operation was achieved. Steady state was the case for the last 3 days of the experiment on the 8 m^2 scale and only the last day of the experiment on the 50 m^2 scale. Nevertheless, a steady biomass concentration was observed in both processes after 22 days.

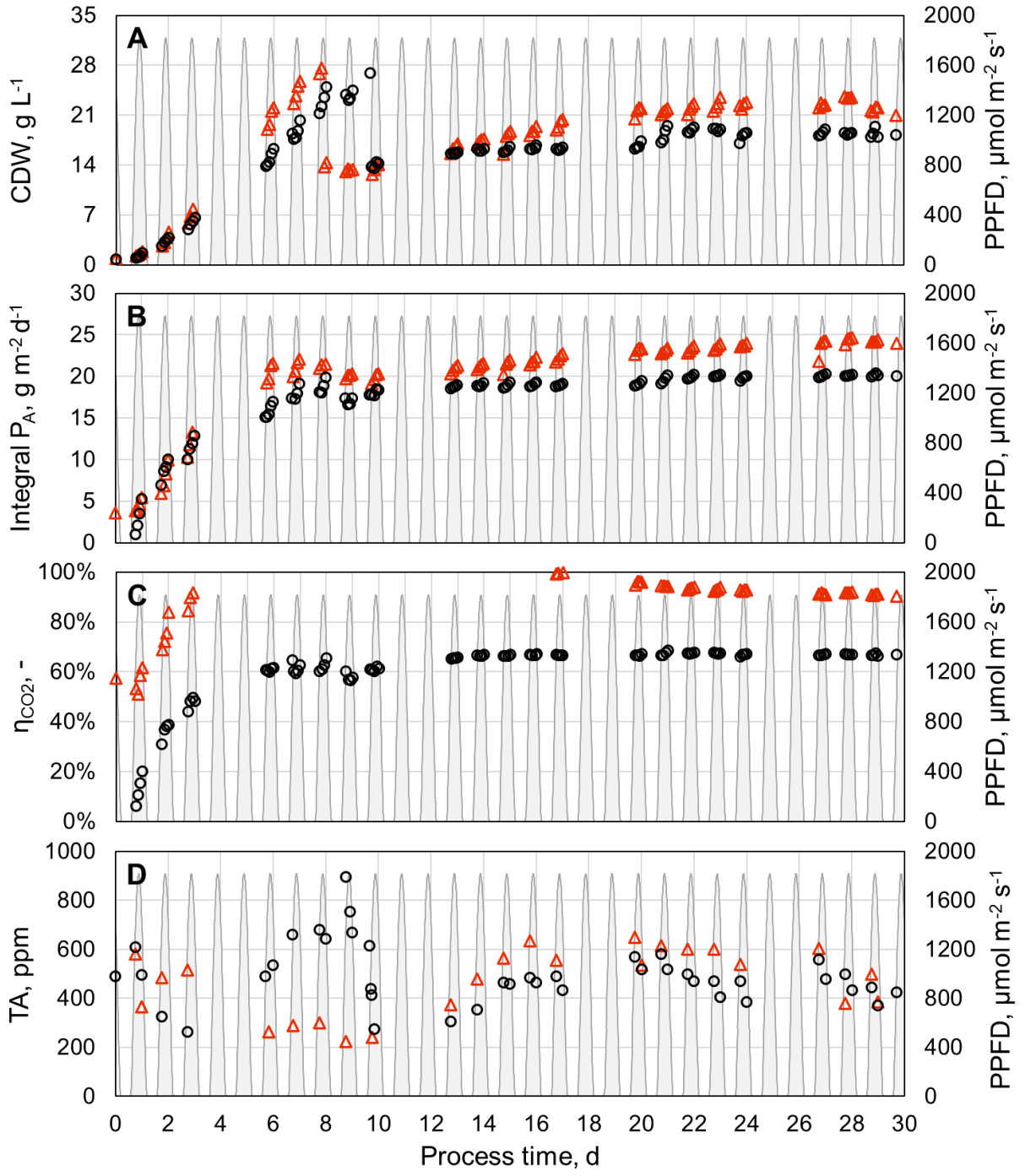

Figure 5.8: Scale-up of biomass production with *M. salina* in continuous mode to 50 m^2 TLC photobioreactor. Presented are continuous processes with a dilution rate of 0.175 d^{-1} on an 8 m^2 scale (△) and on a 50 m^2 scale (○). Nutrient feed rate was 3.5× ASW per day. **A**: CDW concentration (c_X); **B**: integral areal productivity (P_A); **C**: CO_2 fixation efficiency (η_{CO_2}); **D**: total alkalinity (TA). Photosynthetic photon flux density (PPFD) is given on the secondary vertical axis and marked in grey to highlight the daytime.

Figures 5.8 A and B show the course of the CDW concentration and the integral areal productivity

throughout these processes. Similarly to the first scale-up experiment, the biomass concentration and productivity achieved on the 50 m^2 scale were slightly lower but similar to the values on the 8 m^2 scale. In the experiments on the 8 m^2 and the 50 m^2 scales, an average CDW concentration of 22.4 g L^{-1} and 18.4 g L^{-1} and an average integral areal productivity of 24.1 g m^{-2} d^{-1} and 20.1 g m^{-2} d^{-1} were reached on steady state, respectively. As seen in Figure 5.8 D, the TA was kept below 650 ppm except for a short time between days 6-10 on the pilot scale. Although the CO_2 fixation efficiency measured on the 8 m^2 scale was above 100% temporarily, in the steady state, an average CO_2 fixation efficiency of 91% was recorded. Similar to the previous scale-up experiment, CO_2 fixation efficiency on the pilot scale was by 24% lower than on the 8 m^2 scale, reaching an average of 67% on steady state.

In the scale-up experiment with a dilution rate of 0.150 d^{-1} and a nutrient feed rate of 2.5× ASW per day, an average urea concentration of 0.52 g L^{-1} was measured in the microalgae suspension. With a dilution rate of 0.175 d^{-1} and a feed rate of 3.5× ASW per day, the average urea concentration measured was 1.62 g L^{-1} at steady state. In both processes the urea concentration was kept above 0.35 g L^{-1} at all times.

Discussion

Two scale-up experiments in the TLC PBR with 50 m^2 surface area were performed. The first one was with a dilution rate of 0.150 d^{-1} and a nutrient feed rate of 2.5× ASW per day, and the second one was with a dilution rate of 0.175 d^{-1} and a feed rate of 3.5× ASW per day. Interestingly, with a lower feed rate, a slightly higher areal productivity of 21.5 g m^{-2} d^{-1} was achieved at the steady state compared to 20.1 g m^{-2} d^{-1} in the second experiment with a higher feed rate. On the other hand, CO_2 fixation efficiency was by 19% higher in the second experiment with a higher feed rate. Even though these two experiments cannot be directly compared, since different dilution rates were used, the results are consistent with the conclusion in Subsection 5.3.2 suggesting that an increase of the nutrient feed rate above 2.5× ASW per day does not influence productivity but results in an increase in the CO_2 fixation efficiency.

It is important to note that in both scale-up experiments of continuous biomass production, areal productivities were similar to that on the 8 m^2 scale, while CO_2 fixation efficiency was around 25% lower in the pilot-scale TLC reactor. This was also the case for the scale-up experiments of semi-continuous biomass production. There are some differences between the 8 m^2 scale and pilot-scale TLC reactors, which could affect the CO_2 fixation efficiency. One difference is the temperature of microalgae suspension being higher in the TLC reactor with 50 m^2 surface area due to the lower water evaporation rate as shown in Section 5.2. A higher temperature in the reaction medium would eventually cause a reduction of CO_2 fixation efficiency due to the lower gas solubility and a shift in the distribution of DIC species in water at higher temperatures. Another difference is the type of gassing hoses and the volume-specific gas exchange surface area, which is the area of the gassing hose in contact with the reaction medium and is lower for the pilot-scale TLC reactor. The influence of the latter is examined in the following subsection.

5.3.4. Effect of volume-specific gas exchange area on CO_2 fixation efficiency

CO_2 fixation efficiency is one of the main performance indicators of microalgal biomass production in this work. In TLC PBR with 8 m^2 surface area under optimal conditions, it was possible to consistently achieve over 95% CO_2 fixation efficiency. However, in scale-up experiments in TLC PBR with 50 m^2 surface area, CO_2 fixation efficiency stayed below 70%. One of the differences in these experiments that could affect the CO_2 fixation efficiency compared to the 8 m^2 scale reactors is the difference in the gas supply system, which are the type of gassing hoses and the volume-specific gas exchange surface area, which is the area of the gassing hose in contact with the reaction medium.

Table 5.1: Specifications of different CO_2 gassing units used in TLC PBR.

Specification	**1**	**2**	**3**
TLC PBR surface area, m^2	8	50	50
TLC PBR working volume, L	55	350	350
Hose type	Solvox® B	Solvocarb®	Solvox® B
Hose diameter, cm	2.1	2.6	2.1
Total hose length per gassing unit, cm	72	45	120
Gas exchange area per gassing unit, m^2	0.048	0.037	0.079
Number of gassing units per reactor	1	2	2
Volume-specific gas exchange area, m^{-1}	0.864	0.210	0.452

TLC reactors with 8 m^2 surface area had CO_2 gassing units made of Solvox® B hoses (Linde, Pullach, Germany), whereas the CO_2 gassing units of the TLC reactor with 50 m^2 surface area were made of Solvocarb® hoses (Linde, Pullach, Germany), which have slightly larger pores to allow a higher gas flux rate through the perforated material and double the amount of pores per unit hose length compared to Solvox® B hoses. Since smaller pores produce smaller gas bubbles and thus improve the gas diffusion into the liquid phase, the usage of Solvox® B hoses could have a positive effect on CO_2 fixation efficiency as previously demonstrated by Schädler (2020). Hence, the gassing units of the 50 m^2 TLC reactor were modified replacing the Solvocarb® hoses with Solvox® B hoses. Since Solvox® B hoses allow a lower gas flux rate, it must be ensured that the CO_2 supply into the reactor stays sufficient to keep the pH at a given set-point under any circumstances by providing a large enough volume-specific gas exchange surface area. In an experiment using Solvox® B hoses in the CO_2 supply unit without changing the total hose length, it was observed that the gas flux rate was not enough to keep the pH at 8.5 at all times throughout the process (data not shown), which indicated that an increase of the volume-specific gas exchange area definitely have to be increased, if Solvox® B hoses are to be used. This was achieved by increasing the length of the gassing hoses from 45 cm to 120 cm per gassing unit to yield a larger gas exchange surface area as specified in Table 5.1. Even though the volume-specific gas exchange surface area of the 50 m^2 TLC reactor was still below that of the 8 m^2 TLC reactors as seen in Table 5.1, a further increase of the hose

length was not feasible, since this would require a change of the technical design and structural parts of the pilot-scale TLC reactor.

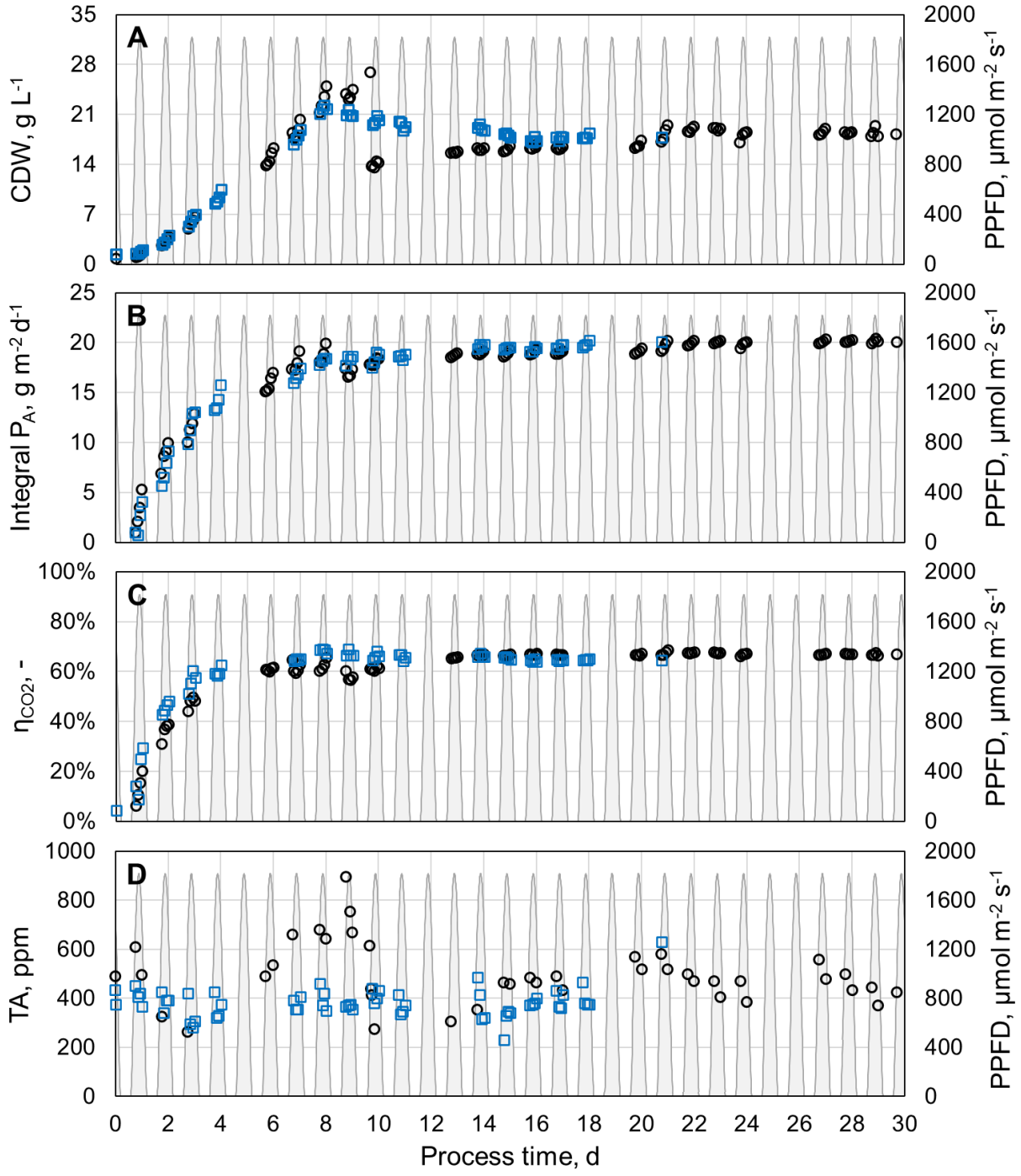

Figure 5.9: Effect of increasing the volume-specific gas exchange surface area and smaller gas bubble size on microalgal biomass production in continuous mode in a pilot-scale TLC PBR. Presented are two experiments on a 50 m^2 scale with volume-specific gas exchange surface area of 0.210 m^{-1} (○) and 0.452 m^{-1} (□). In both processes, a dilution rate of 0.175 d^{-1} was applied. The nutrient feeding rate was 3.5× ASW per day and 3.0× ASW per day in the experiments with the lower and the higher gas exchange surface area, respectively. **A**: CDW concentration (c_X); **B**: integral areal productivity (P_A); **C**: CO_2 fixation efficiency (η_{CO_2}); **D**: total alkalinity (TA). Photosynthetic photon flux density (PPFD) is given on the secondary vertical axis and marked in grey to highlight the daytime.

After implementing the modifications mentioned above on the CO_2 gassing system, an experiment was carried out using the same parameters as in the continuous process with a dilution rate of 0.175 d^{-1} on the pilot scale already presented in Subsection 5.3.3 as the reference with the previous gassing system for comparison as shown in Figure 5.9. Both experiments were performed in continuous mode with a dilution rate of 0.175 d^{-1} and an initial nutrient feed rate of 3.5× ASW per day. After a batch phase of 8 days, which is 2 days shorter than in the reference experiment, a CDW concentration of 22.2 g L^{-1} was reached, and continuous operation was started. A steep increase in the urea concentration was observed after one day of continuous operation. Therefore, the nutrient feeding rate was reduced to 3.0× ASW per day to keep the measured urea concentration below 1.5 g L^{-1}. A steady state was observed after 1.5 times the mean hydraulic residence time in continuous operation, which corresponds to the last 4 days of the experiment.

As seen in Figure 5.9 D, the TA was kept below 500 ppm successfully until the last process day. In the steady state, an average CDW concentration of 17.8 g L^{-1}, a mean integral areal productivity of 23.2 g m^{-2} d^{-1}, and a mean CO_2 fixation efficiency of 64% were recorded. These results are very similar to the values achieved in the reference experiment at steady state, as can be seen in Figure 5.9, meaning that neither the process productivity nor the CO_2 fixation efficiency was noticeably affected by the modifications made to the CO_2 gassing system.

Discussion

By changing the type of gassing hoses to another with smaller pores and increasing the volume-specific gas exchange surface area, it was not possible to further increase the CO_2 fixation efficiency for continuous biomass production in the pilot-scale TLC reactor. As mentioned in Subsection 5.2, another difference between the 8 m^2 and 50 m^2 TLC reactors is the evaporation rate being lower in the pilot-scale reactor. According to Apel (2017), the evaporation rate in the pilot-scale TLC reactor can be 45% lower than in the 8 m^2 scale TLC reactors. According to measurements in this study, the evaporation rate was determined to be approximately 25% lower in the pilot-scale TLC reactor. This results in a much higher maximum temperature of the microalgae suspension during daytime in the 50 m^2 scale TLC reactor, more precisely around 6 °C higher than in processes in 8 m^2 scale reactors. For water with a salinity of 30 ppt, the water temperature increasing from 28–34 °C to 34–40 °C would result in a 0.12–0.16 g L^{-1} decrease in the CO_2 solubility in water (Weiss, 1974). Hence, the microalgae suspension temperature quickly rising to around 40 °C during midday every day may cause more CO_2 to escape from the water phase into the air in the pilot-scale TLC reactor.

5.4. Effect of pH

A series of experiments in semi-continuous mode at various pHs ranging from pH 7.5 to pH 8.5 was performed to investigate the influence of pH on microalgal biomass production. Figure 5.10 A shows the results of six experiments carried out in TLC PBRs at different pH on both 8 m^2 and 50 m^2 scales. On the 8 m^2 scale, increasing the pH from pH 7.5 to pH 8.0 leads to a significant increase of CO_2 fixation efficiency by 30%, from 38% to 68%. A further increase to pH 8.5 had a less significant impact, increasing CO_2 fixation efficiency by 13% to 81%. As anticipated based on previous experiments, CO_2 fixation efficiency was lower on the pilot scale than on the 8 m^2 scale

at the same pH. Still, the positive correlation between the pH and the CO_2 fixation efficiency was observed also on the pilot scale. Here, a pH increase from pH 8.0 to pH 8.5 increased CO_2 fixation efficiency by 30%, from 29% to 59%. Thus, it was demonstrated that the CO_2 fixation efficiency increases with increasing pH in TLC PBRs on both scales in the examined pH range.

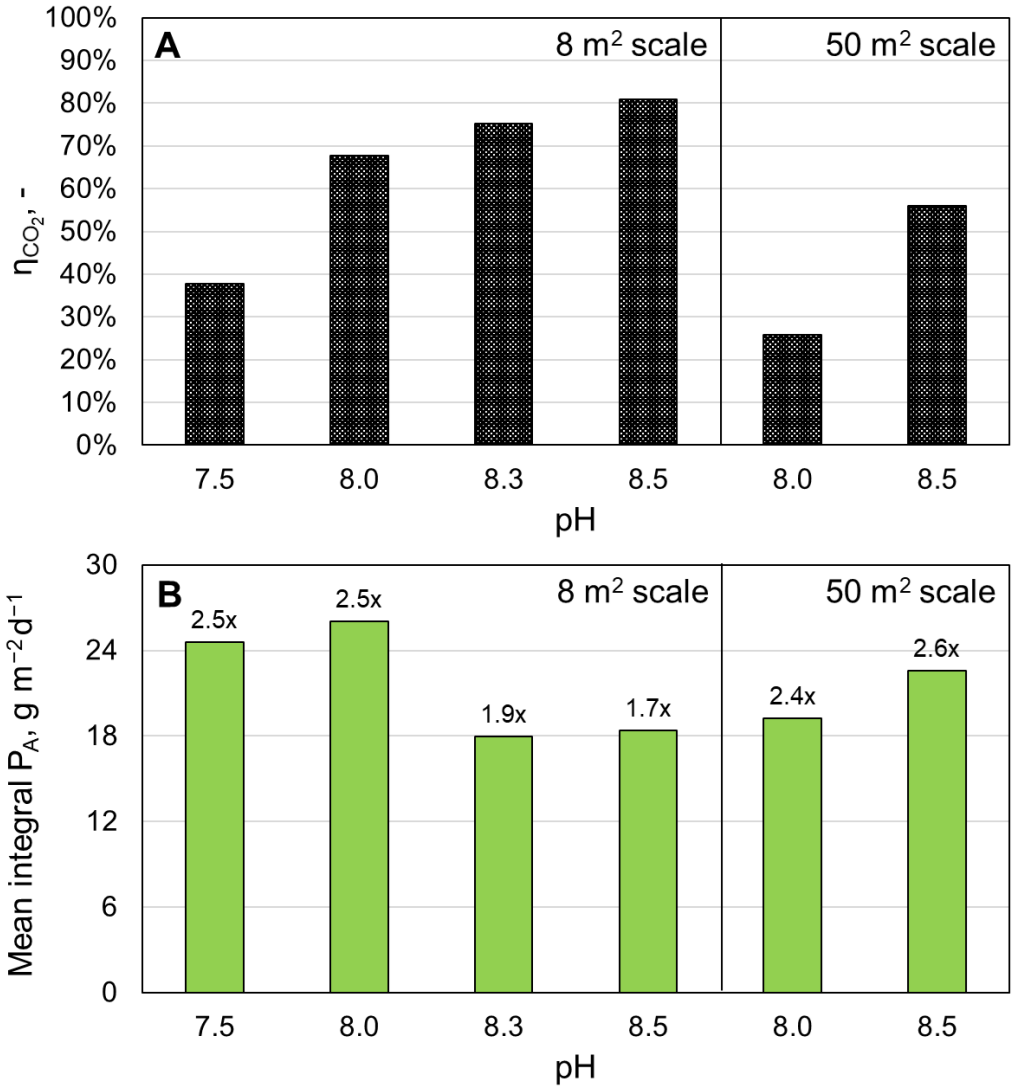

Figure 5.10: Influence of pH on biomass production with *M. salina* in open TLC photobioreactors in semi-continuous mode. Presented are experiments with a similar daily initial CDW concentration of around 20 g L^{-1} at pHs ranging from pH 7.5 to pH 8.5 on both 8 m^2 and 50 m^2 scales. **A**: CO_2 fixation efficiency (η_{CO_2}); **B**: mean integral areal productivity (P_A). Data labels indicate the average nutrient feed rate in terms of a factor (F) of the ASW medium nutrient concentration per day.

Figure 5.10 B shows the mean integral areal productivity in six semi-continuous processes operated at the same daily initial biomass concentration but at different pH on both scales. The data labels on the diagram indicate the average nutrient feed rate as a factor (F) of the nutrient concentration in the ASW medium per day, resulting from the different nutrient concentrations in the feed medium. The results indicate that the areal productivity is only marginally affected by the pH. With pH increasing from pH 7.5 to pH 8.0 at the same nutrient feed rate, the integral areal productivity exhibits only a

slight gain by 1.4 g m^{-2} d^{-1} on the 8 m^2. Likewise, a pH increase from pH 8.0 to pH 8.5 on the 50 m^2 increases the integral areal productivity only by 3.4 g m^{-2} d^{-1}. On the other hand, increasing the nutrient feed rate from 1.9 $\times$ to 2.5 $\times$ ASW per day at an almost constant pH (pH 8.0–8.3) leads to a more significant increase in the areal productivity, namely by 8.0 g m^{-2} d^{-1} on the 8 m^2 scale. Similarly to the observations in previous experiments, lower productivities and CO_2 fixation efficiencies are reached on semi-continuous mode on a 50 m^2 scale compared to the 8 m^2 scale under the same conditions. Still, these figures are highest in operation at pH 8.5 within the investigated pH range in both cases.

Discussion

The pH optimum for *M. salina* is given as pH 7.5–8.0 in literature (Boussiba et al., 1987; Bartley et al., 2014). Surprisingly, the highest biomass productivity was achieved at pH 8.5, which is above the reported optimal range. Since biomass productivity depends on CDW concentration as well as growth rate, the data suggests that at constant CDW concentration, *M. salina* has a higher pH optimum when cultivated in TLC PBR. Due to the effect of pH on the distribution of dissolved carbon species, it was already anticipated that the highest CO_2 fixation efficiency would be reached at pH 8.5. Also, the effect of a pH increase from pH 8.0 to pH 8.5 was much bigger on the pilot scale than on the 8 m^2 scale. This raises the question of whether a further increase of the pH on the pilot scale would further improve the CO_2 fixation efficiency. As shown in Section 5.2, the average temperature of the microalgae suspension under the same climate conditions is higher in TLC PBRs on the pilot scale than on the 8 m^2 scale. It is known that temperature affects the dissolved organic carbon (DIC) balance in water, with the dissociation constants of carbonic acid increasing with rising temperature (Woosley, 2021). Thus, it is possible that increasing the pH further above pH 8.5 would influence the CO_2 fixation efficiency positively. However, it should be noted that pH 8.5 is already above the optimal range for *M. salina* growth and a further increase in pH could drastically reduce the areal productivity.

5.5. Effect of automated switch-off of the circulation pumps overnight

Energy consumption for the circulation of microalgae suspension makes up the largest portion of the process costs for the production of microalgal biomass in open TLC PBR. To reduce energy consumption, circulation pumps are switched off overnight from 8 p.m. to 6 a.m., and the algae suspension in the reactor's retention tanks is mixed only by the movement caused by bubbling pressurized air through the suspension. To investigate how this affects areal productivity and CO_2 fixation efficiency on the 50 m^2 scale, an experiment in continuous operation mode was performed with automated switch-off of the circulation pumps and pressurized air supply overnight. Figure 5.11 shows the results of this experiment (black) and another one carried out under the same conditions but without the automated pump switch-off (red) for comparison. The reference experiment was described in detailed in Subsection 5.3.3.

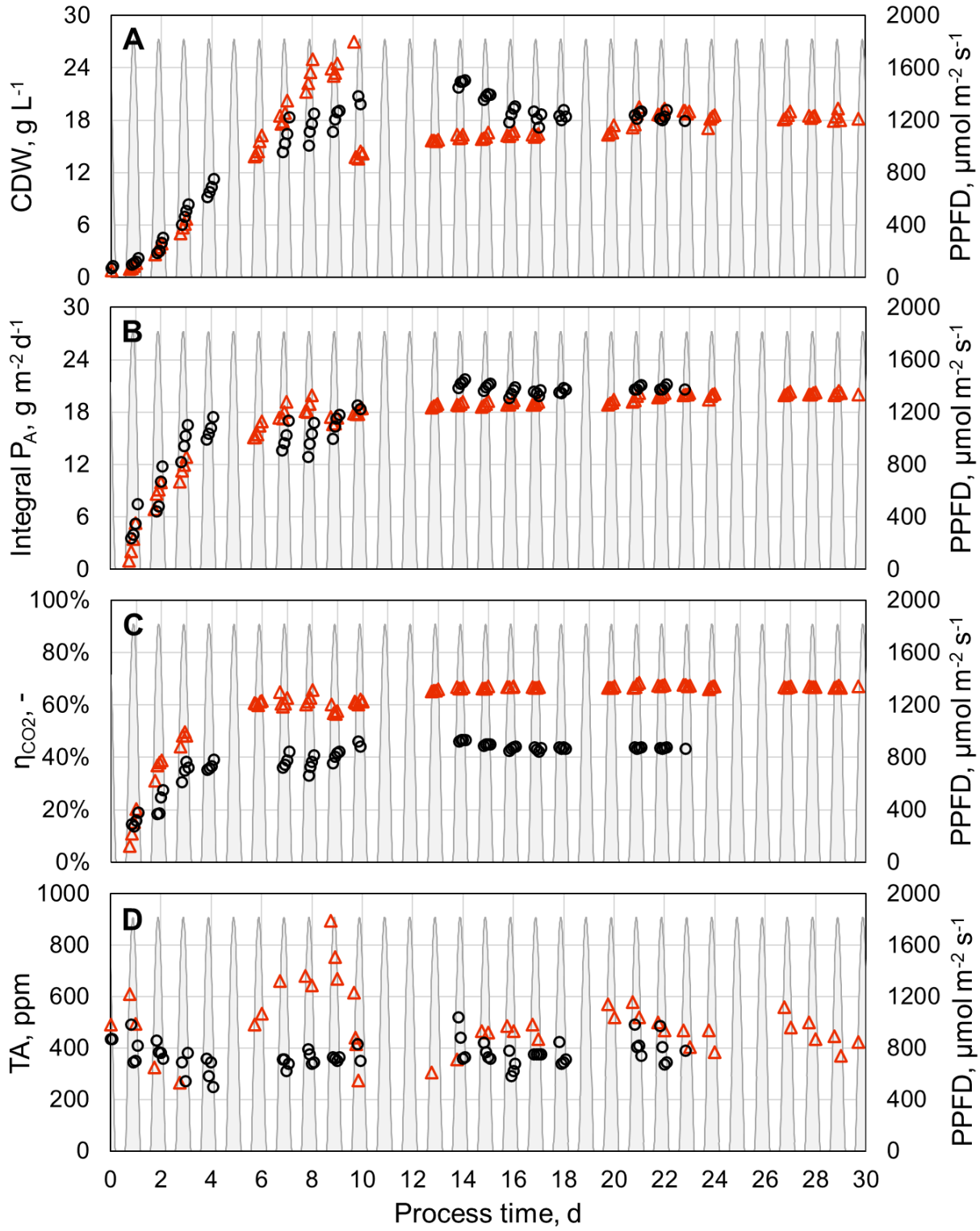

Figure 5.11: Effect of switching off the circulation pumps overnight on biomass production with *M. salina* in continuous mode in a TLC PBR on a 50 m^2 scale. Presented are two continuous processes with a dilution rate of 0.175 d^{-1} and a nutrient concentration (CF) of 20$\times$ that of the ASW medium in the feed medium, corresponding to a nutrient feed rate of 3.5$\times$ ASW per day, with and without the automated pump switch-off mechanism. The experiment with the automated pump switch-off is marked in black (o), while the reference experiment with uninterrupted circulation of the microalgae suspension is marked in red (△). The circulation pump switch-off was for 10 hours overnight from 8 p.m. to 6 a.m., during which the mixing of the algae suspension was done via pressurized air supply at the bottom of the reactor's retention tanks. **A**: CDW concentration (c_X); **B**: integral areal productivity (P_A); **C**: CO_2 fixation efficiency (η_{CO_2}); **D**: total alkalinity (TA). Photosynthetic photon flux density (PPFD) is given on the secondary vertical axis and marked in grey to highlight the daytime.

Both experiments had a batch phase of 10 days. After reaching the desired biomass concentration, the continuous operation was started with a dilution rate of 0.175 d^{-1} and a nutrient concentration (CF) of 20$\times$ that of the ASW medium, corresponding to a nutrient feed rate of 3.5$\times$ ASW per day. A steady state was observed after a process duration of two times the mean hydraulic residence time. An average CDW concentration of 18.4 g L^{-1} was recorded at steady state, which is very similar to the average CDW concentration of 18.3 g L^{-1} in the reference experiment. Furthermore, the average integral areal productivity of 20.1 g m^{-2} d^{-1} was also very similar to 20.8 g m^{-2} d^{-1} recorded in the reference experiment. This means that the areal productivity is not noticeably affected by the switch-off of the circulation pumps overnight. On the other hand, CO_2 fixation efficiency went down by 24%, from 67% to 43%, even though the TA was kept successfully below 500 ppm throughout the experiment.

Besides reducing energy consumption, another advantage of switching off the circulation pumps overnight is reducing the water evaporation rate in the TLC PBR. Figure 5.12 shows the evaporation rate per unit reactor area compared to the reference process shown in Figure 5.11. By operating the circulation pumps only for 14 h during the daytime, the water evaporation rate was decreased by 40% from 4.5 L m^{-2} d^{-1} to 2.7 L m^{-2} d^{-1}, which presents a major advantage in operation costs.

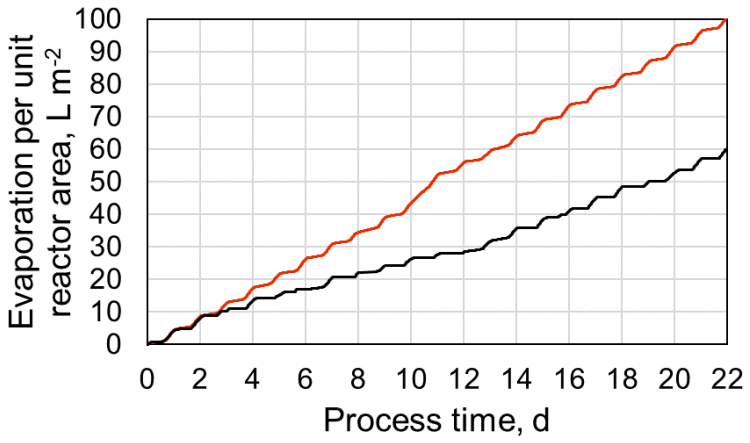

Figure 5.12: Effect of switching off the circulation pumps overnight on water evaporation rate in continuous processes in a TLC PBR on a 50 m^2 scale. Water evaporation rate per reactor surface area is presented for two continuous processes with a dilution rate of 0.175 d^{-1} and a nutrient concentration (CF) of 20$\times$ that of the ASW medium in the feed medium, corresponding to a nutrient feed rate of 3.5$\times$ ASW per day, with and without the automated pump switch-off mechanism. The experiment with the automated pump switch-off is marked in black (**–**), while the reference experiment with uninterrupted circulation of the microalgae suspension is marked in red (**–**). The circulation pump switch-off was for 10 hours overnight from 8 p.m. to 6 a.m., during which the mixing of the algae suspension was done via pressurized air supply at the bottom of the reactor's retention tanks.

Discussion

The switch-off of the circulation pumps with simultaneous pressurized air supply in the retention tanks for 10 hours overnight in a pilot-scale continuous process over 23 days did not have a significant influence on the biomass productivity but resulted in a decrease of CO_2 fixation efficiency by 24%. Additionally, the water evaporation rate, and thus the water consumption required for operation, was decreased by 40% in this way. The same method was previously applied by Schädler

(2020) on a TLC PBR with 8 m^2 surface area, demonstrating that the pump switch-off overnight did not have any effect on microalgae growth or biomass productivity and reporting a reduction of the power input required for TLC PBR operation by 42%, as also verified in this study on pilot scale (50 m^2 TLC PBR). Consequently, implementing an automated pump switch-off mechanism proved very profitable for an industrial-scale application, considering around 40% savings in water supply and energy costs. The only drawback of this modification was the drop in CO_2 fixation efficiency, which was probably caused by the insufficient mixing of the algae suspension overnight, which was accomplished by gassing with pressurized air at only one location at the bottom of the reaction tank. Thus, the drop in CO_2 fixation efficiency could probably be reduced by better mixing of the microalgae suspension in retention tanks, for instance, by pressurized air supply through a perforated floor mat system covering the whole bottom area of the retention tanks. This could, however, not be investigated due to the difficulty of making the necessary technical changes to the TLC reactors.

5.6. Comparison between modes of operation and optimal conditions

Multiple series of experiments were carried out with *M. salina* in open TLC PBRs to determine the optimal process conditions for microalgal biomass production achieving maximum productivity and CO_2 fixation efficiency. In total, three batch, ten semi-continuous, and eight continuous processes were carried out on an 8 m^2 scale. Eventually, one batch, three semi-continuous, and four continuous processes were performed successfully on a pilot scale in the TLC reactor with 50 m^2 surface area. In this section, the results of these experiments are summarized and compared to each other in terms of productivity and CO_2 fixation efficiency.

In batch processes on an 8 m^2 scale maximum integral areal productivity and CO_2 fixation efficiency recorded were 15–20 g m^{-2} d^{-1} and 70–86%, respectively, at a CDW concentration range of 25–35 g L^{-1} after 11–13 days. The daily areal productivity varied from 13.4 g m^{-2} d^{-1} to 25.2 g m^{-2} d^{-1} on these days. In the batch process on a 50 m^2 scale maximum integral areal productivity and CO_2 fixation efficiency observed were 12–14 g m^{-2} d^{-1} and 78–82%, respectively, at a CDW concentration range of 21–24 g L^{-1} after 11 days. A daily areal productivity of 17.8 g m^{-2} d^{-1} was recorded on this day. Both areal productivity and CO_2 fixation efficiency declined after reaching the maximum at day 11. The main issue with using batch production mode, apart from the low areal productivity, is that the maximum productivity and efficiency achieved are limited to only a couple of days, corresponding to only 20% of the total operation time, which makes it unsuitable for an industrial-scale production facility. For this reason, only semi-continuous and continuous modes of operation are considered for microalgal biomass production on an industrially relevant scale.

A summary of the key performance indicators of all semi-continuous and continuous processes carried out in this study for microalgal biomass production is illustrated in Figure 5.13. For productivity comparison, the daily areal productivity was averaged over the whole semi-continuous operation time or, in the case of continuous operation, over the steady-state continuous operation time. Figure 5.13 A shows the key performance indicators for biomass production in TLC PBR with 8 m^2 surface area in continuous mode for various dilution rates using the same nutrient feeding rate of 2.5× ASW per day. As anticipated, the CDW concentration achieved at the steady state was inversely

proportional to the dilution rate. The highest average daily areal productivity of 24.8 g m^{-2} d^{-1} was reached with a dilution rate of 0.150 d^{-1} at an average CDW concentration of 24.6 g L^{-1}. However, these conditions also resulted in a CO_2 fixation efficiency of 77%, which is the lowest recorded in continuous production mode.

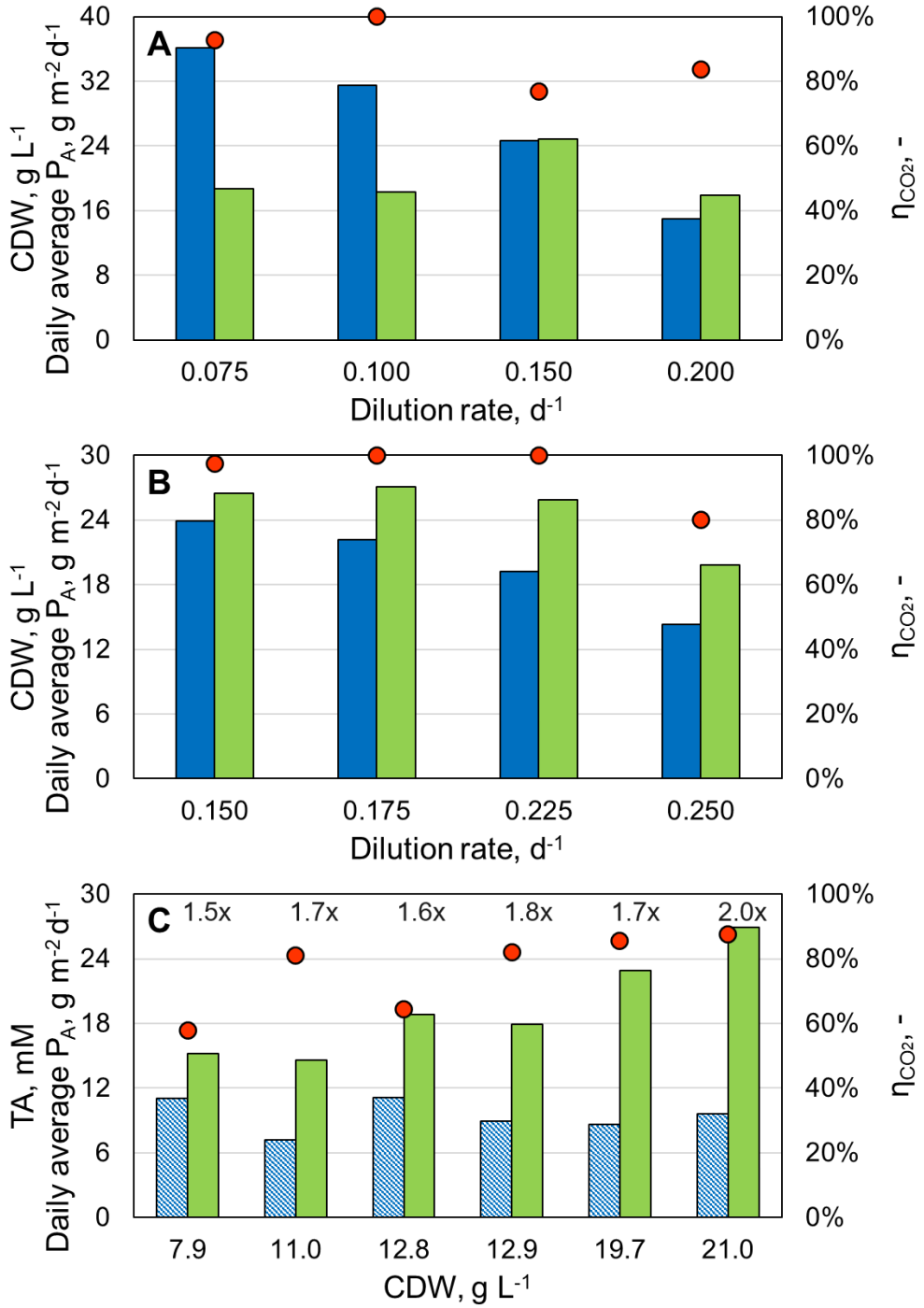

Figure 5.13: Summary of experiments for microalgal biomass production in TLC PBRs on an 8 m^2 scale on an 8 m^2 scale in different operational modes. Presented are CDW concentration (c_X) in blue (■), average daily areal productivity ($P_{A,daily}$) in green (■), total alkalinity (TA) in dashed blue (▨), and CO_2 fixation efficiency (η_{CO_2}) in red (●). **A**: Variation of the dilution rate in continuous mode with a constant nutrient feed rate of 2.5× ASW per day; **B**: variation of the dilution rate in continuous mode using 20× concentrated ASW medium as feed medium (CF=20); **C**: variation of the daily starting biomass concentration in semi-continuous mode with data labels indicating the nutrient feed rate in terms of a factor (F) of the ASW medium nutrient concentration per day.

Figure 5.13 B shows the performance indicators for biomass production in TLC PBR with 8 m^2 surface area in continuous mode for various dilution rates using the same feed medium concentration, namely 20 times of the nutrient concentration in ASW medium per day, meaning that the feeding rate increases with increasing dilution rate. This corresponds to a nutrient feed rate of 3.0×, 3.5×, 4.5× and 5.0× ASW per day for the dilution rates of 0.150 d^{-1}, 0.175 d^{-1}, 0.225 d^{-1} and 0.250 d^{-1}, respectively. The results for a dilution rate of 0.150 d^{-1} indicate that increasing the feeding rate positively influences both productivity and CO_2 fixation efficiency. In this process, an average daily areal productivity of 26.5 g m^{-2} d^{-1} and a CO_2 fixation efficiency of 98% were achieved, corresponding to an increase by 1.7 g m^{-2} d^{-1} and by 21%, respectively, in comparison to the same process with a feed rate of 2.5× ASW per day. Nevertheless, the best results were achieved in the continuous process with a dilution rate of 0.175 d^{-1} with a CDW concentration of 22.2 g L^{-1}, an average daily areal productivity of 27.1 g m^{-2} d^{-1} and a CO_2 fixation efficiency of 100%.

Figure 5.13 C displays the key figures for biomass production in TLC PBR with 8 m^2 surface area in semi-continuous mode with various daily starting CDW concentrations ranging from 7.9 g L^{-1} to 21.0 g L^{-1}. The data demonstrates that the average daily areal productivity increases with growing CDW concentration within the investigated range. Although it is possible to observe a slight rise in the CO_2 fixation efficiency with increasing CDW concentration, there is another factor with a stronger influence on it. An average TA of over 10 mM in a semi-continuous process directly correlates with a sharp drop of CO_2 fixation efficiency by 15–20% compared to other processes with a similar CDW concentration but an average TA of below 10 mM. Comparing the two semi-continuous experiments with CDW concentrations of 12.8 g L^{-1} and 12.9 g L^{-1} presented in Figure 5.13 C, with average TA values of 11.1 mM and 9.0 mM, respectively, shows how maintaining a TA value below 10 mM resulted in an increase of CO_2 fixation efficiency by 18% in this case. Among all the semi-continuous processes presented in Figure 5.13 C, the maximum average daily areal productivity of 26.9 g m^{-2} d^{-1} and the maximum CO_2 fixation efficiency of 88% were achieved in the same process with a daily starting CDW concentration of 21.0 g L^{-1}. Comparing these values to the continuous processes in Figure 5.13 B shows that in both production modes, the highest areal productivity is reached at a similar CDW concentration of 21.0–22.2 g L^{-1}. The maximum values of mean daily areal productivity recorded were almost the same between continuous and semi-continuous processes on an 8 m^2 scale, namely 27.1 g m^{-2} d^{-1} and 26.9 g m^{-2} d^{-1}, respectively. There was, however, a remarkable difference in the highest mean CO_2 fixation efficiency achieved, which was 100% and 88% for continuous and semi-continuous processes on the 8 m^2 scale, respectively.

Figure 5.14 presents the best results achieved using different operational modes for biomass production in TLC PBR on a 50 m^2 scale. Although the highest CO_2 fixation efficiency recorded is in batch mode, this value was sustained only for a day and started to decline afterwards. In contrast, the values in semi-continuous and continuous modes are mean values maintained over a long process time of at least one week, with no subsequent drop observed until the end of the process. CO_2 fixation efficiency achieved in batch, semi-continuous and continuous production of microalgal biomass was 80%, 59% and 66%, respectively. Maximum mean daily areal productivity achieved was 17.7 g m^{-2} d^{-1}, 21.1 g m^{-2} d^{-1} and 22.1 g m^{-2} d^{-1} in batch, semi-continuous and continuous modi, respectively. Mean daily areal productivity was highest in continuous production mode, while

the difference to semi-continuous process is only 1.0 g m^{-2} d^{-1}. These results suggest that the most suitable mode of operation for microalgal biomass production is continuous. Nonetheless, it should be noted that both CO_2 fixation efficiency and areal productivity are lower for biomass production on the 50 m^2 scale in comparison to the 8 m^2 scale. Especially the maximum CO_2 fixation efficiency achieved presents the most significant difference, being by 34% lower on the 50 m^2 scale compared to the 100% reached on the 8 m^2 scale.

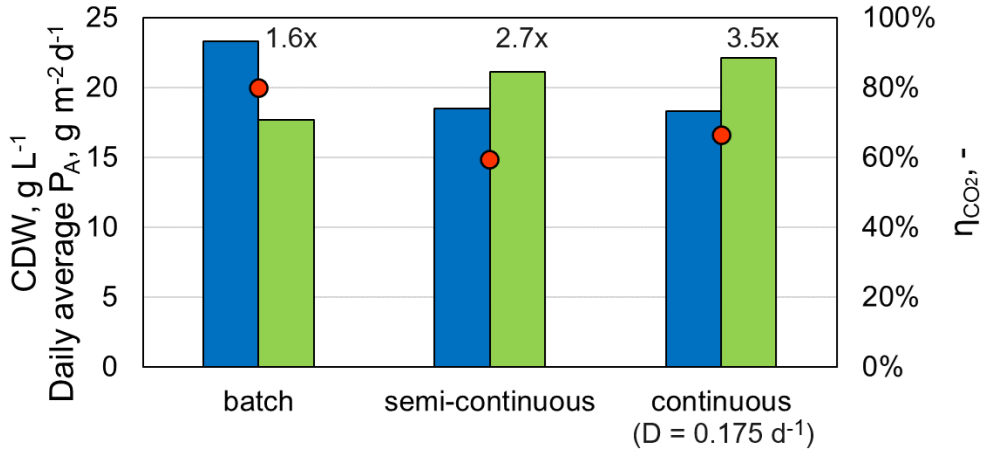

Figure 5.14: Comparison of the best performing processes with different operational modes for microalgal biomass production in TLC PBRs on an 50 m^2 scale. Presented are CDW concentration (c_X) in blue (■), average daily areal productivity ($P_{A,daily}$) in green (■), and CO_2 fixation efficiency (η_{CO_2}) in red (●). For the batch mode, data from the day of maximum areal productivity are presented. For the semi-continuous mode, CDw concentration is the set-point of the daily initial biomass concentration. Data labels indicate the nutrient feed rate in terms of a factor (F) of the ASW medium nutrient concentration per day.

Table 5.2: Optimal process conditions to achieve maximum areal productivity and CO_2 fixation efficiency for microalgal biomass production with *M. salina* in open TLC PBRs. Nutrient concentration in the feed medium is given as a factor (CF) of the nutrient concentration in the ASW medium with unchanged salt concentration. Nutrient feed rate is expressed using a factor (F) of the nutrient concentration in the ASW medium per day.

	Mode of operation	
Parameter	**Semi-continuous**	**Continuous**
CDW concentration	20–25 g L^{-1}	19–24 g L^{-1}
Dilution rate	–	0.150–0.225 d^{-1}
Nutrient concentration in feed medium	–	20× ASW
Nutrient supply to the reactor	2.5–3.5× d^{-1} ASW	3.0–4.5× ASW d^{-1}
pH	8.5	
Total alkalinity (TA)	200–400 ppm	
Volume-specific gas exchange surface	$>$ 0.850 m^{-1}	

Table 5.2 outlines the determined optimal conditions to achieve a mean daily areal productivity of >25 g m^{-2} d^{-1} and an average CO_2 fixation efficiency of >90% consistently in TLC PBR with 8 m^2 surface area. On the pilot scale, these same conditions guarantee an areal productivity of >21 g m^{-2} d^{-1} and a CO_2 fixation efficiency of at least 60%. Under these conditions, around 30 mL of concentrated sulphuric acid per day was required to keep the TA in the range of 4–8 mM (200–400 ppm)

in case of continuous operation. Based on the results presented in Subsection 5.3.4, it should also be mentioned that ensuring a volume-specific gas exchange area of over 0.850 m^{-1} between the CO_2 supply hoses and the reaction medium is crucial to reaching the high CO_2 fixation efficiencies specified above.

Figure 5.15 shows the water evaporation rate in TLC PBRs on different scales and operational modes. For processes on the 50 m^2 scale, the mode of operation had no significant influence on the evaporation rate. In the batch (P-B) and semi-continuous (P-S) processes the average water evaporation rate was the same with 4.3 L m^{-2} d^{-1}, which is very similar to but slightly lower than the values of 4.4–4.9 L m^{-2} d^{-1} recorded in continuous processes (P-C1, P-C2 and P-C3). By operating the circulation pumps of the TLC PBR only for 14 h during daytime (P-C4), the water evaporation rate in a continuous process was successfully reduced by 40% from 4.5 L m^{-2} d^{-1} to 2.7 L m^{-2} d^{-1}. In continuous processes on the 8 m^2 scale (C1 and C2), the evaporation rate was in a range of 5.2–5.5 L m^{-2} d^{-1} and thus higher compared to the 50 m^2 scale.

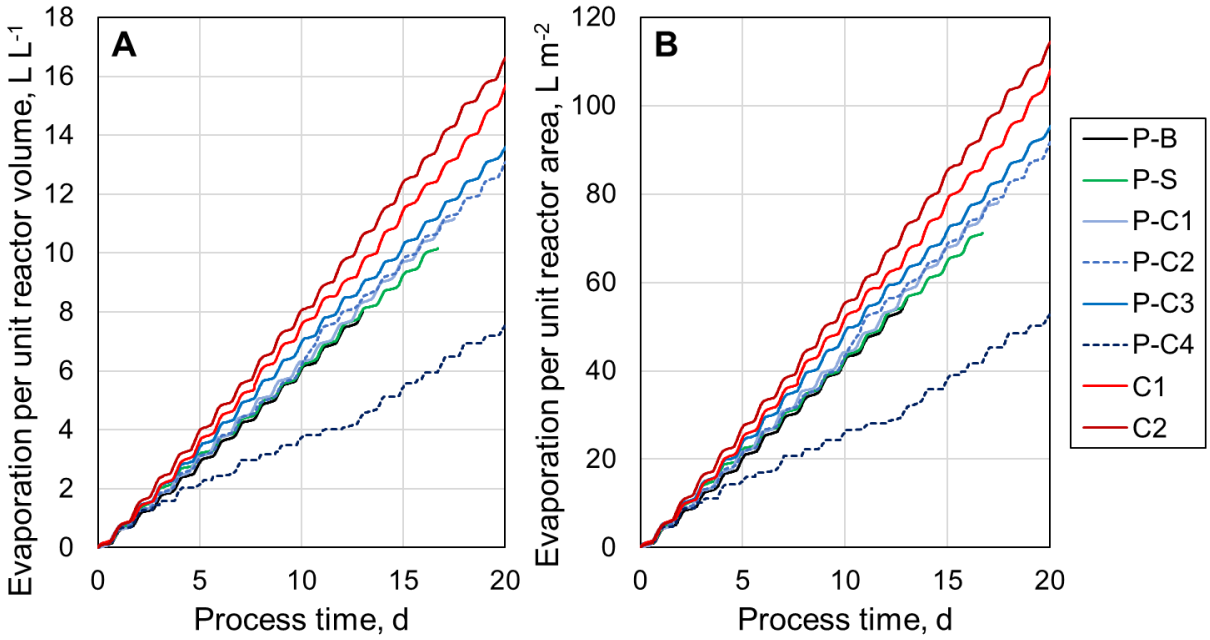

Figure 5.15: Comparison of water evaporation rate in TLC PBRs on different scales and operational modes. P-B and P-S are batch and semi-continuous processes, respectively, whereas P-C1, P-C2 and P-C3 are continuous processes on the 50 m^2 scale. P-C4 is a continuous process on the 50 m^2 scale with the automated switch-off of the circulation pumps overnight. C1 and C2 are continuous processes on the 8 m^2 scale. **A**: Water evaporation rate per unit liquid volume in reactor; **B**: water evaporation rate per unit reactor area.

Discussion

Ketchum and Redfield (1938) demonstrated for the first time that continuous microalgae cultivation allows for keeping biomass productivity at its highest over a longer period than batch cultivation. In this work, it was shown that semi-continuous and continuous modes are both suitable for achieving high areal productivities over 27 g m^{-2} d^{-1} on a daily average. However, continuous operation enabled higher CO_2 fixation efficiency of up to 100%, performing better than the semi-continuous operation in this regard. One of the most important factors affecting CO_2 fixation efficiency was shown to be the TA. Keeping the TA below 10 mM in continuous processes consistently yielded

CO_2 fixation efficiency over 80% as demonstrated previously by Schädler et al. (2019) for batch processes. Additionally, cultivation of *M. salina* at pH 8.5 provided the highest biomass productivity and CO_2 fixation efficiency, although this value is above the optimal pH range of *M. salina* according to literature (Boussiba et al., 1987; Bartley et al., 2014). Both productivity and CO_2 fixation efficiency achieved under the determined optimal conditions were higher than 17.9 g m^{-2} d^{-1} areal productivity and 84% CO_2 fixation efficiency reported in the most recent studies using the same cultivation set-up in continuous mode with a dilution rate of 0.4 d^{-1} (Schädler et al., 2019, 2021). For outdoor TLC PBR on larger scales up to 2,500 L, daily areal productivity of about 10–30 g m^{-2} d^{-1} is found in literature, which conforms with the values achieved in this study (Borowitzka & Moheimani, 2013).

In the process scale-up to the TLC PBR with 50 m^2 surface area, both areal productivity and CO_2 fixation efficiency achieved under optimal conditions remained below the values recorded on the 8 m^2 scale. In particular, the maximum CO_2 fixation efficiency reached on the pilot scale was 66%, which is 34% lower than on the 8 m^2 scale. Thus, a modification of the pilot scale TLC reactor was made, which included a change of the type of the gassing hoses used and increasing the gas exchange surface area, as this was previously shown to increase CO_2 fixation efficiency in the 8 m^2 scale TLC PBR (Schädler, 2020). Unfortunately, modifying the gassing system did not improve CO_2 fixation efficiency on the pilot scale. On the other hand, the maximum CO_2 fixation efficiency achieved in this study on the pilot scale still competes with the literature values for comparable continuous processes in large-scale outdoor systems, such as 63% achieved in a 50 L tubular airlift PBR (Mazzuca Sobczuk et al., 2000) or 70-77% reported for 100–224 m^2 scale TLC PBRs (Doucha & Livansky, 2006).

On the 8 m^2 and the 50 m^2 scale TLC reactors, water evaporation rates of 5.2–5.5 L m^{-2} d^{-1}, and 4.4–4.9 L m^{-2} d^{-1} were measured, respectively. These are in accordance with the previously reported 7.4 L m^{-2} on the 8 m^2 scale and 4.5 L m^{-2} on the 50 m^2 scale (Apel, 2017). To reduce the water and energy demand of the TLC PBR operation, a circulation pump switch-off overnight with simultaneous mixing of the microalgae suspension in retention tanks by pressurized air supply as previously described for the 8 m^2 scale TLC reactors by (Schädler, 2020) was implemented in the pilot-scale TLC reactor. It was successfully verified that the pump switch-off mechanism applied does not affect either microalgae growth or biomass productivity but causes a reduction of CO_2 fixation efficiency. In addition, it was shown that this method provides 40% savings in energy and fresh water supply costs due to the reduction of evaporation rate in the reactor.

5.7. Microalgal biomass harvest

The recovery of microalgae biomass from the reaction medium and biomass dewatering are essential in microalgae processes. These steps, which account for a large portion of the energy consumption in microalgal biomass production, are also essential in this study. Since the microalgae biomass is to be hydrolysed into a sugar-containing cultivation medium, preferably with the highest possible sugar concentration, it is crucial to reduce the water content of the biomass as much as possible to obtain a high-density microalgae paste. In this work, the biomass recovery and dewatering took place in a single step by centrifugation using a dynamic settler with spiral plate technology as described in Section 4.5. Microalgal biomass harvested this way had a CDW mass fraction of

31.2% ($\pm$ 0.7%), which corresponds to a water content of 68.8% *(w/w)*. Table 5.3 shows the separation efficiency achieved using this type of dynamic settler on two different scales. The settler model Evodos 10 (Evodos B.V., Raamsdonksveer, Netherlands) has a maximum capacity of 4 kg biomass per batch with manual discontinuous harvesting between batches. Evodos 50A (Evodos B.V., Raamsdonksveer, Netherlands) is the settler model designed for commercial use with an automated continuous harvesting system and thus without a capacity limit for the harvested biomass. In both cases, the biomass recovery efficiency was around 85%, and the biomass concentration factor was around 15 for dewatering of the microalgae suspension with a CDW concentration of 20 g L^{-1}.

Table 5.3: Performance evaluation of microalgae biomass harvest and dewatering using dynamic settlers with spiral plate technology (Evodos B.V., Raamsdonksveer, Netherlands). Evodos 10 has a maximum capacity of 4 kg biomass per batch with manual discontinuous harvesting between batches, whereas Evodos 50A is a model designed for commercial use with an automated continuous harvesting system without a capacity limit.

	Centrifuge model	
	Evodos 10	**Evodos 50A**
Microalgae suspension volume	50.0 L	710.0 L
CDW concentration	19.6 g L^{-1}	20.7 g L^{-1}
Total dry weight	0.98 kg	14.7 kg
Harvested wet biomass	2.7 kg	40.1 kg
Harvested dry mass	0.85 kg	12.4 kg
Recovery efficiency	86.5%	84.6%
Concentration factor	15.8	15.0

Discussion

Using a dynamic settler with spiral plate technology it was possible to concentrate the microalgae biomass to 31% solids content. A solids fraction of 0.4–22.0% in discharge are reported for other centrifugal methods such as disc stacked centrifuge or decanter, while among filtration based dewatering operations solids concentrations reaching 18% with continuous and 22–27% with discontinuous methods are indicated in literature (Pahl et al., 2012). Thus, a dynamic settler with spiral plate technology proves itself to be the best option, if the highest possible solids concentration is aimed as is the case in this work. Nonetheless, the biomass recovery efficiency of around 85% measured in this study is lower than the range of 95–99% stated for spiral plate technology in literature (Fasaei et al., 2018). This was mainly due to the loss of microalgae suspension at the end of each solids discharge step, since the microalgae suspension inside the centrifuge drum was drained completely before each discharge. This loss could be avoided by directing the discharged algae suspension back into the feed tank, which would yield a higher recovery efficiency. Spiral plate technology has a high performance for microalgal biomass harvest and dewatering in general and is considered an efficient, scalable and continuous method suited for industrial application. However, the high energy requirement of 0.95–2.0 kWh m^{-3} compared to other dewatering methods should also be taken into account in the selection of equipment depending on process requirements (Fasaei et al., 2018).

6. Yeast Oil Production with *Cutaneotrichosporon oleaginosus* Using a Membrane Bioreactor [1]

This chapter focuses on yeast oil production with *C. oleaginosus* under phosphorus-depleted conditions in a membrane bioreactor (MBR) with total cell retention. First, different C/P ratios in the batch medium were examined for lipid production in fed-batch mode on a 3 L scale, and the feed rate was adjusted to give low sugar concentrations in the reaction medium during cultivation. Then, high-cell-density yeast cultivation with a dilute substrate with phosphorus limitation was carried out in an MBR with total cell retention on a 1.5 L scale. Finally, this process was scaled up to 50 L and reproduced multiple times successfully. In addition, simultaneous utilization of different sugars present in microalgae hydrolysate by *C. oleaginosus* was investigated.

6.1. Utilization of sugars

In biomass hydrolysates, different types of carbon sources, particularly different kinds of sugars, are present. In order to determine if *C. oleaginosus* is able to utilize all sugars found in a microalgae hydrolysate simultaneously, a batch process in a stirred-tank reactor (STR) with 3 L working volume was carried out using a defined medium with a sugar mixture of 40 g L^{-1} glucose, 10 g L^{-1} mannose, 10 g L^{-1} galactose and 3 g L^{-1} rhamnose. In this experiment, a cell dry weight (CDW) concentration of 25.8 g L^{-1} was achieved after 45 hours. The highest volumetric productivity of lipids, or lipid space-time-yield (STY_L), with 0.30 g L^{-1} h^{-1} was reached between 22–25 hours. At this process time, a biomass yield ($Y_{X/S}$) of 0.50 g g^{-1} and a lipid yield of ($Y_{L/S}$) of 0.18 g g^{-1} were achieved. The maximum specific growth rate of 0.32 h^{-1} was recorded after 5 hours. The results of the whole experiment are presented in Figure 6.1. After 20 hours, the ammonia concentration in the medium fell below 3 mg L^{-1} as seen in Figure 6.1 (d). As a result of nitrogen limitation, 39% cellular lipid content was achieved at the end of the process with a total lipid concentration of 10.0 g L^{-1}. Figure 6.1 (c) shows that all sugars except for galactose are utilized simultaneously by *C. oleaginosus*. Galactose, however, is taken up first after the concentrations of all other sugars fell below 0.5 g L^{-1}.

Discussion

The sugar content of the defined medium used in this experiment was determined based on the known sugar composition of *M. salina* biomass (Schädler et al., 2019). An examination of sugar utilization by *C. oleaginosus* was necessary since the presence of some sugars inhibiting the take-up of others, such as glucose repression, was reported for *C. oleaginosus* (Gong et al., 2013, 2016). It was verified that glucose, mannose and rhamnose are taken up simultaneously by *C. oleaginosus*. The insight that galactose is not utilized by *C. oleaginosus* simultaneously with other sugars is very important for using microalgae hydrolysate as a substrate for yeast cultivation and is in line with findings in literature (Meo et al., 2017). Although the fraction of galactose in the total sugar content of dry *M. salina* biomass is only 6.8%, a complete loss of galactose contained in the microalgae

[1] Part of the results presented here has already been published in: Koruyucu, A., Blums, K., Peest, T., Schmack-Rauscher, L., Brück, T., & Weuster-Botz, D. (2023). High-cell-density yeast oil production with diluted substrates imitating microalgae hydrolysate using a membrane bioreactor. *Energies, 16*(4), 1757. doi:10.3390/en16041757

hydrolysate would still reduce the carbon conversion efficiency into lipids to some degree and should be therefore avoided, if possible. In high-cell-density yeast oil production in an MBR system with total cell retention, high cell densities and low volumetric flow rates through the reactor would favour the complete utilization of all sugars so that the sugar concentration stays very close to 0 g L^{-1} and thus no sugar exits the reactor unused.

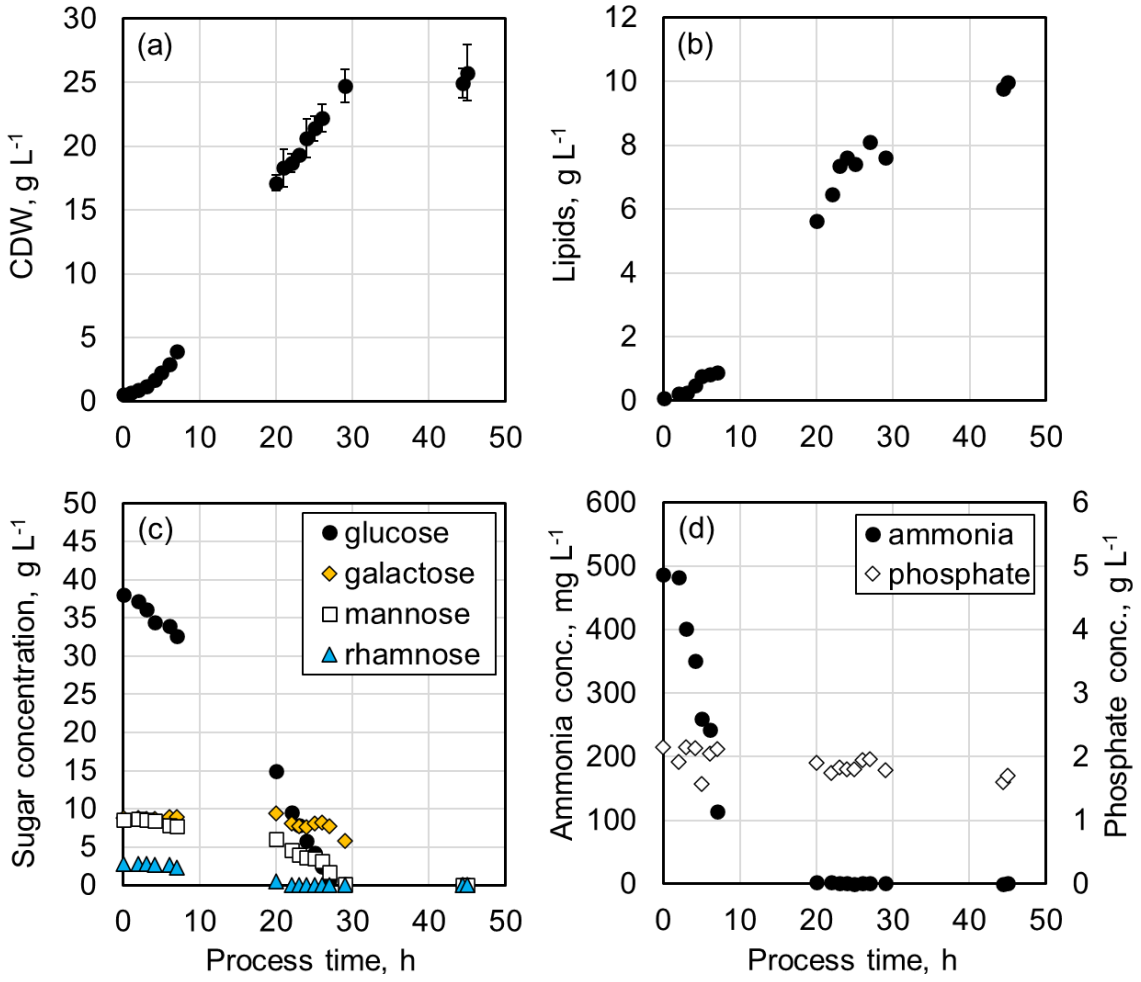

Figure 6.1: A batch process with *C. oleaginosus* in a stirred-tank bioreactor on a 3 L scale to check for possible substrate preferences. A defined medium was used with a mixture of sugars, which are likely to be present in a microalgal biomass hydrolysate. The medium composition was as in Table 4.5 with the following differences: 10.0 g L^{-1} galactose; 3.0 g L^{-1} rhamnose; 2.45 g L^{-1} $(NH_4)_2SO_4$; 2.40 g L^{-1} KH_2PO_4; 0.91 g L^{-1} $NaHPO_4$. The following process settings were applied: pH=6.5; T=30 °C; dissolved oxygen level (DO)$\geq$20%. (a) CDW concentration; (b) lipid concentration; (c) sugar concentrations; (d) concentration of ammonia on the primary vertical axis and of phosphate on the secondary axis.

6.2. Variation of the C/P ratio in fed-batch processes on a litre scale

High productivity lipid production with *C. oleaginosus* under phosphorus-depleted conditions with a C/P ratio of 3512 g g^{-1} in cultivation medium was previously demonstrated by Meo et al. (2017). Thus, a similar C/P ratio was also applied in this study with glucose as the sole carbon source with a 20 g L^{-1} concentration in the batch and with 400 g L^{-1} in the feed medium (see Table 4.5). In order to determine if a lower initial C/P ratio in the batch phase affects the biomass and lipid productivity of the yeast oil production process, two fed-batch processes were carried out in a stirred-tank reactor (STR) on a 3 L scale with different C/P ratios of 470 g g^{-1} and 3515 g g^{-1} in the batch medium. The C/P ratio of the feeding medium was 3515 g g^{-1} in both cases. Figure 6.2 illustrates the results of

these experiments with the first and the second green vertical lines indicating the start of medium feed with 4.0 g L^{-1} h^{-1} glucose after 4 hours and reduction of the feed rate to 1.7 g L^{-1} h^{-1} glucose after 24 hours, respectively.

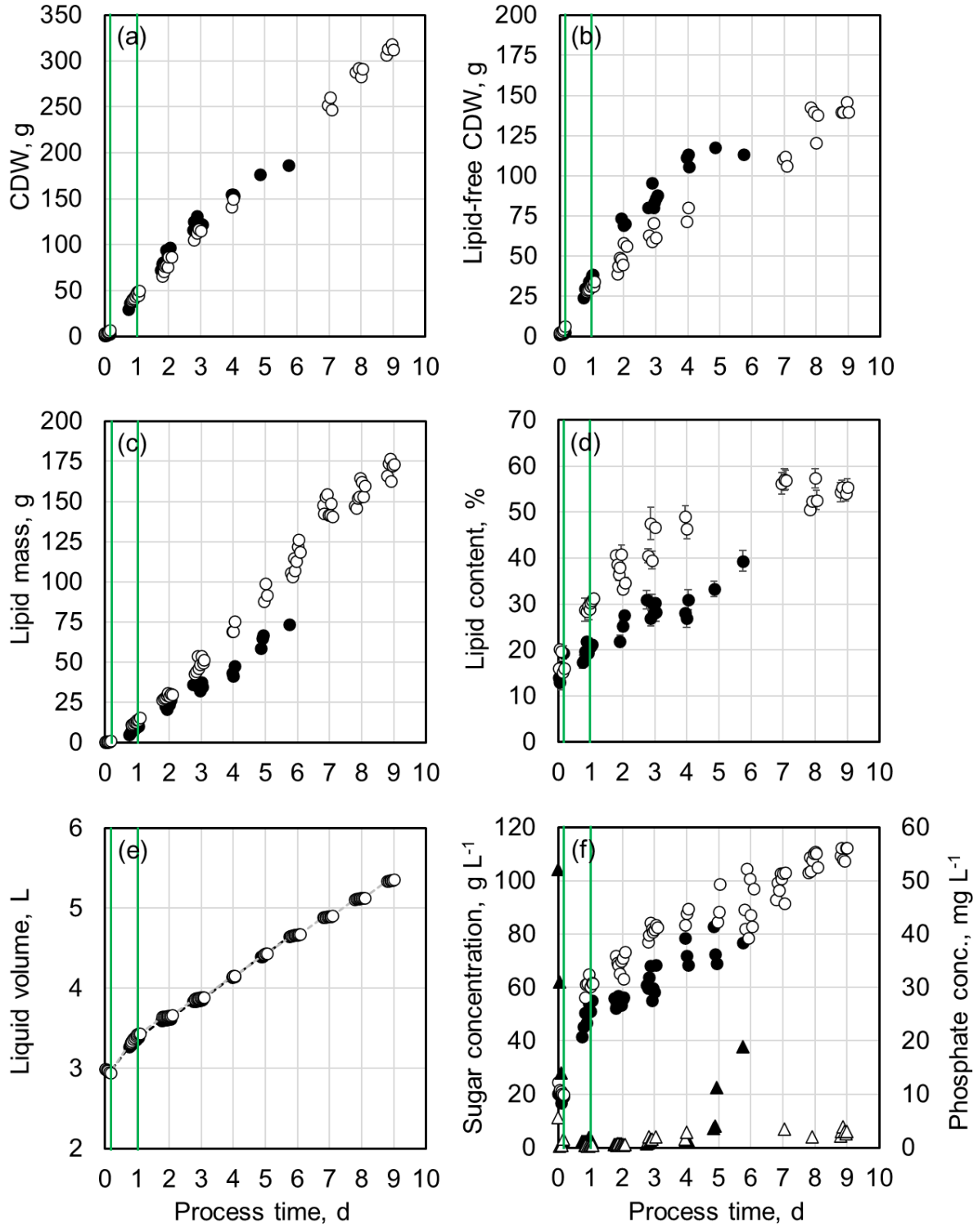

Figure 6.2: Variation of the C/P ratio in batch medium for yeast oil production in fed-batch processes on a litre scale. Batch medium C/P ratio of 470 g g^{-1} represented with black (●) and 3515 g g^{-1} with white marks (○). C/P ratio of the feed medium was 3515 g g^{-1} in both cases. The first and the second green vertical lines indicate the start of feed with 4.0 g glucose L^{-1} h^{-1} and reduction of feed rate to 1.7 g glucose L^{-1} h^{-1}, respectively. The following process parameters were used: pH=6.5; T=30 °C; DO≥20%. (a) CDW; (b) lipid-free CDW; (c) lipid mass; (d) cellular lipid content; (e) liquid volume in reactor; (e) liquid volume in reactor; (f) concentrations of glucose (●) and mannose (◆) on the primary vertical axis and of phosphate (▲) on the secondary axis.

In the first experiment with a C/P ratio of 470 g g^{-1} in the batch medium, a steady biomass increase was observed until day 3, after which it stagnated, reaching a maximum of 186.6 g CDW corresponding to a biomass concentration of 40.1 g L^{-1}. Lipid-free CDW followed a similar pattern, reaching a final mass of 113.1 g (24.3 g L^{-1}) at the end of the process. On the other hand, lipid weight increased continuously throughout the process with a maximum of 73.4 g (15.8 g L^{-1}) at the end. Lipid accumulation continued until the end of the process, as the lipid weight and lipid content did not show a saturation pattern. The cells reached a maximum lipid content of 39.4%. The steady accumulation of glucose in the reaction medium indicates that the feeding rate was too high, resulting in a high glucose concentration of 76.9 g L^{-1} after 6 days. Besides, a steep increase in the phosphate concentration was observed after day 5, simultaneously with a decrease in the lipid-free CDW, implying a possible degradation of the cell mass.

The second process with a C/P ratio of 3515 g g^{-1} in the batch medium lasted 9 days. A steady biomass increase was observed until day 2, after which biomass productivity declined, reaching a maximum CDW of 312.7 g (58.4 g L^{-1}) at the end of the process. The course of lipid-free CDW was similar, with a final value of 139.6 g (26.1 g L^{-1}) at the end. Lipid weight increased almost constantly until day 7 but slowed down after that. At the end of the process, a lipid mass of 173.1 g (32.3 g L^{-1}) was recorded. Cellular lipid content continued increasing over the whole process, showing a saturation behaviour around 55–60% with 55.3% lipid quota after 9 days. As in the previous experiment, the feed rate was set too high, resulting in an accumulation of sugars in the reaction medium with a very high glucose concentration of 112.3 g L^{-1} after 9 days.

In order to prevent sugar accumulation in the reaction medium and to keep the sugar concentration as close to 0 g L^{-1} as possible, another fed-batch process with a C/P ratio of 3515 g g^{-1} in both batch and feed media, but with a lower feed rate was carried out. Total sugar concentration was adjusted to 50 g L^{-1} in the batch medium and 200 g L^{-1} in the feeding medium (with a sugar mixture of 80% glucose and 20% mannose). In addition, the concentration of $(NH_4)_2SO_4$ in batch and feeding media was adjusted to 25.0 g L^{-1} and 12.5 g L^{-1}, respectively. On the first night of cultivation, the dissolved oxygen (DO) level fell to 6.2% due to a failure of the control sequence. The control sequence was restarted after a process time of 19.2 hours, and the DO level was kept above 30% after that. However, this has probably led to a prolonged batch phase of around 2 days. After the glucose concentration fell below 6 g L^{-1}, medium feed was started with a rate of 0.9 g L^{-1} h^{-1} glucose. The cultivation was carried out over 10 days, reaching a final reaction volume of 4.8 L. Ammonia concentration in the reaction medium remained above 10 g L^{-1} at all times excluding a nitrogen-depletion aided lipid accumulation.

Total biomass productivity was mostly stable over the process with a CDW increase rate of 24.3 g d^{-1} corresponding to a productivity of 0.34 g L^{-1} h^{-1}. After the first process day, the rate of lipid-free CDW growth sank, and the lipid production rate increased, which resulted in a steep increase in the cellular lipid content. Lipid quota reached 49.2% on day 3 and increased only marginally by 6.6% over the next 7 days. A final CDW of 245.5 g (51.2 g L^{-1}) and a lipid mass of 136.9 g (28.5 g L^{-1}) were achieved after 10 days. Using a feed rate of 0.9 g L^{-1} h^{-1} sugars, concentrations of both glucose and mannose were kept relatively constant around 3–7 g L^{-1} each until day 8. After that,

sugar concentrations started to fall, reaching values below 1.5 g L^{-1} on day 10.

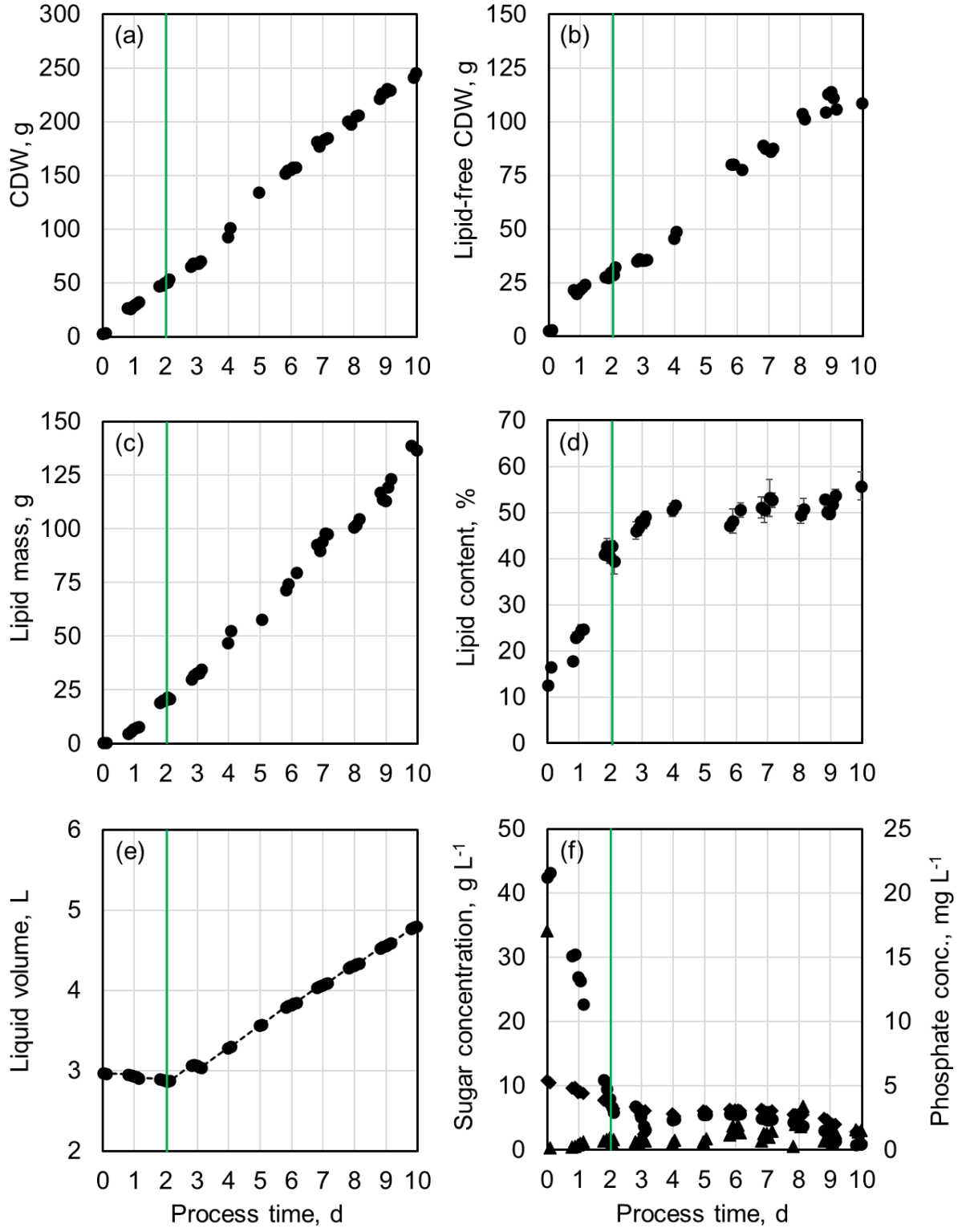

Figure 6.3: Adjustment of feed rate for yeast oil production with low sugar concentration in a fed-batch process on a litre scale. C/P ratio was 3515 g g^{-1} in both batch and feed media. Total sugar concentration was adjusted to 50 g L^{-1} in the batch medium and 200 g L^{-1} in the feeding medium (with a sugar mixture of 80% glucose and 20% mannose). The first green vertical line indicate the start of feed with 0.9 g L^{-1} h^{-1} sugars. The following process parameters were used: pH=6.5; T=30 ℃; DO≥20%. (a) CDW; (b) lipid-free CDW; (c) lipid mass; (d) cellular lipid content; (e) liquid volume in reactor; (f) concentrations of glucose (●) and mannose (◆) on the primary vertical axis and of phosphate (▲) on the secondary axis.

Table 6.1 summarises process parameters, metrics and carbon conversion for three yeast oil production processes with phosphorus limitation in fed-batch mode on a 3 L scale. The fraction of carbon taken up by yeasts, which was converted into lipids, is also referred to as carbon conversion efficiency (η_C). In the final experiment, the flow of carbon was distributed as 21.4% into lipid-free dry cell mass and 44.0% into lipids, with 34.5% released in the form of CO_2 and other by-products. A higher C/P ratio in batch medium yielded a higher lipid productivity and a higher carbon conversion efficiency.

Table 6.1: Process parameters, metrics and carbon conversion for three yeast oil production processes with phosphorus limitation in fed-batch mode on a 3 L scale.

	Experiment #		
Parameters	**I**	**II**	**III**
C/P ratio in batch medium	470 g g^{-1}	3515 g g^{-1}	3515 g g^{-1}
C/P ratio in feed medium	3515 g g^{-1}	3515 g g^{-1}	3515 g g^{-1}
Sugar feeding rate	1.7–4.0 g L^{-1} h^{-1}	1.7–4.0 g L^{-1} h^{-1}	0.9 g L^{-1} h^{-1}
Final reaction volume	4.7 L	5.4 L	4.8 L
Process time	5.7 d	9.0 d	10.0 d
Process metrics			
CDW	40.1 g L^{-1}	58.4 g L^{-1}	51.2 g L^{-1}
Lipid concentration	15.8 g L^{-1}	32.3 g L^{-1}	28.5 g L^{-1}
Lipid quota	39.4%	55.3%	55.8%
STY_{X+L}	0.45 g L^{-1} h^{-1}	0.48 g L^{-1} h^{-1}	0.34 g L^{-1} h^{-1}
STY_L	0.18 g L^{-1} h^{-1}	0.27 g L^{-1} h^{-1}	0.19 g L^{-1} h^{-1}
$Y_{(X+L)/S}$	0.37 g g^{-1}	0.46 g g^{-1}	0.40 g g^{-1}
$Y_{L/S}$	0.15 g g^{-1}	0.26 g g^{-1}	0.22 g g^{-1}
Fraction of carbon converted into			
Lipids	28.5%	50.1%	44.0%
Lipid-free CDW	27.3%	24.9%	21.4%
CO_2 and by-products	44.2%	24.9%	34.5%

Discussion

Generally, a higher C/P ratio results in a higher cellular lipid content in oleaginous yeasts (Meo, 2016; Wu et al., 2010). The C/P ratio of the feeding medium in the fed-batch experiments was adjusted to 3515 g g^{-1}, since Meo (2016) previously showed that this is sufficient for lipid production with high space-time-yield (STY) using *C. oleaginosus*. Meo (2016) also reported that the C/P ratio (in a

range of 702–7024 g g^{-1}) in batch medium does not affect the cellular lipid content of *C. oleaginosus* in the millilitre scale fed-batch cultivations over 4.3 days using the same feeding strategy as in this work, indicating 38–39% final lipid quota achieved. However, the results of the fed-batch cultivations on the 3 L scale in this study show that the C/P ratio (range of 470–3515 g g^{-1}) in batch medium does influence the cellular lipid content of *C. oleaginosus*. After a process time of 4 days, the lipid quota achieved with an initial C/P ratio of 470 g g^{-1} was 30%, while with an initial C/P ratio of 3515 g g^{-1} 50% lipid quota was recorded. Even though it is possible that, in the long term, the lipid content of *C. oleaginosus* would be the same independent of the initial C/P ratio, it would apparently take longer with a lower C/P ratio in batch medium, ultimately affecting the lipid productivity.

STY of lipid production (STY_L) ranged between 0.18–0.27 g L^{-1} h^{-1}, which is much higher than 0.11 g L^{-1} h^{-1} reported by Meo et al. (2017) in a very similar experiment examining phosphorus-depleted fed-batch cultivation of *C. oleaginosus*. A lipid productivity of 0.03 g L^{-1} h^{-1} was indicated by G. Zhang et al. (2011) for phosphorus-depleted batch cultivation of *C. oleaginosus* using N-acetylglucosamine as the carbon source. Nevertheless, similar lipid productivities in a range of 0.16–1.00 g L^{-1} h^{-1} were reported for lipid production induced by nitrogen limitation (Meesters et al., 1996; Hassan et al., 1996).

Carbon flow into lipid synthesis was higher with an initial C/P ratio of 3515 g g^{-1}, resulting in a higher carbon conversion efficiency (η_C). This also shows itself in the higher lipid yield ($Y_{L/S}$) of 0.22–0.26 g g^{-1}, which lies a little below the theoretical maximum that has been calculated by Ratledge (2014) to be approximately 0.33 g g^{-1}. In general, lipid yield achieved in fed-batch cultivations in this study lies above literature values (0.05–0.10 g g^{-1}) for phosphorus-depleted cultivation of *C. oleaginosus* (Meo et al., 2017; G. Zhang et al., 2011).

6.3. Yeast oil production in an MBR on a litre scale

A membrane bioreactor (MBR) with total cell retention was used for high-cell-density yeast cultivation using a defined medium with low sugar concentration on a 1.5 L scale. The MBR was composed of an STR and a cross-flow microfiltration unit connected to it as an external bypass, making up a total working volume of 1–6 L (110 mL of it bypass). A hollow fibre membrane unit made of polysulfone with a pore size of 0.20 µm and a filtration area of 0.042 m^2 was employed. A semi-continuous mode of operation was applied for cultivation in the MBR. Cultivation was started in batch mode, and after complete depletion of the sugars in the medium, the MBR operation was switched to semi-continuous mode. In the semi-continuous mode of operation, the feed is supplied into the MBR continuously at a constant rate, whereas filtering out of the used-up medium from the reactor is completed only for 8 hours during the day. This method entails a constant change in liquid volume inside the reactor in a preset range; however, it also reduces the time of microfiltration per process time so that energy consumption associated with medium filtration is reduced by two-thirds compared to a fully continuous operation. The design and operation of the MBR, as well as the applied semi-continuous production mode, were described in detail in Section 4.7.

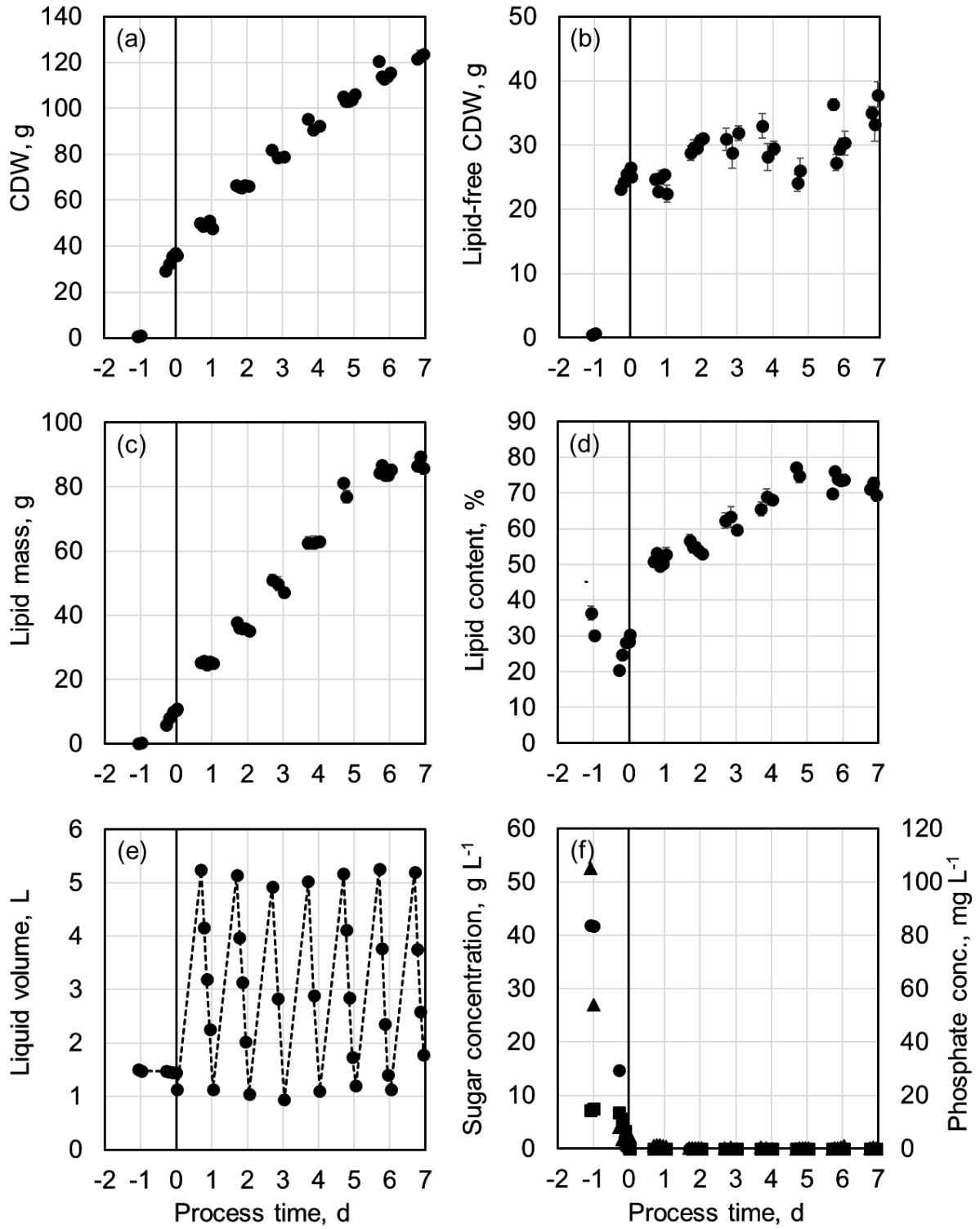

Figure 6.4: A semi-continuous processes for yeast oil production with *C. oleaginosus* in a membrane bioreactor on a 1.5 L scale with total cell retention. A defined medium (Table 4.5) was used with a low sugar concentration of 50 g L^{-1} and a C/P ratio of 3515 g g^{-1} in both batch and feed media with a feed rate of 1.1 g L^{-1} h^{-1} sugars. The following process parameters were used: pH=6.5; T=30 ℃; DO≥20%. The black line shows the end of the batch phase and switch to semi-continuous mode of operation. The error bars show the standard deviation of the triplicate measurements. (a) CDW; (b) lipid-free CDW; (c) lipid mass; (d) lipid content of the yeast cells; (e) liquid volume in reactor; (f) concentrations of glucose (●) and mannose (◆) on the primary vertical axis and of phosphate (▲) on the secondary axis.

Oleaginous yeast *C. oleaginosus* was cultivated under phosphate-depleted conditions with a C/P ratio of 3515 g g^{-1} in both batch and feeding media to induce lipid production. However, the initial

C/P ratio was lower (581 g g^{-1}) after inoculation since the preculture cells were not washed before inoculation. Total sugar concentration was adjusted to 50 g L^{-1} in both batch and feed media (with a sugar mixture of 80% glucose and 20% mannose) since the microalgae hydrolysate to be used as substrate in this work is expected to have a similar sugar concentration. The results of this experiment are presented in Figure 6.4.

The batch phase took 26 hours, and during this time, the sugars were utilized simultaneously by the yeast, meaning there was no preference for one sugar over the other, as already shown in Section 6.1. After complete consumption of sugars in the batch medium, the semi-continuous mode of operation started with a feed rate of 1.1 g L^{-1} h^{-1} sugars. The liquid volume inside the reactor was initially 1.5 L and kept in a range of 0.9–5.3 L throughout the semi-continuous phase. The initial lipid content of the cells was 36.3%, which suggests that a nutrient limitation had already occurred in the preculture. However, the cellular lipid content decreased quickly after the transfer into a nutrient-replete fresh medium by inoculation of the reactor.

After the start of the semi-continuous operation, CDW kept increasing at a slowly decreasing rate. Lipid mass constantly increased at a rate of 13 g d^{-1} until 5 days into the semi-continuous operation but fell abruptly to 4 g d^{-1} thereafter. A very high maximum cellular lipid content of 77.1% was achieved on day 5 of the semi-continuous phase, which declined to 69.4% at the end of the process. This is, however, most likely due to a measurement error in CDW since the calculated lipid-free CDW shows a sharp drop on day 5, followed by a sharp increase on the next day, simultaneously with the changes in cellular lipid quota. Hence, the final value of 69.4% lipid content is more reliable than the peak value. Maximum lipid productivity of 0.39 g L^{-1} h^{-1} was reached simultaneously with maximum lipid quota. Eventually, it was shown that a feeding rate of 1.1 g L^{-1} h^{-1} sugars is sufficiently low to keep the sugar concentrations in reaction medium below the detection limit at all times (Fig. 6.4 f), which is very important to ensure that no valuable carbon source exits the MBR unused.

Discussion

After a total process time of 8 days in an MBR with total cell retention, final cellular lipid content (69.4%), lipid productivity (0.30 g L^{-1} h^{-1}) and lipid yield (0.25 g g^{-1}) were all higher than in the fed-batch cultivation with the same sugar feeding rate, despite a higher initial phosphate availability due to omission of the preculture washing step. An essential difference between the experiments was the sugar concentration in the reaction medium. In the fed-batch experiment described in Section 6.2, the lowest measured sugar concentrations were 0.86 g L^{-1} glucose and 1.2 g L^{-1} mannose, both measured at the end of the process. Here, both sugars were below the detection threshold already after a process time of 1.2 days. A potential effect of carbon depletion on signalling pathways resulting in increased lipogenesis has been reported (Bracharz, Redai, et al., 2017). Thus, lower sugar concentrations may have contributed to increased lipid biosynthesis in this experiment, compared to the fed-batch process.

Although sugar concentrations below the detection level limited the carbon availability, no decrease in lipid-free cell mass or lipid degradation was observed throughout the process. It has been re-

ported that the main bottleneck of lipid accumulation is not the uptake of carbon but rather the flow of carbon to fatty acids and triacylglycerides (Ykema et al., 1986). That means even though no carbon source was detected in the reaction medium, it is likely that the sugars taken up by the cells were present intracellularly and sufficient for ensuring cell maintenance.

High-cell-density cultivation of *C. oleaginosus* in an MBR with total cell retention in continuous mode on a 3 L scale was previously studied by Meo et al. (2017) reporting a final cellular lipid content of 70%, an overall lipid yield of 0.26 g g^{-1} and a STY of 0.53 g L^{-1} h^{-1}. Although lipid content and yield achieved in this study were similar to these values, lipid productivity was significantly lower with 0.30 g L^{-1} h^{-1}. It must, however, be noted that a sugar feed rate of 1.95 g L^{-1} h^{-1} was applied in the mentioned experiment by Meo et al. (2017), which is around 77% higher than in this study and perfectly explains the 77% higher lipid STY. The choice of semi-continuous operation in this study did not allow a higher feeding rate, unfortunately, since this would cause the reaction volume to exceed the maximum working volume of the MBR overnight, where no filtration is performed. Moreover, the semi-continuous operation was necessary in this work since the continuous operation of the 50 L scale MBR used for the scale-up was not possible. Hence, the relatively low lipid productivity is caused by the conservative selection of the feeding rate but can be increased using a higher feed rate in a different operational mode.

6.4. Yeast oil production scale-up to 50 L

The MBR used for the high-cell-density yeast cultivation on a 50 L scale was composed of an STR and a cross-flow microfiltration unit connected to it as an external bypass, constituting a total working volume of 40–67 L (7.25 L of it bypass). A ceramic capillary microfilter with a pore size of 0.25 µm and a filtration area of 0.8 m^2 was employed. Due to technical reasons, an unsupervised operation of the cross-flow microfiltration unit overnight was not possible. Thus, a semi-continuous mode of operation was developed to allow intermittent microfiltration with continuous medium feed. The semi-continuous mode of operation was applied as described for the yeast cultivation in the 1.5 L MBR, with the continuous supply of the feed medium to the MBR at a constant rate and intermittent filtering out of the used-up medium from the reactor only for 8 hours during the day. The design and operation of the MBR, as well as the applied semi-continuous production mode, were described in detail in Section 4.7. In addition, a comparison of the specifications and operating conditions of the 1.5 L and 50 L MBRs is given in Table 4.13.

As in the previous experiment in a 1.5 L scale MBR, *C. oleaginosus* was cultivated under phosphate-depleted conditions with a C/P ratio of 3515 g g^{-1} in both batch and feeding media to induce lipid production. However, the initial C/P ratio was lower (617.5 g g^{-1}) after inoculation since the preculture cells were not washed before inoculation. The results of this experiment and the previous experiment on 1.5 L as reference are presented in Figure 6.5. Instead of plotting the measured values of CDW, lipid-free CDW and lipid concentrations, these were normalised to the initial reaction volume in each experiment by multiplying the concentration with the actual reaction volume at the time of sampling and then dividing by the initial reaction volume at inoculation. In this way, a comparison of the measured values for two different scales with changing reaction volumes is made possible.

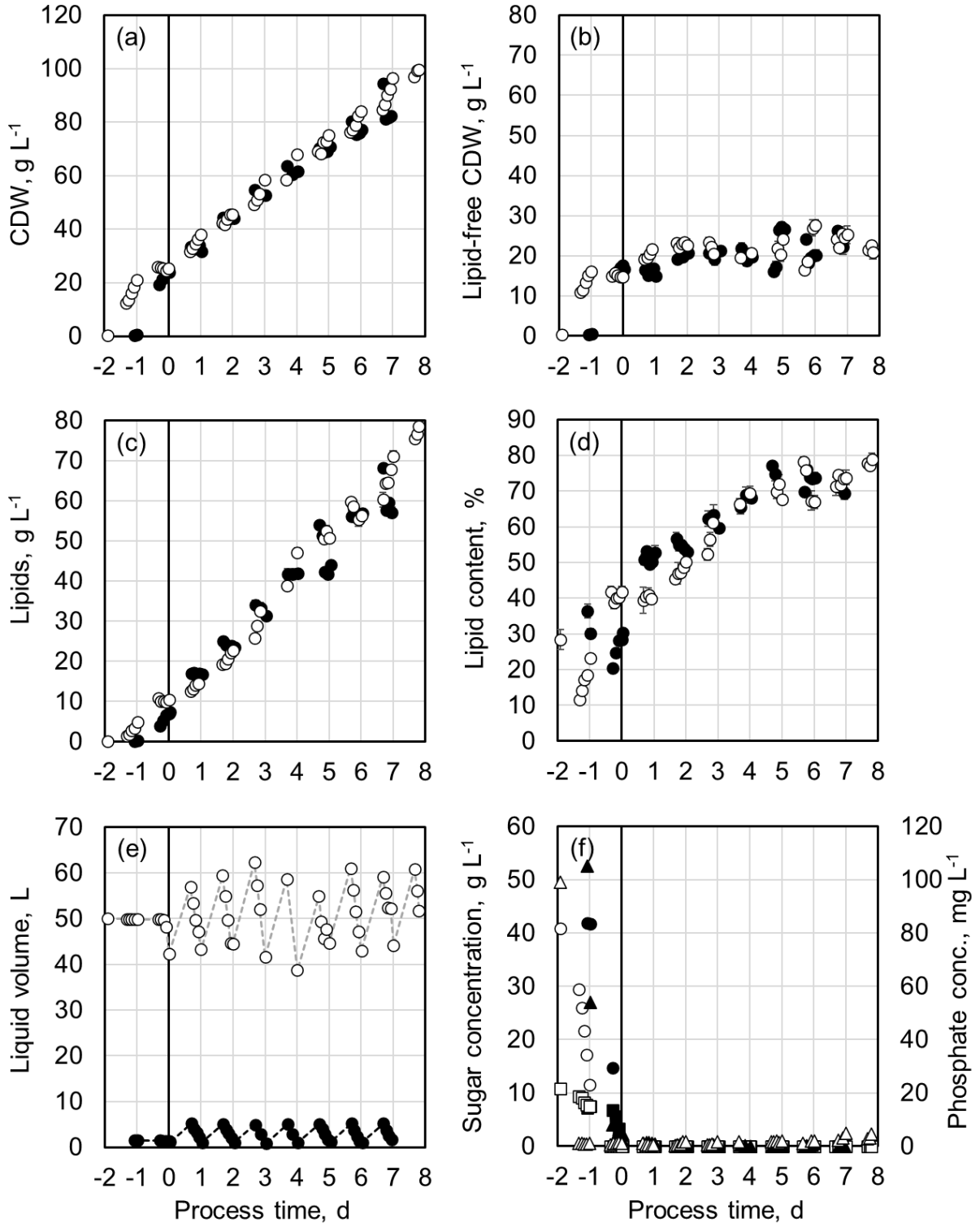

Figure 6.5: Comparison of two semi-continuous processes for yeast oil production with *C. oleaginosus* in MBRs with total cell retention on a 1.5 L and a 50 L scale. The data values are normalized to initial liquid volume in each reactor. A defined medium (Table 4.5) with a low sugar concentration of 50 g L^{-1} and a C/P ratio of 3515 g g^{-1} was used as both batch and feed media with a feed rate of 1.1 g L^{-1} h^{-1} sugars. The following process parameters were used: pH=6.5; T=30 ℃; DO≥20%. The black line shows the end of the batch phase and switch to semi-continuous mode of operation. The results of the experiment on the 1.5 L scale are marked in black (●), while those of the experiment on the 50 L scale are marked in white (○). The error bars show the standard deviation of the triplicate measurements. (a) CDW concentration; (b) lipid-free CDW concentration; (c) lipid concentration; (d) lipid content of the yeast cells; (e) liquid volume in reactor; (f) concentrations of glucose (●) and mannose (◆) on the primary vertical axis and of phosphate (▲) on the secondary axis.

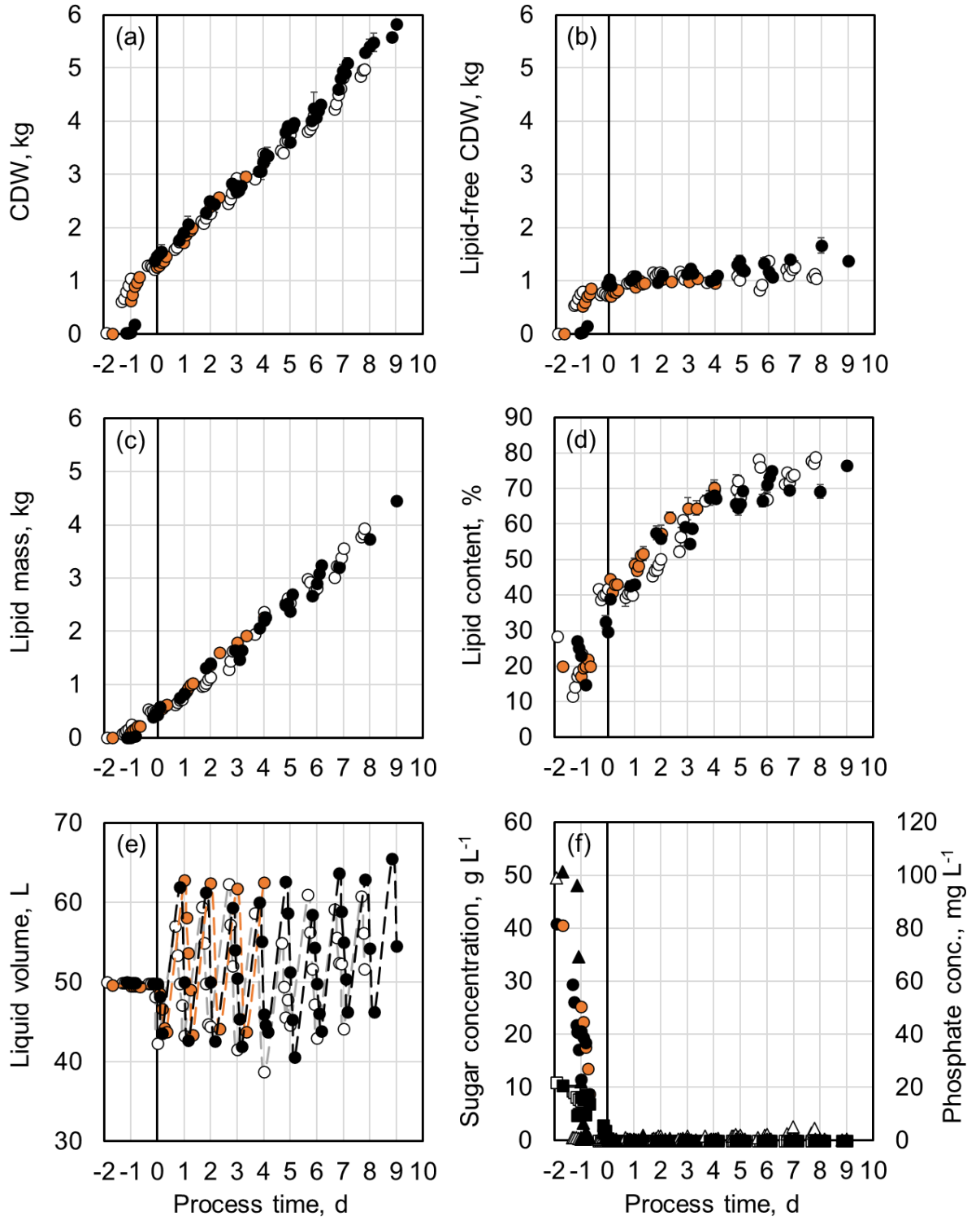

Figure 6.6: Three semi-continuous processes for yeast oil production with *C. oleaginosus* in a membrane bioreactor on a 50 L scale with total cell retention. A defined medium (Table 4.5) with a low sugar concentration of 50 g L^{-1} and a C/P ratio of 3515 g g^{-1} was used as both batch and feed media with a feed rate of 1.1 g L^{-1} h^{-1} sugars. The following process parameters were used: pH=6.5; T=30 °C; DO≥20%. The black line shows the end of the batch phase and switch to semi-continuous mode of operation. The results of Experiment 1 are marked in orange (●), those of Experiment 2 in white (○), and those of Experiment 3 in black (●). The error bars show the standard deviation of the triplicate measurements. (a) CDW; (b) lipid-free CDW; (c) lipid mass; (d) lipid content of the yeast cells; (e) liquid volume in reactor; (f) concentrations of glucose (●) and mannose (◆) on the primary vertical axis and of phosphate (▲) on the secondary axis.

In the experiment on a 50 L scale (Exp. 1), the sugars in the batch medium were completely used up after around 27 hours. However, it took longer until the medium feed and semi-continuous operation could be started, resulting in a batch phase of 46 hours, 20 hours longer than on the 1.5 L scale. As shown in Figure 6.5, normalized values of CDW and lipid concentrations are very much in accordance with each other on both scales throughout the whole process. A cellular lipid content of 73.8% was achieved after 7 days into the semi-continuous mode of operation on the 50 L scale, which is exactly the same as on the 1.5 L scale. Nevertheless, unlike on the 1.5 L scale, lipid quota did not start declining after reaching a maximum but kept increasing until the end of the experiment, reaching a final value of 78.9%. A feed rate of 1.1 g L^{-1} h^{-1} sugars was sufficiently low to keep the sugar concentrations below the detection level also on the 50 L scale. Phosphate concentration increased slightly on the last three days of the experiment but still stayed below 5 mg L^{-1} at all times. These results prove that the scale-up of the high-cell-density yeast oil production in an MBR from the 1.5 L to the 50 L scale was successful.

High-cell-density yeast oil production in an MBR on a 50 L scale was carried out three times to demonstrate the reproducibility of the results, which are illustrated in Figure 6.6. Batch phase duration varied between the experiments due to the lag time between the complete depletion of sugars in the medium and the start of the fresh medium feed. This resulted in stagnation of cell growth of around 1.5 days after inoculation in Experiments 1 and 2. In Experiment 3, the cell density at the time of inoculation was adjusted to prevent this delay. Furthermore, Experiment 2 had to be terminated sooner than intended due to technical problems. During the process, the maximum permeate flow rate achievable by the microfiltration unit decreased over time as a function of increasing biomass concentration. Therefore, Experiments 1 and 3 were stopped as soon as the required permeate flow rate could not be ensured any more.

The batch phase took 28–46 hours for all experiments on a 50 L scale. After complete consumption of sugars in the batch medium, the semi-continuous mode of operation was applied as described in Section 4.7. Small fluctuations in the actual values of flow rates from the set points during the semi-continuous operation led to changes in liquid volume inside the MBR between 40–67 L, with slight deviations from the planned range of 44–63 L. In all the experiments, a defined medium with a C/P ratio of 3515 g g^{-1} (Table 4.5) was used, which contains 17 mg L^{-1} phosphate. After inoculation with unwashed preculture cells, an initial phosphate concentration of 100 mg L^{-1} was measured in each experiment. The initial lipid content of the cells was between 20–30% in all the experiments (Fig. 6.6 d), suggesting that a nutrient limitation had already occurred in the preculture. However, the cellular lipid quota decreased quickly after the transfer into nutrient-replete fresh medium by inoculation of the MBR.

After the start of the semi-continuous operation, the CDW kept increasing at a constant rate of approximately 0.48 kg per day until the end of the process (Fig. 6.6 a). It is remarkable that the lipid concentration also kept rising constantly, although at a slightly lower rate of 0.44 kg per day (Fig. 6.6 c). Accordingly, on average, the lipid-free CDW only marginally increased by 40 g per day (Fig. 6.6 b). Assuming that these rates remain constant, it follows that, with infinite process time, the cellular lipid content would converge to approximately 91.7%. In this way, up to 117 g L^{-1} CDW

concentration in 50 L reaction volume was achieved, and, on average, around 5.83 kg of CDW was formed 9 days after the start of the semi-continuous operation (Fig. 6.6 a). The lipid productivity thereby achieved corresponds to around 8.88 g L^{-1} d^{-1} (0.37 g L^{-1} h^{-1}). Around 4.46 kg lipids (81.7 g L^{-1} lipids in 54.5 L) were present in the yeast suspension at the end of the process (Fig. 6.6 c), which corresponds to a cellular lipid content of 76.5%, although, in all the experiments, 70% lipid quota was already achieved after 4–5 days into the process (Fig. 6.6 d). The results of all the experiments were significantly similar, demonstrating very high reproducibility.

Table 6.2: Process parameters, metrics and carbon conversion for high-cell-density yeast oil production in MBRs with phosphorus limitation on a 1.5 L and a 50 L scale.

	Experiment #			
C/P ratio	**IV**	**1**	**2**	**3**
Batch medium	3515 g g^{-1}	3515 g g^{-1}	3515 g g^{-1}	3515 g g^{-1}
After inoculation	581 g g^{-1}	618 g g^{-1}	603 g g^{-1}	637 g g^{-1}
Feed medium	3515 g g^{-1}	3515 g g^{-1}	3515 g g^{-1}	3515 g g^{-1}
Parameters				
Initial reaction volume	1.5 L	50 L	50 L	50 L
Sugar feeding rate	1.1 g L^{-1} h^{-1}	1.1 g L^{-1} h^{-1}	1.1 g L^{-1} h^{-1}	1.1 g L^{-1} h^{-1}
Semi-conti. process time	6.9 d	7.8 d	3.9 d	9.0 d
Process metrics				
CDW	123.6 g	5.0 kg	3.2 kg	5.8 kg
	(82.4 g L^{-1})	(100.0 g L^{-1})	(64.0 g L^{-1})	(116.0 g L^{-1})
Lipids	85.7 g	3.9 kg	2.3 kg	4.5 kg
	(57.1 g L^{-1})	(78.0 g L^{-1})	(46.0 g L^{-1})	(90.0 g L^{-1})
Lipid quota	69.4%	78.9%	70.3%	76.4%
STY_{X+L}	0.43 g L^{-1} h^{-1}	0.43 g L^{-1} h^{-1}	0.47 g L^{-1} h^{-1}	0.48 g L^{-1} h^{-1}
STY_L	0.30 g L^{-1} h^{-1}	0.34 g L^{-1} h^{-1}	0.44 g L^{-1} h^{-1}	0.37 g L^{-1} h^{-1}
$Y_{(X+L)/S}$	0.35 g g^{-1}	0.40 g g^{-1}	0.40 g g^{-1}	0.42 g g^{-1}
$Y_{L/S}$	0.25 g g^{-1}	0.32 g g^{-1}	0.28 g g^{-1}	0.32 g g^{-1}
Fraction of carbon converted into				
Lipids	45.9%	60.3%	53.3%	61.3%
Lipid-free CDW	12.1%	9.6%	13.4%	11.4%
CO_2 and by-products	42.0%	30.1%	33.3%	27.3%

Table 6.2 summarizes the process parameters and metrics for all high-cell-density yeast oil production processes carried out in MBRs on a 1.5 L and a 50 L scale. In addition, the calculated fraction of the total carbon consumed by the yeast, which was converted into lipid-free CDW, lipids, or CO_2 at the end of the specified process time, is also provided in Table 6.2. In processes on the 50 L scale, on average, 58.3% ($\pm$3.6%) of the carbon was successfully converted into lipids, while the remaining 30.3% ($\pm$2.5%) was assumed to be completely oxidized and released as CO_2 in the exhaust gas. In Figure 6.7, the carbon conversion efficiency (η_C) achieved in all experiments is displayed schematically. Considering that the short process duration in Experiment 1 was the apparent cause of the somewhat lower carbon conversion efficiency, an average of Experiment 2 and 3 is more meaningful to note, which equals 60.8% ($\pm$0.5%).

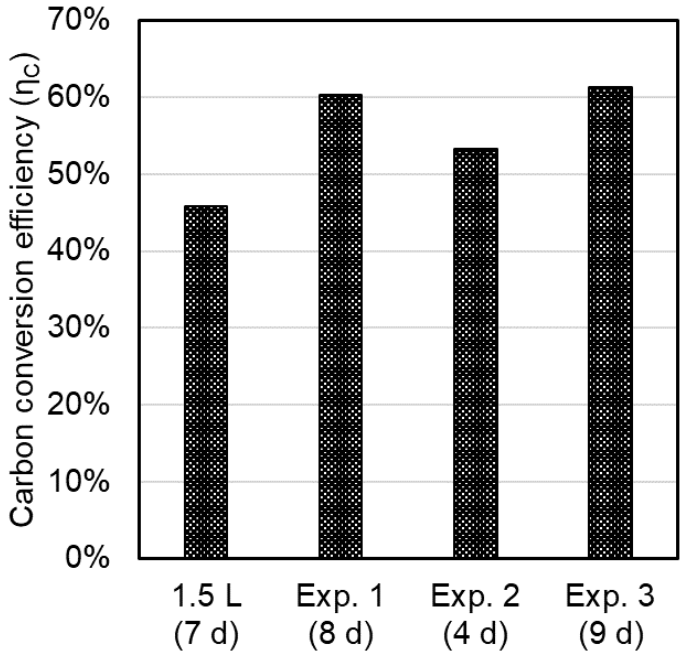

Figure 6.7: Overall carbon conversion efficiency (η_C) achieved with *C. oleaginosus* at the end of each experiment in 1.5 L and 50 L MBRs with semi-continuous mode of operation and a diluted substrate as cultivation medium (Table 4.5).

Figure 6.8 shows light microscope images tracking the morphological changes of *C. oleaginosus* cells over the course of a semi-continuous process for lipid production in a phosphorus-depleted medium in the MBR on the 50 L scale. An increase in the size of cells and lipid droplets is evident. Furthermore, the cell morphology changes from ovoid to almost completely round, with cellular lipid content increasing from 16% on the first day to 79% on the 10th day. It can also be seen that even with increasing overall lipid content, new cells are being formed, with smaller cell sizes and lipid droplets being visible.

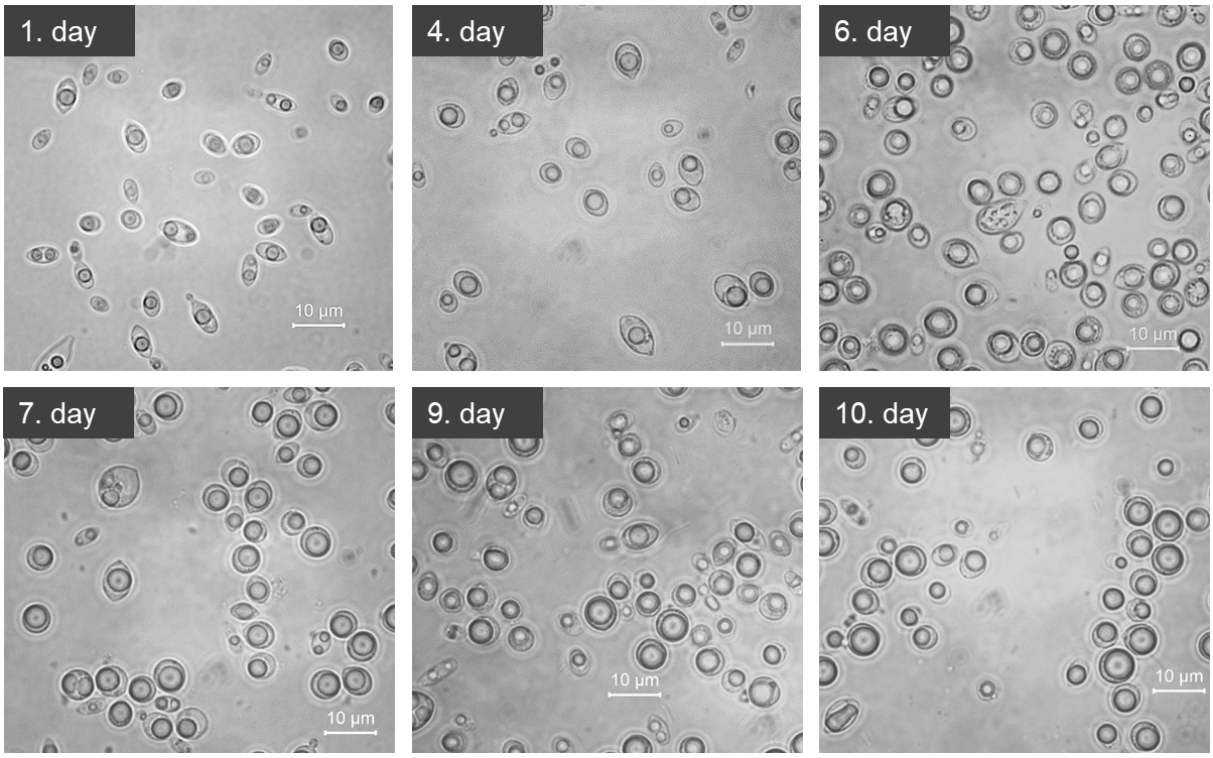

Figure 6.8: Light microscope images of *C. oleaginosus* (50x magnification in bright field) showing the change of cell morphology over a semi-continuous cultivation in an MBR with total cell retention on a 50 L scale for lipid production in phosphorus-depleted medium (Exp. 1). Cells after a process time of 1–10 days with a lipid content ranging from 16% to 79% are shown.

Discussion

Lipid yield ($Y_{L/S}$) and productivity (STY_L), as well as carbon conversion efficiency (η_C), achieved in high-cell-density cultivation of *C. oleaginosus* in an MBR are all higher on the 50 L scale. All process parameters were the same between the two scales except for the material and other specifications of the microfiltration module (Table 4.13). Even though the bypass volume and residence time in bypass without aeration of the yeast suspension were higher on the 50 L scale, the shear stress applied on the yeast cells due to pumping at high flow rates through the filtration module was 12.7-fold in the 1.5 L scale MBR (Table 4.13). So, the higher shear rate in the 1.5 L scale MBR might have influenced the yeast cells negatively, causing stress or cell disruption, especially for cells with very high lipid content and, thus, very large intracellular lipid droplets.

Lipid STY achieved corresponds to around 8.88 g L^{-1} d^{-1}, which is comparable to the values reported with *C. oleaginosus* so far (2.64–14.16 g L^{-1} d^{-1}) (Meo et al., 2017; G. Zhang et al., 2011; Meesters et al., 1996). As mentioned earlier, lipid productivity achieved in this study was limited mainly by the conservative choice of feed flow rate. The feed flow was kept relatively low since it was crucial to ensure that no valuable carbon source exits the MBR unused by keeping the sugar concentrations below the detection limit of 0.004 g L^{-1} glucose and 0.014 g L^{-1} mannose at all times. Additionally, the choice of semi-continuous operation did not allow a higher feeding rate, unfortunately, since this would cause the reaction volume to exceed the maximum working volume of the MBR overnight, where no filtration is performed. Still, the semi-continuous operation was necessary in this work since the continuous operation of the 50 L scale MBR was not possible. Hence,

it would be possible to increase the lipid productivity further using a higher feed rate in a different operational mode.

G. Zhang et al. (2011) and Shaigani et al. (2021) reported achieving 35% and 28% lipid content of dry biomass of *C. oleaginosus* using a phosphate-depleted medium with N-acetylglucosamine as the carbon source after 4 days of process time. In a more comparable study by Zhou et al. (2019), in which a phosphate-depleted hydrolysate from water hyacinth was used as the carbon source, 60% lipid content of *C. oleaginosus* CDW was indicated. In the study by Meo et al. (2017), which is the most analogous study to this one due to the use of a very similar phosphate-depleted medium and an MBR concept on a litre scale, around 70% cellular lipid content was recorded after 3–4 days. The lipid quota achieved in this study after 4 days is much higher than or at least identical to all the data cited above for this yeast. Moreover, to the best of our knowledge, 76.5% lipid content reported in this study is the highest reported so far with *C. oleaginosus* using P limitation. The lipid yield ($Y_{L/S}$) calculated at the end of the process was 0.32 g g^{-1}, which is also higher than the range (0.20–0.26 g g^{-1}) stated in comparable studies using P limitation with *C. oleaginosus* (Meo et al., 2017; G. Zhang et al., 2011; Zhou et al., 2019).

76.5% lipid content achieved in this study is also on the higher spectrum of 43-85% lipid quota reported for *C. oleaginosus* using other methods to induce lipid biosynthesis, such as nitrogen limitation (Moon et al., 1978; Donzella et al., 2022) or co-substrate feeding with acetate (Masri et al., 2019; Rerop et al., 2023), which proves that the method applied in this study is competitive with respect to other strategies suggested in the literature. The conversion efficiency of substrate carbon into lipid carbon has not yet been studied very often. Rerop et al. (2023) have recently reported achieving 20.4–33.6% carbon conversion efficiency in the bio-conversion of lignocellulosic hydrolysate to microbial oils with *C. oleaginosus*. To the best of my knowledge, 60.8% carbon conversion efficiency by *C. oleaginosus* achieved in this study is the highest reported so far.

7. Hydrolysis of Microalgal Biomass [1]

This chapter covers the hydrolysis of the microalgae biomass produced as described in Chapter 5 with *M. salina* in thin-layer cascade (TLC) photobioreactors (PBRs). First, the rheology of the microalgae biomass with various cell densities is examined since this influences the process design for most mechanical cell disruption methods. Then, mechanical disruption of the microalgae cells using various methods is studied. Chemical and enzymatic hydrolysis of *M. salina* biomass with undisrupted cells, as well as with mechanically disrupted cells, are investigated. Mixtures of commercially available enzymes with various compositions were tested for microalgal biomass hydrolysis, and a final enzyme mixture was used for scale-up to the 200 L scale. Finally, phosphorus elimination of microalgal biomass hydrolysate using a precipitating agent is examined.

7.1. Rheology of microalgal cell suspensions

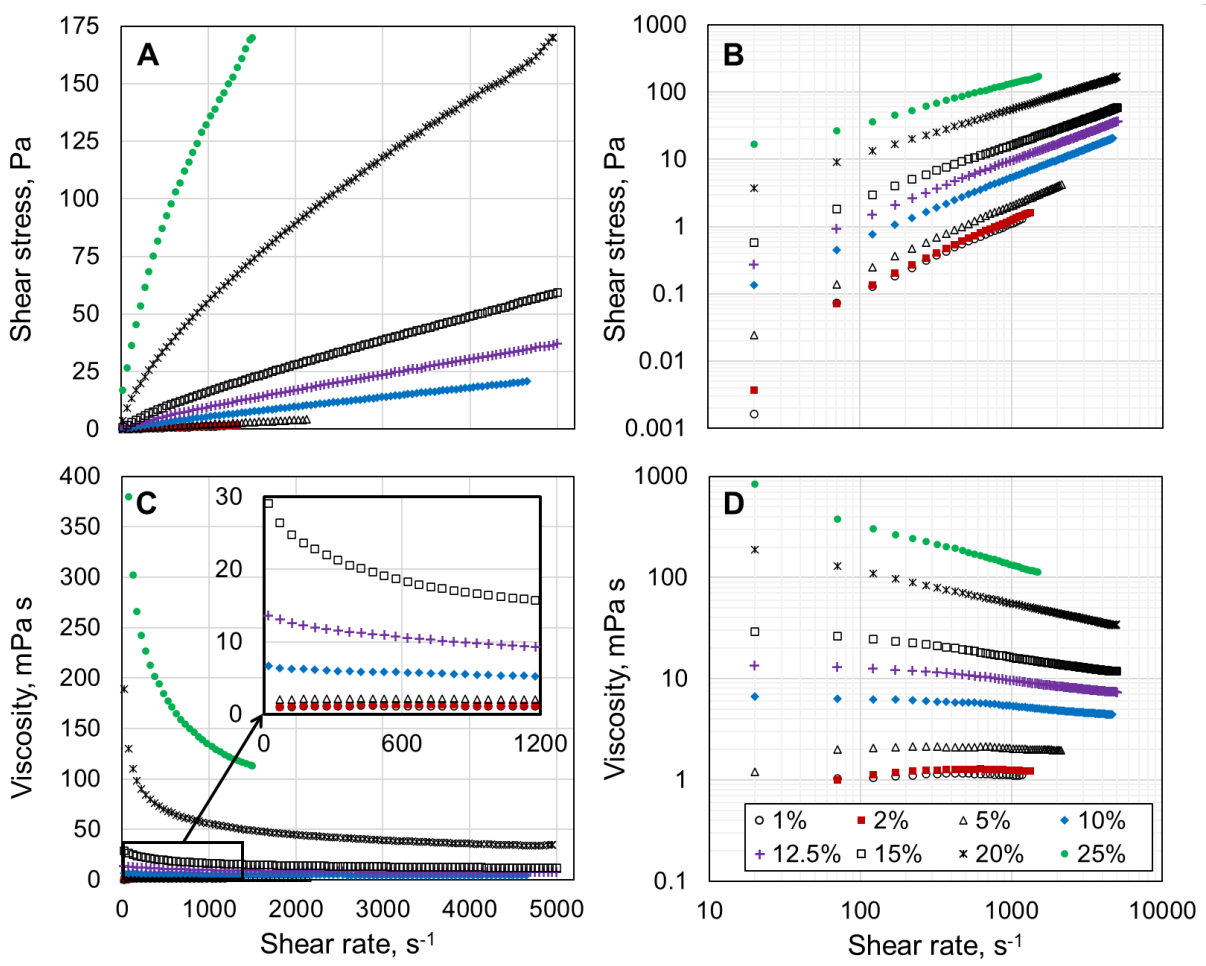

Figure 7.1: Rheology of *M. salina* biomass with various cell dry weight (CDW) concentrations at 25 °C. **A**: Shear stress with respect to shear rate; **B**: log–log plot of shear stress with respect to shear rate; **C**: viscosity with respect to shear rate; **D**: log–log plot of viscosity with respect to shear rate.

[1] Part of the results presented here has already been published in: Koruyucu, A., Peest, T., Korzin, E., Gröninger, L., Patricia, Brück, T., & Weuster-Botz, D. (2024). Cell Disruption and Hydrolysis of *Microchloropsis salina* Biomass as a Feedstock for Fermentation. *Applied Sciences, 14*(21), 9667. doi:10.3390/app14219667

Preliminary cell disruption experiments showed that the flow characteristics of the microalgal biomass change significantly depending on its solids content, temperature and degree of cell disruption. Flow properties of the microalgal biomass are important for all the mechanical cell disruption methods investigated in this study, particularly for the high-pressure homogenization, since the biomass has to be pumped and pushed through very small channels. Most high-pressure homogenizers (HPHs) have a specified upper limit on the viscosity of the material to be processed. Besides, the performance of some processes, such as enzymatic hydrolysis, is affected significantly by how well the reaction mixture is mixed. Therefore, prior to cell disruption experiments, the rheology of microalgal biomass was thoroughly examined with varying solids content and temperature values as described in Subsection 4.9.1.

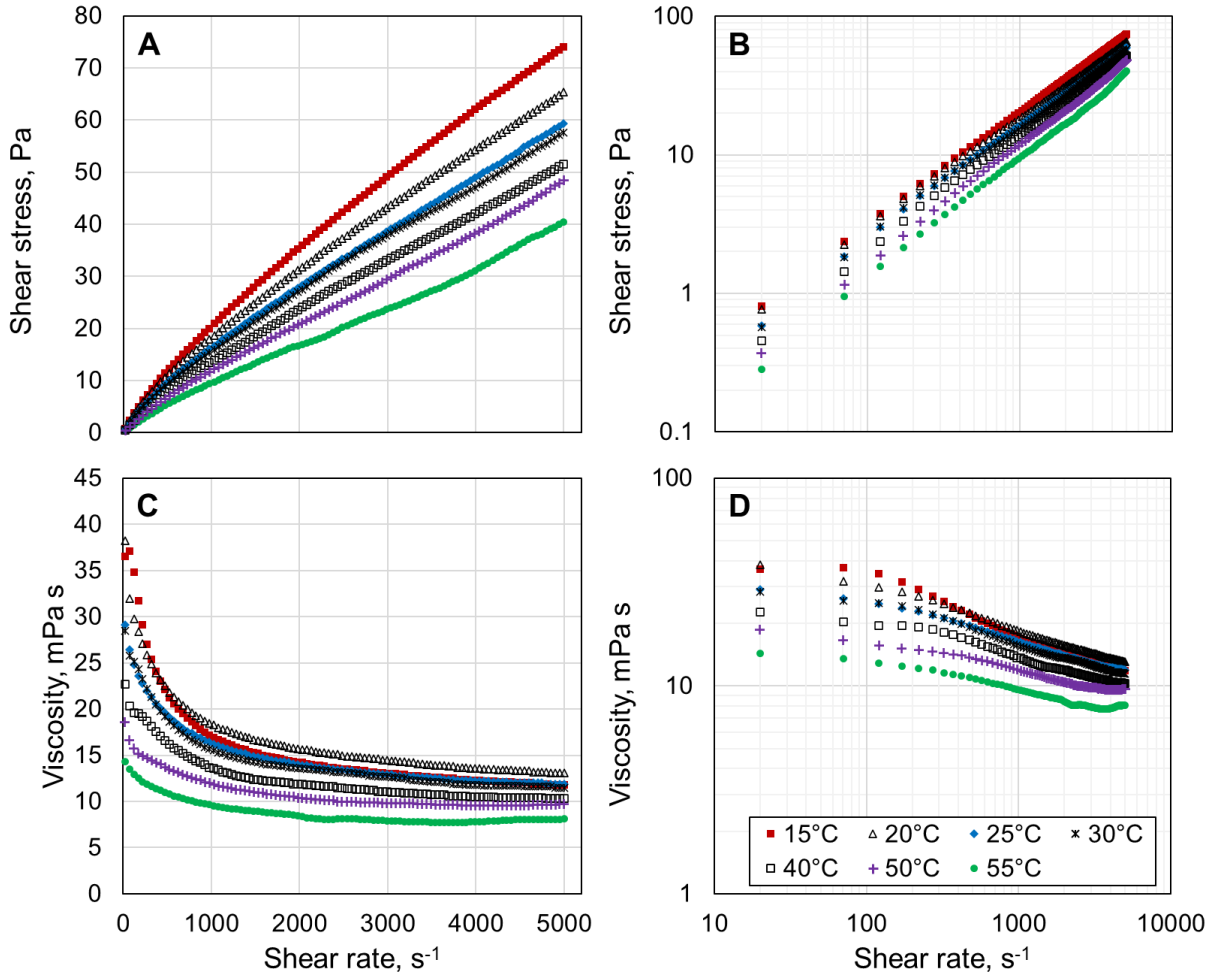

Figure 7.2: Rheology of *M. salina* biomass with a cell dry weight (CDW) concentration of 150 g L^{-1} (15%) at various temperatures. **A**: Shear stress with respect to shear rate; **B**: log–log plot of shear stress with respect to shear rate; **C**: viscosity with respect to shear rate; **D**: log–log plot of viscosity with respect to shear rate.

Figure 7.1 illustrates the viscosity measurement results of microalgal biomass with solids content ranging from 1% to 25%. The equipment used had an upper limit of 175 Pa for shear stress measurements. For this reason, the viscosity of biomass with 25% solids content could not be measured for shear rates over 1500 s^{-1}. Besides, unusually high and changing values were measured above a certain shear rate for microalgae biomass with low solids content (viscosity below 5 mPa s). For the equipment used, the manufacturer explains this phenomenon with the formation of turbulences at high velocities resulting in faulty measurements. Hence, for biomass with a solids content from

1% to 5%, only the correct values measured until this phenomenon has occurred are displayed. As expected, the highest viscosity values were measured with the highest cell densities. Biomass with a solids content of 20–25% is a thick microalgae paste rather than a cell suspension and showed a shear thinning behaviour. For 20% and 25% solids content, the lowest viscosities measured were 34 mPa s and 113 mPa s, respectively. 15% solids content had a viscosity changing between 12–29 mPa s, which can be handled more easily in downstream processing. For even lower solids content of 1–2%, the viscosity of the microalgae suspension lies between 1.0–1.3 mPa s. The shear thinning effect became weaker for solids content between 10–15%, while the microalgae biomass with a solids content between 1–5% behaved like a Newtonian fluid.

Figure 7.2 shows the viscosity measurement results of microalgal biomass with a constant solids content of 15% at various temperatures ranging from 15 °C to 55 °C. As anticipated, microalgal biomass has a lower viscosity at higher temperatures. At an initial shear rate of 20 s^{-1}, the viscosity of the biomass changes from 42.6 mPa s to 14.3 mPa s with a temperature drop from 15 °C to 55 °C. On the other hand, at a shear rate of 5000 s^{-1}, the viscosity of the microalgae biomass decreases only from 14.5 mPa s to 8.1 mPa s with the same temperature drop. Generally, biomass with 15% solids content exhibits a slight shear thinning behaviour, as suggested above. Interestingly, it is also apparent (Fig. 7.2 C and D) that the microalgae biomass behaves almost like a Newtonian fluid for temperatures above 50 °C when the shear rate is above 3000 s^{-1} (Fig. 7.2 C and D).

Discussion

Goudar et al. (1999) reported a viscosity of 60 mPa s for a suspension of *Penicillium chrysogenum* with 17.7% solids content at 28 °C and a shear rate of 200 s^{-1}. Olmstead et al. (2013) stated the viscosity of a *Microchloropsis* sp. paste with 20–25% solids content to be below 1 Pa s at a shear rate of 100 s^{-1}. In this work, for a microalgae biomass with 15–20% solids content at 25 °C and a shear rate of 220 s^{-1}, a viscosity of 21–80 mPa s was measured, while for biomass with 25% solids at a shear rate of 120 s^{-1} a viscosity of 300 mPa s was recorded. Hence, the results of the viscosity measurement prove to be in accordance with literature data. Moreover, the viscosity of microalgae suspension with 1–2% solids, a viscosity of 1.0–1.3 mPa s was measured, which is slightly above the viscosity of water at the same temperature (White, 2011).

Based on the viscosity measurements, the upper limit of solids content of the microalgal biomass for cell disruption using HPH was determined to be between 15–20%. Furthermore, since most cellulases have their optimal working temperature around 50–60 °C, the insight that *M. salina* biomass with 15% cell dry weight (CDW) has a pleasantly low viscosity below 10 mPa s at temperatures above 50 °C is very useful and a good signal for sufficient mixing of the reaction medium during enzymatic hydrolysis.

7.2. Mechanical disruption of microalgal cells

Mechanical disruption of highly dense *M. salina* biomass using ultrasonication, bead milling and high-pressure homogenization was investigated. These methods were selected specifically for their effectiveness with microalgae (Günerken et al., 2015) and applicability in continuous processes on

an industrial scale (Chmiel, 2018).

7.2.1. Ultrasonication

Figure 7.3 shows the disruption of *M. salina* biomass by ultrasonication. Microalgal biomass with various solids content ranging between 10–25% was ultrasonicated for 40 minutes (Fig. 7.3 A) as described in Subsection 4.9.2. Cell disruption progressed very similarly for solids content between 10–20%, reaching nearly 40% after 40 minutes of ultrasonication. Only for a solids content of 25% degree of cell disruption reached 12% after 20 minutes and did not increase with further treatment. Normally, during ultrasonication, there is visible jet stream formation in the liquid medium, which also helps mix the sample. In this experiment, this was also the case for all the treated biomass samples except for biomass with 25% solids content, meaning that this sample was not mixed sufficiently during ultrasonication. Moreover, it was noted for biomass with a solids content of 25% that a dry biomass layer formed on the surface of the sonotrode, which got thicker over time. Thus, it was concluded that ultrasonication is not suited for cell disruption of microalgal biomass with such a high solids content and viscosity since the forces that accomplish the cell disruption by ultrasonication act mainly through the liquid medium, which is not sufficiently present in this case.

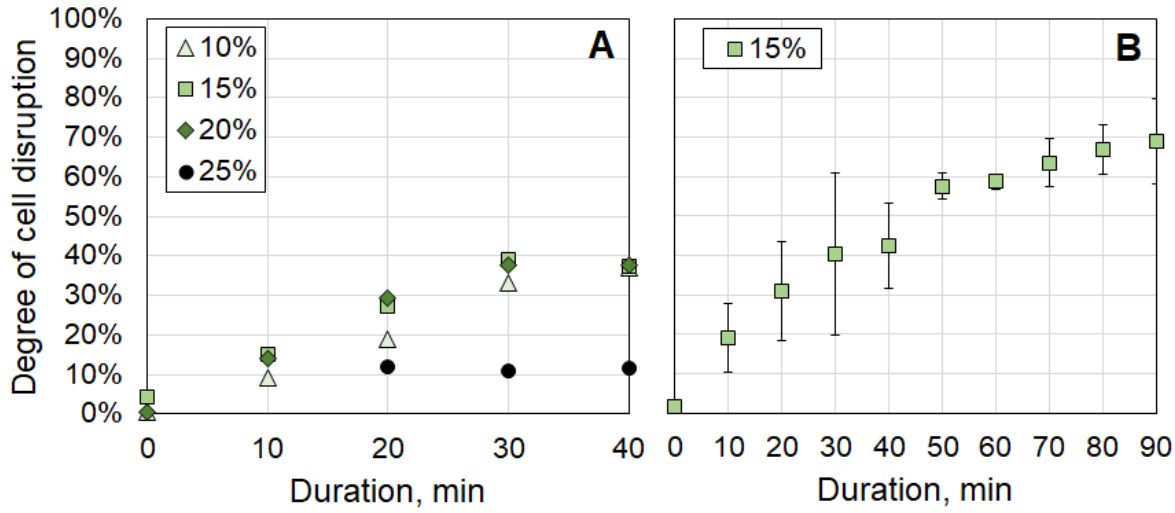

Figure 7.3: Disruption of *M. salina* biomass by ultrasonication. **A**: Ultrasonication of microalgal biomass with various solids content ranging between 10–25% over 40 min; **B**: ultrasonication of microalgal biomass with 15% solids content over 90 min. Error bars show standard deviation of triplicate experiments.

To determine if the disruption degree of *M. salina* cells would further increase with increasing ultrasonication time, a subsequent experiment with microalgal biomass with 15% solids content was performed for a total treatment duration of 90 minutes (Fig. 7.3 B). It was shown that the cell disruption efficiency indeed increased to 60% after 60 minutes and to 70% after 90 minutes of ultrasonication.

Discussion

Yao et al. (2018) examined the effect of high-intensity ultrasound on lipid extraction from high-solids viscous slurries of *Microchloropsis* species. The extraction yields were similar at 12% and 20% solids but decreased considerably for 25% solids content of biomass. It was also verified in this

study that the disruption efficiency of *M. salina* biomass with 25% solids is significantly worse than with 20% solids, whereas the disruption degrees achieved at different concentrations below 20% were very similar. Yao et al. (2018) suggest that such a decrease in efficiency can be due to an increased attenuation of ultrasound waves, which could result in less efficient cell rupture. This is attributed to the increase in biomass viscosity and decrease in speed of sound with increasing solid content.

In this study, the highest disruption efficiency of *M. salina* cells achieved was 70%, while 10–20% was reached after 10 minutes. This is in accordance with the literature values reported for ultrasonication at 20 kHz frequency for 10 minutes (Kurokawa et al., 2016), whereas 60–90% disruption of *Microchloropsis* species after 10–20 minutes is also reported for ultrasonication at much higher frequencies (1.0–4.3 MHz) (Kurokawa et al., 2016; McMillan et al., 2013). For ultrasonic disruption of *Microchloropsis oculata* cells, M. Wang et al. (2014) reported increased effectiveness by a combination of high-frequency focused ultrasound (3.2 MHz) and low-frequency non-focused ultrasound (20 kHz) treatments. However, frequencies applied at a large scale are usually lower due to energy consumption concerns (D'Hondt et al., 2017).

Literature regarding microalgal cell disruption using ultrasonication focuses more on the extraction efficiency of lipids or other products after the treatment, mostly without direct statements about the actual disruption efficiency. Nevertheless, its efficiency depends on microalgae species, biomass concentration and operational conditions such as temperature, time, and frequency (Günerken et al., 2015). Ultrasonication of microalgae has been mainly applied as a pretreatment for biodiesel, bioethanol and biogas production and has been shown to adequately break algal cells in low-density biomass suspensions, increasing the soluble fraction of organic matter, proteins, carbohydrates, and lipids (D'Hondt et al., 2017).

7.2.2. Bead milling

Disruption of *M. salina* cells in a mixer mill was examined using beads of various materials and sizes. In this work, cell disruption experiments using a mixer mill are considered a preliminary exploration for a possible process transfer to an industrial-scale agitated media mill. Microalgal biomass with solids content varying between 10–25% was disrupted by bead milling for 40 minutes as described in Subsection 4.9.3.

Figure 7.4 shows the cell disruption degree over time using beads with 0.5–1.0 mm diameters. The beads were made of zirconium oxide and agate, which have very similar densities of 6.0–7.0 g mL^{-1} (Tab. 4.18). As expected, disruption efficiency increases with declining biomass solids content and increasing milling time. The results were very similar for zirconium oxide and agate beads with the same diameter. With these beads, the highest degree of disruption achieved was 76–78% with a solids content of 10% after 40 minutes. For higher solids content, disruption efficiency remained below 25%. With a smaller bead size of 0.5 mm, the highest degree of disruption achieved for a solids content of 10% was 53% after 40 minutes, which is much lower than with a bead size of 1 mm. Interestingly, on the contrary, the disruption efficiency of biomass with solids content above 15% was higher with a smaller bead size of 0.5 mm than with 1.0 mm.

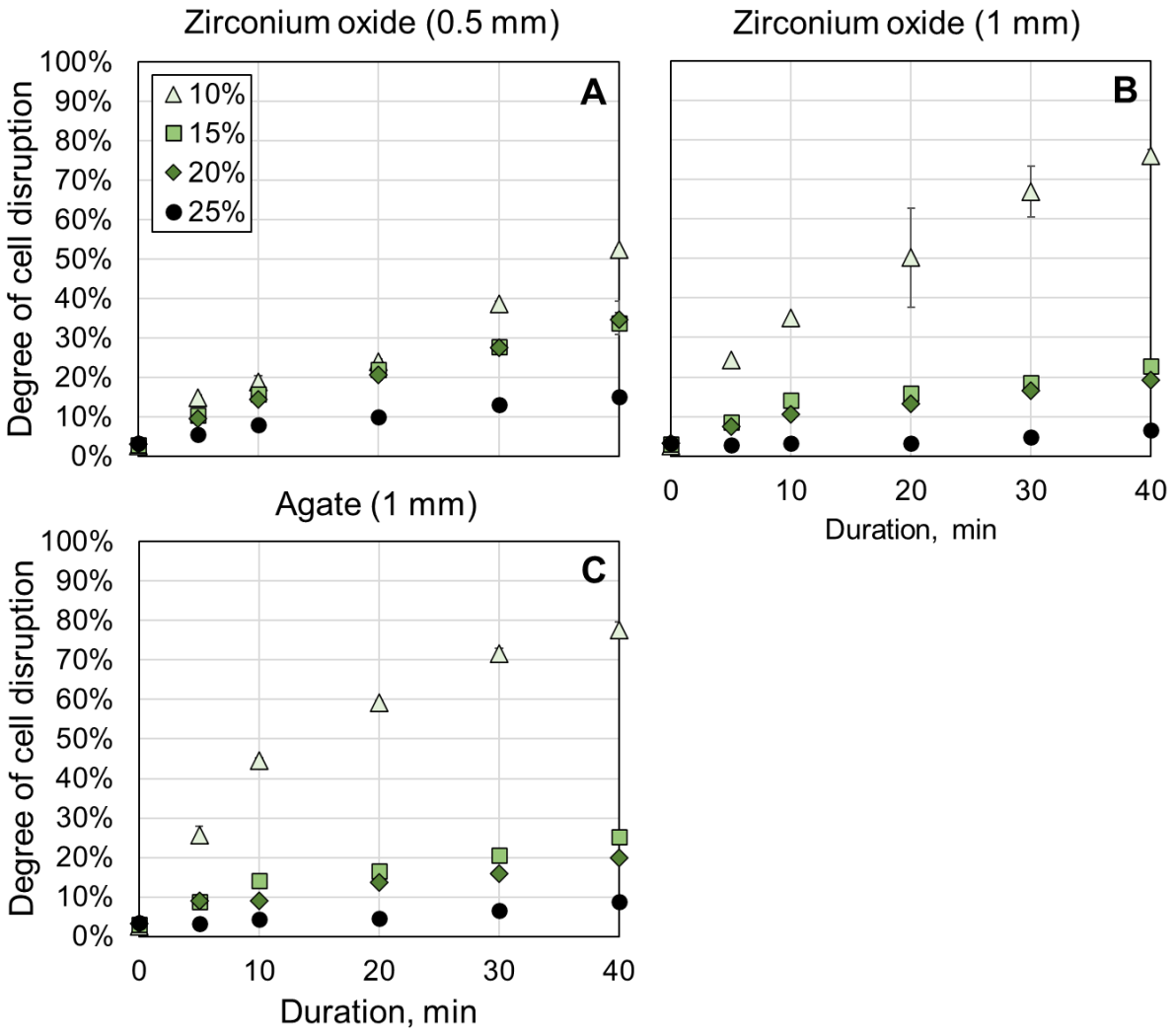

Figure 7.4: Disruption of *M. salina* biomass by bead milling using beads of various materials and sizes. Microalgal biomass with various solids content ranging between 10–25% was milled over 40 min. **A**: Zirconium oxide (0.5 mm); **B**: zirconium oxide (1.0 mm); **C**: agate (1.0 mm). Error bars show standard deviation of duplicate experiments.

Figure 7.5 shows the microalgal cell disruption over time using beads with a diameter between 2–5 mm. The beads were made of glass, stainless steel and tungsten carbide, with material densities of 2.9 g mL^{-1}, 7.7 g mL^{-1} and 15.0 g mL^{-1}, respectively. Using steel beads of 5 mm size, the disruption efficiency was almost independent of solids content and in a range of 46–54% for all biomass concentrations after 40 minutes. On the other hand, reducing the diameter of steel beads from 5 mm to 2 mm resulted in a remarkable increase in disruption degree. For biomass with a solids content of 10–20%, 87–97% of the cells were disrupted after 40 minutes. For 25% solids content, only 67% of the cells were disrupted after 40 minutes, which is still the highest disruption degree achieved with 25% solids content in this work. Using glass beads (3 mm) resulted in the lowest disruption efficiency of the dense *M. salina* biomass, as expected due to its low density (Fig. 7.5 D). However, with tungsten carbide beads (3 mm), which have the highest density among the tested materials, a lower disruption efficiency than with the steel beads (2 mm) was measured (Fig. 7.5 C). Very high sample temperatures and cell agglomeration with visible clumps were observed during cell disruption with tungsten carbide beads. Hence, the measurements might be faulty and lower than the actual values

due to clumped cell debris being counted as intact cells. Nonetheless, a higher material density of the same sized beads is determined to be more effective for disrupting dense biomass of *M. salina* with an optimal bead size of 2–3 mm.

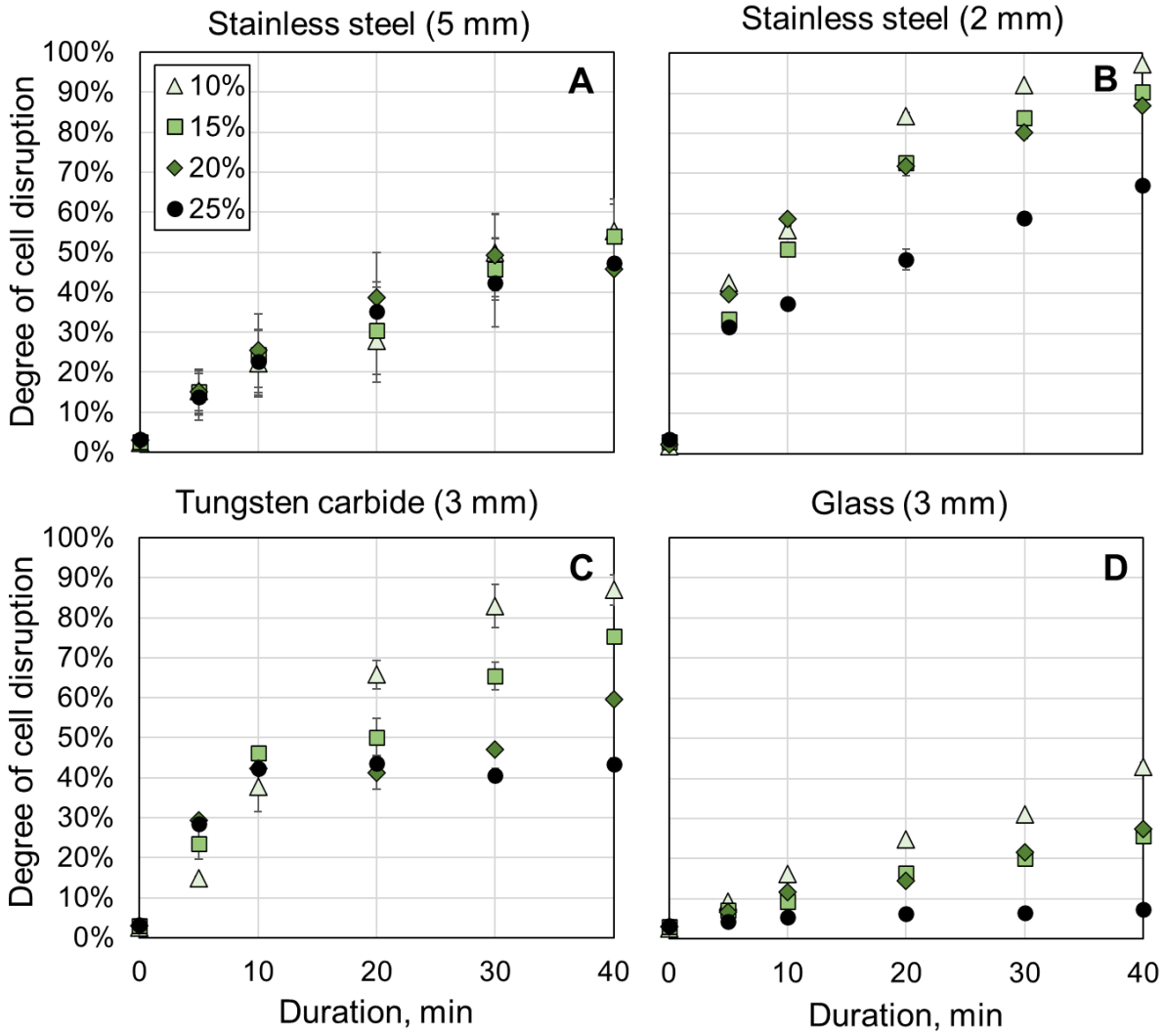

Figure 7.5: Disruption of *M. salina* biomass by bead milling using beads of various materials and sizes. Microalgal biomass with various solids content ranging between 10–25% was milled over 40 min. **A**: Stainless steel (5 mm); **B**: stainless steel (2 mm); **C**: tungsten carbide (3 mm); **D**: glass (3.0 mm). Error bars show standard deviation of duplicate experiments.

Discussion

With zirconium oxide and agate beads at a constant bead size of 1 mm, the disruption degree of *M. salina* cells was very similar. This is to be expected since the densities of these two materials are quite similar (Tab. 4.18). For disruption of microalgae, but also specifically of *Microchloropsis* species, by bead milling, a bead size of 0.3–0.6 mm has been reported to yield higher disruption efficiency than bead sizes over 1 mm (Molina Grima et al., 2013; Quesada-Salas et al., 2021; Montalescot et al., 2015; Pan et al., 2017). This was verified for biomass with solids content greater than 15% in this study. For biomass with 10% solids, however, in contrast to the literature, beads with a diameter of 1 mm performed significantly better than those with 0.5 mm, achieving a 24% higher disruption degree.

In this study, for disruption of *M. salina* cells, the best-performing beads proved to be the stainless steel beads with a diameter of 2 mm, achieving the highest disruption efficiency for all biomass concentrations. Increasing the bead size from 2 mm to 5 mm drastically reduced the disruption degree by 20–43%. Moreover, by showing that tungsten carbide beads perform significantly better than glass beads of the same size, it was demonstrated that beads with higher material density are more effective at disrupting *M. salina* cells. It has been indicated in literature that *Microchloropsis* species are harder to disrupt than most other microalgae species (Kröger et al., 2018; Spiden et al., 2013; Quesada-Salas et al., 2021) and high bead material densities are more effective on microalgal cell disruption by bead milling (Molina Grima et al., 2013; Doucha & Livansky, 2008). For instance, Quesada-Salas et al. (2021) used the same set-up as Montalescot et al. (2015) for mechanical disruption of *Microchloropsis* species with the only difference being the bead material, namely zirconium oxide instead of glass. This resulted in an increase of disruption efficiency by 40% compared to that reported by Montalescot et al. (2015) after one single pass.

For *Microchloropsis* species biomass with 1% solids content, Quesada-Salas et al. (2021) achieved 76–93% cell disruption after milling with zirconium oxide beads (0.4 mm) for 40 minutes. Pan et al. (2017) reported 85% cell disruption for *Microchloropsis* species biomass with 15% solids after milling with zirconium oxide beads (0.8–1.0 mm) for 40 minutes. In this study, disruption efficiency achieved using the same bead size and material after the same milling duration was much lower. However, it must be noted that these studies used agitator bead mills (0.6–1.0 L grinding chamber), while in the current study, a mixer mill (20 mL grinding jars) was used, which is known to be less efficient than agitator mills (D'Hondt et al., 2017). Optimal bead size depends on agitator design and mill geometry and might vary for different bead mills (Doucha & Livansky, 2008). In this study, the highest degree of disruption recorded for *M. salina* biomass with 10% solids was 97%, using 2 mm steel beads and after 40 minutes of treatment.

7.2.3. High-pressure homogenization

High-pressure homogenization for the disruption of *M. salina* cells was examined first on a laboratory scale using a bench-top HPH, followed by a scale-up to 200 L using an industrial HPH as described in Subsection 4.9.4. Microalgal biomass with solids content varying between 10–25% was homogenized for up to 10 passes through the HPH on a laboratory scale. Figure 7.6 shows the results of cell disruption using HPH at two different exiting pressures. At a pressure of 1500 bars, for all CDW concentrations, disruption efficiency kept increasing with each pass through the HPH, reaching a final value between 40–63% after ten passes (Fig. 7.6 A). At a pressure of 3000 bars, a higher disruption degree between 56–78% was achieved for all CDW concentrations after ten passes (Fig. 7.6 B). However, the difference between various solids content was more apparent at 3000 bars. With 10% solids content, a cell disruption degree of 75% was achieved already after four passes, while it took eight passes with a solids content of 15%. Still, disruption efficiency stayed below 80% in both cases despite further treatment. For biomass with 20–25% solids content, maximum disruption efficiency reached only 56–60%.

Figure 7.7 shows the results of the scale-up experiments to 200 L using an industrial HPH. Microal-

gal biomass with a solids content of 15% was homogenized with up to 5 passes at 1000 bar. The degree of cell disruption is plotted with respect to the number of equivalent passes, which is the time equivalent of a single pass when the biomass is circulated in an agitated tank during homogenization. On the 30 L scale, cell disruption efficiency reached 94% after 4.5 equivalent passes. In contrast, on the 60 L and the 200 L scale, cell disruption efficiency reached around 80% after 2–3 passes and did not increase afterwards despite further homogenization. Nevertheless, the industrial HPH was more effective than the bench-top HPH, achieving over 70% cell disruption of biomass with 15% solids after 2 passes at 1000 bar, whereas this required 6 passes at 3000 bar with the bench-top HPH (Fig. 7.6 B and 7.7 B).

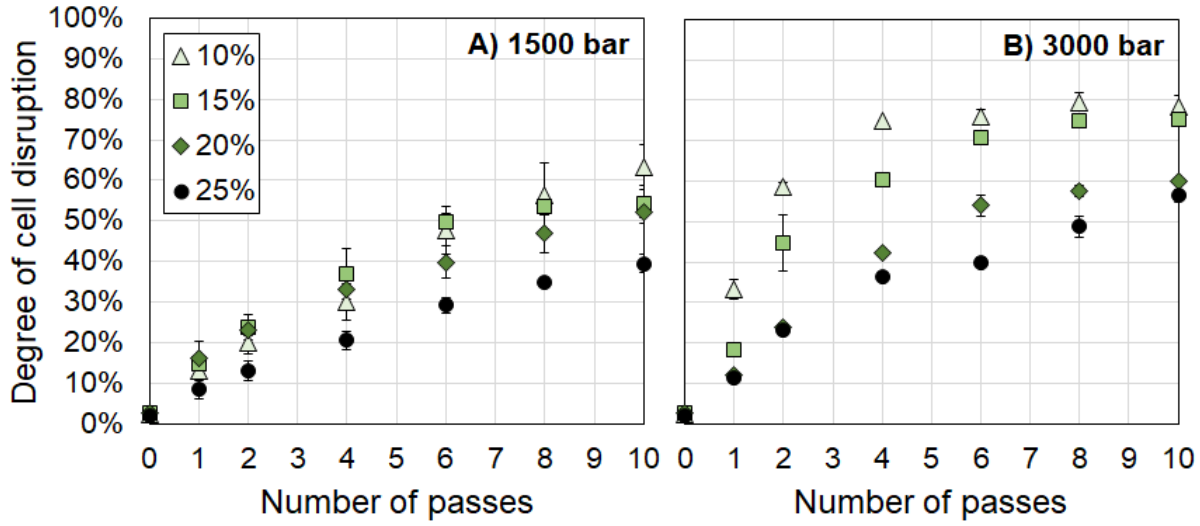

Figure 7.6: Disruption of *M. salina* biomass with HPH on a 200 mL scale. Microalgal biomass with various solids content ranging between 10–25% was homogenized with up to 10 passes. **A**: Exit pressure of 1500 bar; **B**: exit pressure of 3000 bar. Error bars show standard deviation of triplicate experiments.

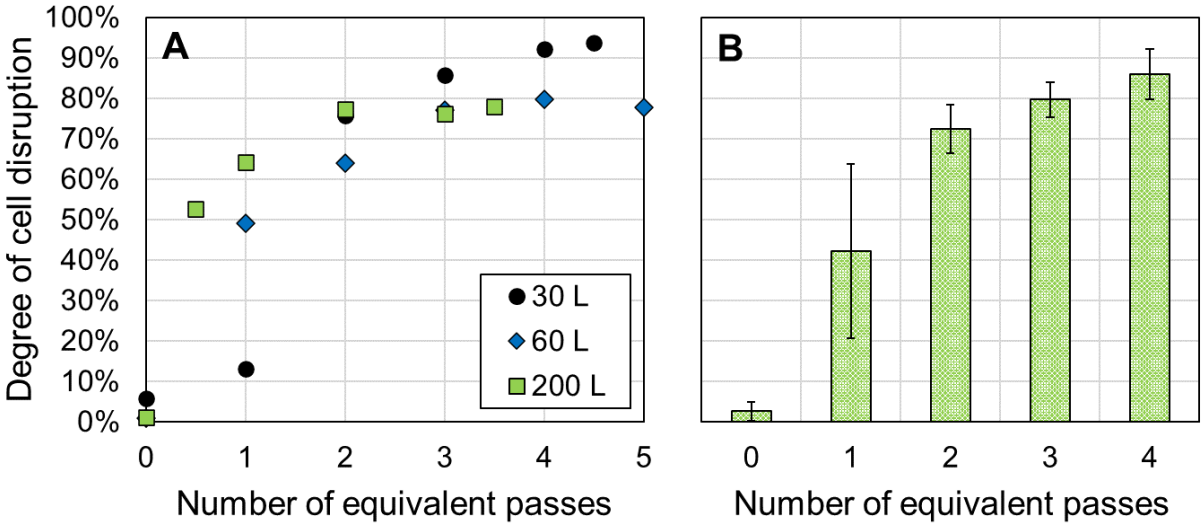

Figure 7.7: Disruption of *M. salina* biomass with HPH on 30–200 L scales at 1000 bar. Microalgal biomass with a solids content of 15% was homogenized with up to 5 passes. Degree of cell disruption is plotted with respect to the number of equivalent passes, which is the time equivalent of a single pass when the biomass is circulated in an agitated tank during homogenization. **A**: Degree of cell disruption on different scales; **B**: mean value of disruption degree on different scales. Error bars show standard deviation between different experiments.

Discussion

In this study, the industrial HPH proved more effective than the bench-top HPH, achieving a higher degree of cell disruption after fewer passes at a lower pressure. This is not surprising since the efficacy of HPH depends highly on the material and design of its mechanical parts, especially of the homogenizing valve (Chmiel, 2018). In general, HPH has proved to be an effective method for disrupting *M. salina* cells, even though the maximum disruption efficiency (86%) achieved with 15% solids content remained below that with bead milling using 2 mm stainless steel beads (90%).

The literature describes the best method of cell disruption as depending on the microalgae strain. (Halim et al., 2012) stated the most effective mechanical disruption method for *Chlorococcum* sp. cells to be HPH, whereas (Lee et al., 1998) demonstrated bead milling is significantly more efficient than HPH for disruption *Botryococcus braunii* cells. At the same time, both agree that ultrasonication is inefficient compared to these methods, as confirmed in this study, as well as others (Günerken et al., 2015). Grimi et al. (2014) stated that HPH was the most effective disruption technique for extracting proteins from *Microchloropsis* species, but also requires the highest power consumption. Generally, a high solids content of the biomass to be processed helps reduce the specific energy consumption of both HPH and bead mills. However, contrary to the common view in literature (Günerken et al., 2015; Yap, Dumsday, Scales, & Martin, 2015), the solids concentration of the *M. salina* biomass did influence the effectiveness of all mechanical cell disruption methods examined in this study. Hence, special caution is recommended when choosing a high biomass concentration above 15% dry weight for mechanical cell disruption.

Microalgal cell disruption using HPH has been examined mostly as a pretreatment method to improve the extraction yield of lipids or other intracellular products (Molina Grima et al., 2013; Grimi et al., 2014; Olmstead et al., 2013). However, there is some quantitative data on the cell disruption of *Microchloropsis* species using HPH. For *Microchloropsis* species, 67–100% cell disintegration degree has been reported using biomass with low solids content below 1% and pressures up to 3000 bar (Spiden et al., 2013; Günerken et al., 2015). Similar disintegration efficiencies of 56–94% were achieved in this study using high-density *M. salina* biomass with 10–25% solids. Additionally, a similar disruption efficiency of 86% was reproducibly achieved in this study using an industrial HPH on a pilot scale and with a high biomass density of 15% dry weight. This is considered to be a high disruption efficiency, considering that *Microchloropsis* species are known to have a very resistant and recalcitrant cell wall containing a layer of algaenan, which is a nonhydrolyzable biopolymer (Scholz et al., 2014), making them easier to cultivate under physically stressful conditions, while at the same time harder to disrupt compared to other species (D'Hondt et al., 2017; Spiden et al., 2013).

7.3. Hydrolysis of microalgal biomass

7.3.1. Chemical and enzymatic hydrolysis of undisrupted cells

Since mechanical disruption of microalgae cells requires high energy consumption, enzymatic hydrolysis of undisrupted *M. salina* cells with and without acid pretreatment was investigated first. The experiment was performed as described in Subsection 4.9.5 using *M. salina* biomass with a CDW

concentration of 163 g L^{-1}. Figure 7.8 shows the results of this experimental series using the same enzyme doses but with prior proteolysis (18 h) using proteases working at different pH optima of pH 3.5 and pH 7.0 followed by autoclaving (at 121 °C for 20 min) at the specified pH for both sterilization and protease inactivation purposes. After autoclaving, pH was adjusted to pH 5.0 for all batches and the specified amounts of cellulase and mannanase mixtures were added for enzymatic hydrolysis (72 h). Since changes in reaction volume due to pH adjustments throughout the process were not negligible, sugar concentrations normalized to the initial reaction volume are presented in addition to the measured values.

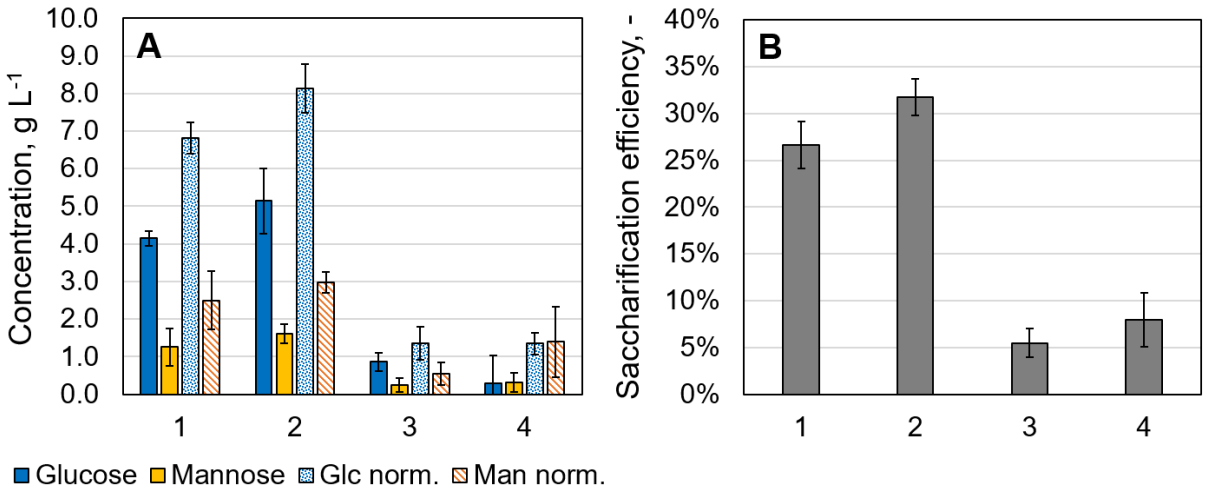

#	Pretreatment	Proteolysis	Enzymatic hydrolysis
1 – 2	Autoclaving at pH 3.5	Protease from *A. saitoi*	1% P + 5.9% C + 0.12% M
3 – 4	Autoclaving at pH 7.0	Protamex®	1% P + 5.9% C + 0.12% M

Figure 7.8: Chemical and enzymatic hydrolysis of undisrupted *M. salina* cells. Enzyme doses given as percent mass ratio of CDW are 1% protease (as specified in figure), 5.9% cellulase (Cellic® CTec3 HS), and 0.12% mannanase (Rohalase® GMP). Since changes in reaction volume due to pH adjustments throughout the process were not negligible, sugar concentrations normalized to initial reaction volume are presented additionally to the measured values. **A**: Actual and normalized final concentrations of glucose and mannose; **B**: saccharification efficiency (η_{sac}). Error bars indicate standard deviation of triplicate experiments.

Around 2.0 g L^{-1} glucose and 2.5–2.7 g L^{-1} mannose were released already after the proteolysis and following heat pretreatment at pH 3.5, which corresponds to a saccharification efficiency of 13%. In contrast, no sugar release was observed for heat pretreatment at pH 7.0. Final concentrations of 4.1–5.1 g L^{-1} glucose and 1.3–1.6 g L^{-1} mannose were achieved with heat pretreatment at acidic pH. On the other hand, final concentrations as low as 0.3–0.9 g L^{-1} glucose and 0.2–0.3 g L^{-1} mannose were measured when the same pretreatment procedure was applied at a neutral pH. Consequently, a significantly higher saccharification efficiency of 27–32% was achieved with acidic heat pretreatment followed by enzymatic hydrolysis, while it remained at 6–8% with heat pretreatment at neutral pH.

Discussion

Most studies on the hydrolysis of microalgal biomass focus on either product extraction, such as

lipids, or utilize already extracted biomass containing disrupted cells (R. Zhang et al., 2019; Zuorro et al., 2016). Some report over 90% carbohydrate solubilization of mechanically or chemically disrupted microalgae cells after enzymatic hydrolysis (Younes et al., 2020; Ho et al., 2013; Meo et al., 2017). Direct enzymatic hydrolysis of undisrupted microalgae cells, especially with conclusions on biomass saccharification, is uncommon in the literature. Few studies focusing on enzymatic disruption of microalgal cell wall use diluted biomass with 1–10% dry weight, which would yield a very dilute hydrolysate with around 2–20 g L^{-1} sugars at best (Demuez et al., 2015). In these studies, using cellulases or a combination of proteases and carbohydrases accomplished saccharification yields of 47–96% with other microalgae species.

Saccharification efficiency of 27–32% achieved with acidic hydrolysis followed by enzymatic hydrolysis is relatively low compared to literature reports for other microalgae strains mentioned above. Scholz et al. (2014) determined that the cell wall of *M. gaditana* contains around 14% algaenan, which is a nonhydrolyzable biopolymer, presenting itself as an insoluble residue following severe acid and base hydrolysis, that is well established also in other species of *Microchloropsis* including *M. salina* (Gelin et al., 1996). Thus, a relatively low saccharification efficiency is to be expected with *Microchloropsis* species even after chemical hydrolysis.

Hernández et al. (2015) carried out a comparable study regrading saccharification of undisrupted *M. gaditana* biomass with acidic hydrolysis followed by enzymatic treatment. They report that 93 mg sugars per g dry weight (DW) were released after diluting the biomass with 7% *(v/v)* sulphuric acid and autoclaving (at 121 °C for 30 min). In this study, pretreatment with proteases and autoclaving the biomass at pH 3.5 (at 121 °C for 20 min) released only 27–29 mg g^{-1} DW sugars. They also note that alkaline pretreatment (5 M NaOH, 90 °C for 30 min) of the biomass had a sugar release yield of 14 mg g^{-1} DW, which is lower than with acidic hydrolysis. Furthermore, Hernández et al. (2015) demonstrated that acidic hydrolysis improved the efficacy of subsequent enzymatic hydrolysis with cellulases significantly with an increase of sugar release from 15 mg g^{-1} DW to 129 mg g^{-1} DW. In the current study, even though this effect was confirmed, the influence of acidic hydrolysis prior to enzymatic hydrolysis was less remarkable with an increase of sugar release from 12–17 mg g^{-1} DW to merely 57–68 mg g^{-1} DW. This difference might originate from using *M. salina* cells grown in nutrient-replete medium, since these have a different macromolecular and cell wall composition (Schädler et al., 2019), which could result in increased structural stability of the cell wall and make it harder to disrupt or hydrolyse.

Although acidic hydrolysis of *M. salina* biomass improved the saccharification yield, it should be noted that it also resulted in a substantial dilution of the biomass due to the addition of acid and base to adjust the pH of the reaction medium. More precisely, dilution of the biomass by a factor of 1.3–1.6 resulted in a decrease of final glucose concentration from 6.8–8.1 g L^{-1} to 4.1–5.1 g L^{-1}. Moreover, the excessive addition of acid and base results in an increase in the salt content of the hydrolysate, which might negatively affect yeast growth when it is used as a cultivation medium for yeast oil production. Hence, the acidic hydrolysis approach was avoided in further hydrolysis experiments in this work.

7.3.2. Enzymatic hydrolysis after mechanical cell disruption

Enzymatic hydrolysis of mechanically disrupted *M. salina* cells was performed as described in Subsection 4.9.5. Table 7.1 shows the disruption degree of microalgal biomass prior to enzymatic hydrolysis and enzyme dosing used in experiments on a millilitre scale together with their label numbers as they come up in the following figures in this subsection. First, the effects of the sterilization method and degree of cell disruption on the effectiveness of enzymatic hydrolysis were investigated, considering the impact on a subsequent scale-up. Then, the dosing of various enzymes was examined for increased saccharification efficiency, and the hydrolysis was scaled up to 200 L using the best-performing enzyme composition.

Table 7.1: Disruption degree of microalgal biomass prior to enzymatic hydrolysis and enzyme dosing (g enzyme per g CDW) used in experiments on a millilitre scale.

#	disruption degree	Cellic® CTec3 HS (Cellulase)	Rohament® CEP (Cellulase)	Rohalase® GMP (Mannanase)	Hemicellulase from *A. niger*	Protamex® (Protease)
1	92%	5.92%	–	0.12%	–	–
2	92%	5.92%	–	0.12%	1.0%	–
3[a]	75%	5.92%	–	0.12%	–	–
4	75%	5.92%	–	0.12%	–	1.0%
5	75%	5.92%	–	0.12%	–	–
6	70%	5.92%	–	0.12%	–	–
7	70%	–	5.0%	0.12%	–	–
8	70%	–	10.0%	0.12%	–	–
9[b]	70%	–	–	–	–	–
10	78%	–	10.0%	0.12%	–	–
11	78%	–	15.0%	0.12%	–	–
12	78%	–	10.0%	2.00%	–	–
13[b]	78%	–	–	–	–	–

[a] Pretreated by autoclaving at 121 °C for 20 min for sterilization. No antibiotics added.

[b] Control without enzyme addition.

Figure 7.9 illustrates the results of experiments examining the influence of sterilization method and cell disruption degree on subsequent enzymatic hydrolysis of mechanically disrupted *M. salina* cells. First, autoclaving at 121 °C for 20 minutes was compared with the addition of antibiotics (each 100 mg L^{-1} of kanamycin and tetracycline) to inhibit the growth of contaminants in respect of saccharification efficiency (η_{sac}). It was demonstrated that skipping the autoclaving step and using antibiotics instead did not affect hydrolysis efficiency, which reached 10% in both cases (Fig. 7.9 B). Therefore, the addition of antibiotics was preferred to prevent contamination effects on biomass hydrolysis in the following experiments. On the other hand, the degree of cell disruption had a great influence

on the effectiveness of hydrolysis. An increase of initial cell disintegration degree from 70% to 92% increased saccharification efficiency by 6% from 10% to 16% (Fig. 7.9 D).

Figure 7.10 A and B present the results of an experiment examining the effects of an addition of hemicellulase or protease to the enzyme mixture on hydrolysis efficiency. Adding 1% hemicellulase to the enzyme mixture in addition to cellulase and mannanase improved biomass hydrolysis, increasing its efficiency by 2% from 16% to 18% (Fig. 7.10 B1). On the other hand, adding 1% protease to the enzyme mixture in addition to cellulase and mannanase increased hydrolysis efficiency only by 1% to 11% (Fig. 7.10 B2).

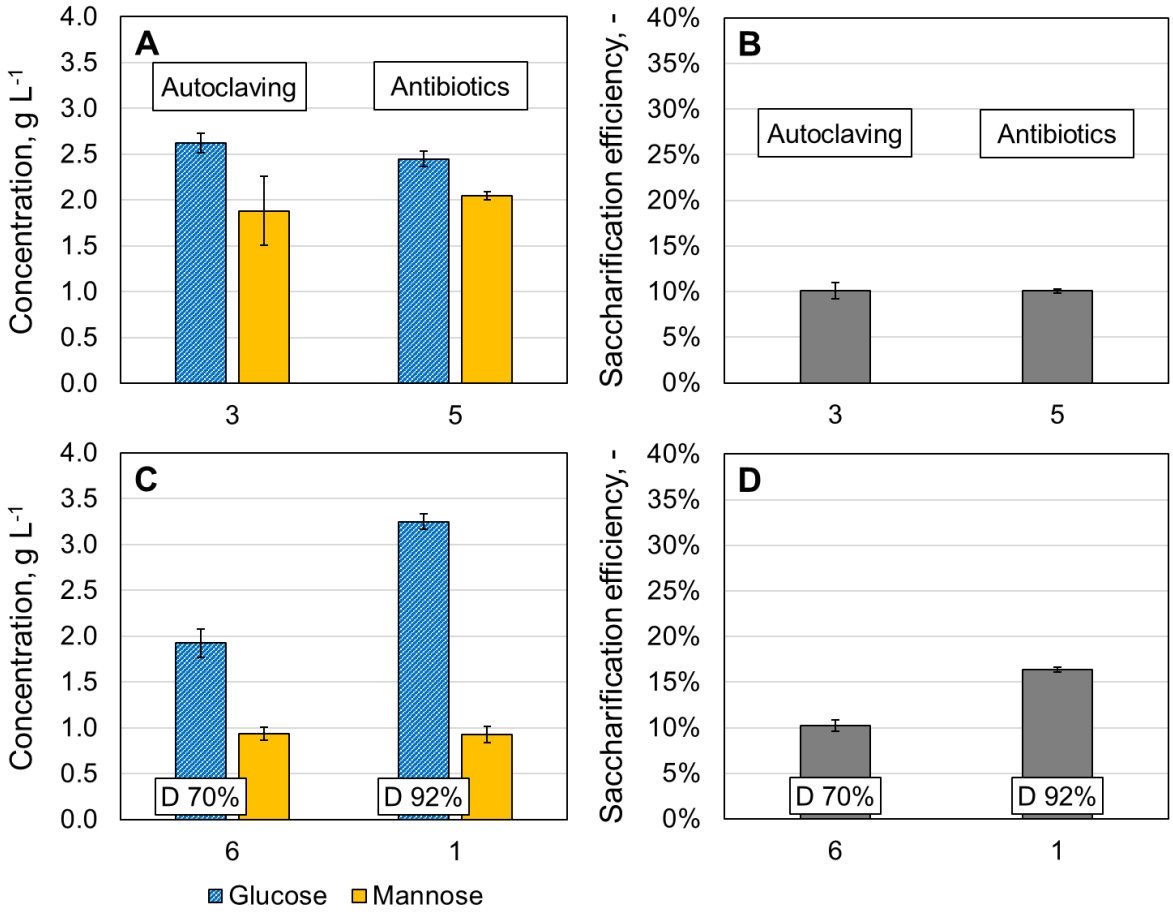

Figure 7.9: Influence of sterilization method and cell disruption degree on subsequent enzymatic hydrolysis of mechanically disrupted *M. salina* cells. Enzyme doses given as percent mass ratio of CDW are as listed in Table 7.1. (**A**) Final concentrations of glucose and mannose and (**B**) saccharification efficiency (η_{sac}) with autoclaving or antibiotic addition as sterilization method. (**C**) Final concentrations of glucose and mannose and (**D**) saccharification efficiency (η_{sac}) with different degrees of mechanical cell disruption as indicated by data labels. Error bars indicate standard deviation of triplicate experiments.

Figure 7.10 C and D present the results of an experiment comparing two different cellulase mixes, namely Cellic® CTec3 HS and Rohament® CEP, labelled as C1 and C2, respectively, with respect to the saccharification efficiency. Only 2% of the carbohydrates were solubilized using a mannanase dose of 0.12%. Using 5% of Cellic® CTec3 HS in addition to mannanase improved the biomass hydrolysis efficiency by 8% to 10%, whereas with Rohament® CEP, the same increased the saccharification efficiency by 10% to 12% (Fig. 7.10 D). With Cellic® CTec3 HS, more mannose was

released, while Rohament® CEP solubilized more glucose (Fig. 7.10 C). Due to its better performance than Cellic® CTec3 HS, as well as its easy-to-use powder form, Rohament® CEP was used as cellulase mix in further enzymatic hydrolysis experiments.

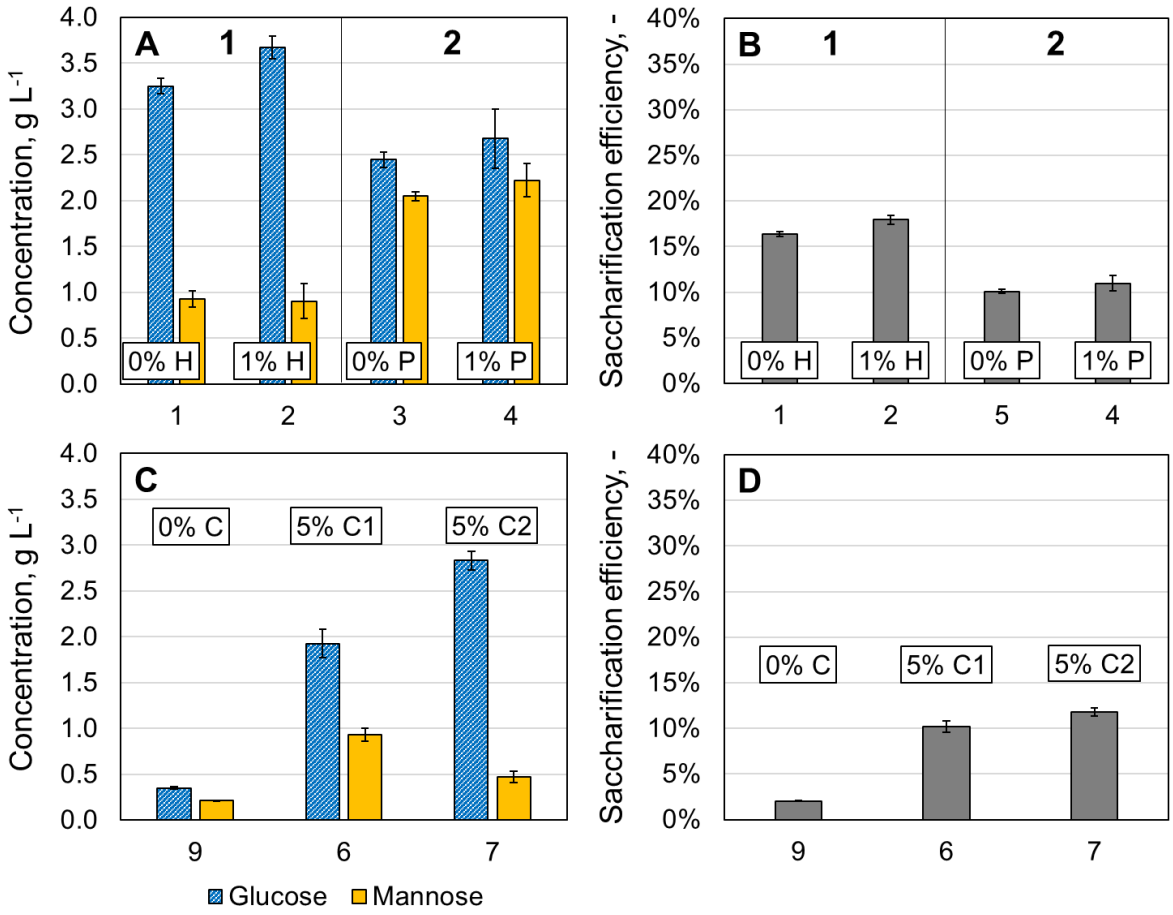

Figure 7.10: Influence of hemicellulase or protease addition and selection of cellulase on the effectiveness of enzymatic hydrolysis of mechanically disrupted *M. salina* cells. Enzyme doses given as percent mass ratio of CDW are as listed in Table 7.1 in detail. (**A**) Final concentrations of glucose and mannose and (**B**) saccharification efficiency (η_{sac}) for **1** hemicellulase and **2** protease addition. Data labels indicate the dosing of hemicellulase (H) and protease (P). (**C**) Final concentrations of glucose and mannose and (**D**) saccharification efficiency (η_{sac}) using different cellulase mixes as indicated by data labels with C1 and C2 being Cellic® CTec3 HS and Rohament® CEP, respectively. Error bars indicate standard deviation of triplicate experiments.

Figure 7.11 A and B display the results of an experiment investigating the effect of cellulase dosing on saccharification efficiency. The difference between sets 1 and 2 is the initial degree of cell disruption, which is 70% and 78%, respectively. This difference led to 1.8 g L^{-1} more sugar (glucose and mannose) in set 2 compared to set 1. In experiment set 1, using 5% and 10% cellulase in addition to mannanase increased hydrolysis efficiency by 10% and 16%, respectively. Moreover, in experiment set 2, using 10% and 15% cellulase in addition to mannanase resulted in an efficiency increase by 16% and 18%, respectively. Although the best results of 7.2 g L^{-1} sugars (glucose and mannose) and 26% saccharification efficiency were reached with 15% cellulase dosing, the difference to 10% cellulase was not significant enough to consider it better with respect to price-performance ratio. For hydrolysis of the biomass with 78% cell disruption, adding 10% cellulase together with 0.12% mannanase yielded 6.9 g L^{-1} sugars and 25% saccharification efficiency. Thus, a cellulase dose of

10% was used in the enzyme mixture in further hydrolysis experiments.

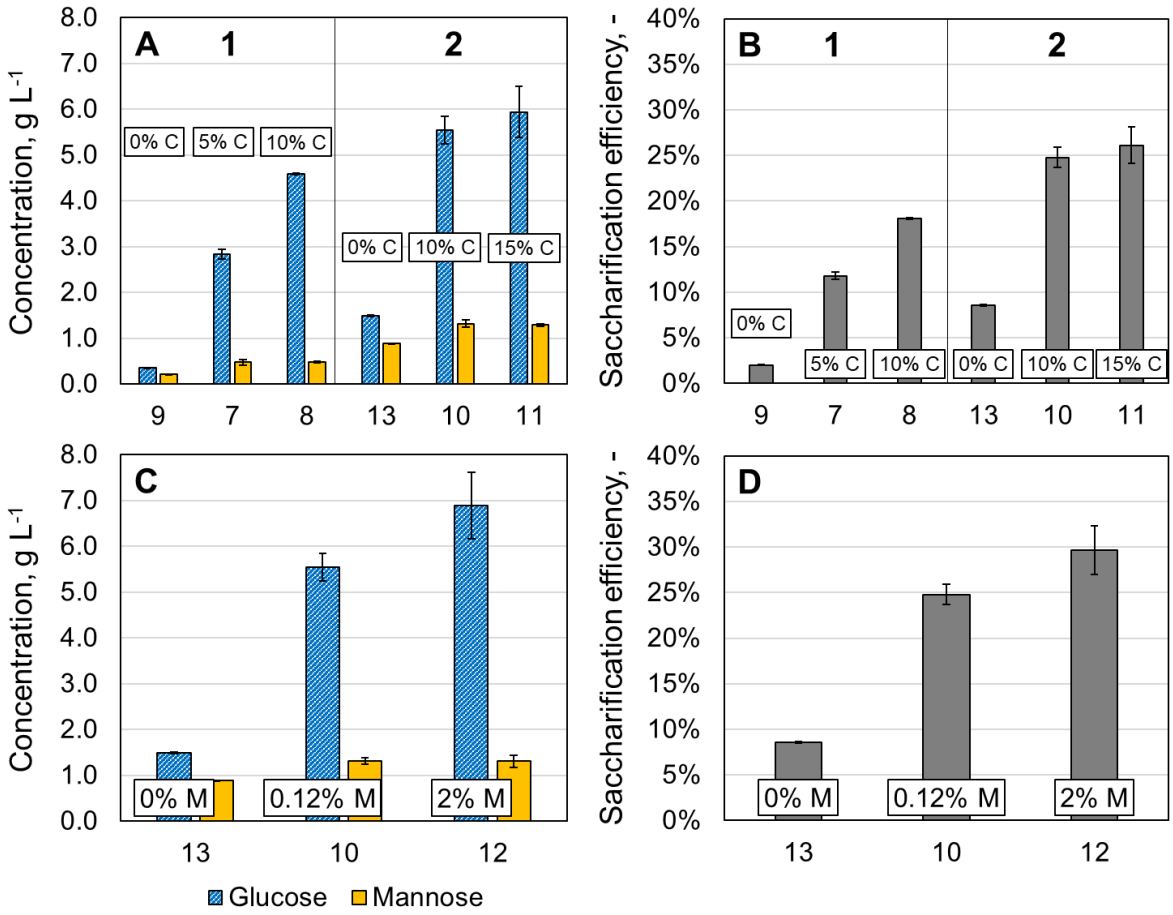

Figure 7.11: Influence of cellulase and mannanase dosing on the effectiveness of enzymatic hydrolysis of mechanically disrupted *M. salina* cells. Enzyme doses given as percent mass ratio of CDW are as listed in Table 7.1 in detail. (**A**) Final concentrations of glucose and mannose and (**B**) saccharification efficiency (η_{sac}) for various cellulase doses with **1** 70% and **2** 78% disruption degree. Data labels indicate the dosing of cellulase (C). (**C**) Final concentrations of glucose and mannose and (**D**) saccharification efficiency (η_{sac}) for various mannanase doses. Data labels indicate the dosing of mannanase (M). Error bars indicate standard deviation of triplicate experiments.

Figures 7.11 C and D reveal the results of an experiment investigating the effect of mannanase dosing on saccharification efficiency. Using 10% cellulase only, 9% of the carbohydrates of the microalgal biomass were solubilized. Adding 0.12% mannanase into the enzyme mixture increased hydrolysis efficiency by 16% to 25%, and a further increase of mannanase dosing to 2.0% increased efficiency by another 5% to 30%. Moreover, the sum of glucose and mannose released increased from 2.4 g L^{-1} to 6.9 g L^{-1} and 8.2 g L^{-1}, respectively. Figure 7.11 C indicates a possible synergy between cellulase and mannanase, which leads to improved glucose release with increased dosing of mannanase, even though the amount of mannose released remains the same.

Scale-up of the enzymatic hydrolysis of mechanically disrupted *M. salina* biomass to first 60 L, and finally to 200 L, was performed as described in Subsection 4.9.5 using a CDW concentration of 150 g L^{-1}. The duration of enzymatic hydrolysis was kept shorter on the large scale since previous experiments showed that the results did not change after 40 hours (data not shown). Figure 7.12

shows the results of the scale-up experiments. On both scales, a cellulase dosing of 10% of CDW was applied. Even though a higher mannanase dose (1.0%) was used on the 200 L scale, no improvement in hydrolysis efficacy was observed compared to the 60 L scale with 0.12% mannanase dosing. Final concentration of released glucose was 5.7 g L^{-1} and 5.9 g L^{-1}, whereas 1.4 g L^{-1} and 1.3 g L^{-1} mannanose was solubilized, respectively. Hence, the resulting saccharification efficiency was very similar, namely 22.2% and 22.6% in the 60 L and the 200 L scale processes, respectively.

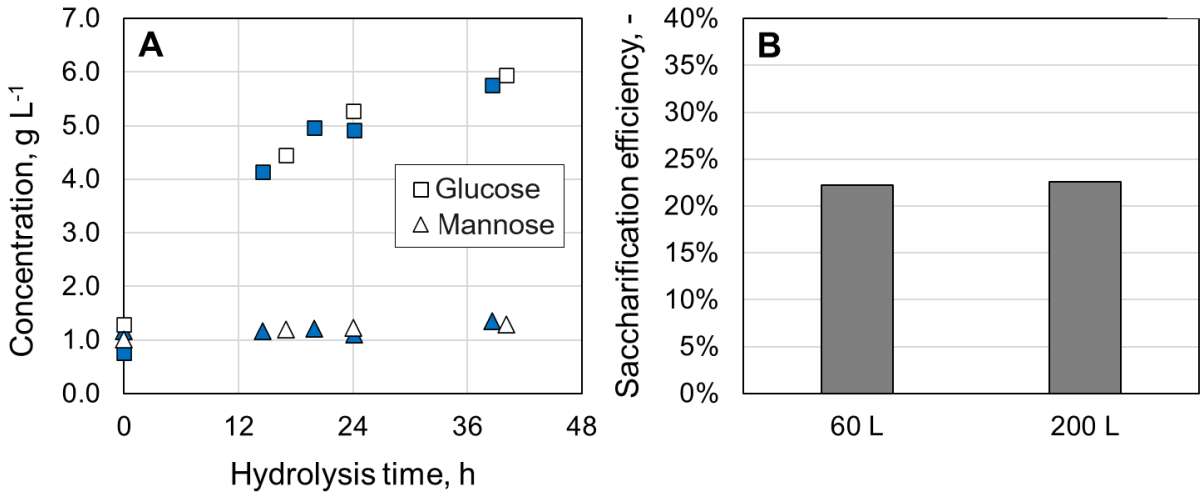

Figure 7.12: Enzymatic hydrolysis of mechanically disrupted *M. salina* cells on 60 L (blue) and 200 L (white) scales. Degree of cell disruption was 78% in both experiments. Enzyme doses given as percent mass ratio of CDW are 10.0% cellulase (Rohament® CEP) and 0.12% and 1.00% mannanase (Rohalase® GMP) for hydrolysis on the 60 L and the 200 L scales, respectively. **A**: Final concentrations of glucose (□) and mannose (△); **B**: saccharification efficiency (η_{sac}).

Discussion

As anticipated, higher degrees of mechanical cell disruption at the beginning of enzymatic hydrolysis resulted in a higher hydrolysis efficiency since the carbohydrates in the cell wall become more exposed, making them more readily available for the enzymes. Increasing cellulase and mannanase doses in the enzyme mixture improved hydrolysis efficiency, and they also exhibited synergistic effects with each other since increasing the mannanase dosing further improved the glucose yield. The addition of hemicellulase to the enzyme cocktail or performing proteolysis prior to the addition of carbohydrases increased the effectiveness of enzymatic hydrolysis only marginally in contrast to literature reports for other microalgae strains (Demuez et al., 2015) and was therefore omitted in the final procedure used for the scale-up to 200 L. Nonetheless, saccharification efficiency achieved on the 200 L scale was 7% lower than the 30% recorded on the millilitre scale, reaching only 23%.

Based on the carbohydrate and sugar composition of *M. salina* grown in a nutrient-replete medium in TLC PBR as reported by Schädler et al. (2019), with an initial CDW concentration of 250 g L^{-1} and 100% saccharification efficiency, the resulting microalgae hydrolysate would have 53.4 g L^{-1} total concentration of glucose and mannose. However, technical equipment used in the current study allowed the processing of only 150 g L^{-1} CDW containing microalgal biomass since the industrial HPH used for mechanical cell disruption did not allow higher feed stream viscosity. Hence, calculating with an initial CDW concentration of 150 g L^{-1} and 100% saccharification efficiency, the resulting

microalgae hydrolysate would have 32.1 g L^{-1} total concentration of glucose and mannose. Nevertheless, the best results obtained in this experimental series were 8.2 g L^{-1} on a millilitre scale and 7.2 g L^{-1} on a 200 L scale. In this work, the maximum saccharification efficiency achieved was 30%, which corresponds to 77.3 mg released sugars per g CDW, very similar to the yield reported by Mirsiaghi and Reardon (2015) using commercial enzyme mixtures on disrupted *M. salina* biomass. Nevertheless, 30% saccharification yield is way below the expected range of 47–90% (Demuez et al., 2015), yielding much lower sugar concentrations than the 50 g L^{-1} presumed for yeast cultivation as described in Chapter 6. One solution to the unexpectedly low sugar content of the microalgae biomass hydrolysate would be concentrating the hydrolysate using an evaporator, which was not demonstrated in this study due to the lack of appropriate equipment for a large-scale application.

It might be possible to improve the carbohydrate saccharification yield for high-density *M. salina* biomass by adding other commercially available enzymes with various activities into the enzyme cocktail used. With the help of a growth inhibition screen, Gerken et al. (2013) suggested that chitinase, lysozyme, pectinase, sulfatase, b-glucuronidase, and laminarinase could aid the enzymatic cell wall degradation of *Microchloropsis* strains. Moreover, Horst et al. (2012) could improve the lipid extraction yield for autoclaved *M. oculata* biomass by around 20% using Viscozyme (a multi-enzyme mixture containing a wide range of carbohydratases) and Proteinase K (an alkaline serine protease of fungal origin). However, the prospects of success at improving the effectiveness of enzymatic hydrolysis seem to be low with *M. salina* cells grown in nutrient-replete medium, since these have a different macromolecular and cell wall composition (Schädler et al., 2019; Jeong et al., 2017), and are apparently harder to disrupt and hydrolyse than the *M. salina* cells grown in nutrient-limited medium (Klassen et al., 2015; Jeong et al., 2017). Applying nutrient limitation on the microalgae culture, on the other hand, would reduce biomass productivity. Alternatively, other microalgae strains that are richer in carbohydrate content and easier to disrupt than *M. salina*, such as the members of *Porphyridium* and *Scenedesmus* genera (González-Fernández & Ballesteros, 2012; Kröger et al., 2018), could be used for a more efficient production of microalgal biomass hydrolysate.

7.4. Elimination of phosphorus in microalgae hydrolysate

Preliminary precipitation experiments with phosphate buffer

Preliminary experiments on phosphate precipitation were carried out as described in Subsection 4.9.6 using a phosphate buffer and $FeCl_3$ as the precipitating agent at a pH range of pH 4.5 to pH 5.5. In the first experiment series, various ratios of iron to phosphorus were examined, adding different amounts of concentrated $FeCl_3$ solution to the buffer. As seen in Figure 7.13 A, using a Fe:P stoichiometric ratio of 1:1 resulted in a reduction of phosphate concentration from 164 mg L^{-1} to 51 mg L^{-1}, yielding a phosphate depletion of only 69%. On the other hand, a Fe:P ratio of 1.5:1 and 2:1 reduced the phosphate concentration to 6 mg L^{-1} and 1 mg L^{-1}, achieving 96% and 99% phosphate depletion, respectively. In the second experiment, the influence of the centrifugation time on phosphate precipitation efficiency was investigated, keeping the Fe:P ratio at 1.5. Figure 7.14 shows that even before centrifugation, the precipitation was so effective that the phosphate concentration was reduced by 97% to 6 mg L^{-1}. A centrifugation time of 10 minutes lowered the phosphate con-

centration to 5 mg L^{-1}, while further centrifugation yielded only higher concentrations, indicating that a centrifugation duration longer than 10 minutes is not necessary for effective phosphate elimination.

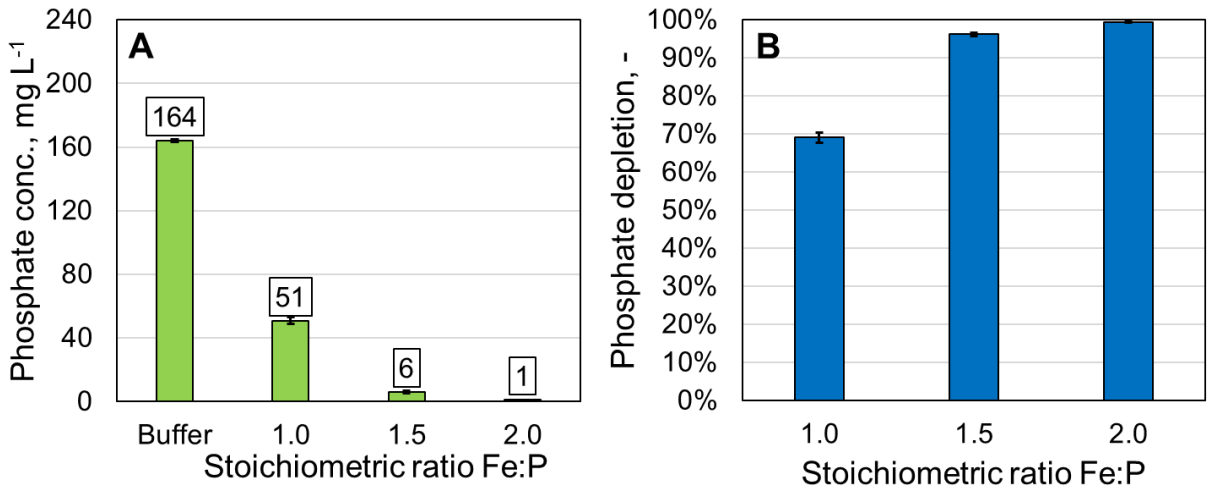

Figure 7.13: Variation of the Fe:P stoichiometric ratio for phosphate precipitation of a phosphate buffer using $FeCl_3$. **A**: Phosphate concentration in the buffer solution and after precipitation with various Fe:P ratios; **B**: degree of phosphate depletion with various Fe:P ratios.

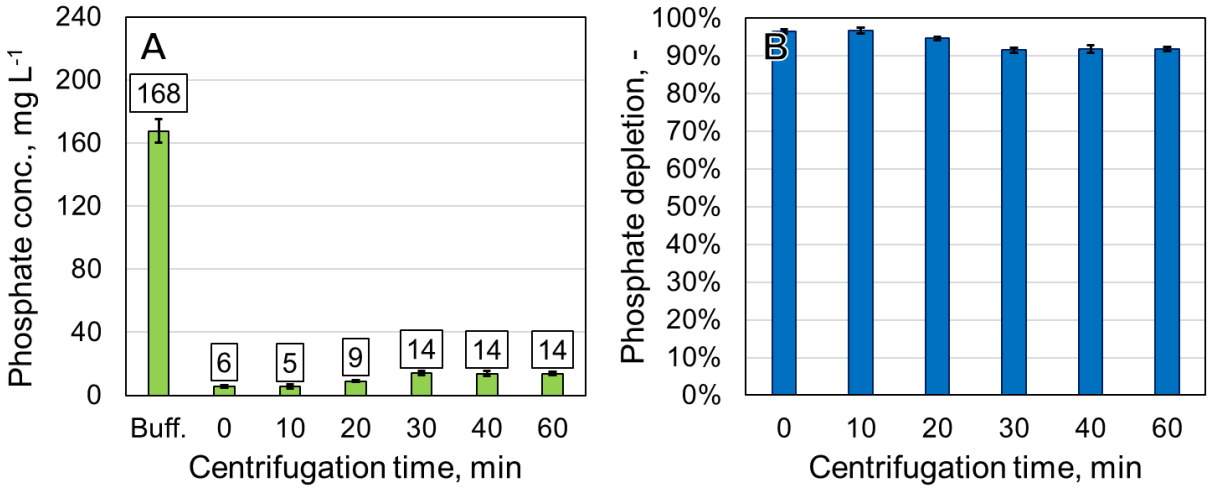

Figure 7.14: Variation of the centrifugation time for phosphate precipitation with a constant Fe:P stoichiometric ratio of 1.5. **A**: Phosphate concentration in the buffer solution and after precipitation and centrifugation for different durations; **B**: degree of phosphate depletion with various centrifugation durations.

Precipitation of phosphate in microalgae hydrolysate

Microalgal biomass hydrolysate produced on the 60 L scale as described in Subsection 7.3.2 had a very high phosphate concentration of 3.7 g L^{-1}, meaning that a single-step precipitation with a stoichiometric excess of iron over phosphorus would require uneconomically large amounts of $FeCl_3$. Moreover, initial experiments with microalgae hydrolysate showed that a single-step process is not as effective as demonstrated with the phosphate buffer (data not shown). Hence, a stepwise reduction of phosphorus content was worked out. For practicality in large-scale applications, it was also examined whether centrifugation of the hydrolysate after each step is necessary. Figure 7.15 shows the results of a stepwise phosphate precipitation of microalgae hydrolysate in three steps with

a Fe:P ratio of 1.5:1 with and without centrifugation after each step. When centrifuged after each precipitation step, the phosphate depletion was 97% in the first step but declined to 44% and 67% in the following steps. Phosphate concentration was reduced from 3.7 g L^{-1} to 101 mg L^{-1}, 57 mg L^{-1}, and finally to 19 mg L^{-1} after each step. This corresponds to a similar phosphate depletion as in the preliminary experiments with phosphate buffer in the first step but a drastic reduction of precipitation efficiency in the following steps. Without centrifuging the hydrolysate after each precipitation step, but only at the end of the final step, a phosphate concentration of 85 mg L^{-1}, 87 mg L^{-1}, and 29 mg L^{-1} were measured after each step. Although the overall degree of phosphate depletion was very similar for the centrifuged and non-centrifuged variants with 99.5% and 99.2%, respectively, the final phosphate concentration was by 10 mg L^{-1} higher in the latter case. This would make a big difference in the C/P ratio of the microalgae hydrolysate if it has a very low sugar content, which is the case for the microalgae hydrolysate produced in this work. Hence, centrifugation after each step was found to be necessary for this work.

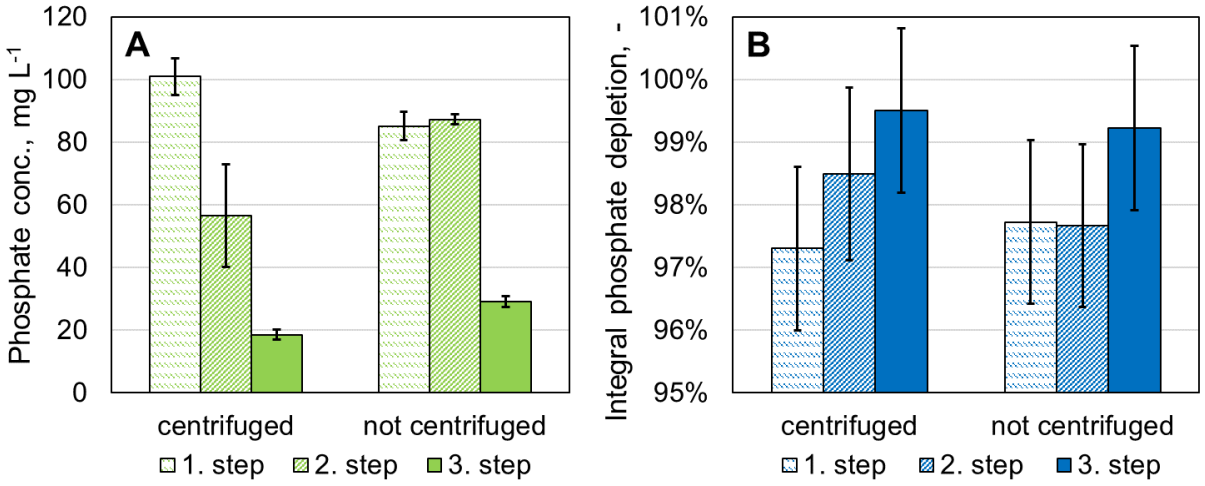

Figure 7.15: Effect of centrifugation on stepwise phosphate precipitation of microalgae hydrolysate. "Centrifuged" label means that the reaction medium was centrifuged after each step and only the supernatant was used for the next precipitation step, whereas "not centrifuged" indicates that centrifugation was not performed between precipitation steps, but only at the end of the experiment. Initial phosphate concentration of the microalgae hydrolysate was 3.747 g L^{-1}. A constant Fe:P stoichiometric ratio of 1.5 was used. **A**: Phosphate concentration after each precipitation step; **B**: cumulative degree of phosphate depletion after each precipitation step.

The stepwise precipitation approach was adopted for the scale-up of the phosphate precipitation to the 200 L scale using the equipment described in Subsection 4.9.6. A Fe:P stoichiometric ratio of 1.2:1 was used in the first step, which was increased to 2:1 for the second step. To avoid diluting the microalgae hydrolysate, the precipitation agent $FeCl_3$ and KOH for pH adjustment were added to the reaction mixture in solid form. As shown in Figure 7.16 A, the initial phosphate concentration in the microalgae hydrolysate was 6.5 g L^{-1}, which is much higher than in the previous experiment, but was still successfully reduced to 83 mg L^{-1} and then to 28 mg L^{-1} after each step. A phosphate depletion of 98.7% and 66.6% was achieved after the first and second precipitation steps, respectively, reaching an overall depletion degree of 99.6%. Performing additional steps attempting further phosphate precipitation on the millilitre scale were unable to decrease the phosphate concentration below 25 mg L^{-1}, even if much higher Fe:P ratios of up to 10:1 were applied, and hence were omitted here (data not shown).

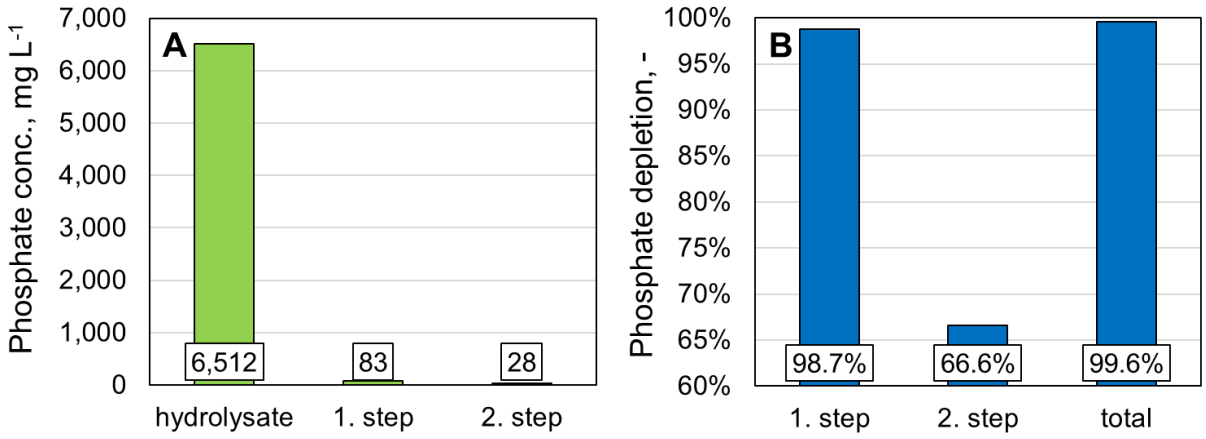

Figure 7.16: Stepwise phosphate precipitation of microalgae hydrolysate on a 200 L scale. A Fe:P stoichiometric ratio of 1.2 and 2.0 were used in 1st and 2nd steps, respectively. Reaction mixture was centrifuged using a disc separator after each step. Precipitating agent $FeCl_3$ and KOH for pH adjustment were added to the reaction mixture in solid form to prevent dilution of the hydrolysate. **A**: Phosphate concentration before and after each precipitation step; **B**: degree of phosphate depletion after each precipitation step and final total phosphate depletion.

Discussion

The conditions selected for phosphorus elimination of microalgal biomass hydrolysate by precipitation using $FeCl_3$, more specifically the pH range of 4.5–5.5 and the stoichiometric excess of iron to phosphorus, are reasonable according to procedures applied in large-scale wastewater treatment plants with extremely low phosphorus levels in effluent streams ($<$ 0.5 mg L^{-1}) due to strict regulations (Takács et al., 2006). Preliminary experiments using a phosphate buffer showed that very low phosphate concentrations down to 1 mg L^{-1} can be obtained by applying the chosen procedure for phosphate precipitation as described in Subsection 4.9.6.

Due to the low sugar concentration of 8.1 g L^{-1} in the microalgae hydrolysate, a very low phosphate concentration of 2.82 mg L^{-1} was required to achieve a C/P ratio of 3515 g g^{-1}, based on the amount of carbon present in sugars and ignoring the other organic carbon sources in the hydrolysate. However, when the same procedure of phosphate precipitation is applied to the microalgae hydrolysate, its effectiveness declined as soon as a phosphate concentration around 100 mg L^{-1} was reached, not allowing a reduction of the phosphate concentration below 25 mg L^{-1}. Using a very similar procedure with a FE:P ratio of 1.5:1 on a different microalgae hydrolysate, Meo et al. (2017) successfully reduced the phosphate content of the hydrolysate by 99.7% from 1.62 g L^{-1} to 10 mg L^{-1}. In this study, initial phosphate level in the hydrolysate was much higher (3.75–6.51 g L^{-1}), and, although a similar phosphate depletion degree of 99.6% was achieved using a two-step precipitation process, final phosphate concentration remained around 19–36 mg L^{-1}, even if further precipitation steps were performed at much higher Fe:P ratios of up to 10:1 (data not shown).

Takács et al. (2006) suggest that there might be various reasons making it hard to achieve very low phosphorus levels in streams containing high amounts of organic matter, such as the formation of organic side products with Fe^{3+} and other components, most importantly, charged organics (through ion-pairing and binding), also stating that the extent of these reactions is unknown. Furthermore,

soluble ferric–phosphate and ferric–hydroxide complexes might form, which hinders the conversion of soluble phosphorus to the particulate form by binding up Fe^{3+} or PO_4^{3-} ions in soluble complexes.

Another strategy to achieve a C/P ratio of 3515 g g^{-1} in the microalgae hydrolysate would be performing phosphate precipitation after concentrating the hydrolysate by evaporation, for instance, using a thin-film evaporator. The increased sugar concentration would then allow a higher C/P ratio at the same phosphate level of around 25 mg L^{-1} after phosphate precipitation.

7.5. Composition of microalgae hydrolysate

Table 7.2 shows the sugar composition, as well as the phosphate and protein concentrations, of the microalgae hydrolysate produced on the 200 L scale as described in Subsection 7.3.2 after phosphate precipitation, which is later used as fermentation medium for yeast oil production in a membrane bioreactor (MBR) (see Section 8.1).

Table 7.2: Measured sugar composition, protein and phosphate content of microalgae hydrolysate after phosphate precipitation.

Component	**Concentration, g L^{-1}**	**Fraction in Sugars, –**
Glucose	5.32	65.9%
Mannose	1.14	14.1%
Galactose	1.52	18.8%
Rhamnose	0.08	1.0%
Xylose	0.02	0.2%
Total sugars	8.08	100.0%
Phosphate	0.036	–
Protein	13.4	–

Table 7.3: Elemental composition of microalgae hydrolysate after phosphate precipitation.

	C	H	N	S	P	O
Mass fraction, %	2.52	10.84	1.65	0.00	0.001[a]	84.99[b]

[a] Calculated from measured phosphate concentration, since detection limit was 0.5% (w/w).

[b] Calculated as the remaining mass fraction after subtraction of all other elements listed above.

The elemental composition of the microalgae hydrolysate after final processing is presented in Table 7.3. Based on these values, microalgae hydrolysate had a C/N ratio of 1.54 g g^{-1} and a C/P ratio of 2044 g g^{-1}. However, it should be noted that the C/P ratio is so high due to the high protein content despite the low sugar concentration. Assuming that sugars are the only carbon source utilized by the yeast, the C/P ratio of the hydrolysate would be only 221 g g^{-1}.

Discussion

Based on the sugar composition of *M. salina* grown in nutrient-replete medium (Schädler et al., 2019), microalgae biomass with a CDW concentration of 150 g L^{-1} contains 24.2 g L^{-1} glucose, 7.5 g L^{-1} mannose, 2.6 g L^{-1} galactose, and 1.9 g L^{-1} rhamnose with the remaining carbohydrates amounting to 2.4 g L^{-1}. According to these values, only 15.2% of mannose could be solubilized with the applied hydrolysis protocol, whereas 58.5% saccharification efficiency of galactose was achieved. Nevertheless, considering an overall saccharification efficiency of 23%, sugar concentrations measured in the final microalgae hydrolysate are in accordance with these values. Meo et al. (2017) reported 40.8 g L^{-1} glucose, 2.0 g L^{-1} mannose, 4.3 g L^{-1} galactose and 13.3 g L^{-1} proteins in the microalgae hydrolysate of *Scenedesmus* species starting with a CDW concentration of 250 g L^{-1}. Even though the total sugar concentration achieved by Meo et al. (2017) was much higher, the protein content is very similar to the concentration measured in this work.

The final C/P ratio of the microalgae hydrolysate after phosphorus elimination was much lower than the desired 3515 g g^{-1}. On the 200 L scale, with a carbon concentration of 25.44 g L^{-1} in the hydrolysate, 22.14 mg L^{-1} phosphate was required to achieve a C/P ratio of 3515 g g^{-1}. It could, however, be reduced to merely 36 mg L^{-1}, reaching a much lower C/P ratio of 2044 g g^{-1}. As mentioned before, one solution to the unexpectedly low C/P ratio of the hydrolysate is to concentrate it by evaporation, for example, using a thin-film evaporator, which could not be demonstrated in this study due to the lack of appropriate equipment for a large-scale application. Phosphate precipitation applied after hydrolysate concentration by evaporation would yield a higher C/P ratio due to higher sugar concentration with a phosphorus concentration of 12 mg L^{-1} (36 mg L^{-1} phosphate) achieved in this work.

8. Process Integration: Yeast Oil Production Using Microalgal Biomass Hydrolysate [1]

This chapter reports on the integration of microalgal biomass production, biomass hydrolysis, and yeast oil production into a single process for microbial oil production from CO_2. First, yeast cultivation using microalgae hydrolysate is presented. Then, the separation of the yeast oil and its fatty acid (FA) composition will be covered, followed by a carbon balance of the whole process. Finally, the integrated process developed in this work is compared with microbial oil production using only microalgae regarding carbon conversion efficiency, productivity, and process costs.

8.1. Yeast oil production in a 1.5 L MBR using microalgae hydrolysate

High-cell-density yeast cultivation using microalgae hydrolysate as the feed medium was performed in the 1.5 L scale membrane bioreactor (MBR) with total cell retention. As there was not enough hydrolysate available, process scale-up to 50 L was not possible. The design and operation of the MBR, as well as the applied semi-continuous production mode, were described in Section 4.7 in detail. This experiment with microalgae hydrolysate was analogous to the cultivation presented in Section 6.3 except for the feeding medium used, which was microalgae hydrolysate with a total sugar concentration of 8.08 g L^{-1} sugars and a C/P ratio of 2044 g g^{-1}. The batch medium was the defined medium described in Table 4.5. The volumetric flow rate of the feed medium was adjusted according to its sugar concentration so that a feeding rate of 1.1 g L^{-1} h^{-1} sugars would be maintained throughout the semi-continuous operation as in the reference experiment. The initial C/P ratio after inoculation was 499 g g^{-1} since the preculture was not washed prior to inoculation. Figure 8.1 shows the results of this experiment using microalgae hydrolysate as the feed medium together with the previously presented experiment using a synthetic medium as reference.

The batch phase took 23 hours, which is 2.6 hours shorter than in the reference experiment. After complete consumption of sugars in the batch medium, the semi-continuous mode of operation started with a hydrolysate feed rate of 1.1 g L^{-1} h^{-1} sugars. The liquid volume inside the reactor was initially 1.5 L and kept in a 1.5–5.5 L range throughout the process. The semi-continuous phase lasted only 17 hours, and the experiment had to be stopped after that since the maximum possible permeate flow rate declined drastically over time, making it impossible to keep the reaction volume below the reactor capacity. This reduction in the permeate flow rate was most probably the result of increasing cell dry weight (CDW) concentration and accumulation of other molecules present in the microalgae hydrolysate in the reactor. After 17 hours of semi-continuous operation, 105.9 g CDW was formed, which is more than twice the 50.1 g after the same process time in the reference experiment. 67.2 g of this was lipid-free CDW, whereas only 38.7 g was lipids. In this way, 36.6% lipid quota was achieved, which is only by 7.2% higher than at the time of inoculation and by 14.2% lower than in the reference experiment after the same production time. Phosphate concentration started rising at the beginning of the semi-continuous phase and reached 62.0 mg L^{-1}, although

[1] Part of the results presented here has already been published in: Koruyucu, A., Blums, K., Peest, T., Schmack-Rauscher, L., Brück, T., & Weuster-Botz, D. (2023). High-cell-density yeast oil production with diluted substrates imitating microalgae hydrolysate using a membrane bioreactor. *Energies, 16(4)*(1757).

glucose and mannose stayed below the detection limit, which lies at 0.004 g L^{-1} and 0.014 g L^{-1}, respectively. At the end of the process, a lipid space-time-yield (STY) of 0.63 g L^{-1} h^{-1} and a lipid yield of 0.34 g per g sugars were recorded.

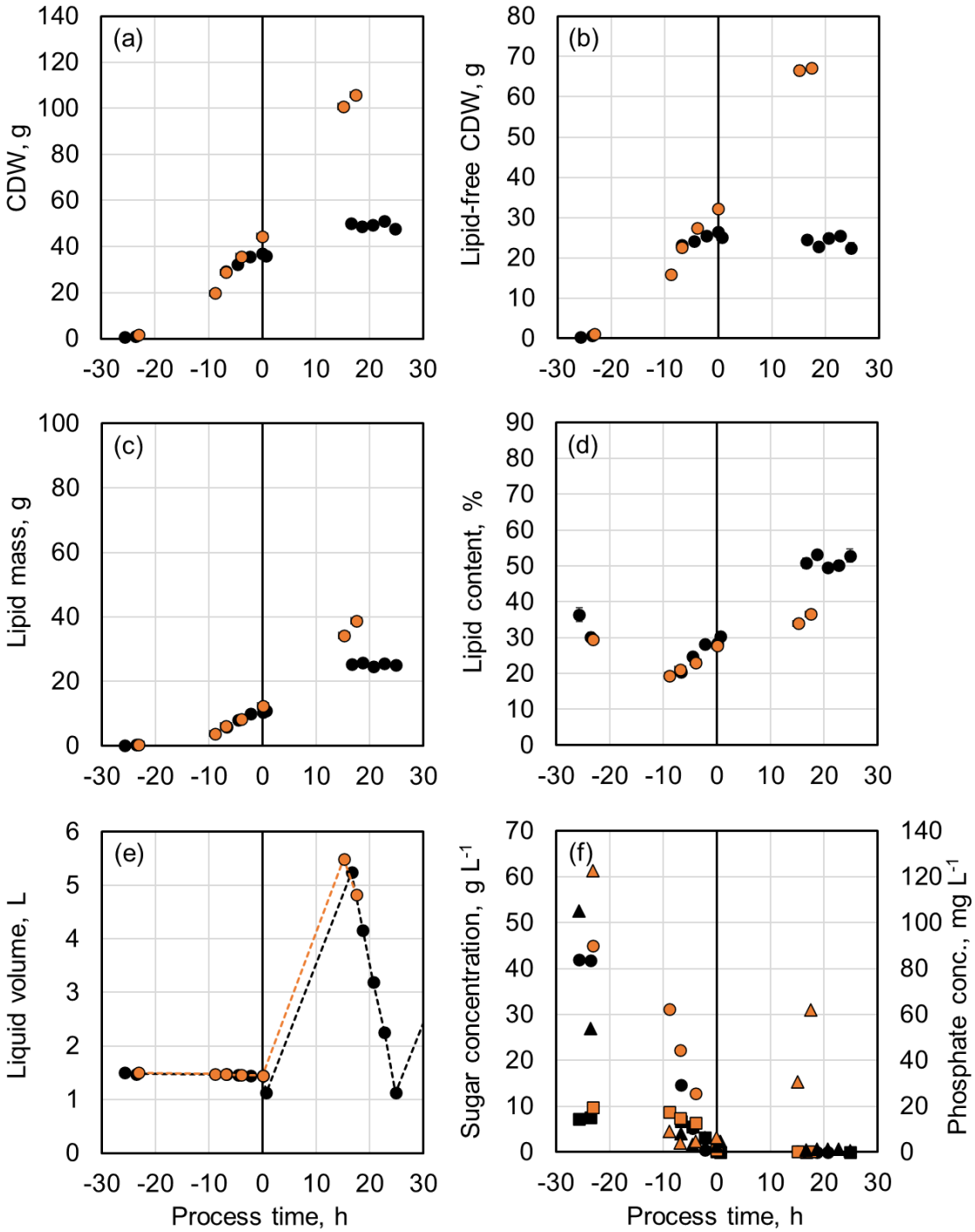

Figure 8.1: Yeast oil production using microalgae hydrolysate as the feed medium in a membrane bioreactor on a 1.5 L scale with total cell retention in a semi-continuous mode. This experiment using hydrolysate as feed is marked in orange (●) and the reference experiment using only defined medium is marked in black (●). A defined medium (Table 4.5) with 50 g L^{-1} sugars and a C/P ratio of 3515 g g^{-1} was used as batch medium, whereas microalgae hydrolysate with 8.08 g L^{-1} sugars and a C/P ratio of 2044 g g^{-1} was used as feed medium with a feeding rate of 1.1 g L^{-1} h^{-1} sugars. The black line shows the end of the batch phase and switch to semi-continuous mode of operation. The error bars show the standard deviation of the triplicate measurements. (a) CDW; (b) lipid-free CDW; (c) lipid mass; (d) lipid content of the yeast cells; (e) liquid volume inside the MBR; (f) concentrations of glucose (●) and mannose (◆) on the primary vertical axis and of phosphate (▲) on the secondary axis.

The carbon balance of the yeast oil production using microalgae hydrolysate as feed was made using the results of elemental analysis. The mass fraction of carbon in microalgae hydrolysate ($x_{C,MAH}$) and in permeate ($x_{C,perm}$) were measured to be 2.52% and 0.81%, respectively. These values were used to calculate the total carbon taken up by the yeast cells. The resulting carbon conversion efficiency (eta_C) into lipids was 29.0%.

Discussion

There were two major problems when using microalgae hydrolysate for high-cell-density yeast oil production in an MBR. The first one is the low C/P ratio of 2044 g g^{-1} in microalgae hydrolysate compared to 3515 g g^{-1} in the defined medium used for yeast cultivation in the reference experiment. Thus, cellular lipid content achieved using microalgae hydrolysate as feed medium (36.6%) was noticeably lower than in the reference process (50.8%). The second major problem was the maximum possible permeate flow rate declining significantly over time from 5 L h^{-1} to 0.3 L h^{-1} after 17 hours into the semi-continuous operation. This is much lower than the flow rate of 0.76 L h^{-1} required to keep the reaction volume below the maximum capacity of the MBR (6 L) at all times and forced a premature termination of the experiment.

The reduction in the permeate flow rate was most probably due to a combined effect of increasing cell density and accumulation of other molecules present in the microalgae hydrolysate in the MBR, causing the formation of a colloid, which is a suspension of microscopically dispersed insoluble particles. Even though microalgae hydrolysate was filter-sterilized (0.22 µm filter) prior to its use as a feed medium, further particle precipitation and coagulation were observed in the MBR after the start of hydrolysate feed. The presence of these particles was confirmed in the samples taken, as a cloudy translucent supernatant with orange colour was formed even after centrifugation at 20,000 rcf. On the other hand, these particles were not observed in the permeate, which was always a fully transparent yellow liquid, meaning that the particles could not pass through the membrane unit and accumulated inside the reactor.

Regarding phosphor elimination in wastewater with $FeCl_3$ as precipitating agent, Takács et al. (2006) emphasise the complexity of mechanisms playing a role in the conversion of various P and Fe species, in both soluble and insoluble forms. They state that the stoichiometry of the present Fe species depends on the wastewater composition and pH. Moreover, they indicate that the formation of organic side products with Fe^{3+} and other wastewater components, particularly charged organics (through ion-pairing and binding), does happen, however, to an unknown extent. This means that a biomass hydrolysate with high organics content, treated with $FeCl_3$ for phosphor elimination, would contain many complex molecules causing colloid formation and flocculation by destabilisation and particle aggregation when these come into contact with a high-density cell culture. The presence of charged organic species, such as dissolved proteins and peptides, in a biomass hydrolysate makes this especially likely to happen.

The reduced permeate flow rate would not be so problematic if the sugar concentration in microalgae hydrolysate was higher or the hydrolysate was later on concentrated by evaporation. For instance,

with a feeding rate of 1.1 g L^{-1} h^{-1} sugars and a sugar concentration of 50 g L^{-1} in hydrolysate, a permeate flow rate of only 0.10 L h^{-1} would be necessary to keep the reaction volume below 2 L at all times in semi-continuous operational mode. Moreover, such a high sugar concentration would drop the required flow rate of feed medium by 87% to 33 mL h^{-1}, thus slowing down the accumulation of species causing particle formation inside the reactor. Alternatively, continuous operation of the MBR with a feeding rate of 1.1 g L^{-1} h^{-1} sugars and a sugar concentration of 6.5 g L^{-1} in hydrolysate would require a permeate flow rate of merely 0.25 L h^{-1}. Unfortunately, these options could not be explored in this study due to time restrictions.

Table 8.1: Process parameters, metrics and carbon conversion for yeast oil production in an MBR under defined conditions or using microalgal biomass hydrolysate (MAH) as feed medium.

	Experiment #		
	IV	**V**	**Meo et al. (2017)**
C/P ratio	**(Defined medium)**	**(MAH as feed)**	**(MAH as medium)**
Batch medium	3515 g g^{-1}	3515 g g^{-1}	4826 g g^{-1}
After inoculation	581 g g^{-1}	499 g g^{-1}	–
Feed medium	3515 g g^{-1}	2044 g g^{-1}	4826 g g^{-1}
Process parameters			
MBR scale	1.5 L	1.5 L	3.0 L
Batch phase duration	25.7 h	23.1 h	69.6 h
Semi-continuous phase	16.6 h	17.5 h	–
Continuous phase	–	–	24.0 h
Process metrics			
Lipid quota	50.8%	36.6%	53%
STY_{X+L}	0.78 g L^{-1} h^{-1}	1.71 g L^{-1} h^{-1}	0.63 g L^{-1} h^{-1}
STY_L	0.40 g L^{-1} h^{-1}	0.63 g L^{-1} h^{-1}	0.33 g L^{-1} h^{-1}
$Y_{(X+L)/S}$	0.49 g g^{-1}	0.93 g g^{-1}	0.82 g g^{-1}
$Y_{L/S}$	0.25 g g^{-1}	0.34 g g^{-1}	0.43 g g^{-1}
Fraction of carbon converted into			
Lipids	46.9%	29.0%	–
Lipid-free CDW	27.2%	30.1%	–
CO_2 and by-products	26.6%	40.9%	–

Table 8.1 summarizes the results of high-cell-density yeast oil production in an MBR with P-limitation using a defined medium as both batch and feeding media (Exp. IV), using microalgal biomass hydrolysate as feeding medium (Exp. V), and an experiment by Meo et al. (2017) using a very similar MBR set-up and microalgae hydrolysate as both batch and feeding media. Values recorded after

a similar semi-continuous or continuous production time are listed for a better comparison. Using microalgae hydrolysate as the feed medium, a much higher lipid STY was achieved, although the lipid quota was by 14.2% lower compared to the use of a defined medium. This is due to more lipid mass being formed after the same process time despite the lower C/P ratio of the feed medium. Also, lipid yield ($Y_{L/S}$) was higher, meaning that more lipid mass was generated per amount of sugars consumed. However, a higher fraction of carbon flew into lipid-free CDW and CO_2 production, resulting in a lower carbon conversion efficiency (η_C) of 29.0%.

The lipid quota achieved in the experiment by Meo et al. (2017) was by 16.4% higher than in this study, which results from a much higher C/P ratio in the hydrolysate they used. Still, STYs of both total CDW and lipids were higher in this study. In both experiments, lipid yield was above the theoretical maximum calculated by Ratledge (2014) to be approximately 0.33 g g^{-1} using glucose as the carbon source. This is due to the presence of other carbon sources in biomass hydrolysate, such as peptides, which were not considered in the calculation of lipid yield on sugars.

Yeast oil production with *C. oleaginosus* using various waste streams and hydrolysates as cultivation medium has been researched at an increasing rate in recent years. Examples of the cultivation media investigated are whey permeate (Moon et al., 1978), various lignocellulosic hydrolysates such as corn cob or wastepaper hydrolysates (Gong et al., 2016; Zhou et al., 2019; Di Fidio et al., 2021; Grubišić et al., 2021, 2022), and algal biomass hydrolysate (Meo et al., 2017; Masri et al., 2017; Younes et al., 2020). In these studies using a variety of methods to induce lipid production using hydrolysates as cultivation medium, maximum values reported for cellular lipid quota were 27.2–59.7%, for lipid STY 0.02–0.35 g L^{-1} h^{-1}, and for lipid yield 0.13–0.24 g g^{-1}, except for the study by Meo et al. (2017) with 0.43 g g^{-1} lipid yield. In the current study, the lipid quota achieved (36.6%) is rather on the lower half of the spectrum of reported literature values. On the other hand, lipid productivity (0.63 g L^{-1} h^{-1}) and yield (0.34 g g^{-1}) recorded in this study are the highest among all the literature mentioned above.

8.2. Fatty acid composition of yeast oil

The fatty acid (FA) composition of the *C. oleaginosus* cells after lipid production under P-depleted conditions using a defined medium, as well as microalgal biomass hydrolysate, is shown in Table 8.2. Among all, two FAs stand out as the main constituents of this yeast oil, namely oleic acid and palmitic acid, with 50–56% and 24–27%, respectively. These are followed by stearic acid and linoleic acid but with much smaller fractions of around 8–11% and 7%. As anticipated, the FA composition using microalgae hydrolysate as the feed medium was very similar to that using a defined medium. For comparison, the compositions of olive and palm oils are presented as well. Even though this yeast oil consists of primarily oleic acid, its overall FA profile resembles that of palm oil rather than olive oil.

As shown in Figure 8.2, the FA composition of *C. oleaginosus* changes only marginally over the process time with increasing lipid content of yeast cells. The most noticeable changes are the increase in the oleic acid fraction by 6.6% and the decrease in the palmitic acid fraction by 3.2%.

Table 8.2: Fatty acid (FA) composition of yeast oil produced with *C. oleaginous* using phosphor-depleted medium and microalgae hydrolysate in this study presented together with data from other comparable studies in the literature and FA profiles of similar plant oils, namely olive oil and palm oil.

		Mass fraction in total fatty acids, %			
Fatty Acid	Trivial Name	P-limitation	P-depleted MAH[a]	Olive oil[b]	Palm oil[b]
C14:0	Myristic acid	0.6	0.6	0	1
C16:0	Palmitic acid	23.5	26.6	11.5	43.8
C16:1	Palmitoleic acid	0.7	0.7	1.5	0.5
C18:0	Stearic acid	8.4	11.4	2.5	5
C18:1 (n-9)	Oleic acid	56.4	49.9	75.5	39
C18:2 (n-6)	Linoleic acid	7.1	6.7	7.5	10
C18:3 (n-3)	α-Linolenic acid	0.4	1.0	1.0	0.2
C20:0	Arachidic acid	0.3	0.4	0.5	0.5
C22:0	Behenic acid	0.2	0.6	–	–
C24:0	Lignoceric acid	1.4	1.0	–	–
C22:6 (n-3)	DHA	0.6	0.7	–	–
C24:1 (n-9)	Nervonic acid	0.0	0.5	–	–
	Others	0.3	–	–	–

[a] MAH stands for microalgae hydrolysate.

[b] Data taken from Belitz et al. (2008).

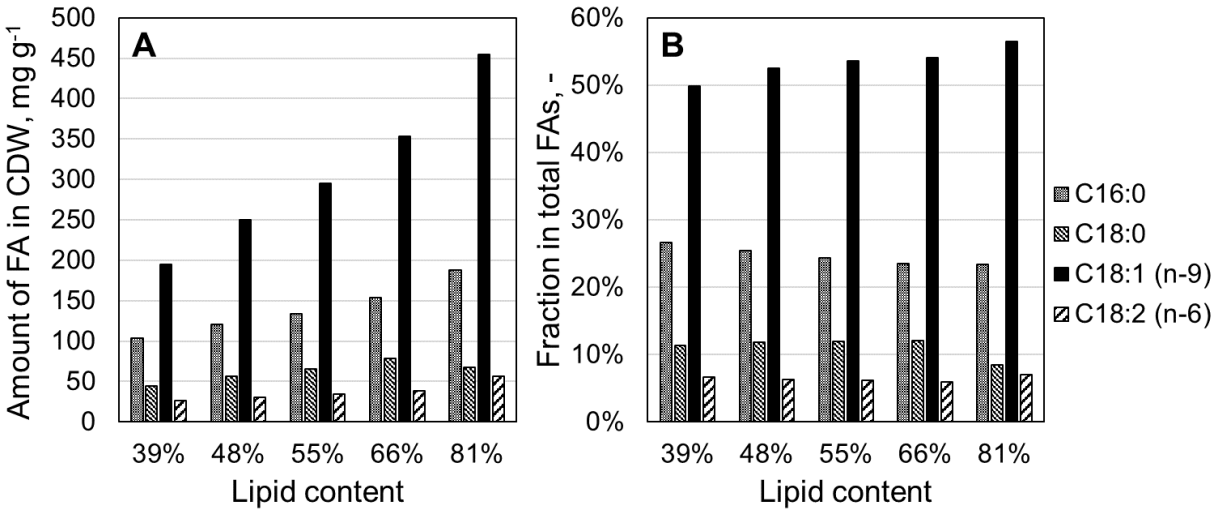

Figure 8.2: Change in (**A**) the amount of certain FAs in the CDW and (**B**) the fraction of these in the total FA content of *C. oleaginosus* cells with respect to the cellular lipid quota.

Discussion

It is reported in the literature that the exact FA composition of *C. oleaginosus* oil might vary depending on the carbon and nitrogen sources present in the substrate; however, the differences are relatively small (Shaigani et al., 2021; Awad et al., 2019; Grubišić et al., 2022; Karayannis et al., 2023). The FA composition measured for yeast oil produced under P-limited conditions in this study is in accordance with the literature data (G. Zhang et al., 2011; Meo et al., 2017). Moreover, using microalgal biomass hydrolysate for yeast oil production under P-limited conditions did not cause a significant change in the FA composition, as previously reported by Meo et al. (2017).

8.3. Separation of yeast oil

The main focus of this work is the process integration for yeast oil production from CO_2; however, some conventional downstream processing possibilities were also explored to present a concept covering a complete production process. Solvent extraction was the preferred method for separating microbial oils from the fermentation broth. For this, various solvents and pre-treatment methods were tested and compared based on the separation efficiency and the FA composition of the resulting product. Solvents selected for examination were ethyl acetate, n-hexane, and ethanol in combination with potassium carbonate (K_2CO_3) to induce or enhance phase separation in water-solvent mixtures. Additionally, the effects of various pre-treatment methods on solvent extraction of the yeast oil from actual fermentation broth were investigated in different combinations. These pre-treatment methods are enzymatic hydrolysis of the yeast cell wall, mechanical disruption of yeast cells using a high-pressure homogenizer (HPH) and treatment with 1% *(v/v)* sulfuric acid as demulsifier. The procedure for each pre-treatment is described in detail in Section 4.8.

Enzymatic treatment of yeast cells directly at the end of fermentation was carried out to see if cell disruption and a subsequent release of the intracellular lipids was possible without mechanical cell disruption methods. For enzymatic disruption of *C. oleaginosus* cells, commercial enzyme mixtures listed in Table 4.14 were used. These were selected based on previous work by Masri et al. (2019) stating the enzyme activities required for enzymatic cell disruption of this yeast strain. It was also considered that the enzymes should be commercially available in large amounts and cost-efficient enough to be used on an industrial scale. However, only enzymatic hydrolysis of the yeast cells was insufficient to release the intracellular lipids since no lipid layer was observed after subsequent centrifugation of the enzymatically treated yeast broth (data not shown). Chemical hydrolysis of yeast cells was not considered since adding a base or an acid at amounts required for chemical hydrolysis would also alter the chemical structure of the yeast oil. The addition of large amounts of a base would cause saponification of lipids, whereas the addition of an acid would generate free FAs by hydrolysing phospholipids (Khot et al., 2020).

High-pressure homogenization

Disruption of *C. oleaginosus* cells was performed on a 30 L scale using an industrial HPH. Directly after a high-cell-density fermentation in the 50 L MBR, yeast broth was concentrated to a volume of 30 L using the microfiltration unit of the MBR. Subsequently, concentrated yeast broth with a

CDW content of around 10% and a lipid content of 79% was homogenized for two passes through the HPH. Already after the first pass, the disintegration degree of the yeast cells reached 87.6%. Nonetheless, only a slight increase to 89.0% was observed after the second pass; thus, further homogenization of the yeast broth was omitted.

Changes in the yeast broth during cell disruption by HPH are also visualized using light microscope images as depicted in Figure 8.3. Initially, yeast cells with intracellular lipid droplets are clearly visible. After one pass through the HPH, larger and extracellular lipid droplets appeared, indicating the release of intracellular lipids. Although some intact cells are still present, mostly cell debris is to be seen. After the second pass, very large extracellular lipid droplets formed, while small amounts of intact cells were still observed.

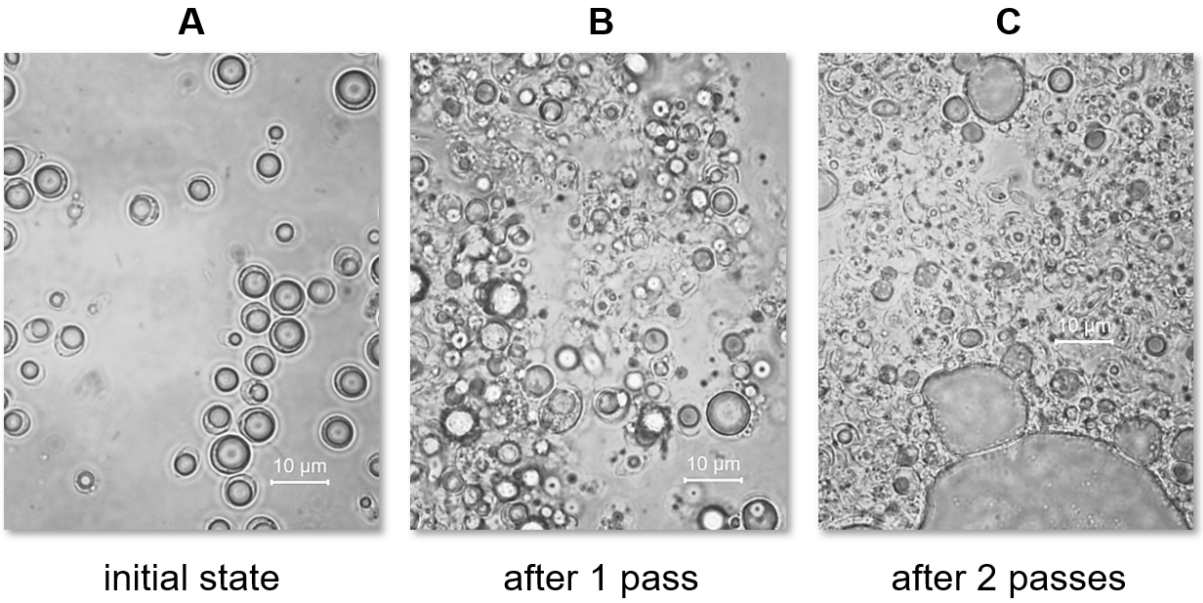

Figure 8.3: Light microscope image (50x magnification in bright field) of *C. oleaginosus* cells after high-pressure homogenisation to release intracellular lipids. HPH was performed at 900 bar exit pressure with 200 L h^{-1} flow rate. Yeast broth homogenized contained 96 g L^{-1} CDW with a lipid content of 79%. **A**: Initial state at the end of fermentation; **B**: yeast broth after 1 pass; **C**: yeast broth after 2 passes.

Separation by centrifugation

After the disruption of lipid-containing yeast cells by two passes through an industrial HPH, a sample was taken and centrifuged at 3221 rcf for 10 minutes to evaluate yeast oil separation qualitatively as illustrated in Figure 8.4. Four phases are visible in the centrifugation tube from bottom to top: a cell debris sediment, a transparent aqueous phase, an opaque layer presumed to be cell debris suspended in an emulsion of lipids and aqueous phase, and a clear liquid oil phase.

Various demulsifiers were examined to break the emulsion, forming between the aqueous and oil phases shown in Figure 8.4 and, thus, to enhance oil separation by centrifugation only. The demulsifiers tested are listed in Table 8.3 grouped according to their solubility in aqueous or oil phases. With a dosing of 0.1–1.0% *(v/v)*, none of the emulsion breakers examined was effective enough to allow efficient oil separation by centrifugation (data not shown). Moreover, with sulphuric and hydrochlo-

ric acid doses above 2% *(v/v)*, unwanted hydrolysis of the yeast biomass was observed through a strong colour change and reduction of the pellet size. However, the addition of 1.0% *(v/v)* sulphuric or hydrochloric acid was determined to improve the phase separation between aqueous and solvent phases in the subsequent solvent extraction of the yeast oil. Therefore, the addition of 1.0% *(v/v)* sulphuric acid as a demulsifier was used as a pretreatment method to enhance phase separation in the oil extraction using solvents.

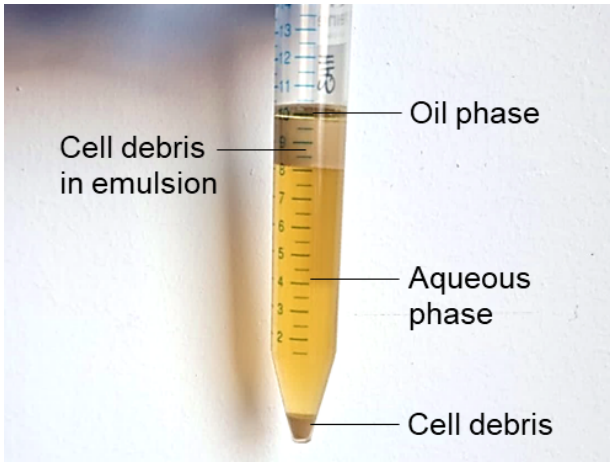

Figure 8.4: Image of an oil containing yeast broth centrifuged after cell disruption with HPH. From bottom to top, the four phases formed were cell debris, aqueous phase, cell debris suspended in emulsion, and oil phase as indicated in the image. Yeast broth processed contained 96 g L^{-1} CDW with a lipid content of 79%.

Table 8.3: Demulsifiers tested for breaking the water-oil emulsion of homogenized yeast broth. Sulphuric and hydrochloric acid were tested with a dosing range of 0.1–10.0% *(v/v)*, while all other demulsifiers were tested with 0.1–1.0% *(v/v)* dosing.

Water soluble	**Water miscible**	**Oil soluble**
Polyethylene glycol 600	n-Butanol	Renoclean Aktiv DA[a]
1,2-Propanediol	tert-Butanol	
Sulphuric acid	Ethanol	
Hydrochloric acid		
Urea		

[a] Product by Fuchs Lubricants GmbH, Mannheim, Germany.

Separation by solvent extraction

Efficient separation of yeast oil from fermentation broth was performed by solvent extraction. The influence of solvent and pre-treatment methods on extraction efficiency was examined. Solvents tested for yeast oil extraction were ethyl acetate, n-hexane, and ethanol in combination with potassium carbonate (K_2CO_3) to induce or enhance phase separation in water-solvent mixtures. Different pre-treatment methods examined for yeast cell wall disruption were enzymatic hydrolysis and me-

chanical disruption using HPH. Sulfuric acid was used as a demulsifying agent for better phase separation in the following solvent extraction. Pre-treatment with 1% *(v/v)* sulfuric acid was carried out at 25 °C and 70 °C to determine the effect of pre-treatment temperature on extraction efficiency.

Figure 8.5 depicts the yeast oil extraction efficiency (η_{ext}) achieved and solvent recovery measured with different pre-treatment methods and solvents, including an elaborate list of methods applied in each case. With no prior cell disruption but pre-treatment with sulfuric acid at 25 °C, lipid extraction efficiency using ethyl acetate was 52%. Performing a combination of enzymatic and mechanical cell disruption methods before acidic treatment and extraction increased extraction efficiency by 18% to 70%. In addition to this modification, increasing the temperature of acidic treatment from 25 °C to 70 °C further increased extraction efficiency by 22% to 92%. Nevertheless, when the exact same procedure was applied using potassium carbonate to facilitate phase separation instead of centrifugation, extraction efficiency dropped by 45% to 46%. Additionally, excluding only the enzymatic treatment of the yeast broth prior to mechanical cell disruption from the procedure reduced the extraction efficiency only by 7% to 85%. Thus, enzymatic treatment of the yeast broth was omitted in further experiments.

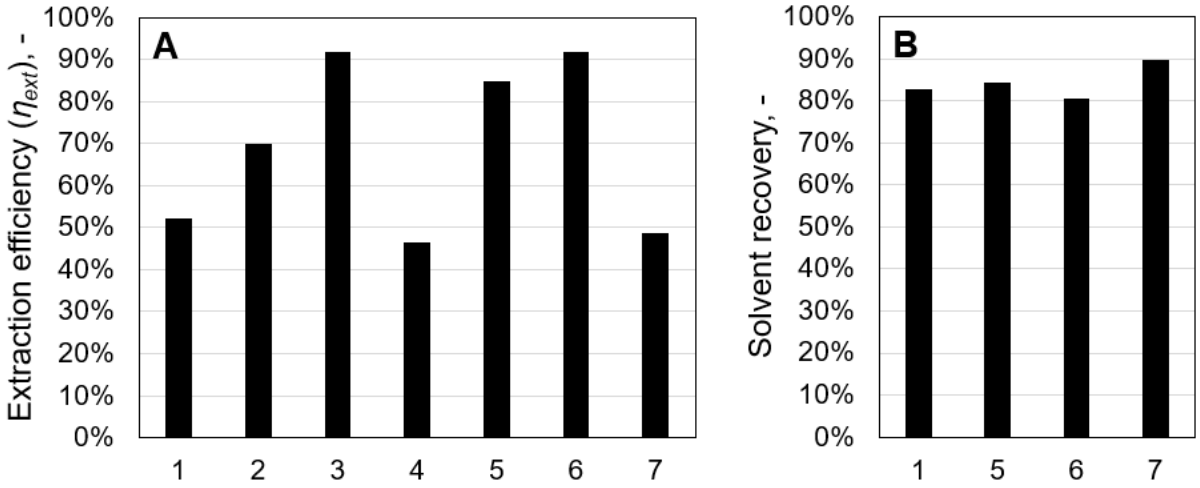

#	Cell disruption method	Separation protocol	Phase separation method
1	No cell disruption	Pretreatment with 1% (v/v) H_2SO_4 at 25°C + extraction with ethyl acetate	Centrifugation
2	Enzymatic + mechanical	Pretreatment with 1% (v/v) H_2SO_4 at 25°C + extraction with ethyl acetate	Centrifugation
3	Enzymatic + mechanical	Pretreatment with 1% (v/v) H_2SO_4 at 70°C + extraction with ethyl acetate	Centrifugation
4	Enzymatic + mechanical	Pretreatment with 1% (v/v) H_2SO_4 at 70°C + extraction with ethyl acetate	K_2CO_3 addition
5	Mechanical	Pretreatment with 1% (v/v) H_2SO_4 at 70°C + extraction with ethyl acetate	Centrifugation
6	Mechanical	Pretreatment with 1% (v/v) H_2SO_4 at 70°C + extraction with n-hexane	Centrifugation
7	Mechanical	Pretreatment with 1% (v/v) H_2SO_4 at 70°C + extraction with ethanol	K_2CO_3 addition + centrifugation

Figure 8.5: Solvent extraction of yeast oil using various pre-treatment methods and different solvents. **A**: Extraction efficiency (η_{ext}); **B**: Solvent recovery using a rotary vacuum evaporator.

Examination of different solvents for yeast oil extraction was carried out using the procedure improved in previous experiments. This included mechanical cell disruption with an HPH, pretreatment with 1% *(v/v)* sulfuric acid at 70 °C to aid in phase separation, extraction with the corresponding solvent, phase separation by centrifugation, solvent recovery with a rotary vacuum evaporator, and finally removal of the remaining solvent in an explosion-proof vacuum drying chamber. Only in the case of ethanol as an extraction solvent, which is miscible with water, was potassium carbonate added to allow phase separation, but subsequent centrifugation was still the method of phase separation. Using this procedure, lipid extraction efficiencies of 85%, 92% and 49% were achieved using ethyl acetate, n-hexane and ethanol, respectively. Overall solvent recovery of the extraction step was over 80% for all solvents used after separation by a rotary vacuum evaporator as described in Section 4.8, while the highest recovery of 90% was recorded with ethanol.

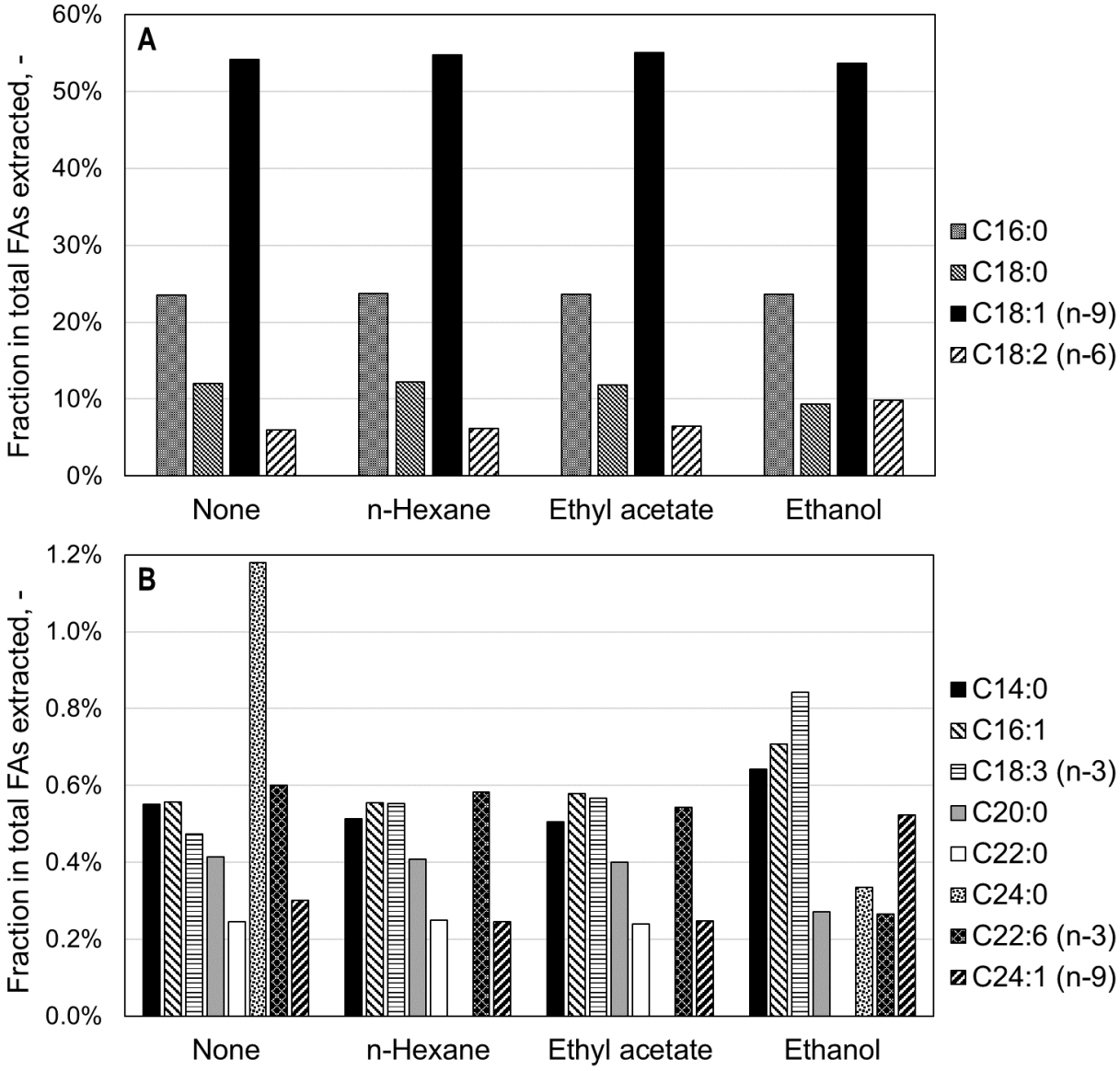

Figure 8.6: FA composition of microbial oils extracted using various solvents. Relative amounts of FAs in yeast oil without extraction and in extracts using n-hexane, ethyl acetate and ethanol are given. **A**: Fractions of palmitic acid (C16:0), stearic acid (C18:0); oleic acid (C18:1) and linoleic acid (C18:2); **B**: fractions of remaining FAs.

Figure 8.6 shows the FA composition of microbial oils extracted using different solvents. In general, the extracts obtained with n-hexane and ethyl acetate had very similar compositions, which were also very close to the original yeast oil, except for lignoceric acid (C24:0). More differences were noted in the oil extracted using ethanol. Fractions of palmitic acid and oleic acid were very similar in all extracted oils. However, the oil extracted using ethanol contained less stearic acid and more linoleic acid compared to n-hexane and ethyl acetate. Nonetheless, the difference was mild, with only around 2.5% for both FAs. Fractions of myristic acid (C14:0), palmitoleic acid (C16:1), α-linolenic acid (C18:3) and nervonic acid (C24:1) were slightly higher in the oil extracted with ethanol, whereas arachidic acid (C20:0) and DHA (C22:6) portions were lower. Interestingly, no behenic acid (C22:0) was extracted with ethanol, while lignoceric acid (C24:0) could be extracted only with ethanol among the examined solvents.

Table 8.4 compares the saturation ratio of yeast oil extracted using different solvents to the original yeast oil and correlates it with solvent hydrophobicity. The correlation indicates that the fraction of unsaturated fatty acids (UFAs) in extracted lipids increases with decreasing solvent hydrophobicity, resulting in a lower saturation ratio.

Table 8.4: Saturation ratio of yeast oils extracted using various solvents (n-hexane, ethyl acetate, ethanol) and solvent hydrophobicity. The saturation ratio of yeast oil prior to extraction is also given for easier comparison.

	Solvent			
	None	n-Hexane	Ethyl acetate	Ethanol
Saturation ratio (SFA:UFA)	1:1.63	1:1.69	1:1.73	1:1.92
Hydrophobicity (log *P*)[a]	–	4.11	0.68	–0.30

[a] Octanol/water partition coefficient for different solvents (Sangster, 1989).

Discussion

Drévillon et al. (2018) investigated the disruption of *Yarrowia lipolytica* biomass with 15% CDW using a table-top HPH at an exit pressure of 1500 bar and reported a cell disintegration degree over 50% already after the first pass, while 80% cell disruption was achieved after six passes. Similarly, in this study, a very high cell disintegration degree of 88% was measured only after one pass using an industrial HPH, confirming that high-pressure homogenization is a highly effective method for disrupting oleaginous yeasts. Further passes increased the cell disintegration only slightly, a phenomenon also reported by Drévillon et al. (2018). Despite the high degree of cell disintegration, only a small portion of the yeast oil could be separated by subsequent centrifugation. This was mainly due to the formation of an oil-water emulsion stabilized by fine particles generated during cell disruption using HPH, which could not be broken adequately by adding various demulsifiers. Only the addition of hydrochloric or sulphuric acid at a dose of 1.0% *(v/v)* proved to break the emulsion slightly, which supports the findings of Fazullin et al. (2022) suggesting that small doses of sulphuric acid act more effectively as a demulsifier than various commercially available surfactants.

The highest lipid extraction yield recorded in this study was 92%, achieved by yeast cell disruption with HPH and pretreatment with 1.0% *(v/v)* sulphuric acid at 70 °C followed by extraction using n-hexane. In literature, relatively lower lipid recovery yields around 75–80% were reported using n-hexane to extract lipids from HPH-treated wet yeast biomass (Kruger et al., 2018; Drévillon et al., 2018). Kruger et al. (2018) obtained a similar lipid extraction yield of 93% with n-hexane, applying an acidic pretreatment of the wet yeast biomass with 1% *(v/v)* sulphuric acid at 170 °C for an hour. Besides, they indicated that an enzymatic treatment of the yeast broth with a mixture of chitinase, mannanase, glucanase and protease yielded an extraction efficiency of 70%. The positive influence of an enzymatic treatment was also confirmed in this work, however, to a smaller extent, since additional enzymatic treatment of the wet biomass prior to cell disruption with HPH improved extraction yield with ethyl acetate by 7% to 92%. In comparison, mechanical disruption of yeast cells using HPH prior to extraction has increased the extraction efficiency by 18%, and thus, was determined to be a more important factor in achieving high extraction yields. Similarly, Thiru et al. (2011) also reported that homogenizing the yeast broth using HPH before solvent extraction improved the yield from 10% to 40–50%.

Using n-hexane and ethyl acetate as solvents, lipid extraction yields over 85% were achieved, while only less than 50% of the yeast oil could be extracted with ethanol using the same protocol. Imatoukene et al. (2020) studied the bead milling assisted lipid extraction from *Y. lipolytica* dry biomass and also reported achieving 82% and 85% extraction yield with n-hexane and ethyl acetate, respectively, whereas the yield remained at 42% with ethanol. Therefore, it is concluded that ethanol, yielding a significantly lower extraction efficiency compared to n-hexane, is an unsuitable solvent for yeast oil extraction. On the other hand, the extraction performance of ethyl acetate was determined to be comparable with n-hexane. FA compositions of the lipid extracts obtained using different solvents were very similar. Interestingly, the fraction of UFAs in the extracts was determined to grow slightly with increasing solvent polarity (Sangster, 1989). However, this should not be considered a generally valid phenomenon since there are also findings in literature contrasting this suggestion (Breil et al., 2016). Lipid extracts consist mainly of free FAs, diacylglycerides (DAGs) and triacylglycerides (TAGs). Nevertheless, Breil et al. (2016) reported that highly polar solvents such as isopropanol and ethanol also extracted certain phospholipids from *Y. lipolytica* biomass, which was not the case for n-hexane or ethyl acetate, suggesting selectivity in the extraction of phospholipids.

8.4. Overall carbon balance of the integrated process

In this work, conversion of CO_2 into microbial oils with the highest efficiency possible is one of the most important objectives. To draw an accurate mass balance on carbon is the key to calculating the overall carbon conversion efficiency of the integrated process. Therefore, an elemental analysis of the microalgae biomass, the yeast cells and the yeast oil was performed. Macromolecular compositions of *M. salina* and *C. oleaginosus* biomass were determined using a combination of measurements and literature values as described in Subsection 4.10.7. Shortly, lipid content was measured, total protein content was calculated from nitrogen content using a correlation factor, ash content was assumed according to literature values, and the remaining portion of the biomass was presumed to be carbohydrates. Overall carbon balance of the integrated process was then calculated based on this analysis.

8.4.1. Macromolecular and elemental composition of *M. salina*

Figure 8.7 illustrates the elemental and macromolecular composition of the microalgae *M. salina*. The carbon content of dry *M. salina* biomass grown under nutrient-replete conditions was measured to be 53%. The molecular formula of *M. salina* biomass was determined as $CH_{1.69}O_{0.39}N_{0.17}$ based on its elemental composition. Dry *M. salina* biomass was determined to contain 26% carbohydrates and 46% proteins, which indicates that around 68% of dry microalgae biomass could be utilized by yeast in a subsequent fermentation using microalgal biomass hydrolysate.

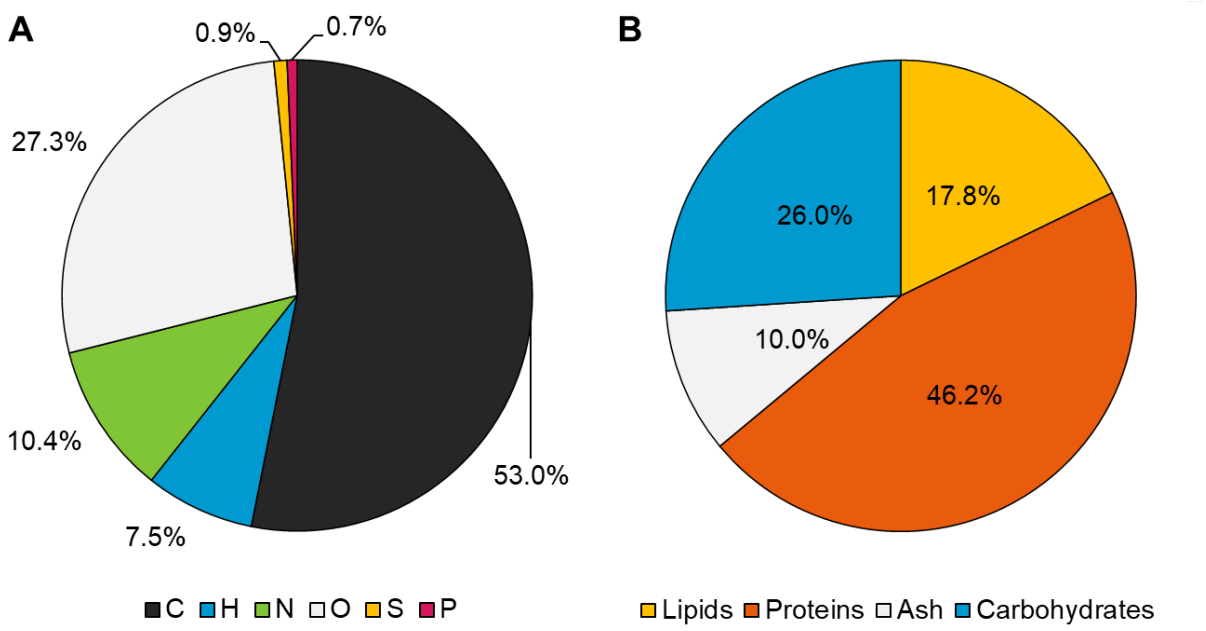

Figure 8.7: (**A**) Elemental and (**B**) macromolecular composition of *M. salina* biomass grown in nutrient-replete medium. Measurements and calculations were done as described in Subsection 4.10.7. Ash content was assumed to be as reported by Schädler et al. (2019).

Discussion

53.0% carbon content of the dry *M. salina* biomass, as well as its overall elemental composition, determined in this work are in accordance with the literature values (50–55% C in CDW) (Schlagermann et al., 2012; Toor et al., 2013). The ash content 10.0% reported by Schädler et al. (2019), which was used for calculations in this study, is also in the range of 4.2–11.7% reported for various algae species (Duboc et al., 1999).

In literature, a protein content between 30–60% of the dry biomass has been indicated for various microalgae species (López et al., 2010; Toor et al., 2013). Toor et al. (2013) measured 35% carbohydrates, 13% lipids and 39% protein in the dry *M. salina* biomass, when the remaining moisture content is excluded. On the other hand, Schädler et al. (2019) reported 26% carbohydrates, 16% lipids and 48% proteins in the dry mass of *M. salina*, which is much closer to the macromolecular composition determined in this study.

8.4.2. Macromolecular and elemental composition of *C. oleaginosus*

Figure 8.8 shows the elemental and macromolecular composition of the oleaginous yeast *C. oleaginosus* grown under nutrient-replete conditions. The carbon content of dry *C. oleaginosus* biomass was measured to be 50%. The molecular formula of *C. oleaginosus* biomass was calculated to be $CH_{1.76}O_{0.47}N_{0.16}$ based on its elemental composition. Dry *C. oleaginosus* biomass was determined to contain 15% lipids, 24% carbohydrates and 54% proteins.

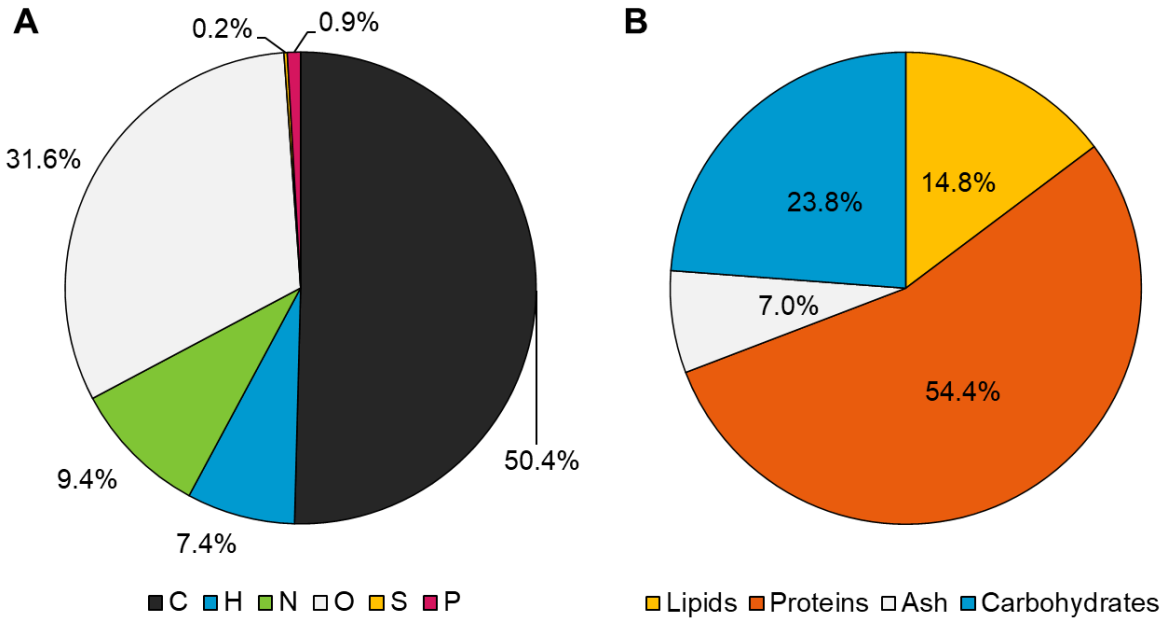

Figure 8.8: (**A**) Elemental and (**B**) macromolecular composition of *C. oleaginosus* biomass grown in nutrient-replete medium. Measurements and calculations were done as described in Subsection 4.10.7. Ash content was calculated based on data reported by Agboola et al. (2021).

Table 8.5: Elemental composition of the yeast oil and the lipid-free *C. oleaginosus* cells. The composition of the lipid-free yeast dry mass was calculated by general mass balancing based on the other two measurements (dry cells and yeast oil) and the measured lipid content (14%) of the yeast cells.

	Mass fraction of the element, %					
	C	H	N	S	P	O
Dry yeast cells (14.8% lipids)	50.42	7.44	9.39	0.23	31.62	0.91
Yeast oil	76.21	12.63	0.03	0.00	11.05	0.06
Lipid-free yeast dry mass (calculated)	45.94	6.54	11.01	0.26	35.19	1.06

The elemental composition of the *C. oleaginosus* cells, as well as that of the yeast oil produced under P-limited conditions, are listed in Table 8.5. The elemental composition of the lipid-free dry yeast biomass was calculated based on these data considering the 14.8% lipid quota of the biomass. Based on this elemental analysis data, the molecular formula of the yeast oil was determined to be $CH_{1.97}O_{0.11}$, whereas that of the lipid-free dry yeast biomass was $CH_{1.70}O_{0.58}N_{0.21}$.

Discussion

The mass fractions of the elements in the dry cell biomass of *C. oleaginosus* are very similar to the values reported for various oleaginous yeast strains considering the given cellular lipid content (Minkevich et al., 2010). Furthermore, the elemental composition of the lipid-free biomass is very much in conformity with the mass fractions of the elements reported for the oleaginous yeast strain *Rhodosporidium toruloides* (C 43.9%, H 6.7%, O 42.6%, and N 6.8% for a lipid content of 1%) by Zhou et al. (2012). Based on its FA composition, Meo (2016) calculated the molecular formula of *C. oleaginosus* yeast oil to be $CH_{1.74}O_{0.10}$, which is very close to the formula determined in this work, although the stoichiometric H:C ratio was found to be by 0.23 higher. Duboc et al. (1999) stated the elemental formula of an average yeast to be $CH_{1.65}O_{0.54}N_{0.14}$, which is consistent with the formula determined for *C. oleaginosus* in this work.

The lipid content of oleaginous microorganisms depends very much on the specific strain and growth conditions. 14.8% lipid content measured for *C. oleaginosus* indicates that a slight nutrient limitation might have started (Morin et al., 2011), although it is still below the oleaginicity mark of 20%. For various yeast species, an ash content of 3.1–10.1% (Duboc et al., 1999; Agboola et al., 2021) and a protein content of 40.3–56.3% (Agboola et al., 2021) have been reported, which conform with the values given for *C. oleaginosus* dry mass in this study. Nonetheless, no data could be found on the carbohydrate content of dry yeast mass.

8.4.3. Carbon balance

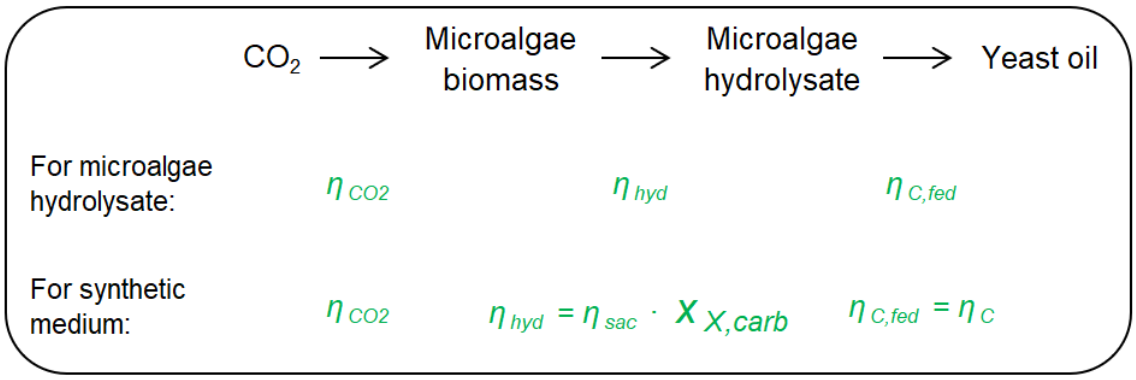

Figure 8.9: Parameters used to make a carbon balance of the integrated yeast oil production process with different approaches for the use of synthetic medium and of microalgae hydrolysate as cultivation medium.

After a thorough investigation of each step of the integrated process using microalgae and oleaginous yeast for the production of microbial oils, an overall carbon balance was made combining CO_2 fixation into biomass by microalgae, biomass hydrolysis, and lipid production by yeast. Since the processes using defined synthetic medium and microalgae hydrolysate as cultivation media for yeast oil production had different outcomes, two different approaches were adopted for making the carbon balance as outlined in Figure 8.9. One was considering saccharification efficiency (η_{sac}) in the biomass hydrolysis step and carbon conversion efficiency (η_C) into lipids using the synthetic medium for yeast cultivation. The other one was considering total hydrolysis efficiency (η_{hyd}) in the

biomass hydrolysis step and fed-carbon conversion efficiency ($\eta_{C,fed}$) into lipids using the microalgae hydrolysate for yeast cultivation.

η_{CO_2}, η_{sac} and η_C are calculated using Equations (4.12), (4.17) and (4.16), respectively. However, these equations are formulated for the use of a synthetic medium, considering only the solubilization of sugars for biomass hydrolysis efficiency. Hence, they were modified to allow a complete carbon balance in the case of actual microalgae hydrolysate used as feed medium. Thus, total hydrolysis efficiency (η_{hyd}) of the microalgal biomass, considering all carbon sources present in it, was calculated as follows:

$$\eta_{hyd} = \frac{x_{C,MAH} \cdot \rho_{MAH}}{c_X \cdot x_{C,Ms}} \tag{8.1}$$

where $x_{C,MAH}$ is the mass fraction of carbon in microalgae hydrolysate, ρ_{MAH} is the density of microalgae hydrolysate, c_X is the CDW concentration of microalgae biomass to be hydrolysed, and $x_{C,Ms}$ is the mass fraction of carbon in *M. salina* dry mass. c_X was adjusted to 150 g L^{-1}, while $x_{C,MAH} = 2.52\%$ and $x_{C,Ms} = 53.0\%$ were determined by elemental analysis as described in Subsection 4.10.7. Additionally, ρ_{MAH} was measured to be 995.8 g L^{-1}. Thus, a hydrolysis efficiency (η_{hyd}) of 32.9% was used in the carbon balancing of the final integrated process instead of saccharification efficiency (η_{sac}).

Carbon conversion efficiency (η_C) is defined as the fraction of carbon taken up by the yeast cells, which is converted into lipids at the end of the process. In the case of defined synthetic medium being used for yeast oil production, all supplied sugars were taken up by the yeast, therefore $m_{C,out} = 0$, and thus, $m_{C,in} - m_{C,out} = m_{C,in}$ held true. However, in the case of microalgae hydrolysate, although the sugars were used up completely, the permeate still contained some carbon ($m_{C,out} \neq 0$), which has to be considered in the carbon balance. Thus, in this case, a fed-carbon conversion efficiency ($\eta_{C,fed}$) was calculated on the basis of total carbon fed into the system for yeast cultivation as follows:

$$\eta_{C,fed} = \frac{m_L \cdot x_{C,Lipid}}{m_{C,in}} \tag{8.2a}$$

$$m_{C,in} = x_{C,syn} \cdot m_{syn} + x_{C,MAH} \cdot m_{MAH} \tag{8.2b}$$

where m_{syn} is the mass of synthetic medium used in the batch phase of the cultivation, m_{MAH} is the mass of microalgae hydrolysate fed into the reactor, and $x_{C,syn}$ is the mass fraction of carbon in the synthetic medium. In this way, it was calculated that using microalgae hydrolysate as feeding medium, 19.4% of the total carbon fed into the reactor was converted into yeast oil ($\eta_{C,fed}$).

Two different methods were used to calculate the mass of CO_2 generated by yeast during yeast oil production. The first one was using the results of elemental analysis on a general mass balance described in Equations (4.13) and (4.14). The other one was using the results of inlet and exhaust gas analysis to make a molar balance on CO_2 as expressed in Equations (3.24) and (4.15). The latter was used to check the validity of the method making use of mass balance equations. Both methods were explained in Subsection 4.11.4 in detail. Figure 8.10 depicts a comparison of these different methods by presenting the ratio of CO_2 mass calculated using method A to that using method B. The ratio of CO_2 calculated using method A to using B varied remarkably between experiments,

with a standard deviation of 17.6%. Although, a mean value of 93.1% implies a good approximation of total CO_2 mass generated using method A, the results of method B (gas analysis data) varied relatively strongly between individual experiments. Thus, method A was found more suitable for the calculation of CO_2 generated by yeast during yeast oil production.

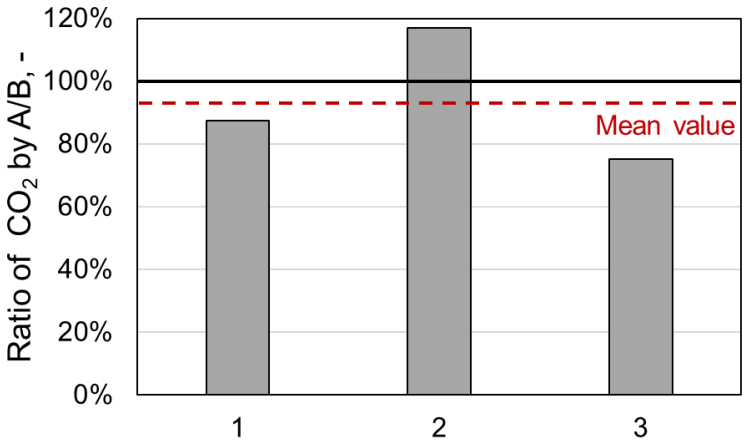

Figure 8.10: Comparison of two different methods for calculating the mass of CO_2 generated by yeast in three different experiments for yeast oil production in an MBR on a 50 L scale. Plotted is the ratio of (A) total mass of generated CO_2 calculated using the results of elemental analysis on a general mass balance to (B) total mass of CO_2 calculated using the results of inlet and exhaust gas analysis to make a molar balance on CO_2. Mean value is 93.1% with a standard deviation of 17.6%.

Table 8.6 shows the overall carbon balance of the integrated process using microalgae and oleaginous yeast for the production of microbial oils according to three different scenarios. The first scenario (A) is considering the saccharification of the carbohydrates in the microalgae biomass with an efficiency of 21.0% followed by the conversion of solubilized sugars into yeast oil with a carbon conversion efficiency (η_C) of 61.3% as determined for the high-cell-density yeast oil production in the MBR on a 50 L scale using a defined synthetic medium. This scenario would result in 2.47% of the carbon entering the system in form of CO_2 to be converted into yeast oil. To point out the significance of the saccharification efficiency (η_{sac}) on the results, the second scenario (B) assumes a higher efficiency of 90.0% in the microalgal biomass hydrolysis step. In this way, 10.61% of the carbon entering the system in form of CO_2 would be converted into yeast oil. Finally, the last scenario (C) takes into account the hydrolysis efficiency (η_{hyd}) with respect to the fraction of carbon solubilized in the biomass hydrolysis step and the fed-carbon conversion efficiency ($\eta_{C,fed}$) actually measured for the high-cell-density yeast oil production in the 1.5 L scale MBR using microalgae hydrolysate as feeding medium. In this case, 6.01% of the carbon entering the system as CO_2 is converted into yeast oil at the end of the process.

Discussion

Elemental analysis of microalgae and yeast cells, as well as the produced yeast oil, enabled accurate overall mass balance calculations of the integrated process using microalgae and oleaginous yeast to produce microbial oils. Many studies report on the CO_2 fixation efficiency in microalgal lipid production processes, however, not the carbon conversion efficiency into lipids. Thus, there is no readily available literature data for comparison. Moreover, this study might be the first one to provide such an elaborate carbon balance of a microbial oil production process using CO_2 as the only carbon

source. In this study, with the integrated process using microalgae and yeast for single-cell oil (SCO) production, an overall carbon conversion efficiency of 2.47% was achieved using synthetic medium and 6.01% using microalgal biomass hydrolysate as feeding medium. Nonetheless, with a higher efficiency of microalgal biomass hydrolysis, higher overall carbon conversion efficiencies could be reached.

Table 8.6: Overall carbon balance of the integrated process using microalgae and oleaginous yeast for the production of microbial oils. Three different scenarios were considered: (A) using synthetic medium with actual microalgae biomass saccharification efficiency (η_{sac}); (B) using synthetic medium with a higher theoretical microalgae biomass saccharification efficiency; (C) using microalgae hydrolysate with actual microalgae biomass hydrolysis efficiency (η_{hyd}).

	Scenario #		
	(A)	(B)	(C)
	using synthetic medium	synt. medium with high η_{sac}	using MAH
Stream	**Mass of C in the corresponding stream, g**		
C in CO_2	100.0	100.0	100.0
C fixated in microalgae biomass[a]	98.0	98.0	98.0
C lost into atmosphere	2.0	2.0	2.0
C solubilized in microalgae hydrolysate	4.0[b]	17.3[c]	30.9[d]
C remaining in microalgal biomass	94.0	80.7	68.1
C converted into yeast oil	2.47[e]	10.61[e]	6.01[f]
C converted into lipid-free yeast biomass	0.46	1.97	6.24
C converted into CO_2 and by-products	1.10	4.72	8.48
C remaining in permeate	0.00	0.00	10.18

[a] Calculated using a CO_2 fixation efficiency (η_{CO_2}) of 98.0%.

[b] Calculated using a saccharification efficiency (η_{sac}) of 21.0%.

[c] Calculated using a saccharification efficiency (η_{sac}) of 90.0%.

[d] Calculated using a hydrolysis efficiency (η_{hyd}) of 32.9%.

[e] Calculated using a carbon conversion efficiency (η_C) of 61.3%.

[f] Calculated using a fed-carbon conversion efficiency ($\eta_{C,fed}$) of 19.4%.

The carbon fed to the yeast is used for cell growth, lipid production, energy gain by respiration generating CO_2, and by-products. It should be noted, that the carbon remaining after subtracting the carbon used for yeast biomass and oil production was allocated to CO_2 and by-product generation without further specification. It has been reported, that many oleaginous yeast species produce by-products, such as polyols, to an extent that is not negligible (Dulermo et al., 2015; Caporusso et al., 2021). However, the exact composition or amount of these by-products are mostly unknown. Since other methods to quantify the amount of CO_2 generation by yeast, such as gas analysis, were not consistent enough between different experiments, a further separation of this CO_2 and by-products stream in the carbon mass balance was omitted.

8.5. Comparison of the integrated process to oil production by microalgae

In this section, the integrated process utilizing microalgae and yeast for microbial oil production is compared with the oil production using only microalgae. For this, lipid productivity, overall carbon conversion efficiency and process costs related to microalgal biomass production are evaluated. Since microalgal biomass production is the less productive and rate-limiting step in the integrated process, lipid productivity is calculated with respect to the unit thin-layer cascade (TLC) reactor area required to produce the corresponding amount of microalgal biomass. Lipid productivity of continuous microalgal oil production with *M. salina* in a TLC photobioreactor (PBR) was previously reported by Schädler et al. (2021) to be 1.65 g m^{-2} d^{-1} (0.25 g L^{-1} d^{-1}). For the integrated process, parameters used to calculate the lipid productivity per unit TLC reactor area are listed in Table 8.7. As indicated in the table, some of these values were varied to construct different hypothetical scenarios to evaluate what could have been achieved theoretically if the parameter value was different. In scenarios (A, B) using the results achieved with a synthetic yeast cultivation medium on the 50 L scale, it was assumed that the yeast would utilize only the sugars present in the microalgal biomass hydrolysate as a carbon source. In scenarios (C, D, E) using the results achieved with microalgae hydrolysate as yeast cultivation medium on the 1.5 L scale, all carbon sources present in the hydrolysate were taken into account in the calculation.

Table 8.7: Parameters used for calculation of lipid productivity per unit thin-layer cascade (TLC) reactor area for the integrated process using microalgae and yeast for microbial oil production.

Parameter	**Value**
CDW productivity of microalgae	24.1 g m^{-2} d^{-1}
Mass fraction of C in dry microalgae mass ($x_{C,Ms}$)	0.53
CDW content of biomass to be hydrolysed	150 g L^{-1}
Microalgal biomass hydrolysis efficiency (η_{hyd})	32%[a]
Fed-C conversion efficiency ($\eta_{C,fed}$)	19%[a]
Mass fraction of C in yeast oil ($x_{C,Lipid}$)	0.76
Carbohydrate content of dry microalgae mass ($x_{X,carb}$)	0.26
Saccharification efficiency[b] (η_{sac})	21%[a]
Weighted mass fraction of C in sugars present in microalgae ($x_{C,S}$)	0.40
C conversion efficiency[b] (η_C)	61%[a]

[a] Values varied to construct different scenarios.

[b] Values used only in scenarios assuming results achieved with synthetic yeast cultivation medium.

Table 8.8 shows the lipid productivity with respect to unit TLC reactor area for microalgal oil production, as well as for the integrated process using microalgae and yeast for oil production, considering different scenarios. Unfortunately, actual lipid productivities achieved in this study (A, C) remain in a

range of 0.25–1.03 g m^{-2} d^{-1}, which is lower than the lipid productivity achieved by microalgae only. Theoretically, higher productivities around 1.81–2.89 g m^{-2} d^{-1} could be achieved if a hydrolysis efficiency of 90% could be realized in the microalgal biomass hydrolysis step (B, D). Furthermore, a significant gain in lipid productivity would be obtained if the carbon conversion efficiency into yeast oil using microalgae hydrolysate was increased to 50%, in addition to 90% hydrolysis efficiency (E). In this case, a lipid productivity of 7.45 g m^{-2} d^{-1} would be achieved, which is 4.5 times that of the lipid productivity achieved by microalgae.

Table 8.8: Productivity comparison of the integrated process using microalgae and yeast for microbial oil production with microalgal oil production. Lipid productivity is calculated with respect to unit TLC reactor area required to produce the necessary amount of microalgal biomass. Data presented for microalgal oil production was previously reported by Schädler et al. (2021). Five different scenarios of the integrated process were considered by varying saccharification efficiency (η_{sac}), hydrolysis efficiency (η_{hyd}), carbon conversion efficiency (η_C) and fed-carbon conversion efficiency ($\eta_{C,fed}$).

Scenario #	Process	Lipid productivity[a], g m^{-2} d^{-1}	Source
M	Lipid production with *M. salina*	1.65	Schädler et al. (2021)
A	Integrated process using synthetic medium ($\eta_{sac} = 21\%$, $\eta_C = 61\%$)	0.25	This study
B	Integrated process using synthetic medium ($\eta_{sac} = 90\%$, $\eta_C = 61\%$)	1.81	Theoretical[b]
C	Integrated process using MAH ($\eta_{hyd} = 32\%$, $\eta_{C,fed} = 19\%$)	1.03	This study
D	Integrated process using MAH ($\eta_{hyd} = 90\%$, $\eta_{C,fed} = 19\%$)	2.89	Theoretical[b]
E	Integrated process using MAH ($\eta_{hyd} = 90\%$, $\eta_{C,fed} = 50\%$)	7.45	Theoretical[b]

[a] Lipid productivity per unit TLC reactor area.

[b] Theoretical values calculated assuming hypothetical η_{sac}, η_{hyd} and $\eta_{C,fed}$ values.

In a biorefinery using CO_2 as the carbon source, converting carbon into microbial oils with the highest efficiency possible would be one of the most important objectives. The carbon conversion efficiency of microalgal oil production is calculated based on own measurements and literature data, assuming 1.65 g m^{-2} d^{-1} lipid productivity with 30.3% cellular lipid quota (Schädler et al., 2021), 0.56 mass fraction of carbon in dry microalgae mass with 30.3% cellular lipid quota (calculated based on elemental analysis), 48.6% CO_2 fixation efficiency (corrected for actual C content of dry microalgae mass) (Schädler et al., 2019), and 0.76 mass fraction of carbon in microalgal oil (Schlagermann et al., 2012). Overall carbon conversion efficiency of the integrated process for yeast oil production from microalgal biomass is calculated using the productivities given in Table 8.8 together with 24.1 g m^{-2} d^{-1} CDW productivity of microalgae, 0.53 mass fraction of C in dry microalgae mass, 98.0% CO_2 fixation efficiency in microalgae cultivation step, and 0.76 mass fraction of carbon in yeast oil.

The mass fraction of carbon in CO_2 was taken as 0.27 in both cases.

Table 8.9 shows overall carbon conversion efficiency for microalgal oil production and the integrated oil production process using both microalgae and yeast, considering different scenarios. Using only microalgae for lipid production, 19.8% of the carbon entering the reactor in the form of CO_2 is converted into lipids. Carbon conversion efficiencies achieved in this study (A, C) remain way below this value with merely 2.5–6.0%. Even with an increase of microalgal biomass hydrolysis efficiency to 90% (B, D), carbon conversion efficiency achieved would be 10.6–16.9%, which is still below the efficiency of microalgal lipid production. This comparison shows that only the combined effect of higher hydrolysis efficiency and higher fed-carbon conversion efficiency in the integrated process (E) could yield a similar carbon conversion efficiency as in microalgal oil production. However, with 90% hydrolysis efficiency and 50% fed-carbon conversion efficiency, the integrated process could reach a very high overall carbon conversion efficiency of 43.6%, corresponding to 2.2 times the efficiency achieved by microalgae only.

Table 8.9: Efficiency comparison of the integrated process using microalgae and yeast for microbial oil production with microalgal oil production. Overall carbon efficiency is defined as the fraction of carbon initially fed into the system in form of CO_2, which is converted into lipids at the end of the process. Data presented for microalgal oil production is based on literature (Schädler et al., 2019, 2021). Five different scenarios of the integrated process were considered by varying saccharification efficiency (η_{sac}), hydrolysis efficiency (η_{hyd}), carbon conversion efficiency (η_C) and fed-carbon conversion efficiency ($\eta_{C,fed}$).

Scenario #	Process	Overall C efficiency[a], -	Source
M	Lipid production with *M. salina*	19.8%	Schädler et al. (2021)
A	Integrated process using synthetic medium ($\eta_{sac} = 21\%$, $\eta_C = 61\%$)	2.5%	This study
B	Integrated process using synthetic medium ($\eta_{sac} = 90\%$, $\eta_C = 61\%$)	10.6%	Theoretical[b]
C	Integrated process using MAH ($\eta_{hyd} = 32\%$, $\eta_{C,fed} = 19\%$)	6.0%	This study
D	Integrated process using MAH ($\eta_{hyd} = 90\%$, $\eta_{C,fed} = 19\%$)	16.9%	Theoretical[b]
E	Integrated process using MAH ($\eta_{hyd} = 90\%$, $\eta_{C,fed} = 50\%$)	43.6%	Theoretical[b]

[a] Fraction of carbon initially fed into the system as CO_2, which is converted into lipids.

[b] Theoretical values calculated assuming hypothetical η_{sac}, η_{hyd} and $\eta_{C,fed}$ values.

In spite of extensive research on lipid production with microalgae, microalgal oils are still not considered profitable for industrial production of low-value-added products due to their lack of cost competitiveness in the current oil market. Hence, cost reduction is an important aspect of the integrated process using both microalgae and yeasts for microbial oil production. An analysis of the

overall costs of this integrated process is not performed in this work since the process was only demonstrated to be feasible but not improved enough to reflect the actual cost of production in an industrial-scale process. Nonetheless, a comparison of the costs pertaining to microalgae cultivation is made between the integrated process and the use of only microalgae for lipid production.

Schädler (2020) has previously determined the cost of microalgal biomass production with *M. salina* in autonomous industrial-scale open TLC PBRs. The plant was presumed to operate under climate conditions similar to that of southern Spain in summer. The autonomous production concept considered that CO_2 would be captured directly from the air, that the water supply would be either seawater or freshwater generated from it by reverse osmosis, and that the required energy would be produced on-site using a photovoltaic system. Microalgal biomass harvest via a dynamic settler with spiral plate technology was also included in the production costs, whereas oil extraction was not considered. In this way, the production cost per dry mass of *M. salina* grown under N limitation was calculated by Schädler (2020) to be 1.77 € per kg CDW. On the other hand, the cost of biomass production without any nutrient limitation was determined as 0.37 € per kg CDW. Not included in these are the cost of labour and the capital costs of land, equipment and infrastructure.

To estimate the cost of microalgal biomass production per lipid mass produced, the amount of lipids produced per microalgae CDW generated was calculated for all cases. For microalgal lipid production, a cellular lipid quota of 30.3% was assumed (Schädler et al., 2021). On the other hand, for the integrated process, yeast oil produced per unit microalgae CDW was calculated by dividing the lipid productivity per TLC reactor area (see Tab. 8.8) by a microalgal CDW productivity of 24.1 g m^{-2} d^{-1}.

Table 8.10 compares costs related to microalgal biomass production between microalgal oil production and the integrated process using both microalgae and yeast for yeast oil production. It should be emphasized that these values represent only the cost of microalgal biomass production per mass of lipids produced in the overall process, not considering the cost of biomass hydrolysis or yeast cultivation. By this calculation, the cost of microalgal lipids produced in a TLC PBR as described by (Schädler et al., 2021) would be 5.84 € kg^{-1} lipids. For all scenarios, lipids produced per microalgae biomass in the integrated process are either below or only similar to that in the microalgae process, but not higher. However, some of these scenarios (B, D, E) still suggest a reduction of microalgae-cultivation-related costs per lipid mass produced. Comparing Table 8.10 with Table 8.8 makes it more apparent that there is a lower limit of lipid productivity per unit TLC reactor area, above which the microalgae-cultivation-related costs per lipid mass produced are lower than in the microalgal lipid production. Using a backwards calculation method, this lipid productivity limit is determined to be 1.51 g m^{-2} d^{-1} for the integrated process, corresponding to 6.3 g lipids produced per 100 g of microalgae dry weight (DW). The cost of microalgal biomass production calculated for the integrated process with actual values achieved in this study (A, C) fall much higher (8.58–20.84 € kg^{-1} lipids) than the 5.84 € kg^{-1} lipids achieved using microalgae only for lipid production. However, increasing the biomass hydrolysis efficiency in the integrated process to 90% (B, D) reduces these costs significantly to 3.05–4.86 € kg^{-1} lipids. Moreover, assuming a fed-carbon conversion efficiency ($\eta_{C,fed}$) of 50% (E) reduces these costs further to 1.18 € kg^{-1} lipids.

Table 8.10: Cost comparison of the integrated process using microalgae and yeast for microbial oil production with microalgal oil production. Only the costs related to microalgal biomass production per mass of lipids produced are evaluated, not considering the cost of biomass hydrolysis or yeast cultivation. The cost of labour and the capital costs of land, equipment and infrastructure were excluded as well. In the case of the integrated process, yeast oil produced per microalgal biomass generated is taken into account. Data presented for microalgal oil production, as well as data on the cost of microalgal biomass production without nutrient limitation, are based on literature (Schädler, 2020; Schädler et al., 2021). Five different scenarios of the integrated process were considered by varying saccharification efficiency (η_{sac}), hydrolysis efficiency (η_{hyd}), carbon conversion efficiency (η_C) and fed-carbon conversion efficiency ($\eta_{C,fed}$).

Scenario #	Process	Lipids/MA[a], g g^{-1} CDW	Cost of MA[b], € kg^{-1} lipids	Source
M	Lipid production with *M. salina*	30.3%	5.84	Schädler (2020)
A	Integrated process using synthetic medium ($\eta_{sac} = 21\%$, $\eta_C = 61\%$)	1.8%	20.84	This study
B	Integrated process using synthetic medium ($\eta_{sac} = 90\%$, $\eta_C = 61\%$)	7.5%	4.86	Theoretical[c]
C	Integrated process using MAH ($\eta_{hyd} = 32\%$, $\eta_{C,fed} = 19\%$)	4.3%	8.58	This study
D	Integrated process using MAH ($\eta_{hyd} = 90\%$, $\eta_{C,fed} = 19\%$)	12.0%	3.05	Theoretical[c]
E	Integrated process using MAH ($\eta_{hyd} = 90\%$, $\eta_{C,fed} = 50\%$)	30.9%	1.18	Theoretical[c]

[a] Mass of lipids produced per dry mass of microalgae generated in a TLC reactor.

[b] Cost of microalgal biomass production per unit mass of lipids produced.

[c] Theoretical values calculated assuming hypothetical η_{sac}, η_{hyd} and $\eta_{C,fed}$ values.

Discussion

Production of microbial oils from CO_2 using microalgae and oleaginous yeast in an integrated process was compared with lipid production using only microalgae in terms of lipid productivity, overall carbon conversion efficiency and process costs related to microalgal biomass production. The lipid productivity achieved using microalgae hydrolysate as feeding medium for yeast cultivation was 1.03 g m^{-2} d^{-1}, which is lower than the productivity of microalgal lipid production. Similarly, the overall carbon conversion efficiency into lipids was determined to be 6.0% in the integrated process, which is by 13.8% lower than with microalgae only. Moreover, a cost analysis regarding only the cost of microalgae cultivation per mass of lipids produced, indicated a cost increase by 2.74 € kg^{-1} lipids to 8.58 € kg^{-1} lipids compared to lipid production with microalgae, although the remaining costs of microalgal biomass hydrolysis and yeast cultivation were not even included into the calculation. Thus, at its current state, production of microbial oils using microalgae and oleaginous yeast in an integrated process is less profitable than microalgal lipid production itself, with no prospects of becoming an industrially applicable process.

The primary aim of this study was to demonstrate the feasibility of the integrated process using microalgae and oleaginous yeast. Since it was obvious, that the current state of the process would not be profitable, different scenarios were constructed to evaluate the theoretical outcomes possible using reasonable hypothetical values for some key process parameters, namely the microalgal biomass hydrolysis efficiency and the carbon conversion efficiency of the yeast cultivation step. In the scenario, with an increase of biomass hydrolysis efficiency from 32% to 90% and of carbon conversion efficiency by yeast from 19% to 50%, all the performance indicators were improved significantly. In this case, a lipid productivity of 7.45 g m^{-2} d^{-1} would be achieved, which is 4.52 times of that reported for microalgal lipid production. Moreover, an overall carbon conversion efficiency of 43.6% and a microalgal biomass production cost of 1.18 € kg^{-1} lipids would be attained. Only in this scenario, the total cost of microbial oils produced with the integrated process could be lower than that of the microalgal oils, considering the remaining process costs related to microalgal biomass hydrolysis and yeast cultivation.

A biomass hydrolysis efficiency of 90% and a carbon conversion efficiency of 50% in the yeast cultivation are reasonably estimated values for an optimized future process. Improving the hydrolysis efficiency is unlikely with *M. salina* cells grown in nutrient-replete medium, as discussed in Subsection 7.3.2. Nevertheless, saccharification yields in a range of 47–90% have been reported in literature (Demuez et al., 2015). Thus, other microalgae strains that are richer in carbohydrate content and easier to disrupt than *M. salina*, such as the members of *Porphyridium* and *Scenedesmus* genera (González-Fernández & Ballesteros, 2012; Kröger et al., 2018), could be used for a more efficient production of microalgal biomass hydrolysate.

On the other hand, there are multiple ways to achieve a higher carbon conversion efficiency of the yeast cultivation step. First of all, the C/P ratio of the microalgal biomass could be set higher than the 2044 g g^{-1} realized in this study, for instance by concentrating the microalgae hydrolysate using an evaporator prior to phosphate precipitation, as discussed in Section 7.4. Secondly, yeast cultivation in the MBR could be performed for a longer duration than merely 17.5 hours in semi-continuous mode, as discussed in Section 8.1. In the end, it was possible to achieve up to 61.3% carbon conversion efficiency with yeast cultivated using synthetic medium in a 50 L scale MBR with a C/P ratio of 3515 g g^{-1} and a process duration of 9 days. It should also be noted, that a higher hydrolysis efficiency, resulting in a higher sugar concentration in the hydrolysate, would already contribute to a higher C/P ratio and a longer process duration in the MBR by reducing the dilution rate required.

Market price of microbial oils are estimated to be around 0.5–3.1 $ kg^{-1} for microalgal oil (Chisti, 2007; He et al., 2016) and 1.6–7.0 $ kg^{-1} for yeast oil (Masri et al., 2019; Koutinas et al., 2014; Bonatsos et al., 2020; Gallego-García et al., 2022). Rerop et al. (2023) have recently reported a price of 2.9–4.0 $ kg^{-1} for yeast oil produced with *C. oleaginosus* using a lignocellulosic hydrolysate as substrate, which is in the price range for organic palm oil. Moreover, Karamerou et al. (2021) pointed out hypothetical ways to further reduce the costs of large-scale yeast oil production down to 0.81 $ kg^{-1} using techno-economic modelling. The cost of yeast oil produced using microalgae and oleaginous yeast in an integrated process, as suggested in this study, could fall into this price range after future optimization. By all means, it should be noted, that the cost calculation for mi-

croalgal biomass production by Schädler (2020), used in this study, was made for an autonomous plant concept with its own integrated CO_2 and fresh water production facilities. In most literature sources estimating relatively low production costs, much cheaper or free of charge CO_2 sources, as well as wastewater treatment options for cheap nutrient and water supply, are considered. Since the costs predicted by Schädler (2020) are at least double the expected microalgal oil price reported in literature, it can be assumed that the cost of microalgae cultivation in the integrated process would actually be lower than half of the predicted value, corresponding to around 0.6 € kg^{-1} for the best case scenario. Yeast oil cost of the integrated process could be further reduced, for instance, if extraction of other valuable products from the microalgal biomass prior to enzymatic hydrolysis, the use of residual biomass for anaerobic biogas production, or recycling of nutrients and CO_2 from the waste streams generated within the process would be considered in the cost calculation.

9. Summary and Outlook

Microbial oil production from CO_2 using microalgae has been researched intensively in recent years. Still, high production costs resulting from low lipid productivity prevent microalgae processes to become sufficiently competitive for the production of low-value-added products. This study suggests an alternative pathway for the production of microbial oils from CO_2, utilizing microalgae and oleaginous yeasts in an integrated process, combining the best features of microalgae as CO_2 capturers and oleaginous yeasts as microbial oil producers.

Marine microalgae can fixate CO_2 into their biomass with an efficiency of up to 90% using sunlight (Schädler et al., 2019). Lipid production in microalgae, like in other oleaginous microorganisms, is induced by the limitation of an essential nutrient such as nitrogen or phosphorus in the presence of a carbon source in excess. It has been previously shown that microalgae growing fast without any nutrient limitation achieve a much higher areal productivity than lipid production under growth-limiting conditions (Schädler et al., 2019). Therefore, it is reasonable to utilize microalgae only for the fast and efficient CO_2 fixation instead of for lipid production. Microalgae biomass generated in this way can then be hydrolysed and used as a cultivation medium for oleaginous yeasts to produce microbial oils with high productivity. The primary aim of this study was to demonstrate the feasibility of this integrated process for the first time and determine the most important aspects for process scale-up and optimization.

Cultivation systems for microalgae can be grouped into two, as open and closed photobioreactors (PBRs). While the microalgae suspension in open PBRs is in direct contact with the atmosphere, the culture in closed reactors is completely separated from its surroundings. Although closed cultivation systems offer advantages such as better control of the growth conditions and protection from external contamination, their high complexity and poor scalability make the installation and operation of closed PBRs too expensive for the industrial production of high-value-added products (Zittelli et al., 2013). Hence, the general assumption is that only simple open cultivation systems can economically produce microalgae biomass as a raw material for the industry. For this reason, an open PBR type was chosen for microalgal biomass production in this work.

Production of microalgal biomass requires large areas due to the dependence of biomass growth on sunlight, which makes high areal productivity crucial for the profitability of any open microalgae cultivation system. Apel et al. (2017) applied a new type of scalable open thin-layer cascade (TLC) PBR to investigate microalgal growth under physical simulation of suitable climate zones. The first objective of this study was to determine the necessary conditions to achieve high biomass productivities and >90% CO_2 fixation efficiency of microalgal biomass production in a TLC reactor on a pilot scale (50 m^2) under realistic climate conditions. Moreover, a suitable mode of operation with high efficiency was to be determined for continuous biomass production.

One of the main challenges of using open PBRs for microalgae cultivation is the risk of contamination by other microorganisms (Ratledge & Wynn, 2020). Thus, it is essential to reduce this risk by applying extreme cultivation conditions that are unfavourable for potential contaminants. The marine

microalgae *Microchloropsis salina* is known to achieve relatively high growth rates of 0.03 h^{-1} with a salinity optimum at 35 ppt and a pH optimum of 7.5–8.0 (Boussiba et al., 1987). Microalgae cultivation under these conditions significantly reduces the amount of contaminants in an open culture. The high salinity of the algae culture also makes it possible to use seawater as the cultivation medium, which reduces freshwater consumption. Moreover, multiple studies have shown that *M. salina* is well suited for biomass production in open TLC PBRs (Apel et al., 2017; Pfaffinger et al., 2019; Schädler et al., 2019, 2021). Therefore, *M. salina* was used for microalgal biomass production in this work.

In order to be used as a substrate for oil production by oleaginous yeasts, microalgal biomass had to be first hydrolysed to make the carbon sources present in the biomass available for uptake by the yeast. *M. salina* biomass grown under nutrient-replete conditions has around 25% *(w/w)* carbohydrates and 50% *(w/w)* proteins (Schädler et al., 2019), which corresponds to around 50 g L^{-1} sugar concentration in a hydrolysate produced using biomass with a cell dry weight (CDW) concentration of 250 g L^{-1} (Meo et al., 2017). Such a low concentration of the carbon source is very diluted in comparison to synthetic media used in industrial processes. Therefore, a dynamic settler with spiral plate technology was employed for biomass harvest and dewatering to get a whole-cell microalgae paste with the highest biomass density possible.

Marine microalgae have rather complex and structurally stable cell walls, which are hard to disrupt both mechanically and chemically (Spiden et al., 2013; Scholz et al., 2014; Hernández et al., 2015). Besides, microalgae grown in nutrient-replete medium can build even stronger cell walls than those grown in nutrient-limited medium (Jeong et al., 2017). Therefore, a combination of different cell disruption and biomass hydrolysis methods, including various mechanical, chemical and enzymatic methods, were examined in this study. For process scalability, commercially available enzyme mixtures were preferred for biomass hydrolysis. Lipid accumulation by oleaginous yeasts is induced by the deficiency of a nutrient required for growth, accompanied by an excess of carbon sources in the medium. Phosphate elimination using precipitating agents, such as $FeCl_3$, is an uncomplicated and cheap option to create nutrient-depleted conditions applicable on an industrially relevant scale (Sabelfeld & Geißen, 2011). Hence, in this study, limiting the phosphorus source was the preferred method for induction of lipid production by oleaginous yeasts, which requires very low phosphorus concentrations below 100 mg per litre depending on the carbon content of the substrate (G. Zhang et al., 2011; Meo et al., 2017).

Using a diluted substrate as a cultivation medium means relatively low product concentrations in the final product stream, resulting in higher costs in downstream processing. A membrane bioreactor (MBR) is very suitable for carrying out high-cell-density yeast cultivation with a diluted medium at low sugar concentrations. In this way, the residence time of the yeast cells in the bioreactor is decoupled from that of the medium, enabling the feeding of large amounts of substrate solution without diluting the yeast suspension inside the bioreactor. In this study, an MBR with a cross-flow microfiltration module in a bypass was employed with total cell retention to get the most out of the lipid-producing yeast cells after the activation of oleaginous metabolism. The objective of the MBR operation was to achieve high volumetric lipid productivity with the yeast while keeping the carbon conversion yield into microbial oils as high as possible. Also, while using an MBR, an accumulation of sugars in

the reaction medium would mean the loss of valuable carbon sources in the permeate stream. In order to prevent that, a dilution rate that is sufficiently low to keep the sugar concentration as low as possible while still supplying adequate substrate to achieve high lipid productivity was determined.

Since its first isolation from cheese plant floors and drains, *Cutaneotrichosporon oleaginosus* has been noted as an oleaginous yeast with high potential due to its ability to utilize a vast spectrum of substrates as carbon source and accumulate over 70% of its CDW as lipids (Moon et al., 1978; Yaguchi, Rives, & Blenner, 2017). This yeast strain not only displays high tolerance against growth inhibitors (Bracharz, Beukhout, et al., 2017; Yu et al., 2011, 2014; Yaguchi, Robinson, et al., 2017) but also can co-utilize various substrates and grow in variable and harsh conditions found in wastewater streams. These remarkable features contribute to the general opinion that *C. oleaginosus* has great potential in the valorization of wastes and residues. Moreover, previous studies had already demonstrated it possible to utilize lipid-extracted and enzymatically hydrolysed microalgae biomass with *C. oleaginosus* on a laboratory scale (Younes et al., 2020; Meo et al., 2017). Therefore, *C. oleaginosus* was selected for oil production in this study, considering the variety of carbon sources and possible inhibitory substances present in microalgal biomass hydrolysate.

Some conventional downstream processing possibilities were also explored in this study to cover a complete production process. Solvent extraction was preferred for separating microbial oils from fermentation broth, since this method is already commonly used in the oil industry. Hence, various solvents and pre-treatment methods were tested and compared based on the separation efficiency and the fatty acid (FA) composition of the resulting extract. Furthermore, a very detailed overall carbon balance of the integrated lipid production process was worked out making use of an elemental analysis of all the intermediate and final products. A final comparison of the microbial oil production using microalgae and oleaginous yeasts in an integrated process with oil production using only microalgae was made to show potential improvements to the microalgal lipid production. This comparison took into account productivity, carbon conversion efficiency and production costs of the two processes. Finally, the most important aspects to be considered for future process optimization were pointed out.

The first objective in this study was to maximize the biomass productivity and CO_2 fixation efficiency of the microalgal biomass production. To this end, production of microalgal biomass with *M. salina* was examined applying different modes of operation in open TLC PBRs with 8 m^2 surface area. In batch mode, maximum integral areal productivity of microalgal biomass ranged between 17–19 g m^{-2} d^{-1}. Thereupon, semi-continuous and continuous modes of operation were investigated, to determine, if higher productivities than in batch mode can be achieved in this way. Besides, continuous production is essential for any process if industrial applicability is of concern. In both semi-continuous and continuous modi, highest productivities were reached at similar CDW densities of 21.0–22.2 g L^{-1} (Fig. 9.1 1A). Maximum values of mean daily areal productivity recorded for long term operation up to 30 days were very similar around 27.0 g m^{-2} d^{-1} in both cases. There was, however, a noticeable difference in the mean CO_2 fixation efficiency achieved, which was 100% and 88% for continuous and semi-continuous processes on the 8 m^2 scale, respectively. Hence, continuous operation was determined to be more suitable for high efficiency microalgal biomass production

than semi-continuous operation, allowing 100% CO_2 fixation efficiency (Fig. 9.1 1C).

For process optimization, the influence of various other parameters, namely pH, total alkalinity and nutrient feed rate, on the process performance was studied. Biomass productivity and CO_2 fixation efficiency were regarded as the key performance indicators. Variation of the pH in a range of pH 7.5–8.5 showed that pH 8.5 was optimal. Besides, keeping the total alkalinity (TA) between 4–8 mM by continuous addition of urea containing medium and concentrated sulphuric acid allowed very high CO_2 fixation efficiencies up to 100% in continuous mode. Medium feed rate was determined to affect first the biomass productivity, and then, above a certain value, improve the CO_2 fixation efficiency at constant productivity. However, there is an upper limit of feed concentration, above which the microalgal growth is affected negatively (Schädler et al., 2019). In this study, for a CDW density of 20–25 g L^{-1}, a nutrient feed rate of 2.5–3.5$\times$ the nutrient concentration in the artificial seawater (ASW) medium per day was determined to be ideal for semi-continuous operation, whereas continuous operation required a higher nutrient feed rate of 3.0–4.5$\times$ the nutrient concentration in the ASW medium.

After determining the optimal operational conditions, microalgal biomass production was successfully scaled up using a pilot-scale TLC reactor with 50 m^2 surface area. On the pilot scale, slightly lower cell densities were achieved in continuous operation at a steady state using the same dilution rate as on the 8 m^2 scale. This resulted in a modest drop of maximal biomass productivity to 22.1 g m^{-2} d^{-1}. However, the most remarkable difference was observed in the CO_2 fixation efficiency, which was 66% at its maximum. This was hypothesized to result from the lower volume-specific gas exchange area between the CO_2 supply hoses and the microalgae suspension compared to the 8 m^2 scale, causing an impaired CO_2 transfer into the liquid phase. However, modifications made to the gas supply system to increase the gas exchange surface area from 0.21 m^{-1} to 0.45 m^{-1} had no success at improving the CO_2 fixation efficiency. Eventually, this was the only problematic aspect of the process scale-up, which requires further research.

For efficient production of microalgal biomass in TLC PBRs, an automated switch-off of the circulation pumps overnight was implemented on a 50 m^2 scale, reducing both the energy requirement for circulation and the fresh water consumption by 40%. Moreover, biomass productivity was not affected by this modification. Although a 24% drop of CO_2 fixation efficiency was observed, this could probably be avoided by better mixing of the microalgae suspension in retention tanks overnight using pressurized air supply, which demands further investigation.

For continuous biomass harvest and dewatering in a single step, a dynamic settler with spiral plate technology was evaluated. With a concentration factor of 15, the final solids content of the harvested microalgal biomass paste was around 30%. In spite of a very high separation efficiency, the biomass recovery was 85%, mainly due to the complete draining of the microalgae suspension inside the centrifuge drum before each solids discharge step. This could be circumvented by directing the discharged algae suspension back into the feed tank. In this way, a higher biomass recovery efficiency around 95–99% could be achieved as reported in literature (Fasaei et al., 2018).

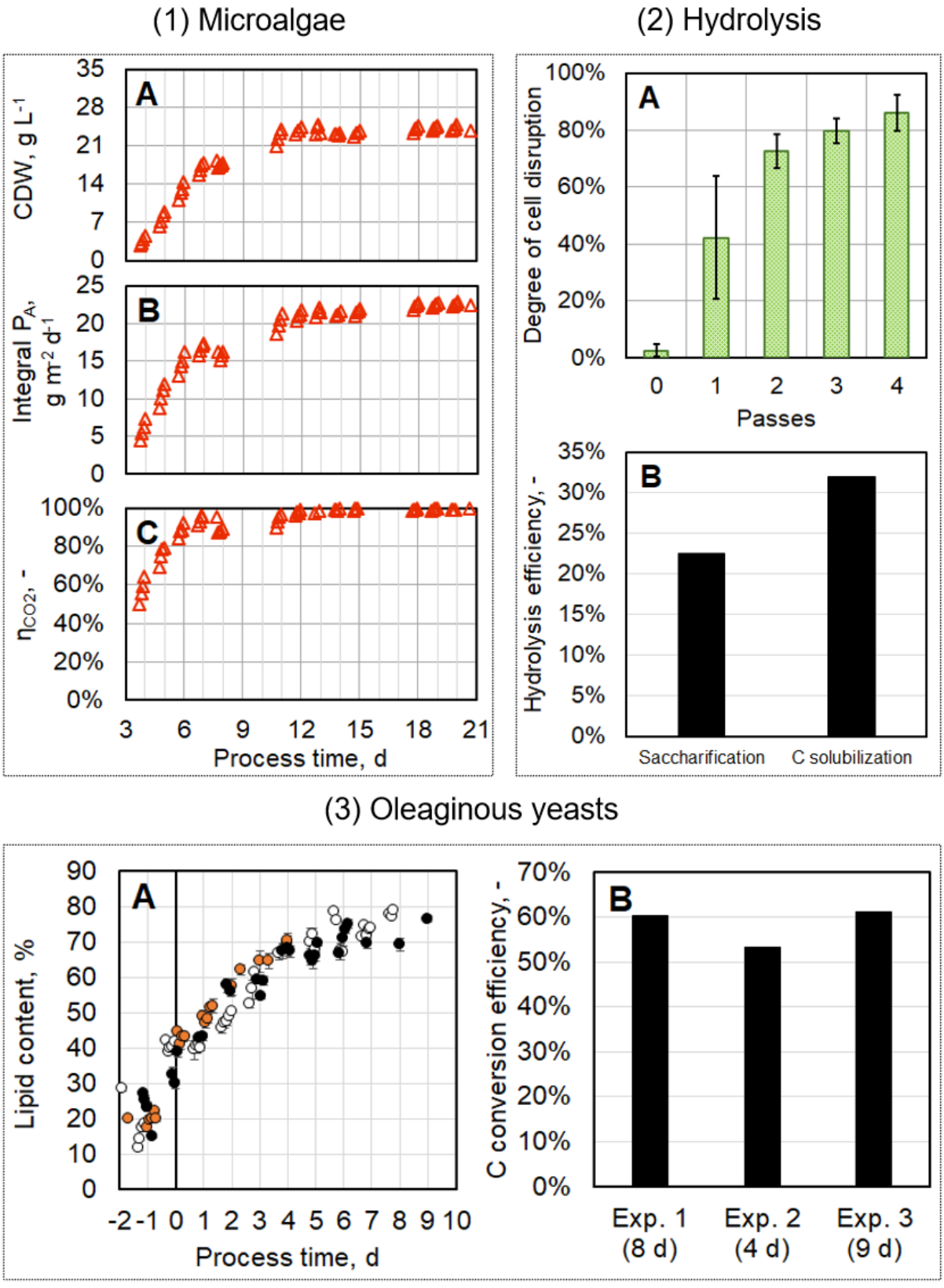

Figure 9.1: Summary of the main results achieved in this work. (1) Continuous microalgal biomass production with *M. salina* in a TLC PBR on a 8 m^2 scale with a dilution rate of 0.15 d^{-1}. **1A**: CDW concentration; **1B**: integral areal productivity; **1C**: CO_2 fixation efficiency. (2) Cell disruption and hydrolysis of *M. salina* biomass on the 30-200 L scales. **2A**: Mechanical cell disruption of microalgal biomass with a solids content of 15% *(w/w)* using an industrial HPH; **2B**: biomass hydrolysis efficiency after enzymatic treatment with commercially available cellulase and mannanase enzyme mixtures. (3) Lipid production with *C. oleaginosus* using a dilute substrate under phosphorus limitation (C/P ratio = 3515 g g^{-1}) in an MBR on a 50 L scale in triplicate. **3A**: Lipid content of the yeast biomass; **3B**: conversion efficiency of the substrate carbon into yeast oil.

One of the main objectives in this study was to maximize the lipid productivity and carbon conversion efficiency of the yeast oil production step. First, the effect of different C/P ratios in the batch medium were examined for lipid production with *C. oleaginous* in fed-batch mode on a 3 L scale. Additionally, the substrate feeding rate was adjusted to reduce the sugar concentration in the reaction medium as much as possible, while keeping the space-time-yield (STY) as high as possible. A C/P ratio of 3515 g g^{-1} in both batch and feed media and a sugar feeding rate of 1.1 g L^{-1} h^{-1} were determined to be optimal. In this way, a lipid STY of 0.19–0.27 g L^{-1} h^{-1} and a carbon conversion efficiency of 44–50% were achieved.

High-cell-density cultivation of *C. oleaginous* was performed in an MBR with total cell retention, first on a 1.5 L and subsequently on a 50 L scale, using a dilute substrate with 50 g L^{-1} sugars. This sugar concentration was anticipated assuming a CDW concentration of 250 g L^{-1} in the microalgae biomass to be hydrolysed and a carbohydrate saccharification efficiency around 80% based on literature (Schädler et al., 2019; Meo et al., 2017). Since the unsupervised operation of the 50 L scale MBR was not possible, a semi-continuous operational mode was applied. In the semi-continuous mode of operation, the feed was supplied into the MBR continuously with a constant rate, whereas filtering out of the used up medium from the reactor was done only for eight hours during the day. This method entails a constant change in liquid volume inside the reactor in a preset range. However, it also reduces the time of microfiltration per process time so that the energy consumption associated with medium filtration is reduced by two-thirds compared to a fully continuous operation. In this way, a lipid STY of 0.30 g L^{-1} h^{-1} and a carbon conversion efficiency of 46% were achieved on the 1.5 L scale.

Scale-up of the high-cell-density yeast cultivation to the MBR on a 50 L scale, as well as two reproductions, were performed successfully, reaching up to 0.37 g L^{-1} h^{-1} lipid STY, 79% cellular lipid quota, 0.32 g g^{-1} lipid yield and 61% carbon conversion efficiency (Fig. 9.1 3A and 3B). The STY achieved using MBRs was limited mainly by the conservative choice of feed flow rate, which was kept relatively low to prevent loss of sugars through the permeate stream. Nonetheless, process performance was even better on the 50 L scale than on the 1.5 L scale, probably because of the lower shear stress applied on the yeast cells due to pumping at lower flow rates through the filtration module on the 50 L scale. Moreover, to the best of my knowledge, 79% lipid content reported in this study is the highest reported so far with *C. oleaginosus* using P limitation.

Microalgae cells were hydrolysed to solubilize the carbon fixated in biomass, enabling its uptake by the yeast. Since sugars are the main carbon source utilized by oleaginous yeasts for oil production, saccharification efficiency of the carbohydrates present in microalgal biomass was used to measure hydrolysis performance. To keep the sugar concentration in the resulting hydrolysate as high as possible, high cell densities from 10% to 25% were used in the microalgae biomass to be hydrolysed. First, direct enzymatic hydrolysis of *M. salina* biomass without prior cell disruption was investigated using a mixture of commercially available enzymes, however without success, yielding only 6–8% saccharification efficiency. Chemical cell disruption by autoclaving at pH 3.5 and 121 ℃ for 20 minutes was successful, yielding a saccharification efficiency of 13% already before and 27–32% after a subsequent enzymatic hydrolysis. Nevertheless, chemical hydrolysis required the addition of large

amounts of acid and base to adjust the pH, and hence was accompanied by a high increase in salt concentrations, which would affect the yeast growth negatively, when the hydrolysate is used as substrate for yeast cultivation. For this reason, mechanical disruption of the *M. salina* cells prior to enzymatic hydrolysis was investigated.

Mechanical disruption of dense *M. salina* biomass was performed using ultrasonication, bead milling and high-pressure homogenization (HPH). These methods were selected specifically for their effectiveness with microalgae (Günerken et al., 2015) and applicability in continuous processes on an industrial scale (Chmiel, 2018). Among these methods, milling with 2 mm steel beads using a mixer mill yielded the highest cell disruption efficiencies for all cell densities examined on a 10–200 mL scale. For comparison, at a cell density of 15%, microalgal cell disintegration reached 90% after 40 minutes by bead-milling, whereas only 70% was achieved by ultrasonication at 20 kHz after 90 minutes and 75% by HPH at 3000 bar after 10 passes. On the other hand, the industrial HPH used for microalgal cell disruption on a 200 L scale, performed much better than the table-top one, achieving 80% cell disintegration degree already after three passes at 1000 bar, reaching a maximum of 86% after four passes (Fig. 9.1 2A). It was however not possible to use the industrial HPH with cell densities above 15%, since this resulted in a significant increase in viscosity, exceeding the limit allowed for this equipment, as verified by an examination of the rheology of microalgal biomass at different densities.

Following the mechanical disruption of microalgae cells, a parameter study was carried out to improve the efficiency of enzymatic hydrolysis of the disrupted microalgae cells. Autoclaving and proteolysis prior to enzymatic hydrolysis were determined to have no effect on the final saccharification efficiency, and were therefore omitted. Hence, inhibition of contaminant growth during enzymatic hydrolysis was ensured using antibiotics instead of heat sterilization. Thereupon, various compositions of the enzyme mixture used are tested for maximal saccharification efficiency. The best performing enzyme mixture on the millilitre scale was 10% Rohament® CEP (Cellulase) and 2% Rohalase® GMP (Mannanase) reaching a saccharification efficiency of 30%. Nonetheless, on the 200 L scale, the same procedure of mechanical cell disruption followed by enzymatic hydrolysis yielded only 23% saccharification efficiency (Fig. 9.1 2B). Based on elemental analysis, this was determined to correspond to 32% hydrolysis efficiency, meaning 32% of the carbon fixated in microalgal biomass was solubilized by enzymatic hydrolysis (Fig. 9.1 2B). The resulting hydrolysate contained 8.1 g L^{-1} sugars with a composition of 66% glucose, 14% mannose, 19% galactose, 1% rhamnose and trace amounts of xylose.

Phosphorus elimination from the microalgae hydrolysate was accomplished by the addition of a precipitating agent, namely $FeCl_3$. Preliminary experiments using a phosphate buffer showed that very low phosphate concentrations down to 1 mg L^{-1} can be obtained using a Fe:P stoichiometric ratio of 2:1 at pH 4.5–5.5, corresponding to a phosphate depletion by 99.4%. Since the initial phosphate concentration in the microalgae hydrolysate was much higher than anticipated, ranging from 3.75 g L^{-1} to 6.51 g L^{-1}, a multi-step precipitation procedure of the hydrolysate was developed to reduce the amount of $FeCl_3$ required. Nonetheless, the effectiveness of phosphate precipitation was much lower and variable when applied on the microalgae hydrolysate, resulting in a final phosphate con-

centration of 19–36 mg L^{-1}. This reduction in the efficacy of the phosphate precipitation procedure used is most probably due to the high organic matter content of the microalgae hydrolysate, causing formation of a variety of unwanted side products with iron (Takács et al., 2006).

Microalgae hydrolysate produced on a 200 L scale had a low sugar concentration of 8.1 g L^{-1}, but a relatively high total carbon concentration of 25.44 g L^{-1}. With a phosphate concentration of 36 mg L^{-1}, corresponding to 12 mg L^{-1} phosphorus, C/P ratio of the microalgae hydrolysate was 2044 g g^{-1} based on its total carbon content. However, it is unclear how much of the carbon sources other than sugars, such as peptides, are actually used by oleaginous yeasts during oil production. C/P ratio of the hydrolysate based on its sugar concentration was as low as 275 g g^{-1}, which entails a failure at inducing oleaginous metabolism of the yeast sufficiently to achieve high lipid yields using this hydrolysate as substrate. Obviously, achieving a higher saccharification efficiency of the microalgal biomass, yielding a higher sugar concentration in the hydrolysate, would automatically increase the C/P ratio. However, in case that is not possible, another strategy to increase the sugar concentration, and consequently the C/P ratio, would be concentrating the biomass hydrolysate prior to phosphate precipitation, for instance using a thin-film evaporator.

Figure 9.1 summarizes the results achieved before integrating the individual process steps. Originally, it was intended to carry out the process integration on a large scale using the MBR with a 50 L working volume. However, the unexpectedly low saccharification efficiency in the biomass hydrolysis step, resulting in an extremely low sugar concentration in the hydrolysate, did not allow yeast oil production with microalgae hydrolysate as substrate using the MBR on the 50 L scale. High-cell-density yeast cultivation performed using a defined synthetic medium on the 50 L scale required around 250 L of feed medium for a single experiment with nine days of semi-continuous operation. A sugar concentration of 8.1 g L^{-1} in the feed medium, instead of the expected 50 g L^{-1}, increased the required feed amount to 1543 L. Therefore, process integration was carried out using the 1.5 L scale MBR. A defined synthetic medium with 50 g L^{-1} sugars was used as the batch medium to keep the biomass density and cellular metabolism at the beginning of the semi-continuous production phase the same as in the reference experiment, allowing a better performance comparison of the two processes.

High-cell-density yeast cultivation in an MBR with total cell retention on a 1.5 L scale using microalgae hydrolysate as the feed medium accomplished 0.63 g L^{-1} h^{-1} lipid STY, 37% cellular lipid quota, 0.34 g g^{-1} lipid yield and 29% carbon conversion efficiency. Due to technical problems arising from using biomass hydrolysate as the feed medium, the semi-continuous operation lasted only 17.5 hours. After that, the experiment had to be terminated prematurely. The biggest problem when using microalgae hydrolysate as the feed medium was the maximum possible permeate flow rate declining significantly over time from 5 L h^{-1} to 0.3 L h^{-1} after 17 hours into the semi-continuous operation. This is much lower than the flow rate of 0.76 L h^{-1} required to keep the reaction volume below the maximum capacity of the MBR (6 L) at all times. This was attributed mainly to the formation and accumulation of colloids inside the reactor caused by high organic matter content and iron-containing by-products of the phosphate precipitation step remaining in the hydrolysate. Although the lipid yield was much higher than the 0.25 g g^{-1} achieved using a synthetic medium, the lipid quota after the same process time was by 14% lower due to the lipid-free biomass generation being much higher, by

0.7 g L^{-1} h^{-1} to be precise. This was mainly because of the combined effect of a lower C/P ratio and the high protein (i.e. polypeptide) content of the microalgae hydrolysate. The higher biomass density also contributed to the reduced permeate flow rate through the filter module, forcing an abrupt termination of the process.

To give an idea about its possible uses in the industry, the FA composition of the yeast oil produced with *C. oleaginosus* under P-limited conditions was determined. Among all FAs, oleic acid and palmitic acid stood out as the main constituents of this yeast oil with 50–56% and 24–27%, respectively. These two were followed by stearic acid and linoleic acid but with much smaller fractions of around 8–11% and 7%. As anticipated based on literature, the FA composition using microalgae hydrolysate as feeding medium was very similar to that using a defined medium (Meo et al., 2017). Furthermore, FA composition of *C. oleaginosus* oil changed only marginally over the process time with increasing cellular lipid content of yeast cells. All in all, overall FA profile of this yeast oil resembles that of palm oil.

For separation of the yeast oil produced in this way, an efficient solvent extraction procedure was devised. This included mechanical cell disruption with a HPH, pretreatment of the homogenized yeast broth with 1% *(v/v)* sulfuric acid at 70 °C to aid in phase separation, extraction with a solvent using a solvent:broth volumetric ratio of 2:1, phase separation by centrifugation, solvent recovery with a rotary vacuum evaporator, and finally, removal of the solvent remains in an explosion-proof vacuum drying chamber. This procedure was applied using three different solvents to evaluate their suitability by extraction efficiency. Using ethyl acetate, n-hexane and ethanol, lipid extraction efficiencies of 85%, 92% and 49% were achieved, respectively. These values are in conformity with the extraction yields reported for the corresponding solvents in literature (Imatoukene et al., 2020; Kruger et al., 2018). Moreover, in all cases, more than 80% of the solvent could be recovered after evaporation. The FA composition of the extracts using different solvents were very similar to each other, with only a slight difference in the FA saturation ratio due to differing hydrophobicity of the solvents. Eventually, ethyl acetate and n-hexane were determined to be suitable for yeast oil extraction, with the selection being dependent on process requirements and the end use of the oil, whereas ethanol proved to be unsuitable yielding a much lower extraction efficiency.

To draw an accurate mass balance on carbon is the key to calculating the overall carbon conversion efficiency of the integrated process. Therefore, an elemental analysis of the microalgae biomass, the yeast cells and the yeast oil was performed. In addition, macromolecular compositions of the *M. salina* and *C. oleaginosus* biomasses produced were determined. An overall carbon balance of the integrated process revealed a very low carbon conversion efficiency with the current state of the process (Fig. 9.2). Even though a very high CO_2 fixation efficiency of 98% was presumed in the microalgae cultivation step, only 31% of the initial carbon could be solubilized by enzymatic hydrolysis of the microalgal biomass due to low hydrolysis efficiency. Hence, using microalgal biomass hydrolysate as feed medium for the yeast cultivation, only 6% of the initial carbon could be converted into yeast oil, while 8% was converted back into CO_2 and 10% left the system unused in the permeate stream. The most important factors causing such a low overall carbon conversion efficiency in the integrated process were determined to be the low biomass hydrolysis efficiency and

the low carbon conversion efficiency during yeast cultivation with biomass hydrolysate, the latter caused by the high phosphorus concentration in the hydrolysate. Figure 9.2 illustrates the process flowchart showing the equipment used for the scale-up of each process step, as well as the carbon flow throughout the integrated process.

The immediate results might seem very unfavourable at first glance. However, it should be noted that the primary aim of this study was to demonstrate, for the first time, the feasibility of an integrated process using microalgae grown without nutrient limitation and oleaginous yeasts to produce microbial oils from CO_2. The insights gained in this study by thoroughly investigating each process step and their integration are very valuable for further process optimization. By implementing the process modifications suggested in this work, it would be possible to improve the key figures of the integrated process sufficiently to turn it into a promising technology. This was verified by a comparison between the integrated process investigated in this study and microbial oil production using only microalgae, to explore under which conditions the integrated process would pose an improvement to the microalgal oil production.

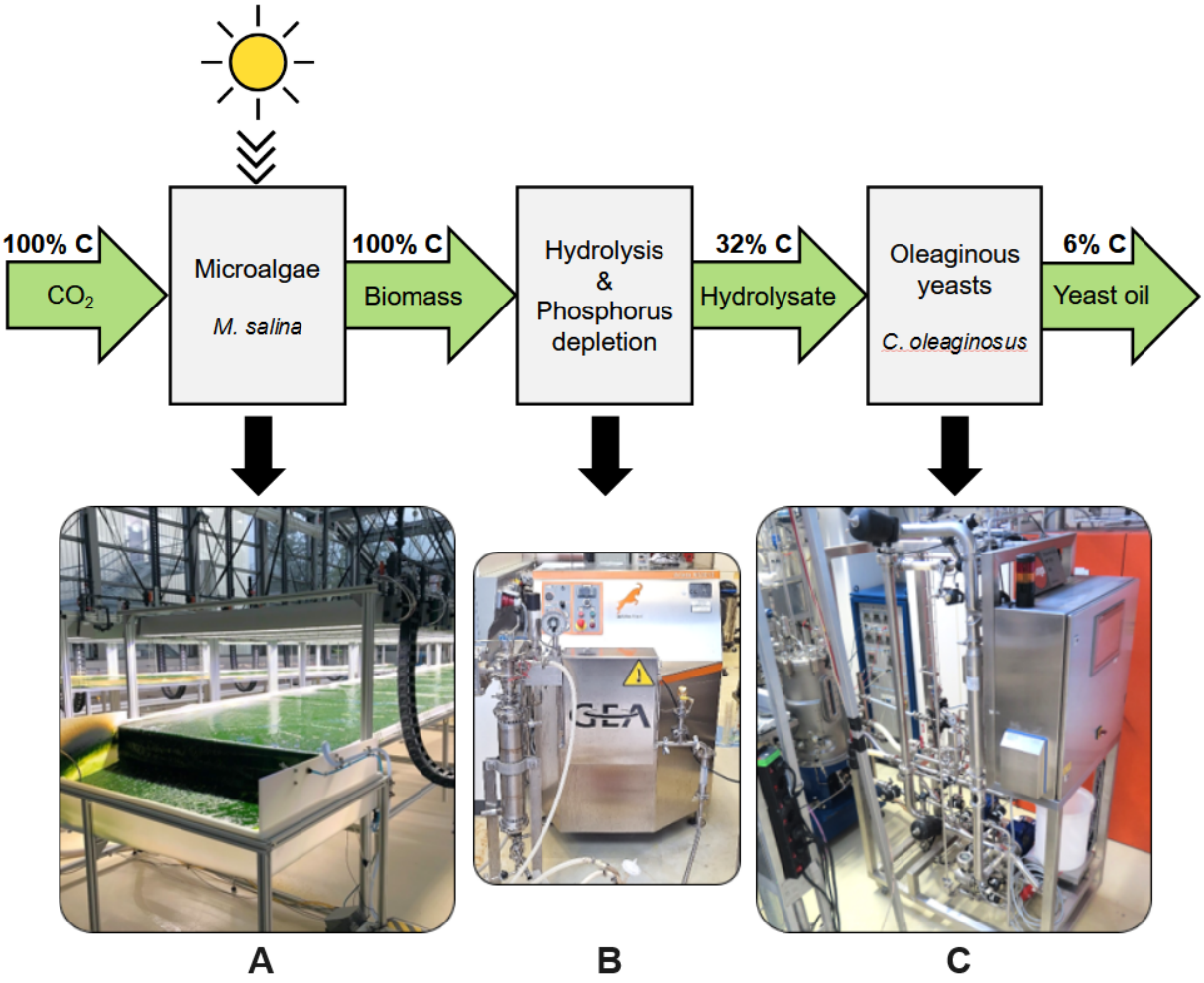

Figure 9.2: Process flow and carbon conversion of the microbial oil production from CO_2 using microalgae and oleaginous yeasts in an integrated process showing the equipment used in each step. **A**: Open TLC photobioreactor on a 50 m^2 scale used for microalgae cultivation; **B**: industrial high-pressure homogenizer used for microalgal cell disruption; **C**: MBR with total cell retention on a 50 L scale used for yeast cultivation.

For the performance comparison of the integrated process to microalgal lipid production, lipid productivity, overall carbon conversion efficiency and process costs related to microalgal biomass pro-

duction are evaluated. The data presented for the microalgal lipid production, as well as the cost of microalgal biomass production, are based on literature studying lipid production with *M. salina* grown in TLC PBR under the same conditions (Schädler, 2020; Schädler et al., 2021), considering autonomous industrial-scale open TLC PBRs for calculating the biomass production costs. Since microalgal biomass production is the less productive and rate-limiting step in the integrated process, lipid productivity is calculated with respect to unit TLC reactor area required to produce the corresponding amount of microalgal biomass. Different scenarios were constructed to evaluate the theoretical outcomes possible using reasonable hypothetical values for some key process parameters. As mentioned above, biomass hydrolysis efficiency and the carbon conversion efficiency during yeast cultivation were determined to have a significant impact on the current process performance, and thus, were varied in this analysis.

The integrated process utilizing microalgae and yeasts as realized in this study yielded 1.03 g m^{-2} d^{-1} lipid productivity per TLC reactor area, an overall carbon conversion efficiency of 6.0% and microalgal biomass production costs of 8.58 € kg^{-1} lipids. With the current state of the process, all of these performance indicators turned out to be worse than in the microalgal lipid production. Nevertheless, assuming a microalgal biomass hydrolysis efficiency of 90% and a carbon conversion efficiency of 50% in the yeast cultivation step provided much better prospects for the integrated process. This hypothetical scenario yielded 7.45 g m^{-2} d^{-1} lipid productivity per TLC reactor area, an overall carbon conversion efficiency of 43.6% and microalgal biomass production costs of 1.18 € kg^{-1} lipids, performing much better than the microalgal lipid production in all aspects. These results imply that the integrated process could, theoretically, exhibit both higher productivity and carbon conversion efficiency if improved as suggested, and pose a reasonable alternative to the lipid production using only microalgae.

Outlook

Since the hydrolysis efficiency of the microalgal biomass was determined to have the most significant impact on the current process performance, future work for process optimization should focus primarily on enhancing the saccharification efficiency of biomass hydrolysis. Improving the carbohydrate saccharification yield for high-density *M. salina* biomass by addition of other commercially available enzymes with various activities, such as chitinase or laminarinase, might be possible (Gerken et al., 2013; Horst et al., 2012). Still, the prospects of success at improving the enzymatic hydrolysis efficiency seem to be low with *M. salina* cells grown in nutrient-replete medium, since these are harder to disrupt and hydrolyse than the *M. salina* cells grown under nutrient limitation (Klassen et al., 2015; Jeong et al., 2017). Applying nutrient limitation on the microalgae culture, on the other hand, would reduce biomass productivity. Alternatively, other microalgae strains that are richer in carbohydrates and easier to disrupt than *M. salina*, such as the members of *Porphyridium* and *Scenedesmus* genera (González-Fernández & Ballesteros, 2012; Kröger et al., 2018), could be used for a more efficient production of microalgal biomass hydrolysate.

Carbon conversion efficiency in the yeast cultivation step was determined to have the second most significant impact on the process performance and should, therefore, also be the focus for process

improvement. There are multiple ways to achieve a higher carbon conversion efficiency in the yeast cultivation step. First of all, the C/P ratio of the microalgal biomass could be set higher than the 2044 g g^{-1} realized in this study, by concentrating the microalgae hydrolysate by evaporation, for instance, using a thin-film evaporator, prior to phosphate precipitation. The increased sugar concentration would then allow a higher C/P ratio at the same phosphate level of around 25 mg L^{-1} after phosphate precipitation. Secondly, yeast cultivation in the MBR could be performed longer than merely 17.5 hours in semi-continuous mode. In the end, it was possible to achieve up to 61.3% carbon conversion efficiency with yeast cultivated using synthetic medium in a 50 L scale MBR with a C/P ratio of 3515 g g^{-1} and a process duration of 9 days. It should also be noted that a higher hydrolysis efficiency, resulting in a higher sugar concentration in the hydrolysate, would already contribute to a higher C/P ratio and a longer process duration in the MBR by reducing the dilution rate required.

The only technical problem in utilizing biomass hydrolysate as a cultivation medium in an MBR was the reduced permeate flow rate, which prevented a long enough process duration for high-efficiency carbon conversion into yeast oil. In order to circumvent the problems caused by a reduced permeate flow rate, a higher sugar concentration in the hydrolysate would be required. For instance, with a sugar concentration of 50 g L^{-1} in hydrolysate, a permeate flow rate of only 0.10 L h^{-1} would be necessary to keep the reaction volume below 2 L at all times in semi-continuous operational mode. Moreover, such a high sugar concentration would reduce the required flow rate of feed medium by 87% to 33 mL h^{-1}, thus slowing down the accumulation of species causing particle formation inside the reactor. Alternatively, continuous operation of the MBR could be considered. With a sugar concentration of 8.1 g L^{-1} in hydrolysate, a permeate flow rate of merely 0.20 L h^{-1} would be required in continuous mode.

An essential step towards making the integrated process more efficient and reducing the production costs of the yeast oil would be recycling unused product streams within the process. For instance, CO_2 produced in yeast cultivation could be captured and reused in microalgae cultivation. The seawater separated at the harvest and dewatering of the microalgae biomass could also be recycled as microalgae cultivation medium. It could also be possible to extract the phosphorus from the $FePO_4$ precipitated for phosphorus elimination and recycle it as a nutrient for microalgae cultivation. Moreover, the microalgal biomass residue that cannot be further hydrolysed enzymatically could be combusted to generate heat energy for use within the process, used for anaerobic biogas production, or converted into biochar by pyrolysis.

Finally, further possibilities to increase the cost-effectiveness of microbial oil production using both microalgae and yeasts in an integrated process should be explored, considering higher value creation and new environmental protection regulations. As suggested in many techno-economic analyses regarding microalgae cultivation, much cheaper or free of charge CO_2 sources from industrial waste streams and exhaust gases, as well as wastewater treatment options for cheap nutrient and water supply, should definitely be considered. Extracting some high-value-added products from the microalgal biomass prior to enzymatic hydrolysis, for instance, specific polyunsaturated fatty acids such as docosahexaenoic acid (Ratledge & Wynn, 2020), as well as various pigments, antioxidants and vitamins, is also a reasonable option to increase the profitability of the overall process.

References

Abeln, F., & Chuck, C. J. (2021). The history, state of the art and future prospects for oleaginous yeast research. *Microbial Cell Factories*, *20*, 221. doi: 10.1186/s12934-021-01712-1

Acién, F. G., Fernández-Sevilla, J. M., & Grima, E. M. (2016). Supply of co $_2$ to closed and open photobioreactors. In S. P. Slocombe & J. R. Benemann (Eds.), *Microalgal production for biomass and high-value products* (1st ed., p. 225–251). Boca Raton: CRC Press. doi: 10.1201/b19464

Agboola, J. O., Øverland, M., Skrede, A., & Øvrum Hansen, J. (2021). Yeast as major protein-rich ingredient in aquafeeds: a review of the implications for aquaculture production. *Reviews in Aquaculture*, *13*(2), 949–970. doi: 10.1111/raq.12507

Andersen, R. A. (2013). The microalgal cell. In A. Richmond & Q. Hu (Eds.), *Handbook of microalgal culture* (p. 1–20). John Wiley & Sons, Ltd. doi: 10.1002/9781118567166.ch1

Andrews, J. F. (1968). A mathematical model for the continuous culture of microorganisms utilizing inhibitory substrates. *Biotechnology and Bioengineering*, *10*(6), 707–723. doi: 10.1002/bit.260100602

Apel, A. (2017). *Offene flachgerinnereaktoren zur massenproduktion von mikroalgen mit physikalischer klimasimulation* (Unpublished doctoral dissertation). Technical University of Munich.

Apel, A., Pfaffinger, C., Basedahl, N., Mittwollen, N., Göbel, J., Sauter, J., ... Weuster-Botz, D. (2017). Open thin-layer cascade reactors for saline microalgae production evaluated in a physically simulated mediterranean summer climate. *Algal Research*, *25*, 381–390. doi: 10.1016/j.algal.2017.06.004

Awad, D., Bohnen, F., Mehlmer, N., & Brück, T. (2019). Multi-factorial-guided media optimization for enhanced biomass and lipid formation by the oleaginous yeast *Cutaneotrichosporon oleaginosus*. *Frontiers in Bioengineering and Biotechnology*, *7*, 54. doi: 10.3389/fbioe.2019.00054

Barsanti, L., & Gualtieri, P. (2022). *Algae : Anatomy, biochemistry, and biotechnology* (3rd ed.). Taylor & Francis Group.

Bartley, M. L., Boeing, W. J., Dungan, B., Holguin, F. O., & Schaub, T. (2014). ph effects on growth and lipid accumulation of the biofuel microalgae *Nannochloropsis salina* and invading organisms. *Journal of Applied Phycology*, *26*, 1431–1437. doi: 10.1007/s10811-013-0177-2

Beardall, J., & Raven, J. A. (2013). Limits to phototrophic growth in dense culture: Co2 supply and light. In M. A. Borowitzka & N. R. Moheimani (Eds.), *Algae for biofuels and energy* (p. 91–97). Dordrecht: Springer Netherlands. doi: 10.1007/978-94-007-5479-9_5

Beardall, J., & Raven, J. A. (2016). Carbon acquisition by microalgae. In M. A. Borowitzka, J. Beardall, & J. A. Raven (Eds.), *The physiology of microalgae* (p. 89–99). Cham: Springer International Publishing. doi: 10.1007/978-3-319-24945-2_4

Becker, E. W. (2013). Microalgae for aquaculture: Nutritional aspects. In A. Richmond & Q. Hu (Eds.), *Handbook of microalgal culture* (p. 671–691). John Wiley & Sons, Ltd. doi: 10.1002/9781118567166.ch36

Belitz, H.-D., Grosch, W., & Schieberle, P. (2008). Lipide. In *Lebensmittelchemie* (6th ed., p. 161–251). Berlin, Heidelberg: Springer Berlin Heidelberg. doi: 10.1007/978-3-540-73202-0_4

Bertolo, A. P., Biz, A. P., Kempka, A. P., Rigo, E., & Cavalheiro, D. (2019). Yeast (*Saccharomyces cerevisiae*): evaluation of cellular disruption processes, chemical composition, functional properties and digestibility. *Journal of Food Science and Technology*, *56*, 3697–3706. doi: 10.1007/s13197-019-03833-3

Bonatsos, N., Marazioti, C., Moutousidi, E., Anagnostou, A., Koutinas, A., & Kookos, I. K. (2020). Techno-economic analysis and life cycle assessment of heterotrophic yeast-derived single cell oil production process. *Fuel*, *264*, 116839. doi: 10.1016/j.fuel.2019.116839

Borowitzka, M. A. (2016). Algal physiology and large-scale outdoor cultures of microalgae. In M. A. Borowitzka, J. Beardall, & J. A. Raven (Eds.), *The physiology of microalgae* (p. 601–652). Cham: Springer International Publishing. doi: 10.1007/978-3-319-24945-2_23

Borowitzka, M. A., & Moheimani, N. R. (2013). Open pond culture systems. In M. A. Borowitzka & N. R. Moheimani (Eds.), *Algae for biofuels and energy* (p. 133–152). Dordrecht: Springer Netherlands. doi: 10.1007/978-94-007-5479-9_8

Boussiba, S., Vonshak, A., Cohen, Z., Avissar, Y., & Richmond, A. (1987). Lipid and biomass production by the halotolerant microalga *Nannochloropsis salina*. *Biomass*, *12*(1), 37–47. doi: 10.1016/0144-4565(87)90006-0

Bracharz, F., Beukhout, T., Mehlmer, N., & Brück, T. (2017). Opportunities and challenges in the development of *Cutaneotrichosporon oleaginosus* atcc 20509 as a new cell factory for custom tailored microbial oils. *Microbial Cell Factories*, *16*(1), 178. doi: 10.1186/s12934-017-0791-9

Bracharz, F., Redai, V., Bach, K., Qoura, F., & Brück, T. (2017). The effects of torc signal interference on lipogenesis in the oleaginous yeast *Trichosporon oleaginosus*. *BMC Biotechnology*, *17*, 27. doi: 10.1186/s12896-017-0348-3

Breil, C., Meullemiestre, A., Vian, M., & Chemat, F. (2016). Bio-based solvents for green extraction of lipids from oleaginous yeast biomass for sustainable aviation biofuel. *Molecules*, *21*(2), 196. doi: 10.3390/molecules21020196

Brenner, A., & Abeliovich, A. (2013). Water purification: Algae in wastewater oxidation ponds. In A. Richmond & Q. Hu (Eds.), *Handbook of microalgal culture* (p. 595–601). John Wiley & Sons, Ltd. doi: 10.1002/9781118567166.ch31

Caporusso, A., De Bari, I., Valerio, V., Albergo, R., & Liuzzi, F. (2021). Conversion of cardoon crop residues into single cell oils by *Lipomyces tetrasporus* and *Cutaneotrichosporon curvatus*: process optimizations to overcome the microbial inhibition of lignocellulosic hydrolysates. *Industrial Crops and Products*, *159*, 113030. doi: 10.1016/j.indcrop.2020.113030

Chisti, Y. (2007). Biodiesel from microalgae. *Biotechnology Advances*, *25*(3), 294–306. doi: 10.1016/j.biotechadv.2007.02.001

Chmiel, H. (2018). Aufarbeitung (downstream processing). In H. Chmiel, R. Takors, & D. Weuster-Botz (Eds.), *Bioprozesstechnik* (4th ed., p. 299–402). Berlin, Heidelberg: Springer Berlin Heidelberg. doi: 10.1007/978-3-662-54042-8_9

Chmiel, H., & Walitza, E. (2018). Rheologie von biosuspensionen. In H. Chmiel, R. Takors, & D. Weuster-Botz (Eds.), *Bioprozesstechnik* (4th ed., p. 107–129). Berlin, Heidelberg: Springer Berlin Heidelberg. doi: 10.1007/978-3-662-54042-8_4

Chmiel, H., & Weuster-Botz, D. (2018). Bioreaktoren. In H. Chmiel, R. Takors, & D. Weuster-Botz (Eds.), *Bioprozesstechnik* (4th ed., p. 157–229). Berlin, Heidelberg: Springer Berlin Heidelberg. doi: 10.1007/978-3-662-54042-8_6

Demuez, M., Mahdy, A., Tomás-Pejó, E., González-Fernández, C., & Ballesteros, M. (2015). Enzymatic cell disruption of microalgae biomass in biorefinery processes. *Biotechnology and Bioengineering*, *112*(10), 1955–1966. doi: 10.1002/bit.25644

Di Fidio, N., Minonne, F., Antonetti, C., & Raspolli Galletti, A. M. (2021). *Cutaneotrichosporon oleaginosus*: A versatile whole-cell biocatalyst for the production of single-cell oil from agro-industrial wastes. *Catalysts*, *11*, 1291. doi: 10.3390/catal11111291

Donzella, S., Fumagalli, A., Arioli, S., Pellegrino, L., D'Incecco, P., Molinari, F., ... Compagno, C. (2022). Recycling food waste and saving water: Optimization of the fermentation processes from cheese whey permeate to yeast oil. *Fermentation*, *8*(7), 341. doi: 10.3390/fermentation8070341

Doucha, J., & Livansky, K. (2006). Productivity, co_2/o_2 exchange and hydraulics in outdoor open high density microalgal (*Chlorella* sp.) photobioreactors operated in a middle and southern european climate. *Journal of Applied Phycology*, *18*, 811–826. doi: 10.1007/s10811-006-9100-4

Doucha, J., & Livansky, K. (2008). Influence of processing parameters on disintegration of *Chlorella* cells in various types of homogenizers. *Applied Microbiology and Biotechnology*, *81*, 431–440. doi: 10.1007/s00253-008-1660-6

Drévillon, L., Koubaa, M., & Vorobiev, E. (2018). Lipid extraction from *Yarrowia lipolytica* biomass using high-pressure homogenization. *Biomass and Bioenergy*, *115*, 143–150. doi: 10.1016/j.biombioe.2018.04.014

Duboc, P., Marison, I., & von Stockar, U. (1999). Quantitative calorimetry and biochemical engineering. In R. Kemp (Ed.), *From macromolecules to man* (Vol. 4, p. 267–365). Elsevier Science B.V. doi: 10.1016/S1573-4374(99)80009-0

Dulermo, T., Lazar, Z., Dulermo, R., Rakicka, M., Haddouche, R., & Nicaud, J.-M. (2015). Analysis of atp-citrate lyase and malic enzyme mutants of *Yarrowia lipolytica* points out the importance of mannitol metabolism in fatty acid synthesis. *Biochimica et Biophysica Acta (BBA) - Molecular and Cell Biology of Lipids*, *1851*(9), 1107–1117. doi: 10.1016/j.bbalip.2015.04.007

D'Hondt, E., Martín-Juárez, J., Bolado, S., Kasperoviciene, J., Koreiviene, J., Sulcius, S., ... Bastiaens, L. (2017). Cell disruption technologies. In C. Gonzalez-Fernandez & R. Muñoz (Eds.), *Microalgae-based biofuels and bioproducts* (p. 133–154). Woodhead Publishing. doi: 10.1016/B978-0-08-101023-5.00006-6

European Comission. (2022). *Green deal: Eu agrees law to fight global deforestation and forest degradation driven by eu production and consumption.* `https://ec.europa.eu/commission/presscorner/detail/en/ip_22_7444`. (Accessed on 16 February 2024)

Fasaei, F., Bitter, J., Slegers, P., & van Boxtel, A. (2018). Techno-economic evaluation of microalgae harvesting and dewatering systems. *Algal Research*, *31*, 347–362. doi: 10.1016/j.algal.2017.11.038

Fazullin, D. D., Fazullina, L. I., Yarovikova, D. A., Mavrin, G. V., Nasyrov, I. A., & Shaikhiev, I. G. (2022). Demulsification and ultrafiltration of water-oil emulsions. *Chemical and Petroleum Engineering*, *57*, 783–791. doi: 10.1007/s10556-022-01007-1

Feldmann, H. (Ed.). (2012). *Yeast : Molecular and cell biology* (2nd ed.). Weinheim: John Wiley & Sons Incorporated.

Gallego-García, M., Susmozas, A., Moreno, A. D., & Negro, M. J. (2022). Evaluation and identi-

fication of key economic bottlenecks for cost-effective microbial oil production from fruit and vegetable residues. *Fermentation*, *8*(7), 334. doi: 10.3390/fermentation8070334

Geankoplis, C. J. (Ed.). (2003). *Transport processes and separation process principles* (4th ed.). New Jersey: Pearson Education.

Gelin, F., Boogers, I., Noordeloos, A. A. M., Damsté, J. S. S., Hatcher, P. G., & de Leeuw, J. W. (1996). Novel, resistant microalgal polyethers: An important sink of organic carbon in the marine environment? *Geochimica et Cosmochimica Acta*, *60*(7), 1275–1280. doi: 10.1016/0016-7037(96)00038-5

Gerken, H. G., Donohoe, B., & Knoshaug, E. P. (2013). Enzymatic cell wall degradation of *Chlorella vulgaris* and other microalgae for biofuels production. *Planta*, *237*, 239–253. doi: 10.1007/s00425-012-1765-0

Gong, Z., Shen, H., Wang, Q., Yang, X., Xie1, H., & Zhao1, Z. K. (2013). Efficient conversion of biomass into lipids by using the simultaneous saccharification and enhanced lipid production process. *Biotechnology for Biofuels*, *6*, 36. doi: 10.1186/1754-6834-6-36

Gong, Z., Shen, H., Zhou, W., Wang, Y., Yang, X., & Zhao, Z. K. (2015). Efficient conversion of acetate into lipids by the oleaginous yeast *Cryptococcus curvatus*. *Biotechnology Biofuels*, *8*, 189. doi: 10.1186/s13068-015-0371-3

Gong, Z., Zhou, W., Shen, H., Zhao, Z. K., Yang, Z., Yan, J., & Zhao, M. (2016). Co-utilization of corn stover hydrolysates and biodiesel-derived glycerol by *Cryptococcus curvatus* for lipid production. *Bioresource Technology*, *219*, 552–558. doi: 10.1016/j.biortech.2016.08.021

González-Fernández, C., & Ballesteros, M. (2012). Linking microalgae and cyanobacteria culture conditions and key-enzymes for carbohydrate accumulation. *Biotechnology Advances*, *30*(6), 1655–1661. (Special issue on ACB 2011) doi: 10.1016/j.biotechadv.2012.07.003

Goudar, C. T., Strevett, K. A., & Shah, S. N. (1999). Influence of microbial concentration on the rheology of non-newtonian fermentation broths. *Applied Microbiology and Biotechnology*, *51*, 310–315. doi: 10.1007/s002530051396

Griffiths, M. J., van Hille, R. P., & Harrison, S. T. L. (2010). Selection of direct transesterification as the preferred method for assay of fatty acid content of microalgae. *Lipids*, *45*(11), 1053–1060. doi: 10.1007/s11745-010-3468-2

Grimi, N., Dubois, A., Marchal, L., Jubeau, S., Lebovka, N., & Vorobiev, E. (2014). Selective extraction from microalgae *Nannochloropsis* sp. using different methods of cell disruption. *Bioresource Technology*, *153*, 254–259. doi: 10.1016/j.biortech.2013.12.011

Grubišić, M., Galić Perečinec, M., Peremin, I., Mihajlovski, K., Šantek, S. B. B., & Ivančić Šantek, M. (2022). Optimization of pretreatment conditions and enzymatic hydrolysis of corn cobs for production of microbial lipids by *Trichosporon oleaginosus*. *Energies*, *15*(9), 3208. doi: 10.3390/en15093208

Grubišić, M., Mihajlovski, K., Gruičić, A. M., Beluhan, S., Šantek, B., & Ivančić Šantek, M. (2021). Strategies for improvement of lipid production by yeast *Trichosporon oleaginosus* from lignocellulosic biomass. *Journal of Fungi*, *7*(11), 934. doi: 10.3390/jof7110934

Günerken, E., D'Hondt, E., Eppink, M., Garcia-Gonzalez, L., Elst, K., & Wijffels, R. (2015). Cell disruption for microalgae biorefineries. *Biotechnology Advances*, *33*(2), 243–260. doi: 10.1016/j.biotechadv.2015.01.008

Halim, R., Harun, R., Danquah, M. K., & Webley, P. A. (2012). Microalgal cell disruption for biofuel

development. *Applied Energy*, *91*(1), 116–121. doi: 10.1016/j.apenergy.2011.08.048

Harun, R., & Danquah, M. K. (2011). Enzymatic hydrolysis of microalgal biomass for bioethanol production. *Chemical Engineering Journal*, *168*(3), 1079–1084. doi: 10.1016/j.cej.2011.01.088

Hassan, M., Blanc, P. J., Pareilleux, L.-M. G. A., & Goma, G. (1996). Influence of nitrogen and iron limitations on lipid production by *Cryptococcus curvatus* grown in batch and fed-batch culture. *Process Biochemistry*, *31*(4), 355–361. doi: 10.1016/0032-9592(95)00077-1

He, Q., Yang, H., & Hu, C. (2016). Culture modes and financial evaluation of two oleaginous microalgae for biodiesel production in desert area with open raceway pond. *Bioresource Technology*, *218*, 571–579. doi: 10.1016/j.biortech.2016.06.137

Hernández, D., Riaño, B., Coca, M., & García-González, M. (2015). Saccharification of carbohydrates in microalgal biomass by physical, chemical and enzymatic pre-treatments as a previous step for bioethanol production. *Chemical Engineering Journal*, *262*, 939–945. doi: 10.1016/j.cej.2014.10.049

Ho, S.-H., Huang, S.-W., Chen, C.-Y., Hasunuma, T., Kondo, A., & Chang, J.-S. (2013). Bioethanol production using carbohydrate-rich microalgae biomass as feedstock. *Bioresource Technology*, *135*, 191–198. (Biorefineries) doi: 10.1016/j.biortech.2012.10.015

Horst, I., Parker, B. M., Dennis, J. S., Howe, C. J., Scott, S. A., & Smith, A. G. (2012). Treatment of *Phaeodactylum tricornutum* cells with papain facilitates lipid extraction. *Journal of Biotechnology*, *162*(1), 40–49. (Photosynthetic microorganisms for bio-fuel production from sun light) doi: 10.1016/j.jbiotec.2012.06.033

Imatoukene, N., Koubaa, M., Perdrix, E., Benali, M., & Vorobieva, E. (2020). Combination of cell disruption technologies for lipid recovery from dry and wet biomass of *Yarrowia lipolytica* and using green solvents. *Process Biochemistry*, *90*, 139–147. doi: 10.1016/j.procbio.2019.11.011

Jacobi, A., & Posten, C. (2013). Energy considerations of photobioreactors. In M. A. Borowitzka & N. R. Moheimani (Eds.), *Algae for biofuels and energy* (1st ed., p. 223–232). Springer Netherlands. doi: 10.1007/978-94-007-5479-9_13

Jeong, S. W., Nam, S. W., HwangBo, K., Jeong, W. J., Jeong, B., Chang, Y. K., & Park, Y. (2017). Transcriptional regulation of cellulose biosynthesis during the early phase of nitrogen deprivation in *Nannochloropsis salina*. *Scientific Reports*, *7*, 5264. doi: 10.1038/s41598-017-05684-4

Kaplan, D. (2013). Absorption and adsorption of heavy metals by microalgae. In A. Richmond & Q. Hu (Eds.), *Handbook of microalgal culture* (p. 602–611). John Wiley & Sons, Ltd. doi: 10.1002/9781118567166.ch32

Karamerou, E. E., Parsons, S., McManus, M. C., & Chuck, C. J. (2021). Using techno-economic modelling to determine the minimum cost possible for a microbial palm oil substitute. *Biotechnology for Biofuels*, *14*, 57. doi: 10.1186/s13068-021-01911-3

Karayannis, D., Papanikolaou, S., Vatistas, C., Paris, C., & Chevalot, I. (2023). Yeast lipid produced through glycerol conversions and its use for enzymatic synthesis of amino acid-based biosurfactants. *International Journal of Molecular Sciences*, *24*(1), 714. doi: 10.3390/ijms24010714

Ketchum, B. H., & Redfield, A. C. (1938). A method for maintaining a continuous supply of marine diatoms by culture. *The Biological Bulletin*, *75*(1), 165–169. doi: 10.2307/1537681

Khot, M., Raut, G., Ghosh, D., Alarcón-Vivero, M., Contreras, D., & Ravikumar, A. (2020). Lipid recovery from oleaginous yeasts: Perspectives and challenges for industrial applications. *Fuel*,

259, 116292. doi: 10.1016/j.fuel.2019.116292

Klassen, V., Blifernez-Klassen, O., Hoekzema, Y., Mussgnug, J. H., & Kruse, O. (2015). A novel one-stage cultivation/fermentation strategy for improved biogas production with microalgal biomass. *Journal of Biotechnology*, *215*, 44–51. (Prospects and challenges for the development of algal biotechnology) doi: 10.1016/j.jbiotec.2015.05.008

Koros, W. J., Ma, Y. H., & Shimidzu, T. (1996). Terminology for membranes and membrane processes (iupac recommendations 1996). *Pure and Applied Chemistry*, *68*(7), 1479–1489. doi: 10.1351/pac199668071479

Kourist, R., Bracharz, F., Lorenzen, J., Kracht, O. N., Chovatia, M., Daum, C., ... Nowrousianf, M. (2015). Genomics and transcriptomics analyses of the oil-accumulating basidiomycete yeast *Trichosporon oleaginosus*: Insights into substrate utilization and alternative evolutionary trajectories of fungal mating systems. *mBio*, *6*(4). doi: 10.1128/mBio.00918-15

Koutinas, A. A., Chatzifragkou, A., Kopsahelis, N., Papanikolaou, S., & Kookos, I. K. (2014). Design and techno-economic evaluation of microbial oil production as a renewable resource for biodiesel and oleochemical production. *Fuel*, *116*, 566–577. doi: 10.1016/j.fuel.2013.08.045

Kruger, J. S., Cleveland, N. S., Yeap, R. Y., Dong, T., Ramirez, K. J., Nagle, N. J., ... Biddy, M. J. (2018). Recovery of fuel-precursor lipids from oleaginous yeast. *ACS Sustainable Chemistry & Engineering*, *6*(3), 2921–2931. doi: 10.1021/acssuschemeng.7b01874

Kröger, M., Klemm, M., & Nelles, M. (2018). Hydrothermal disintegration and extraction of different microalgae species. *Energies*, *11*(2), 450. doi: 10.3390/en11020450

Kurokawa, M., King, P. M., Wu, X., Joyce, E. M., Mason, T. J., & Yamamoto, K. (2016). Effect of sonication frequency on the disruption of algae. *Ultrasonics Sonochemistry*, *31*, 157–162. doi: 10.1016/j.ultsonch.2015.12.011

Kurtzman, C. P., & Piskur, J. (2006). Taxonomy and phylogenetic diversity among the yeasts. In P. Sunnerhagen & J. Piskur (Eds.), *Comparative genomics: Using fungi as models* (p. 29–46). Heidelberg: Springer Berlin. doi: 10.1007/b106654

Lee, S. J., Yoon, B.-D., & Oh, H.-M. (1998). Rapid method for the determination of lipid from the green alga *Botryococcus braunii*. *Biotechnology Techniques*, *12*, 553–556. doi: 10.1023/A:1008811716448

López, C. V. G., del Carmen Cerón García, M., Fernández, F. G. A., Bustos, C. S., Chisti, Y., & Sevilla, J. M. F. (2010). Protein measurements of microalgal and cyanobacterial biomass. *Bioresource Technology*, *101*, 7587–7591. doi: 10.1016/j.biortech.2010.04.077

Masojídek, J., Torzillo, G., & Koblížek, M. (2013). Photosynthesis in microalgae. In A. Richmond & Q. Hu (Eds.), *Handbook of microalgal culture* (p. 21–36). John Wiley & Sons, Ltd. doi: 10.1002/9781118567166.ch2

Masri, M., Garbe, D., Mehlmer, N., & Brück, T. (2019). A sustainable, high-performance process for the economic production of waste-free microbial oils that can replace plant-based equivalents. *Energy Environ. Sci.*, *12*(9), 2717–2732. doi: 10.1039/c9ee00210c

Masri, M., Younes, S., Haack, M., Qoura, F., Mehlmer, N., & Brück, T. (2017). A seagrass-based biorefinery for generation of single-cell oils for biofuel and oleochemical production. *Energy Technology*, *6*(6), 1026–1038. doi: 10.1002/ente.201700604

Mazzuca Sobczuk, T., García Camacho, F., Camacho Rubio, F., Acién Fernández, F. G., & Molina Grima, E. (2000). Carbon dioxide uptake efficiency by outdoor microalgal cultures

in tubular airlift photobioreactors. *Biotechnology and Bioengineering*, *67*(4), 465–475. doi: 10.1002/(SICI)1097-0290(20000220)67:4<465::AID-BIT10>3.0.CO;2-9

McMillan, J. R., Watson, I. A., Ali, M., & Jaafar, W. (2013). Evaluation and comparison of algal cell disruption methods: Microwave, waterbath, blender, ultrasonic and laser treatment. *Applied Energy*, *103*, 128–134. doi: 10.1016/j.apenergy.2012.09.020

Meesters, P., Huijberts, G., & Eggink, G. (1996). High-cell-density cultivation of the lipid accumulating yeast *Cryptococcus curvatus* using glycerol as a carbon source. *Applied Microbiology and Biotechnology*, *45*, 575–579. doi: 10.1007/s002530050731

Meo, A. (2016). *Reaktionstechnische charakterisierung der lipidherstellung aus verdünnten zuckergemischen mit Trichosporon oleaginosus* (Unpublished doctoral dissertation). Technical University of Munich.

Meo, A., Priebe, X. L., & Weuster-Botz, D. (2017). Lipid production with *Trichosporon oleaginosus* in a membranebioreactor using microalgae hydrolysate. *Journal of Biotechnology*, *241*, 1–10. doi: 10.1016/j.jbiotec.2016.10.021

Minkevich, I. G., Dedyukhin, E. G., & Chistyakova, T. I. (2010). The effect of lipid content on the elemental composition and energy capacity of yeast biomass. *Applied Microbiology and Biotechnology*, *88*, 799–806. doi: 10.1007/s00253-010-2766-1

Mirsiaghi, M., & Reardon, K. F. (2015). Conversion of lipid-extracted *Nannochloropsis salina* biomass into fermentable sugars. *Algal Research*, *8*, 145–152. doi: 10.1016/j.algal.2015.01.013

Mishra, S. K., Suh, W. I., Farooq, W., Moon, M., Shrivastav, A., Park, M. S., & Yang, J.-W. (2014). Rapid quantification of microalgal lipids in aqueous medium by a simple colorimetric method. *Bioresource Technology*, *155*, 330–333. doi: 10.1016/j.biortech.2013.12.077

Molina Grima, E., Acién Fernández, F. G., & Robles Medina, A. (2013). Downstream processing of cell mass and products. In A. Richmond & Q. Hu (Eds.), *Handbook of microalgal culture* (p. 267–309). John Wiley & Sons, Ltd. doi: 10.1002/9781118567166.ch14

Molina Grima, E., Belarbi, E.-H., Acién Fernández, F. G., Robles Medina, A., & Chisti, Y. (2003). Recovery of microalgal biomass and metabolites: process options and economics. *Biotechnology Advances*, *20*(7), 491–515. doi: 10.1016/S0734-9750(02)00050-2

Molina Grima, E., García Camacho, F., Sánchez Pérez, J., Acién Fernández, F., & Fernández Sevilla, J. (1997). Evaluation of photosynthetic efficiency in microalgal cultures using averaged irradiance. *Enzyme and Microbial Technology*, *21*(5), 375–381. doi: 10.1016/S0141-0229(97)00012-4

Monod, J. (1949). The growth of bacterial cultures. *Annual Review of Microbiology*, *3*(1), 371–394. doi: 10.1146/annurev.mi.03.100149.002103

Montalescot, V., Rinaldi, T., Touchard, R., Jubeau, S., Frappart, M., Jaouen, P., ... Marchal, L. (2015). Optimization of bead milling parameters for the cell disruption of microalgae: Process modeling and application to *Porphyridium cruentum* and *Nannochloropsis oculata*. *Bioresource Technology*, *196*, 339–346. doi: 10.1016/j.biortech.2015.07.075

Moon, N. J., Hammond, E., & Glatz, B. A. (1978). Conversion of cheese whey and whey permeate to oil and single-cell protein. *Journal of Dairy Science*, *61*(11), 1537–1547. doi: 10.3168/jds.S0022-0302(78)83762-X

Morin, N., Cescut, J., Beopoulos, A., Lelandais, G., Le Berre, V., Uribelarrea, J.-L., ... Nicaud, J.-M.

(2011). Transcriptomic analyses during the transition from biomass production to lipid accumulation in the oleaginous yeast *Yarrowia lipolytica*. *PLOS ONE*, *6*(11), 1–13. doi: 10.1371/journal.pone.0027966

Muller-Feuga, A. (2013). Microalgae for aquaculture: The current global situation and future trends. In A. Richmond & Q. Hu (Eds.), *Handbook of microalgal culture* (p. 613–627). John Wiley & Sons, Ltd. doi: 10.1002/9781118567166.ch33

Olmstead, I., Kentish, S., Scales, P., & Martin, G. (2013). Low solvent, low temperature method for extracting biodiesel lipids from concentrated microalgal biomass. *Bioresource Technology*, *148*, 615–619. doi: 10.1016/j.biortech.2013.09.022

Pahl, S. L., Lee, A. K., Kalaitzidis, T., Ashman, P. J., Sathe, S., & Lewis, D. M. (2012). Harvesting, thickening and dewatering microalgae biomass. In M. A. Borowitzka & N. R. Moheimani (Eds.), *Algae for biofuels and energy* (1st ed., p. 165–185). Springer Dordrecht. doi: 10.1007/978-94-007-5479-9_10

Pan, Z., Huang, Y., Wang, Y., & Wu, Z. (2017). Disintegration of *Nannochloropsis* sp. cells in an improved turbine bead mill. *Bioresource Technology*, *245*, 641–648. doi: 10.1016/j.biortech.2017.08.146

Pfaffinger, C. E., Schöne, D., Trunz, S., Löwe, H., & Weuster-Botz, D. (2016). Model-based optimization of microalgae areal productivity in flat-plate gas-lift photobioreactors. *Algal Research*, *20*, 153–163. doi: 10.1016/j.algal.2016.10.002

Pfaffinger, C. E., Severin, T. S., Apel, A. C., Göbel, J., Sauter, J., & Weuster-Botz, D. (2019). Light-dependent growth kinetics enable scale-up of well-mixed phototrophic bioprocesses in different types of photobioreactors. *Journal of Biotechnology*, *297*, 41–48. doi: 10.1016/j.jbiotec.2019.03.003

Pines, D., Ditkovich, J., Mukra, T., Miller, Y., Kiefer, P. M., Daschakraborty, S., ... Pines, E. (2016). How acidic is carbonic acid? *The Journal of Physical Chemistry B*, *120*(9), 2440–2451. doi: 10.1021/acs.jpcb.5b12428

Quesada-Salas, M. C., Delfau-Bonnet, G., Willig, G., Préat, N., Allais, F., & Ioannou, I. (2021). Optimization and comparison of three cell disruption processes on lipid extraction from microalgae. *Processes*, *9*(2), 369. doi: 10.3390/pr9020369

Radecka, D., Mukherjee, V., Mateo, R. Q., Stojiljkovic, M., Foulquié-Moreno, M. R., & Thevelein, J. M. (2015). Looking beyond *Saccharomyces*: the potential of non-conventional yeast species for desirable traits in bioethanol fermentation. *FEMS Yeast Research*, *15*(6), fov053. doi: 10.1093/femsyr/fov053

Ratledge, C. (2005). Single cell oils for the 21st century. In Z. Cohen & C. Ratledge (Eds.), *Single cell oils* (p. 1–20). AOCS Press. doi: 10.1016/B978-1-893997-73-8.50005-0

Ratledge, C. (2014). The role of malic enzyme as the provider of nadph in oleaginous microorganisms: a reappraisal and unsolved problems. *Biotechnology Letters*, *36*, 1557–1568. doi: 10.1007/s10529-014-1532-3

Ratledge, C., & Wynn, J. (2002). The biochemistry and molecular biology of lipid accumulation in oleaginous microorganisms. *Advances in Applied Microbiology*, *51*, 1–52. doi: 10.1016/S0065-2164(02)51000-5

Ratledge, C., & Wynn, J. P. (2020). Oils from microorganisms. In *Bailey's industrial oil and fat products* (p. 1–34). John Wiley & Sons, Ltd. doi: 10.1002/047167849X.bio006.pub2

Rerop, Z. S., Stellner, N. I., Graban, P., Haack, M., Mehlmer, N., Masri, M., & Brück, T. B. (2023). Bioconversion of a lignocellulosic hydrolysate to single cell oil for biofuel production in a cost-efficient fermentation process. *Fermentation*, *9*(2), 189. doi: 10.3390/fermentation9020189

Sabelfeld, M., & Geißen, S.-U. (2011). Verfahren zur eliminierung und rückgewinnung von phosphor aus abwasser. *Chemie Ingenieur Technik*, *83*(6), 782–795. doi: 10.1002/cite.201000187

Salazar, O., & Asenjo, J. A. (2007). Enzymatic lysis of microbial cells. *Biotechnology Letters*, *29*, 985–994. doi: 10.1007/s10529-007-9345-2

Sangster, J. (1989). Octanol-water partition coefficients of simple organic compounds. *Journal of Physical and Chemical Reference Data*, *18*(3), 1111–1229. doi: 10.1063/1.555833

Sawangkeaw, R., & Ngamprasertsith, S. (2013). A review of lipid-based biomasses as feedstocks for biofuels production. *Renewable and Sustainable Energy Reviews*, *25*, 97–108. doi: 10.1016/j.rser.2013.04.007

Schlagermann, P., Göttlicher, G., Dillschneider, R., Rosello-Sastre, R., & Posten, C. (2012). Composition of algal oil and its potential as biofuel. *Journal of Combustion*, *2012*, 285185. doi: 10.1155/2012/285185

Scholz, M. J., Weiss, T. L., Jinkerson, R. E., Jing, J., Roth, R., Goodenough, U., ... Gerken, H. G. (2014). Ultrastructure and composition of the *Nannochloropsis gaditana* cell wall. *Eukaryotic Cell*, *13*(11), 1450–1464. doi: 10.1128/ec.00183-14

Schramm, G. (2004). *A practical approach to rheology and rheometry* (2nd ed.). Karlsruhe: Thermo Electron GmbH.

Schädler, T. (2020). *Biomasse- und lipidherstellung mit Microchloropsis salina in offenen flachgerinnereaktoren* (Unpublished doctoral dissertation). Technical University of Munich.

Schädler, T., Cerbon, D. C., de Oliveira, L., Garbe, D., Brück, T., & Weuster-Botz, D. (2019). Production of lipids with *Microchloropsis salina* in open thin-layer cascade photobioreactors. *Bioresource Technology*, *289*, 121682. doi: 10.1016/j.biortech.2019.121682

Schädler, T., Thurn, A.-L., Brück, T., & Weuster-Botz, D. (2021). Continuous production of lipids with *Microchloropsis salina* in open thin-layer cascade photobioreactors on a pilot scale. *Energies*, *14*(2), 500. doi: 10.3390/en14020500

Shaigani, P., Awad, D., Redai, V., Fuchs, M., Haack, M., Mehlmer, N., & Brück, T. (2021). Oleaginous yeasts- substrate preference and lipid productivity: a view on the performance of microbial lipid producers. *Microbial Cell Factories*, *20*, 220. doi: 10.1186/s12934-021-01710-3

Sitepu, I. R., Garay, L. A., Sestric, R., Levin, D., Block, D. E., German, J. B., & Boundy-Mills, K. L. (2014). Oleaginous yeasts for biodiesel: Current and future trends in biology and production. *Biotechnology Advances*, *32*(7), 1336–1360. doi: 10.1016/j.biotechadv.2014.08.003

Spiden, E. M., Yap, B. H. J., Hill, D. R. A., Kentish, S. E., Scales, P. J., & Martin, G. J. O. (2013). Quantitative evaluation of the ease of rupture of industrially promising microalgae by high pressure homogenization. *Bioresource Technology*, *140*, 165–171. doi: 10.1016/j.biortech.2013.04.074

Takors, R., & Weuster-Botz, D. (2018). Prozessmodelle. In H. Chmiel, R. Takors, & D. Weuster-Botz (Eds.), *Bioprozesstechnik* (4th ed., p. 71–105). Berlin, Heidelberg: Springer Berlin Heidelberg. doi: 10.1007/978-3-662-54042-8_3

Takács, I., Murthy, S., Smith, S., & McGrath, M. (2006). Chemical phosphorus removal to extremely low levels: experience of two plants in the washington, dc area. *Water Science & Technology*,

53(12), 21–28. doi: 10.2166/wst.2006.402

Talukder, M. R., Das, P., & Wu, J. C. (2012). Microalgae (*Nannochloropsis salina*) biomass to lactic acid and lipid. *Biochemical Engineering Journal*, *68*, 109–113. doi: 10.1016/j.bej.2012.07.001

Thiru, M., Sankh, S., & Rangaswamy, V. (2011). Process for biodiesel production from *Cryptococcus curvatus*. *Bioresource Technology*, *102*(22), 10436–10440. doi: 10.1016/j.biortech.2011.08.102

Thorpe, R. F., & Ratledge, C. (1972). Fatty acid distribution in triglycerides of yeasts grown on glucose or n-alkanes. *Microbiology*, *72*(1), 151–163. doi: 10.1099/00221287-72-1-151

Thurn, A.-L., Stock, A., Gerwald, S., & Weuster-Botz, D. (2022). Simultaneous photoautotrophic production of dha and epa by *Tisochrysis lutea* and *Microchloropsis salina* in co-culture. *Bioresources and Bioprocessing*, *9*, 130. doi: 10.1186/s40643-022-00612-5

Toor, S. S., Reddy, H., Deng, S., Hoffmann, J., Spangsmark, D., Madsen, L. B., ... Rosendahl, L. A. (2013). Hydrothermal liquefaction of *Spirulina* and *Nannochloropsis salina* under subcritical and supercritical water conditions. *Bioresource Technology*, *131*, 413–419. doi: 10.1016/j.biortech.2012.12.144

UNFCCC. (2016). *The paris agreement.* `https://unfccc.int/process-and-meetings/the-paris-agreement`. (Accessed on 16 February 2024)

Wang, M., Yuan, W., Jiang, X., Jing, Y., & Wang, Z. (2014). Disruption of microalgal cells using high-frequency focused ultrasound. *Bioresource Technology*, *153*, 315–321. doi: 10.1016/j.biortech.2013.11.054

Wang, Y., Zhang, S., Zhu, Z., Shen, H., Lin, X., Jin, X., ... Zhao, Z. K. (2018). Systems analysis of phosphate-limitation-induced lipid accumulation by the oleaginous yeast *Rhodosporidium toruloides*. *Biotechnology for Biofuels*, *11*, 148. doi: 10.1186/s13068-018-1134-8

Weiss, R. (1974). Carbon dioxide in water and seawater: the solubility of a non-ideal gas. *Marine Chemistry*, *2*(3), 203–215. doi: 10.1016/0304-4203(74)90015-2

Weuster-Botz, D., & Takors, R. (2018). Wachstumskinetik. In H. Chmiel, R. Takors, & D. Weuster-Botz (Eds.), *Bioprozesstechnik* (4th ed., p. 45–70). Berlin, Heidelberg: Springer Berlin Heidelberg. doi: 10.1007/978-3-662-54042-8_2

White, F. M. (2011). *Fluid mechanics* (7th ed.). New York: McGraw Hill.

Woosley, R. J. (2021). Evaluation of the temperature dependence of dissociation constants for the marine carbon system using ph and certified reference materials. *Marine Chemistry*, *229*, 103914. doi: 10.1016/j.marchem.2020.103914

Wu, S., Hu, C., Jin, G., Zhao, X., & Zhao, Z. K. (2010). Phosphate-limitation mediated lipid production by *Rhodosporidium toruloides*. *Bioresource Technology*, *101*(15), 6124–6129. doi: 10.1016/j.biortech.2010.02.111

Yadav, G., Dubey, B. K., & Sen, R. (2020). A comparative life cycle assessment of microalgae production by co_2 sequestration from flue gas in outdoor raceway ponds under batch and semi-continuous regime. *Journal of Cleaner Production*, *258*, 120703. doi: 10.1016/j.jclepro.2020.120703

Yaguchi, A., Rives, D., & Blenner, M. (2017). New kids on the block: emerging oleaginous yeast of biotechnological importance. *AIMS Microbiology*, *3*(2), 227–247. doi: 10.3934/microbiol.2017.2.227

Yaguchi, A., Robinson, A., Mihealsick, E., & Blenner, M. (2017). Metabolism of aromatics by *Trichosporon oleaginosus* while remaining oleaginous. *Microbial Cell Factories*, *16*, 206. doi: 10.1186/s12934-017-0820-8

Yao, S., Mettu, S., Law, S. Q., Ashokkumar, M., & Martin, G. J. (2018). The effect of high-intensity ultrasound on cell disruption and lipid extraction from high-solids viscous slurries of *Nannochloropsis* sp. biomass. *Algal Research*, *35*, 341–348. doi: 10.1016/j.algal.2018.09.004

Yap, B. H., Dumsday, G. J., Scales, P. J., & Martin, G. J. (2015). Energy evaluation of algal cell disruption by high pressure homogenisation. *Bioresource Technology*, *184*, 280–285. doi: 10.1016/j.biortech.2014.11.049

Yeh, S. W., Ong, L. J., Glazer, A. N., & Clark, J. H. (1987). Fluorescence properties of allophycocyanin and a crosslinked allophycocyanin trimer. *Cytometry*, *8*(1), 1–109. doi: 10.1002/cyto.990080113

Ykema, A., Verbree, E. C., van Verseveld, H. W., & Smit, H. (1986). Mathematical modelling of lipid production by oleaginous yeasts in continuous cultures. *Antonie van Leeuwenhoek*, *52*, 491–506. doi: 10.1007/BF00423410

Younes, S., Bracharz, F., Awad, D., Qoura, F., Mehlmer, N., & Brück, T. (2020). Microbial lipid production by oleaginous yeasts grown on *Scenedesmus obtusiusculus* microalgae biomass hydrolysate. *Bioprocess and Biosystems Engineering*, *43*, 1629–1638. doi: 10.1007/s00449-020-02354-0

Yousuf, A., Sannino, F., Addorisio, V., & Pirozzi, D. (2010). Microbial conversion of olive oil mill wastewaters into lipids suitable for biodiesel production. *Journal of Agricultural and Food Chemistry*, *58*(15), 8630-8635. doi: 10.1021/jf101282t

Yu, X., Zeng, J., Zheng, Y., & Chen, S. (2014). Effect of lignocellulose degradation products on microbial biomass and lipid production by the oleaginous yeast *Cryptococcus curvatus*. *Process Biochemistry*, *49*(3), 457–465. doi: 10.1016/j.procbio.2013.10.016

Yu, X., Zheng, Y., Dorgan, K. M., & Chen, S. (2011). Oil production by oleaginous yeasts using the hydrolysate from pretreatment of wheat straw with dilute sulfuric acid. *Bioresource Technology*, *102*(10), 6134–6140. doi: 10.1016/j.biortech.2011.02.081

Zhang, G., French, W. T., Hernandez, R., Hall, J., Sparks, D., & Holmes, W. E. (2011). Microbial lipid production as biodiesel feedstock from n-acetylglucosamine by oleaginous microorganisms. *Journal of Chemical Technology & Biotechnology*, *86*(5), 642–650. doi: 10.1002/jctb.2592

Zhang, R., Parniakov, O., Grimi, N., Lebovka, N., Marchal, L., & Vorobiev, E. (2019). Emerging techniques for cell disruption and extraction of valuable bio-molecules of microalgae *Nannochloropsis* sp. *Bioprocess and Biosystems Engineering*, *42*, 173–186. doi: 10.1007/s00449-018-2038-5

Zhou, W., Li, Y., Zhang, Y., & Zhao, Z. (2012). Energy efficiency evaluation of lipid production by oleaginous yeast *Rhodosporidium toruloides*. *Journal of Thermal Analysis and Calorimetry*, *108*, 119–126. doi: 10.1007/s10973-011-1659-6

Zhou, W., Tang, M., Zou, T., Peng, N., Zhao, M., & Gong, Z. (2019). Phosphate removal combined with acetate supplementation enhances lipid production from water hyacinth by *Cutaneotrichosporon oleaginosum*. *Biotechnology for Biofuels and Bioproducts*, *12*, 148. doi: 10.1186/s13068-019-1491-y

Zittelli, G. C., Rodolfi, L., Bassi, N., Biondi, N., & Tredici, M. R. (2013). Photobioreactors for microal-

gal biofuel production. In M. A. Borowitzka & N. R. Moheimani (Eds.), *Algae for biofuels and energy* (p. 115–131). Dordrecht: Springer Netherlands. doi: 10.1007/978-94-007-5479-9_7

Zuorro, A., Miglietta, S., Familiari, G., & Lavecchia, R. (2016). Enhanced lipid recovery from *Nannochloropsis* microalgae by treatment with optimized cell wall degrading enzyme mixtures. *Bioresource Technology*, *12*, 35–41. doi: 10.1016/j.biortech.2016.04.025

List of Abbreviations and Symbols

Abbreviation	Meaning
2-PG	2-Phosphoglycolate
ACL	ATP:citrate lyase
AD	Adenosine Deaminase
AMP	Adenosine monophosphate
ASW	Artificial seawater
ATP	Adenosine triphosphate
A/V ratio	Area to volume ratio
CBB cycle	Calvin Benson Bassham cycle
CDW	Cell dry weight
CER	Carbon emission rate
CMP	Cytidine monophosphate
CoA	Coenzyme A
C/P ratio	Mass ratio of carbon to phosphorus
DAG	Diacylglycerol
DCD	Degree of cell disruption
DHA	Docosahexaenoic acid
DIC	Dissolved inorganic carbon
DW	Dry weight
EDTA	Ethylenediaminetetraacetic acid
$F_{640–780}$	Fluorescence in the wavelength range of 640–780 nm
FA	Fatty acid
FAME	Fatty acid methyl ester
FAS	Fatty acid synthase
FC	Flow cytometry
FI	Flame ionization detector
FSC	Forward-scattered light
G3P	3-Phosphoglycerate
GC	Gas chromatography
GC-FID	Gas chromatograph with a flame ionization detector
GMP	Guanosine monophosphate
HPH	High-pressure homogenizer
ICDH	Isocitrate dehydrogenase
IMP	Inosine monophosphate
LED	Light-emitting diode
MA	Microalgae
MAH	Microalgae hydrolysate
MBR	Membrane bioreactor

Continued on the next page.

Abbreviation	Meaning
MDH	Malate dehydrogenase
ME	Malic enzyme
NADPH	Nicotinamide adenine dinucleotide phosphate
NMP	Nucleoside monophosphate
OD_{600}	Optical density at 600 nm
OTR	Oxygen transfer rate
OUR	Oxygen uptake rate
PA	Phosphatidate
PAR	Photosynthetically active radiation
PBR	Photobioreactor
PBS	Phosphate-buffered saline
PFD	Photon flux density
Pi	Inorganic phosphate
PL	Phospholipid
pO_2	dissolved oxygen level
PPFD	Photosynthetic photon flux density
PUFA	Polyunsaturated fatty acid
RNA	Ribonucleic acid
RQ	Respiratory quotient
RuBisCO	Ribulose-1,5-bisphosphat-carboxylase
RuBP	Ribulose-1,5-bisphosphate
SCO	Single-cell oil
SFA	Saturated fatty acid
SPV	Sulfo-phospho-vanillin
STR	Stirred-tank reactor
STY	Space-time-yield
TA	Total alkalinity
TAG	Triacylglycerol
TLC	Thin-layer cascade
TMP	Trans membrane pressure
TUM	Technical University of Munich
UFA	Unsaturated fatty acid
UMP	Uridine monophosphate
YPD	Yeast-peptone-dextrose

Symbol	Unit	Meaning
A	m^2	Surface area
α	–	Reflux ratio
CF	–	Ratio of nutrient concentration in the feed medium to that in the ASW medium
$c_{glucose}$	g L^{-1}	Glucose concentration
c_i	g L^{-1}	Concentration of species i
$c_{i,in}$	g L^{-1}	Concentration of species i at the inlet stream
$c_{i,out}$	g L^{-1}	Concentration of species i at the outlet stream
c_L	g L^{-1}	Lipid concentration
$c_{L,ext}$	g L^{-1}	Lipid concentration of yeast suspension used for extraction
$c_{mannose}$	g L^{-1}	Mannose concentration
$c_{nutrient,ASW}$	g L^{-1}	Nutrient concentration in the ASW medium
c_{O_2}	g L^{-1}	Concentration of oxygen dissolved in reaction medium
$c*_{O_2}$	g L^{-1}	Saturation concentration of oxygen in reaction medium
c_P	g L^{-1}	Product concentration
$c_{P,in}$	g L^{-1}	Product concentration at the inlet stream
$c_{P,out}$	g L^{-1}	Product concentration at the outlet stream
c_S	g L^{-1}	Substrate concentration
$c_{S,0}$	g L^{-1}	Initial substrate concentration
$c_{S,feed}$	g L^{-1}	Substrate concentration of the feed medium
$c_{S,in}$	g L^{-1}	Substrate concentration at the inlet stream
$c_{S,out}$	g L^{-1}	Substrate concentration at the outlet stream
$c_{S,t}$	g L^{-1}	Substrate concentration at process time t
c_X	g L^{-1}	Cell dry weight concentration
$c_{X,0}$	g L^{-1}	Initial cell dry weight concentration
$c_{X,in}$	g L^{-1}	Concentration of cell dry weight at the inlet stream
$c_{X,out}$	g L^{-1}	Concentration of cell dry weight at the outlet stream
CER	mol L^{-1} h^{-1}	Carbon emission rate
D	h^{-1} or d^{-1}	Dilution rate
D_{max}	h^{-1}	Dilution rate at which a wash-out of the cells from the reactor occurs
DCD	–	Degree of cell disruption
ϵ	L g^{-1} cm^{-1}	Specific extinction coefficient
$\dot{\gamma}$	s^{-1}	Shear rate
η_{CO_2}	–	Carbon dioxide fixation efficiency
η_C	–	Carbon conversion efficiency based on C uptake
$\eta_{C,fed}$	–	Carbon conversion efficiency based on C fed into the reactor
η_{ext}	–	Lipid extraction efficiency
η_{hyd}	–	Hydrolysis efficiency based on carbon solubilization
η_{sac}	–	Saccharification efficiency

Continued on the next page.

Symbol	Unit	Meaning
F	–	Ratio of nutrient feed per reaction volume to nutrient concentration in the ASW medium
i_{cells}	–	Incidence count of intact cells with FC
i_{debris}	–	Incidence count of cell debris with FC
I	µmol m^{-2} s^{-1}	Light transmitted over the layer thickness
$I*$	µmol m^{-2} s^{-1}	Mean integral PFD
I_0	µmol m^{-2} s^{-1}	Incident photon flux density
k_La	h^{-1}	Volumetric gas transfer coefficient of oxygen
K_S	g L^{-1}	Saturation constant in Monod equation
K_{SP}	µmol m^{-2} s^{-1}	Saturation constant for photon flux density
K_I	–	Inhibition constant
K_{IP}	µmol m^{-2} s^{-1}	Photoinhibition constant
l	cm	Thickness of the optical path
$m_{C,in}$	g	Mass of carbon added into the reactor
m_{CDW}	g	Mass of CDW produced
m_{C,CO_2}	g	Mass of carbon mass exiting the system in form of CO_2
m_{CO_2}	g	Mass of carbon dioxide supplied into the reactor
$\dot{m}_{CO_2}$	g h^{-1}	Mass flow rate of carbon dioxide supplied into the reactor
m_i	g	Mass of species i
$m_{CDW,0}$	g	Cell dry weight measured at process start
$m_{CDW,t}$	g	Cell dry weight measured at time t
$m_{\dot{CO_2}}$	g h^{-1}	Mass flow rate of CO_2
m_L	g	Mass of lipids produced
$m_{L,0}$	g	Initial mass of lipids produced
$m_{L,t}$	g	Mass of lipids produced at process time t
$m_{L,ext}$	g	Mass of lipids extracted
m_{MAH}	g	Mass of microalgae hydrolysate added into the reactor for yeast cultivation
$m_{nutrient,in}$	g	Mass of nutrients fed to the reactor
$m_{S,in}$	g	Mass of substrate added into the reactor
$m_{S,R}$	g	Mass of remaining unused substrate
$m_{S,up}$	g	Mass of substrate taken up
$m_{S,up,t}$	g	Mass of substrate taken up at process time t
m_{syn}	g	Mass of synthetic medium added into the reactor for yeast cultivation
m_P	g	Mass of product generated
$m_{P,0}$	g	Initial mass of product generated
$m_{P,t}$	g	Mass of product generated at process time t
m_{Urea}	g	Mass of urea supplied into the reactor
$m_{Urea,t}$	g	Total mass of urea supplied into the reactor at process time t

Continued on the next page.

Symbol	Unit	Meaning
$m_{Vit,in}$	g	Mass of vitamins added into the reactor
m_X	g	Mass of lipid-free biomass produced
$m_{X,0}$	g	Initial mass of lipid-free biomass produced
M_{CO_2}	g mol^{-1}	Molar mass of CO_2
μ	Pa s	Dynamic viscosity
μ	h^{-1}	Growth rate
μ_{max}	h^{-1}	Cell specific maximum growth rate
μ_{set}	h^{-1}	Setpoint for a constant growth rate
$n_{CO_2,in}$	mol	Molar flow rate of CO_2 at the inlet stream
$n_{CO_2,out}$	mol	Molar flow rate of CO_2 at the outlet stream
$n_{N_2,in}$	mol	Molar flow rate of N_2 at the inlet stream
$n_{N_2,out}$	mol	Molar flow rate of N_2 at the outlet stream
n_{O_2}	mol	Molar amount of O_2
$n_{O_2,in}$	mol	Molar flow rate of O_2 at the inlet stream
$n_{O_2,out}$	mol	Molar flow rate of O_2 at the outlet stream
OTR	g L^{-1} h^{-1}	Oxygen transfer rate
OUR	g L^{-1} h^{-1}	Oxygen uptake rate
P	atm	Absolute pressure
P_A	g m^{-2} d^{-1}	Areal productivity
P_{in}	bar	Pressure at the inlet stream
P_{out}	bar	Pressure at the outlet stream
P_{perm}	bar	Pressure at the permeate stream
P_V	g L^{-1} h^{-1}	Volumetric productivity
ϕ	–	Sensitivity factor
Q_S	g L^{-1} h^{-1}	Sugar feed rate based on initial fermentation volume
q_P	g g^{-1} h^{-1}	Cell specific product formation rate
q_S	g g^{-1} h^{-1}	Cell specific substrate uptake rate
$q_{S,\mu}$	g g^{-1} h^{-1}	Rate of cell specific substrate uptake for growth
$q_{S,m}$	g g^{-1} h^{-1}	Rate of cell specific substrate uptake for maintenance
$q_{S,P}$	g g^{-1} h^{-1}	Rate of cell specific substrate uptake for product formation
r	m	radius
r_{feed}	g L^{-1} d^{-1}	Nutrient feed rate
$r_{feed,ave}$	g L^{-1} d^{-1}	Average nutrient feed rate
r_i	g L^{-1} h^{-1}	Formation rate of species i
r_S	g L^{-1} h^{-1}	Substrate uptake rate
r_P	g L^{-1} h^{-1}	Product formation rate
r_X	g L^{-1} h^{-1}	Biomass production rate
R	L atm mol^{-1} K^{-1}	Ideal gas constant
R_{rest}	g	Remaining carbon mass presumed to be oxidized by respiration in the carbon balance equation

Continued on the next page.

Symbol	Unit	Meaning
Re	–	Reynold's number
RQ	–	Respiratory quotient
ρ	g L^{-1}	Fluid density
ρ_{MAH}	g L^{-1}	Density of microalgal biomass hydrolysate
STY_i	g L^{-1} h^{-1}	Space-time-yield of species i
STY_L	g L^{-1} h^{-1}	Space-time-yield of lipids
STY_{X+L}	g L^{-1} h^{-1}	Space-time-yield of lipid-containing biomass
T	K	Temperature
t	h or d	Process time
t_0	h	Process starting time (e.g. inoculation time)
TMP	bar	Trans membrane pressure
τ	h	Hydraulic residence time
τ	Pa	Shear stress
V	L	Volume
$\dot{V}$	L h^{-1}	Volumetric flow rate in and out of the reactor when $\dot{V}_{in} = \dot{V}_{out}$
V_{ext}	L	Volume of yeast suspension used for extraction
$\dot{V}_{in}$	L h^{-1}	Volumetric flow rate of the inlet stream
$\dot{V}_{in,filter}$	L h^{-1}	Volumetric flow rate of feed into the filter module
$\dot{V}_{g,in}$	L h^{-1}	Volumetric flow rate of the gas inlet stream
$\dot{V}_{out}$	L h^{-1}	Volumetric flow rate of the outlet stream
$\dot{V}_{out,perm}$	L h^{-1}	Volumetric flow rate of permeate outlet stream
$\dot{V}_{out,ret}$	L h^{-1}	Volumetric flow rate of retentate outlet stream
$\dot{V}_{g,out}$	L h^{-1}	Volumetric flow rate of the gas outlet stream
V_R	L	Liquid volume inside the reactor
$V_{R,0}$	L	Initial liquid volume inside the reactor
$\dot{V}_{reflux}$	L h^{-1}	Volumetric flow rate of retentate fed back to the reactor
$Y_{CO_2,in}$	–	Molar fraction of CO_2 in the inlet gas stream
$Y_{CO_2,out}$	–	Molar fraction of CO_2 in the outlet gas stream
Y_{LS}	g g^{-1}	Lipid yield
$Y_{N_2,in}$	–	Molar fraction of N_2 in the inlet gas stream
$Y_{N_2,out}$	–	Molar fraction of N_2 in the outlet gas stream
$Y_{O_2,in}$	–	Molar fraction of O_2 in the inlet gas stream
$Y_{O_2,out}$	–	Molar fraction of O_2 in the outlet gas stream
Y_{PS}	g g^{-1}	Product selectivity
Y_{PX}	g g^{-1}	Specific productivity
$Y_{(X+L)/S}$	g g^{-1}	Lipid-containing biomass yield coefficient
Y_{XO_2}	g g^{-1}	Biomass yield coefficient of oxygen
Y_{XS}	g g^{-1}	Lipid-free biomass yield
$Y_{XS,\mu}$	g g^{-1}	Biomass yield coefficient
x_C	g g^{-1}	Mass fraction of carbon in a molecule or material

Continued on the next page.

Symbol	Unit	Meaning
x_{C,CO_2}	g g^{-1}	Mass fraction of carbon in CO_2
$x_{C,Lipid}$	g g^{-1}	Mass fraction of carbon in yeast lipids
$x_{C,MAH}$	g g^{-1}	Mass fraction of carbon in microalgal biomass hydrolysate
$x_{C,Ms}$	g g^{-1}	Mass fraction of carbon in dry microalgae mass
$x_{C,S}$	g g^{-1}	Overall carbon fraction of the added sugars
$x_{C,syn}$	g g^{-1}	Mass fraction of carbon in synthetic medium used for yeast cultivation
$x_{C,Urea}$	g g^{-1}	Mass fraction of carbon in urea
$x_{C,Vit}$	g g^{-1}	Carbon fraction of the added vitamins
$x_{carb,glucose}$	g g^{-1}	Glucose mass fraction in the carbohydrates of the microalgae
$x_{carb,mannose}$	g g^{-1}	Mannose mass fraction in the carbohydrates of the microalgae
$x_{X,carb}$	g g^{-1}	Carbohydrate fraction of dry microalgae mass

A. Appendices

A.1. Equipment Used

Table A.1: Components of thin-layer cascade photobioreactors.

Component	Product and Manufacturer
Aluminium frame	Aluminium profile 80x80E/L, Alvarís, Germany
Centrifugal pump	Ventaix, Germany
CO_2 mass flow controller	red-y smart, Voegtlin, Switzerland
CO_2 supply hose	Solvocarb® and Solvox® B, Linde, Germany
Flow meter	MIK, Kobold, Germany
Frequency inverter	Movitrac® LTE-B, SEW Eurodrive, Germany
Level sensor	LFFS, Baumer, Germany
Magnetic valve	Type 52, Gemü, Germany
pH/temperatur probe	tecLine 201020/51-18-04-18-120, Jumo, Germany
pH transmitter	ecoTrans pH 03, Jumo, Germany
Pond liner	PE pond liner 320 g m^{-2}, Daedler, Germany
Process control system	LabView 2017, National Instruments, USA
Pumping tubes	Rauspiraflex Liquitec, REHAU, Germany
Tanks and channels	PE-HD 10 mm, Rauch, Germany
Three-way valve	PVC-Welt, Germany
USB DAQ System	U6, Labjack, USA
Wire mesh	PS3030KFE, 30/3 mm, Mutanox, Germany

Table A.2: Components of stirred-tank and membrane bioreactors on a litre scale.

Component	Product and Manufacturer
Air filter	Acro® 50 (0.2 µm), Cytiva, USA
Ball valve	Minibinox®, Effebi, Italy
Control software	IrisNT Pro Balance v5, Infors AG, Switzerland
DO probe	InPro6800, Mettler Toledo, USA
Microfiltration module	CFP-2-E-4A, Cytiva, USA
Stirred-tank reactor	Labfors 2, Infors HT, Switzerland
Peristaltic feed pump	PD 5001, Heidolph, Germany
Peristaltic permeate pump	BVP Easy-Load, Ismatec, Germany
Peristaltic circulation pump	BVP Easy-Load II, Ismatec, Germany
pH probe	405-DPAS-SC-K8S/425, Mettler Toledo, USA
Pressure gauge	Type 233.50, WIKA, Germany

Table A.3: Equipment used in TUM-AlgaeTec Center.

Equipment	**Product and Manufacturer**
Alkalinity analyser	HI755 Checker HC, Hanna Instruments, USA
Analytical balance	New Classic MS104S, Mettler Toledo, USA
Diaphragm vacuum pump	LABOPORT® N938.50 KN18, KNF Group Int., Germany
Drying cabinet	UF450, Memmert, Germany
Dynamic settler	Evodos 10, Evodos, Netherlands
Dynamic settler	Evodos 50A, Evodos, Netherlands
Harvest tank	Type TR 5/L white PE, Aricon, Germany
Medium tank	Type TR 5/L black PE, Aricon, Germany
Micropipettes	20 µL to 10 mL Transferpette®, Brand, Germany
Microscope	Eclipse E200 Nikon, Germany
Peristaltic pump	120U/DM3, Watson Marlow, Germany
Peristaltic pump	530DuN, Watson Marlow, Germany
pH meter	HandyLab 100, SI Analytics, Germany
Refractometer	HI96822, Hanna Instruments, USA
Spectral radiometer	Flame-T Ocean Optics Inc., USA
Spectrophotometer	Genesys 10S UV-Vis, Thermo Fisher Scientific, USA
Tabletop centrifuge	Espresso, Thermo Fisher Scientific, USA
Tabletop scale	ML6002T, Mettler Toledo, USA
Thermometer	HI98509, Hanna Instruments, USA
Vortex mixer	Vortex-Genie 2 G560 E, Scientific Industries Inc., USA

Table A.4: Equipment used in TUM Pilot Plant for Industrial Biotechnology.

Equipment	**Product and Manufacturer**
Control software	BioSCADALab, Bioengineering, Switzerland
Cross-flow microfiltration unit	Clearflow MF X 01, Heinrich Frings, Germany
Exhaust gas analyser	BCP-CO_2 & BCP-O_2, BlueSens, Germany
High-pressure homogenizer	Ariete NS3015H, GEA Group, Germany
Incubation shaker	innova 44, Eppendorf, Germany
Medium vessel	200 L sterile vessel, Rütten, Germany
Magnetic stirrer	MR Hei-Standard, Heidolph, Germany
Microfilter	Crystar 41-61-3.0 FT250, Saint-Gobain, France
Stirred-tank reactor	LP75L, Bioengineering, Switzerland

Table A.5: Equipment used at the Chair of Biochemical Engineering and Werner Siemens-Chair of Synthetic Biotechnology at TUM.

Equipment	Product and Manufacturer
Analytical balance	XA 204, Mettler Toledo, USA
Autoclave	VX-150, Systec, Germany
Centrifuge	ROTIXA 50 RS, Hettich, Germany
Flow cytometer	CytoFLEX V0-B3-R1, Beckman Coulter, USA
GC-FID	GC-2010 Plus, Shimadzu, Japan
GC column	FAMEWAX, Restek, Germany
High-pressure homogenizer	HPL6, Maximator, Germany
Incubation shaker	Multitron, Infors HT, Switzerland
Lyophilizer	Alpha 1-2 LD plus, Martin Christ, Germany
Magnetic stirrer	MR Hei-Standard, Heidolph, Germany
Micropipettes	10 µL to 10 mL Transferpette®, Brand, Germany
Microplate reader	Infinite® M200 Pro, Tecan, Germany
Microplate reader software	Magellan™ V6.6, Tecan, Germany
Microscope	Axiolab, Carl Zeiss, Germany
Mixer mill	MM 400, Retsch, Germany
pH meter	Five Easy pH/mV, Mettler Toledo, USA
Rotary vacuum evaporator	Hei-VAP Expert, Heidolph, Germany
Ultrasonic homogenizer	Sonopuls, Bandelin, Germany
Stirred-tank reactor	Labfors 5, Infors HT, Switzerland
Tabletop centrifuge	Mikro 220, Hettich, Germany
Thermomixer	basic, CellMedia, Germany
Vortex mixer	Vortex-Genie 2 G560 E, Scientific Industries Inc., USA

A.2. Materials Used

Table A.6: Materials used for analysis and experiments.

Material	Product and Manufacturer
Acetate assay	Acetic acid Assay Kit, R-Biopharm, Germany
Ammonia assay	Ammonia Assay Kit, R-Biopharm, Germany
Cellulase mix	Cellic® CTec3 HS, Novozymes, Denmark
Cellulase mix	Rohament® CEP, AB Enzymes, Germany
Galactose assay	Lactose/D-Galactose Assay Kit, R-Biopharm, Germany
Glass beads	1.04015 (3 mm Ø), Sigma-Aldrich, USA
Glass microfibre filter	Whatman® Grade GF/C (25 mm Ø), Cytiva, USA
Glucose assay	D-Glucose Assay Kit, R-Biopharm, Germany
Hemicellulase	Hemicellulase from *A. niger*, Sigma-Aldrich, USA
Mannanase	Rohalase® GMP, AB Enzymes, Germany
Mannose assay	D-Mannose/D-Fructose/D-Glucose Assay Kit, Megazyme, Ireland

Continued on the next page.

Table A.6: Materials used for analysis and experiments.

Material	**Product and Manufacturer**
Mixer mill grinding jar	01.462.0213, Retsch, Germany
Rhamnose assay	L-Rhamnose Assay Kit, Megazyme, Ireland
Xylose assay	D-Xylose Assay Kit, Megazyme, Ireland
Phosphate assay	Phosphate colorimetric kit, Sigma-Aldrich, USA
Protease	Protease from *A. saitoi*, Sigma-Aldrich, USA
Protease mix	Protamex®, Novozymes, Denmark
Protein assay	Pierce™BCA Protein Assay Kit, Thermo Fisher Scientific, USA
Stainless steel beads	22.455.0010 (2 mm Ø), Retsch, Germany
Stainless steel beads	22.455.0003 (5 mm Ø), Retsch, Germany
Tungsten carbide beads	22.455.0006 (3 mm Ø), Retsch, Germany
Zirconium oxide beads	ZetaBeads® Plus 0.5 (0.5 mm Ø) Netzsch, Germany
Zirconium oxide beads	ZetaBeads® Plus 1.0 (1 mm Ø) Netzsch, Germany